Titre: Title:	Investigation on Multi-Bolted/Bonded Single-lap Composite Joints via 3D Digital Image Correlation (DIC) Technology
Auteur: Author:	Masoud Mehrabian
Date:	2022
Type:	Mémoire ou thèse / Dissertation or Thesis
Référence: Citation:	Mehrabian, M. (2022). Investigation on Multi-Bolted/Bonded Single-lap Composite Joints via 3D Digital Image Correlation (DIC) Technology [Thèse de doctorat, Polytechnique Montréal]. PolyPublie. https://publications.polymtl.ca/10280/

POLYTECHNIQUE MONTRÉAL

affiliée à l'Université de Montréal

Investigation of multi-bolted/bonded single-lap composite joints via 3D digital image correlation (DIC) technology

MASOUD MEHRABIAN

Département de génie mécanique

Thèse présentée en vue de l'obtention du diplôme de *Philosophiæ Doctor*

Génie mécanique

Avril 2022

POLYTECHNIQUE MONTRÉAL

affiliée à l'Université de Montréal

Cette thèse intitulée:

Investigation of multi-bolted/bonded single-lap composite joints via 3D digital image correlation (DIC) technology

présentée par **Masoud MEHRABIAN**

en vue de l'obtention du diplôme de *Philosophiæ Doctor*

a été dûment acceptée par le jury d'examen constitué de :

Aurelian VADEAN, président

Rachid BOUKHILI, membre et directeur de recherche

Daniel THERRIAULT, membre

Abdolhamid AKBARZADEH SHAFAROUDI, membre externe

DEDICATION

This thesis is dedicated to my family, namely:

To my late father, whom I lost during my Ph.D. studies, whose words of encouragement always inspired me;

To my mother for her unconditional love and unwavering support that gave me the strength to keep going;

To my big brother who has been a cherished guide in my life;

And to my big sister for always being there for me, listening to me, and understanding me.

ACKNOWLEDGEMENTS

I would like to express my profound gratitude to my research director, Professor Rachid Boukhili, for trusting me, providing endless support, and giving me the priceless opportunity to pursue a doctoral degree under his supervision. In addition to having practical and theoretical knowledge of a domain, a great mentor should also be able to understand human challenges, give wise solutions, and demonstrate genuine empathy; and Professor Boukhili excelled in both of these attributes.

I would like to extend a special thank you to my friends and colleagues, who provided technical and/or inspirational support during my studies: Rim Ouadday, Seyedmohammad Tabaie, Hamid Ghorbani, Farid Gamdani, Nasrin Golzadeh, Nimâ Machouf, Aouni Jr. Lakis, Kevin Charlebios, Nivine Boussaid, Raphael Blier, Mohammad Ghaedsharaf, Ilyass Tabiai, Isabelle Nowlan, Kambiz Chizari and Mr. Djebar Ait Messaoud.

In light of the fact that I have an amazing network of friends and colleagues that goes beyond making a list, I would like to thank you all for your support, smiles, and encouraging words during the course of my doctoral studies.

As a final note, I would like to express my sincere gratitude to my family, particularly my late father, Alidad, my mother, Aghdas, and my siblings, Babak and Mahnoosh; your thoughtful, unconditional, and sincere encouragement and support have been and continue to be an inspiration, a source of wisdom for me.

RÉSUMÉ

Toute structure compte une panoplie de composantes connectées ensemble. Le concept des joints est essentiel puisqu'il permet l'assemblage de plusieurs sections formant une structure. Par contre, dans une structure, les joints sont toujours considérés comme le point le plus faible de celle-ci, où les problèmes se développent. Un joint peut raccorder des composantes faites de matériaux différents tels que : des métaux, des alliages, des composites, etc. Les caractéristiques inhérentes des matériaux composites donnent cet avantage aux manufacturiers de produire une composante à l'aide d'un simple moule qui se rapproche de la géométrie ou de la forme désirée. Cette particularité réduit significativement le nombre de joints en comparaison avec les composantes métalliques. Toutefois, ceci ne signifie pas que les joints ne sont pas nécessaires pour les composites. Leur manque de ductilité ainsi que le comportement fragile font en sorte que les joints des composites sont différents des joints métalliques. Par conséquent, l'étude des joints pour les matériaux composites est essentielle afin de comprendre leur comportement, ce qui pourrait permettre la mise en place de lignes directrices de design afin d'avoir un joint sécuritaire, durable et fiable.

Cette thèse porte sur l'étude expérimentale du comportement mécanique et de fracture des joints à simple chevauchement (SL) seulement boulonnés (OB) et hybride (boulonnés/collés) (HBB) en utilisant la technologie de corrélation d'image numérique (DIC). Par l'utilisation de cette technique avancée, le déplacement et/ou la déformation (dans le plan ou hors plan) de chaque point peuvent être mesurés à partir du moment où la charge est appliquée jusqu'à la défaillance. Ceci permet donc de caractériser précisément le champ de déformation, l'initiation et la progression des fissures, les mécanismes de défaillance ainsi que tout autre résultat connexe. Les contributions de la présente recherche débutent avec l'étude d'un phénomène typique se produisant dans les joints SL de composites dénommé le moment secondaire (SB). La technologie 3D-DIC a été utilisée pour mesurer le déplacement hors plan (OPD), ce qui représente ledit SB de la surface du spécimen dans les joints à simple recouvrement multiboulonnés pour les drapage croisés (CP) et quasi isotropes (QI) de carbone/époxy pour deux épaisseurs de stratifié. Le modèle analytique de la ligne neutre (NLM) a été utilisé dans ce travail et prédit la même tendance observée par les résultats DIC. Il a été observé que le ratio de SB est 30% plus élevé dans les stratifiés CP que ceux ayant un drapage QI.

Dans la présente thèse, la technologie 3D-DIC a été utilisée pour élucider le comportement en traction des joints SL de type OB et HBB en mesurant la distribution des contraintes et les effets secondaires de moment ainsi que de torsion. Aussi, les données fournies par le DIC ont illustré l'équilibre entre la charge de matage et le contournement de la charge ainsi que le mécanisme de transfert de charge en suivant l'évolution du champ de déformation dans les régions sous les boulons. Les résultats ont montré que l'ajout de l'adhésif comporte deux principaux bénéfices, soit : la diminution de la concentration de contrainte dans l'entourage des boulons et le retard de l'initiation du dommage et donc de la défaillance finale, et la diminution des phénomènes de torsion et de SB ainsi que de leur effet nuisible.

L'élongation du trou boulonnée est un paramètre important dans la détermination de la défaillance des joints boulonnés. La technologie DIC est un outil puissant permettant la mesure de l'élongation du trou (BHE) dans les joints de composites OB et HBB. Dans les joints HBB, il a été observé que l'hybridation diminue fortement l'élongation du trou. Ce phénomène était plus prononcé dans les spécimens CP que ceux QI. Les résultats ont montré que pour les joints HBB, l'élongation du trou n'est pas dépendante du drapage, alors que ce paramètre a un grand impact dans le cas des joints OB. De plus, il a été trouvé que dans le cas des joints OB, la contribution du contournement de charge est supérieure à celle de la charge de matage en ce qui a trait à l'élongation du trou.

Les déformations hors plan dans la région de recouvrement des joints HBB ont été bien capturées en utilisant le DIC. Les composantes de déformation principales : la déformation de décollement (ε_{zz}), la déformation en cisaillement (ε_{xz}) et la déformation longitudinale (ε_{xx}), sont identifiées durant toute la durée du test de traction. Le suivi en temps réel du développement des déformations dans la région mentionnée a aidé à identifier la charge correspondant à l'initiation de la défaillance dans l'adhésif. Il a été trouvé que la défaillance est initiée avant que la charge n'atteigne 50% de sa valeur finale. De plus, les résultats ont illustré que les déformations de décollement et en cisaillement, en plus de la rotation du joint dans les joints HBB-CP sont supérieures à celle des joints HBB-QI.

Les résultats obtenus dans le cadre de ce travail de recherche ont contribué à approfondir la connaissance en ce qui a trait au comportement des joints OB et HBB pour les matériaux composites. La contribution de la technologie DIC pour élargir notre compréhension du comportement mécanique des assemblages mécaniques fut démontrée et devrait donc être

poursuivie. Nous estimons que ces résultats peuvent être utiles pour permettre un design d’un joint structurel en composite optimisé et sécuritaire.

ABSTRACT

Each structure comprises a variety of components connecting to each other. Thus, the joining concept is important as it forms a structure by holding different sections next to each other. However, in a structure, the joints are always considered as the weakest part where the problems stem from. A joint can connect components made of different materials, such as metal, alloys, composites, etc. The inherent characteristic of composite materials gives this edge to manufacturers to produce a composite component using a simple mold yet close to the desired geometry or shape. This feature noticeably reduces the number of joints, particularly when compared with conventional metal components, where numerous joints might be required. This fact does not deny the need for joining composite components while they are brittle and suffer from a lack of ductility. Therefore, the study of composite joints is essential to understand their behavior, which can provide a guideline for a reliable, durable and safe joint design.

This thesis deals with the experimental study of the mechanical and fractural behavior of only-bolted (OB) and hybrid bolted/bonded (HBB) single-lap (SL) composite joints using Digital Image Correlation (DIC) technology. Through this advanced technique, displacement/strain (in-plane or out-of-plane) of each individual point can be measured from the moment of applying load to the final fracture; therefore, strain distribution, crack initiation/propagation, failure mechanism, and such related matters can be precisely characterized. The contributions of the current research start with studying a very common phenomenon that occurs in SL composite joints called secondary bending (SB). 3D-DIC was utilized to measure out-of-plane displacement (OPD), which represents the so-called SB, of the specimen surface in multi-bolt single-lap joints composed of cross-ply (CP) and quasi-isotropic (QI) carbon/epoxy laminates for two laminate thicknesses. The analytical Neutral Line Model (NLM) was used in this work, which predicts the same trend observed by DIC results. The quantified SB ratio was found to be approximately 30% higher in CP than in QI.

In the present thesis, 3D-DIC technology has been widely used to elucidate the tensile behaviors of OB and HBB SL joints through the measurement of stress distribution and bending/torsion side effects. Additionally, the DIC data illustrated the balance between bearing and bypass loads as well as the load transferring mechanism by tracking the strain evolutions in the regions under the bolts. The results showed that added adhesive creates two significant benefits; first, it relieves stress

concentration in the vicinity of the bolts and delays damage initiation and thereby the final fracture, and second, it diminishes the SB and twisting phenomena and their associated deleterious effects.

The elongation of the bolt hole is an important parameter to assess the failure of bolted joints. DIC is a powerful means to measure bolt hole elongation (BHE) in OB and HBB composite joints. In HBB joints, it was observed that hybridization decreases the BHE significantly, which was more pronounced in CP configurations than that of QI. Results exhibited that in HBB joints, hole elongation is not dependent on laminate lay-up, while it is very influential in OB joints. Furthermore, it was found that in OB joints, the contribution of the bypass loads to the elongation of the hole is greater than that of the bearing action.

Through-the-thickness deformations of the overlap region of the thick HBB composite joints can be well captured using DIC. The major strain components, namely peel strain (ε_{zz}), shear strain (ε_{xz}), and longitudinal strain (ε_{xx}), are identified during the entire tensile test. The real-time monitoring of the strain development in the mentioned region helped to find the corresponding load at which the adhesive failure initiates. It was found that failure nucleates before the load reaches 50% of its ultimate value. Moreover, results illustrated that peel and shear strains, as well as joint rotation in HBB-CP, are higher than those of HBB-QI.

The results obtained within the framework of this research contributed to deepening the knowledge on the behavior of OB and HBB composites. The contribution of DIC technology to broaden our understanding of the mechanical behavior of mechanical assemblies has been demonstrated and should therefore be pursued. It is believed that the obtained results can be useful for designing optimized and safe composite joint structures.

TABLE OF CONTENTS

LIST OF TABLES

LIST OF FIGURES

LIST OF ABBREVIATIONS AND SYMBOLS

ε^{br}	Bearing strain
σ^{br}	Bearing stress
k_b	Bending factor
BHE	Bolt hole elongation
CFRE	Carbone fiber reinforced epoxy
CCD	Charge-coupled device
CP	Cross-ply
DIC	Digital image correlation
FL	Failure load
FOV	Field of view
FHT	Filled-Hole-Tension
HBB	Hybrid bolted-bonded
θ	Joint rotation angle
LHE	Longitudinal hole elongation
NLD	Neutral line displacement
NLM	Neutral line model
OB	Only bolted
OHT	Open-Hole-Tension
OPD	Out-of-plane displacement

QI	Quasi-isotropic
SB	Secondary bending
SLJ	Single-Lap joint
SG	Strain gauge
TS	Tensile Strength
THC	Transversal hole compression
VARI	Vacuum Assisted Resin Infusion
VARTM	Vacuum assisted resin transfer molding
VE	Virtual extensometers

LIST OF APPENDICES

CHAPTER 1 INTRODUCTION

1.1 Context of the research

Without question, joining was one of the first, if not the first, manufacturing technology. From the dawn of humankind, the capability of joining different materials to create workable tools, manufacture products, and assemble simple components to erect a structure has been a controversial issue [1]. Therefore, all different materials, from the very primary ones, like stone, wood, bone, etc., to the current ones, such as metals, steel, alloys, composites, and the like, require a technique to be connected. The desired joining method can vary according to the components' material in which bolting (using mechanical fasteners), bonding (using chemical adhesive), and welding (using high heat to melt the parts together) are the most common approaches (Figure 1.1). Conventional materials, like metals and alloys, are more convenient in terms of joining and predicting their behavior. However, when it comes to advanced materials, such as fiber-reinforced composites, choosing a proper method for connecting and being able to analyze its mechanical response are of critical concern since composites are not considered as a material; they are primarily a structure composed of fibers and polymer/metal matrices.

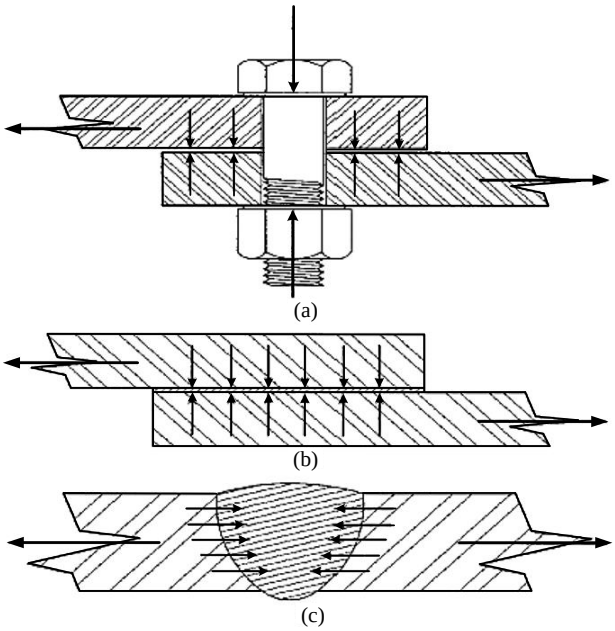

Figure 1.1: Three main classes of joints (a) Bolted joint, (b) Bonded joints (c) Welding [1].

Fiber-reinforced composite materials have been widely used in complex aeronautical structures due to one of their major advantages, which resides in providing substantial weight reduction while possessing a significant amount of strength when compared to traditional counterparts made from metal. Additionally, composite materials are advantageous as they can be formed to the closest desired shape, which in turn reduces the number of joints. However, joining some composite components is unavoidable and has been recognized as a critical feature in aerospace structural design. These situations are even more demanding for advanced thermoset and/or thermoplastic composite structures because they are mostly brittle and lack the ductility to redistribute loads which is so characteristic of conventional metal alloys used widely throughout the industry [2]. The mentioned downside features, i.e., brittleness and less ductility, of composite materials may result in a catastrophic failure without any pre-alerting; hence, it brought about a significant concern among industrial and academic researchers. The most probable location of this sort of failure in a composite structure is the joints, as they are the weakest parts. Thermoset composite components are usually attached using mechanical fasteners, adhesively bonded approaches or hybridization of them. Thus, the mechanical behavior analysis of the composite joints is of vital importance and always more complicated than its homogeneous equivalent like metal.

The most representative analysis of a composite joint to the practical cases can be drawn from the experimental testing while a joint coupon is under a semi-real condition. Different mechanical tests are available like tension, compression, shear, impact, etc., but the utilized equipment and post-processing steps are the predominant factors that yield an approved interpretation of the results and analyze the joint behavior. Amongst various experimental testing tools, a recent image processing-based technology called Digital Image Correlation (DIC) has become an efficient and robust technique to fulfill this purpose. This method can be implemented in either two dimensional (2D) or three dimensional (3D) systems and provides the precise full-field measurement of the displacement as well as strain distribution of the surface of interest. Moreover, DIC overcomes the routine problems being encountered when using conventional measuring tools, like strain gauges and extensometers, as it can probe all the points of a surface. The present research mainly focuses on the contribution of 3D Digital Image Correlation (3D-DIC) on characterizing the joint mechanical response, failure mechanism, and fractural behavior of

multi-bolt and hybrid bolted/bonded single-lap (SL) composite joints to achieve broad insight into this matter and try to deliver fail-safe and reliable composite joint designs.

1.2 Structure of the Thesis

The work carried out to materialize the proposed main goal is presented in this thesis commencing with this introduction. The thesis comprises 9 major chapters. Following this "Introduction", the next chapter (Chapter 2) consists of the literature review. It includes some backgrounds covering the structure of bolted and bonded composite joints, which is followed by surveying the researches on hybrid bolted/bonded composite joints, and a review of the DIC technology concept and related work. Chapter 3 defines the concerning problem that will be addressed in this research using the proposed solution and the general objective of the research, which is further broken down into four sub-objectives. Moreover, the coherence of the articles with the sub-objectives is detailed in this chapter. The four sub-objectives are fulfilled and presented in conducted articles through Chapters 4, 5, 6, and 7, forming the core of this thesis.

In Chapter 4, the out-of-plane displacements, which represent so-called secondary bending, of four different configurations of multi-bolt SL composite joints are quantified using 3D-DIC, and the results' trends are also confirmed with an analytical approach called the Neutral Line method (NLM). In Chapter 5, the DIC is implemented to measure the full-field strain distribution of the surface as well as secondary bending/twisting effects in multi-bolt and hybrid bolted/bonded SL composite joints, and the tensile behavior is analyzed using the corresponding results. Chapter 6 is dedicated to precisely highlighting the influential factors on bolt-hole elongation and its effect on the mechanical responses of multi-bolt and hybrid bolted/bonded SL composite joints. In Chapter 7, the high potential of DIC technology is exploited to monitor and analyze the strain development and fracture progression through-the-thickness of the overlap region of multi-bolt SL hybrid bolted/bonded composite joints. A general discussion, which briefly summarizes the results of the entire research, is provided in Chapter 8. Lastly, the conclusion and recommendations are presented in Chapter 9, and the bibliography will follow.

CHAPTER 2 BACKGROUND AND LITERATURE REVIEW

2.1 Background

Large and complex constructions, such as airplanes, ship hulls, automobiles and other similar crafts, are manufactured using mounting and assembling subsections made of steel, metal, alloys, or composite materials. Interconnecting these sub-components in a way, which will yield a reliable, safe, and the applicable joint is of particular concern for both manufacturers and academic researchers. The main goal of a joint is to transfer a load from one component to another. Given that discontinuities can be brought about in terms of geometry and material (in some cases), the durability and reliability of a joint need to be well understood to guarantee a safe operation. There are three main classes of joints for thermoset composite materials, as displayed in Figure 2.1, namely (a) mechanical fastening, (b) adhesive bonding, and (c) the combination of the two techniques called hybrid bolted/bonded (HBB) joint. Each of them has its pros and cons listed in Table 2.1 [3]. In the following subsections (2.1.1 and 2.1.2), the structure and mechanism of only bolted and only bonded SL composite joints are studied, which will be followed by a literature survey of the work that has been done regarding HBB SL composite joints.

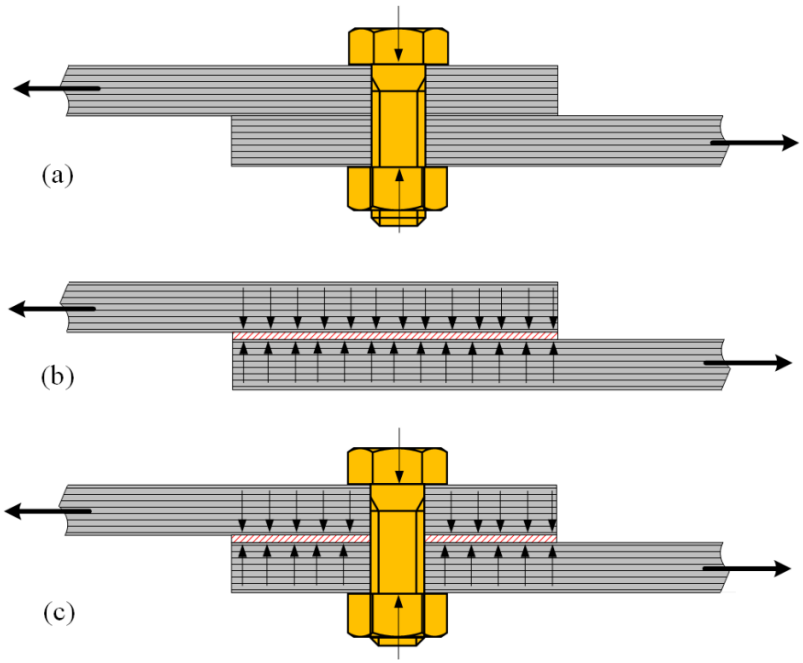

Figure 2.1: Three classes of SL composite joints (a) Bolted joint (b) Bonded joints (c) Hybrid Bolted/Bonded joint.

Table 2.1: Advantages and disadvantages of bolted, bonded and hybrid bolted/bonded joints.

Advantages	Disadvantages
Bolted joints	
Easy to disassemble	Considerable stress concentration
Straightforward manufacturing and inspection	Added weight of mechanical fasteners
Environmentally insensitive	Hole formation can damage composite
Insensitive to peel forces	Composites have poor bearing properties
Bonded joints	
Low stress concentration	Difficult to inspect
Light weight	Prone to environmental effects
Excellent fatigue life	Cannot be disassembled
Damage tolerant	Sensitive to peel and shear stresses
No fretting problems	Catastrophic failure mode
Hybrid bolted/bonded joints	
Improved fatigue life	Marginal strength improvement
Suppressing the crack propagation by mechanical fasteners	Increased weight
Back-up mechanism provided with mechanical fasteners	Better performance in thinner joints

2.1.1 Bolted Composite Joints

It is important to be able to remove and disassemble structural components to conduct repairs, inspections, or replacements. As such, mechanically-fastened joints are the preferred technique for connecting different parts, which may be made from conventional materials, including metal and advanced composite components. Mechanical joints in fiber-polymer composite structures have been studied since the mid-1960s, which corresponds to the first appearances of composite materials due to their high modulus, high strength, lightweight, and good corrosion/fatigue resistance. Early in this period, it was found that the mechanical behavior of composites in bolted joints varied substantially from what occurred with metals [4]. Due to the ductile property of metal, these materials are more workable when compared to their composite counterparts, which are more sensitive to edge distances and hole spacing than metal joints [5]. Hart-Smith [6] demonstrated this behavioral comparison and scaled it as joint structural efficiency (Figure 2.2).

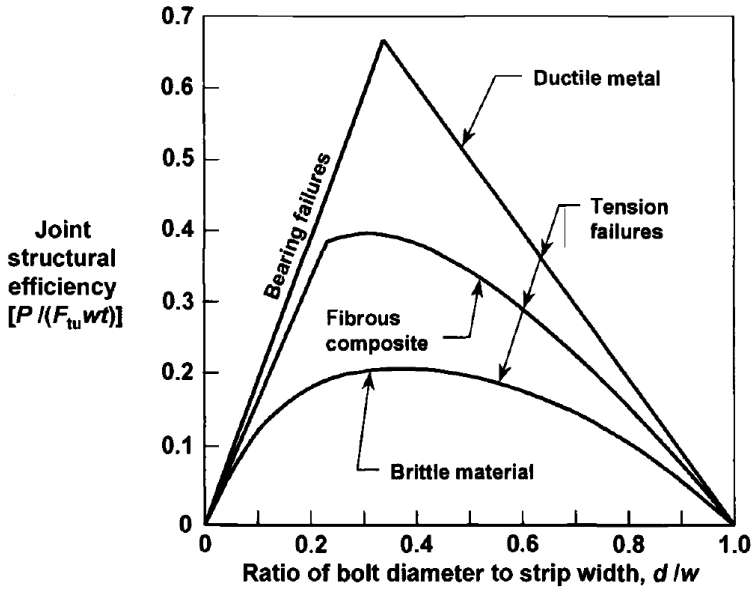

Figure 2.2: Relative efficiencies of bolted joints in ductile, fibrous composite and brittle materials [6].

Generally, there are two major groups of joints, namely single row and multi-row configuration. Obviously, light loaded joints demand the former, while the highly loaded ones require the latter. Another prominent factor concerning bolted composite joints resides in its

diversity of failure modes. The failure mode of a joint could be influenced by factors such as joint geometry and fiber patterns. Common failure modes of bolted joints are shown in Figure 2.3 [6].

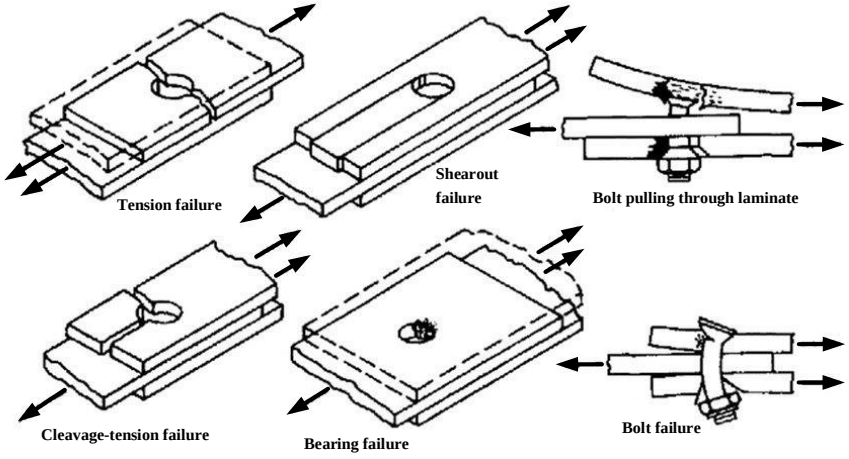

Figure 2.3: Modes of failure for bolted composite joints [6].

Bearing failure is the only non-catastrophic mode caused by the compressive stress consisting of fiber micro buckling, matrix cracking, and considerable delamination [7]. This mode is the preferred failure mode since it is not catastrophic, meaning that the joint will still stand following failure. Bearing is more likely to happen when there is a high ratio of *W/D* [8]. Further, it takes place only in single-row joints, which harshly limits the load that can be transferred through these joints [6]. Another failure mode is net-tension which is associated with fiber and matrix tension failures because of high-stress concentration at the hole edge [9]. This mode is classified as a catastrophic failure given that the crack propagates transversally to the applied load direction. This is the dominated mode of failure in multi-row joints in which high by-pass stresses are born at extreme bolts where the individual bearing stresses are lower [6]. This type of failure catastrophically occurs at $\theta = 90^o$ without any marked warnings prior to final rupture, and no sign of damage takes place until approximately 90% of the applied failure load [10].

The bad arrangement of fiber patterns comprising too many longitudinal fibers in the laminate may lead to shear-out failure [6], which is another type of catastrophic failure. The only warning in this case is the noise heard at 87% of the failure load, and occurs after 0° layer experiences micro-buckling [10]. In most cases, shear-out failures occur in single bolted rows is and associated with bearing failures with a short end distance (small e/d ratio) [8]. Mixing of shear-

out failure and net-tension failure results in cleavage failure, which occurs when there is a sufficient number of 0° (load direction) and $\mp 45^{o}$ fibers combined with inadequate of 90° fibers (perpendicular to the load) [6]. Bolt type failures can also occur when the bolt diameter is too small compared to the laminate thickness.

To understand the mechanical behavior of composite bolted joints, one should also have a good understanding of the load transfer mechanism to comprehend the different factors that can affect the mechanical response of a joint. These may include joint materials, laminate lay-up and thickness (in the case of composite adherends), hole diameter, fastener location (ratio of w/d and e/d), fastener types (protruding head or countersunk), bolt-tightening torque, and bolt-hole clearance [11]. Most importantly, it should be understood what portion of the load is carried by the bolt in a simple single-lap composite joint. In the past, researchers have studied different approaches to measuring the transferred load via bolts for different configurations [12]. There are two major paths for load transfer in bolted joints, the critical one is the bolt itself, and the other path is the friction between adherends. In the single-lap single-bolted joint, when the external load (F) is very small and secondary bending (SB) has not yet initiated, the load is first transferred from one adherend to another via the static friction between the nut (or washer) and the upper plate, f_{l-n}, as well as the friction between two adherends, f_{l-l} [13]. Figure 2.4 displays the free body diagram of a single-lap single bolted joint subjected to the external load.

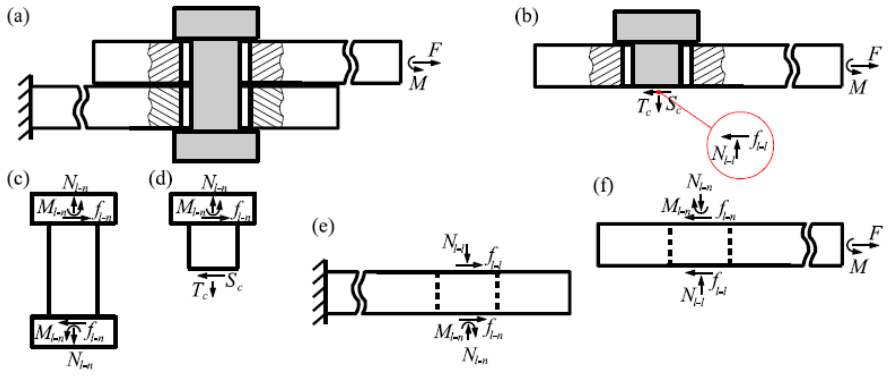

Figure 2.4: Schematic diagrams of the bolt-load carrying mechanism in a single-lap, single-bolt joint with clearance: (a) the single-bolt joint subjected to an external tensile load (b)–(f) free-body diagrams of the upper half of the joint, the bolt-nut combination, the upper half of the bolt, the lower adherend and the upper one [13].

From Figure 2.4, the following equations can be derived:

$$F = f_{l-n} + f_{l-l} \tag{2.1}$$

$$f_{l-n} = S_c \qquad \text{Bolt shear load before SB} \tag{2.2}$$

$$f_{l-l} = F - S_c \tag{2.3}$$

With increasing the external load, the static friction forces will be overcome, and the adherends will start sliding relative to each other. This gradually leads to the elimination of the clearance until there is none, at which point the bolt shank will come in contact with the bolt hole, and SB start to be initiated, as shown in Figure 2.5. At this moment, the majority of the external load ($F\cos\theta$) is transferred by the accumulation of the friction force between the nut (or washer) and upper laminate , f_{l-n}, the friction force between the two substrates , f_{l-l}, and the normal contact force between the bolt shank and bolt hole, N_0 [13]. At this moment, the joint starts rotating, and since the deformation is insignificant, it is presumed that the rotation angle of adherends is equal to that of the bolt with respect to its axis. The equilibrium equations can be stated as:

$$F\cos\theta = f_{l-n} + f_{l-l} + N_0 \tag{2.4}$$

$$F\sin\theta = f_0 + N_{l-n} - N_{l-l} = T_c - N_{l-l} \tag{2.5}$$

$$f_{l-n} + N_0 = S_c \qquad \text{Bolt shear load after SB} \tag{2.6}$$

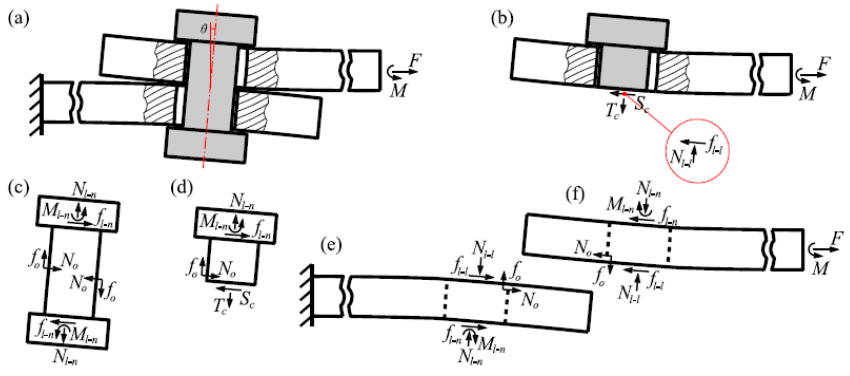

Figure 2.5: Diagrams of the bolt bearing mechanism in a single-lap, single-bolt joint once the clearance has been eliminated: (a) the single-bolt joint subjected to an external tensile load (b)–

(f) free-body diagrams of the upper half of the joint, the bolt-nut combination, the upper half of the bolt, the lower substrate and the upper one [13].

2.1.2 Bonded Composite Joints

Another common type of connection technique is an adhesively bonded joint in which two or more adherend surfaces are attached to each other by solidified chemical polymeric-type substances alone. The science of adhesive bonding technology embraces several fields including mechanics, chemistry, and surface physics [14]. Bonded joints have been being widely used in secondary aircraft structures owing to their advantages, including good fatigue life, weight reduction, high strength-to-weight ratios, good external finishing, the capability to join different/thin substrates, good environmental sealing, and lower fabrication costs [15]. Some of these advantages make the bonded joints an appropriate alternative to conventional mechanical fasteners [16]. On the other hand, some drawbacks limit their application in primary aircraft structural components. These drawbacks include the inability to disassemble bonded joints, that they are severely susceptible to manufacturing processes including proper surface treatments and environmental effects (such as moisture) [15], and moreover, that their failure mode is typically catastrophic in nature. Generally, thin structures with properly defined load paths are suitable candidates for adhesive bonding, whilst thicker structures consisting of complex load paths are preferred candidates for mechanical fastening [17].

There are a variety of adhesives which some are categorized as strong/rigid/brittle while others are classified as weak/flexible/ductile substances. Materials used for structural adhesive bonding are cured at either room or elevated temperatures and should be endowed with a sufficient amount of strength in order to transfer the loads within themselves and through the joint. Several types of structural adhesives can be used, but epoxies, nitrile phenolics, and bismaleimides are the most prevalent [18]. The main function of adhesively bonded joints is to transfer applied load within the adhesive layer, which is mainly occurred due to shear loading. Wide varieties of bonded joint configurations are available to fulfill this intention. Figure 2.6 shows typical bonded configurations.

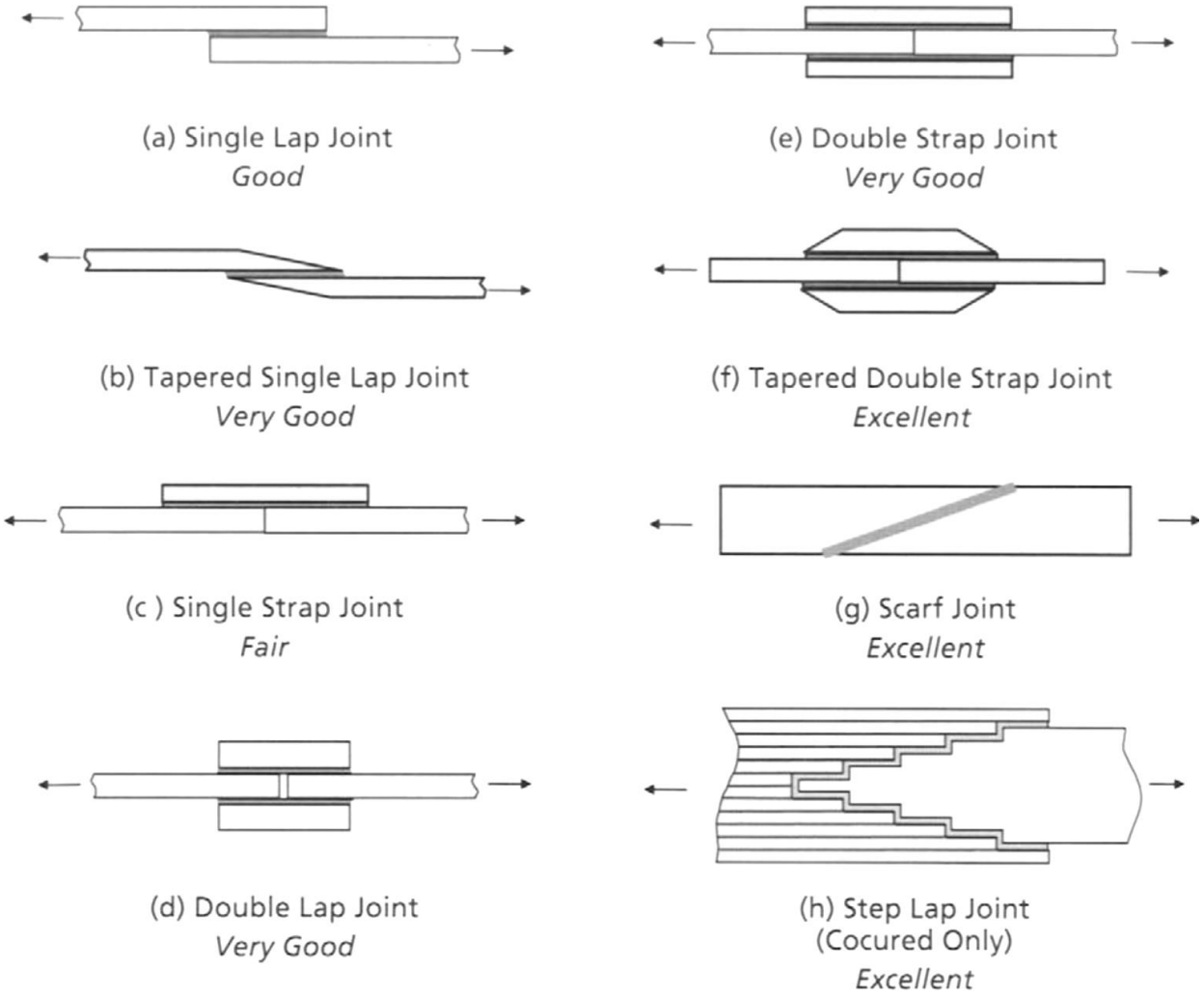

Figure 2.6: Typical adhesively bonded joint configurations [18].

Among these different joint types, the single and double lap (SLJ and DLJ) ones are the most practical and realistic configurations. They are most often used for attaching relatively thin adherends. Fabricating of stepped-lap and scarf joints is more complex, and their goal is generally to transfer high loads within thicker adherends [14]. The effects of the adherend thickness and of the joint configuration on the failure mode are shown in Figure 2.7. The evolution in configurations is shown with an increasing trend in strength capability from the lowest to the highest. In each type, the adherend thickness may be increased to achieve higher load capacity [4].

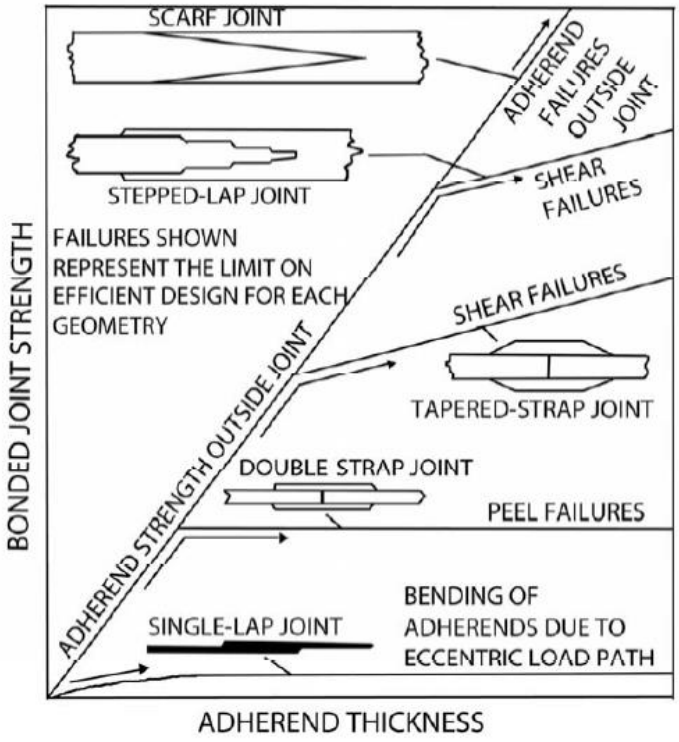

Figure 2.7: Joint geometry effects [19].

The adhesive bond strength is usually measured using the simple single-lap shear test [18], which is also the most frequently investigated configuration in terms of experimental and theoretical approaches (the joint is shown in Figure 2.8). Figure 2.8 also illustrates the typical stress distribution in the adhesive layer comprising of the shear and peel stresses. It can be observed that the highest stresses occur near the edges of the overlap. Due to the load eccentricity, a moment (called secondary bending- SB) is induced at the overlap and the joint rotates when deformed. The peel stress is a by-product of this rotation (SB) which may reduce the joint strength significantly [14]. Adhesively bonded stress analysis' can be formulated from the simplest form of $\sigma = \frac{P}{A}$, which simply takes into account the average amount of shear stress in the bond line, to sophisticated formulas based on elasticity assumptions for applications of fracture mechanics [4]. The first analytical analysis known for calculating the stress in adhesively bonded joints was introduced by Volkersen [20] in 1938. This analysis computed the shear stress in the adhesive, but the shear deformation and bending created by the eccentric load path were not considered, which are essential elements in composite adherends. Goland and Reissner [21] were the first researchers who took into account a bending moment (M) and a transverse force (V) (caused by eccentric load

path at SLJ) at the ends of the bonded joints in addition to the existing shear stress, distribution of adhesive shear and peel stress is the same as illustrated in Figure 2.8. In contrast to both previous pieces of researche, Hart-Smith considered adhesive plasticity for SLJ [22] and DLJ [23]. Hart-Smith developed the analyses of Volkersen [20] for DLJs [23] and the investigation was performed by Goland and Reissner [21] for SLJs [22]. (Da Silva et al [24-26] reported a thorough comparison of analytical studies)

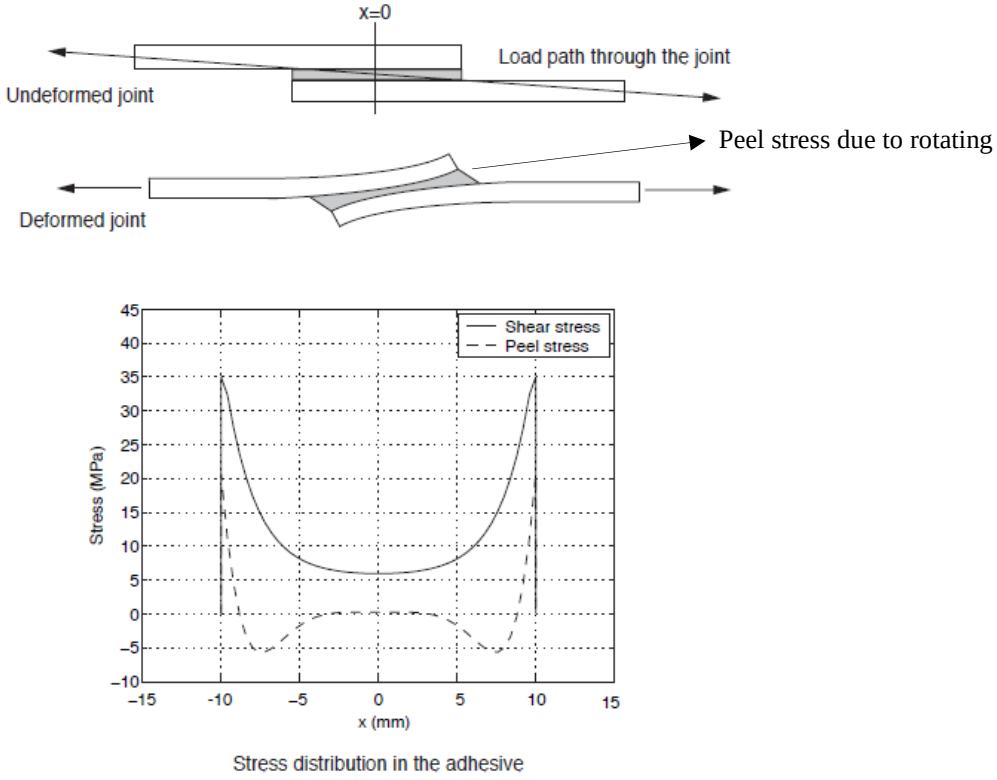

Figure 2.8: Structural behavior of a bonded SLJ [14].

There are two predominant major failure modes in adhesively bonded joints, namely cohesive failure and adhesive failure. By definition, the former takes place within the adhesive or the adherends, while the latter occurs between the adhesive and the adherends (Figure 2.9). If the adhesively bonded joint fails at the interface between the adherend and the adhesive layer due to imperfections in the bonding caused by poor surface treatment, then the adhesive will likely fail in an adhesive mode. This type of failure is not desired, given that the joint will typically experience a failure below the joint's design strength [27].

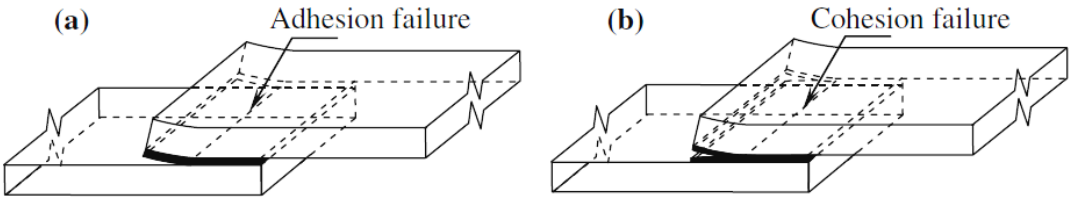

Figure 2.9: Different failure modes in the bonded SLJ [28].

Failure modes in composite bonded joints are determined from the quality of the bonding at each interface, the specimen geometry, and the loading [16]. According to the standard ASTM D5573 [29], FRP bonded joint failures include the classification of seven failure modes (all definitions retrieved from [30]):

(1) Adhesive failure: The separation appears to be at the adhesive–adherend interface (sometimes referred to as interfacial failure).

(2) Cohesive failure: The separation is within the adhesive.

(3) Thin-layer cohesive failure (TLCF): The failure is similar to the cohesive failure, except that the failure is very close to the adhesive–adherend interface, characterized by a 'light dusting' of adhesive on one of the adherend surfaces and a thick layer of adhesive left of the other (sometimes referred to as interphase failure).

(4) Fiber-tear failure (FTF): The failure occurs exclusively within the fiber reinforced plastic (FRP) matrix, characterized by the appearance of reinforcing fibers on both ruptured surfaces.

(5) Light-fiber-tear failure (LFTF): The failure occurs within the FRP adherend near the surface, characterized by a thin layer of the FRP resin matrix visible on the adhesive, with few or no glass fibers transferred from the adherend to the adhesive.

(6) Stock-break failure: This occurs when the separation is within the adherend but outside the bonded region.

(7) Mixed failure: Where the failure is a mixture of different classes.

The failure of an adhesively bonded joint seldom takes place in one specific single mode, but rather, it often occurs in a combination of two or more of the first six modes. Such combinations are classified as mixed failures (Figure 2.10 [16]).

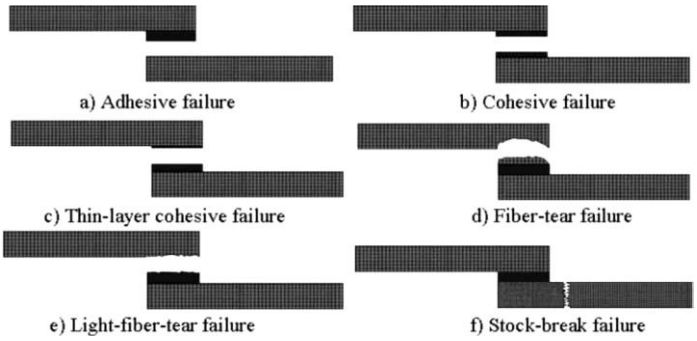

Figure 2.10: Possible failure modes in bonded joints between FRP composite adherends [16].

In principle, the strength of a joint really relies on the stress distribution within the joint and fundamentally depends on the joint geometry and the mechanical properties of the adhesive and the adherends [16]. In the case of brittle adherends (like composite laminates), which possess a relatively low through-thickness strength, in the SLP joint, when SB occurs, high magnitudes of stress concentrations are introduced near the ends of the adhesive, which consequently affects the adjacent substrate surface. As it is observed in Figure 2.11 [31], these spots are the critical locations where failure is often initiated due to interlaminar tensile stresses and results in the fiber-tear adherend failure mode.

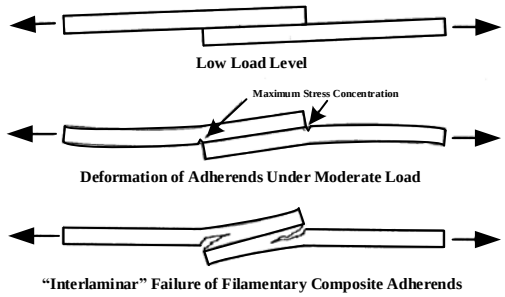

Figure 2.11: Failure of the single-lap bonded joint with brittle adherends [31].

2.2 Hybrid Bolted/Bonded Composite Joints

In order to achieve an efficient and robust joint design, which possesses a higher static strength and longer fatigue life, the combination of bolting and bonding is proposed as another development for use in both industry and academy. Hybridization will be beneficial when the advantages of each underlying bolted and bonded joint contributes towards the structural behavior, e.g., load exerted from different directions (bond joint preferred) or exposure to elevated

temperature ambient (bolt joint preferred) [32]. Therefore, backing up mechanism will be brought about the secondary joint type, which will guarantee an enhanced structural performance of the overall joint.

The hybrid bolted/bonded joints that have been studied by the researchers are mostly SL joints loaded in uniaxial tension [33], which is the concern geometry of the present study as it is the most doable and applicable sort of joints in real practical cases. Hart-Smith started comprehensively analyzing bolted/bonded composite joints in the year 1982 [2] with the Douglas Aircraft Company. He found that the combination of bonding and bolting could be the most appropriate joint design for thicker structures, particularly when made from fibrous composites. He came up with the “fail-safe design” term by which bolts can contribute as a back-up mechanism in the HBB joint and would take up a portion of the applied load after adhesive failure. Stewart [34] experimentally saw the influence of the stacking sequence on crack propagation once the damage was initiated. He mentioned that the 0-degree ply location had a pronounced effect on damage initiation and propagation. Static test outcomes indicated that mixing bonded and bolted joints had a low effect on damage initiation but that it decreased the propagation rate.

Wei-Hwang Lin, Ming-Hwa R. Jen [35] experimentally and through simulation with finite element (FE) modeling studied the failure analysis of single lap multi bolted/bonded composite joints. The authors used different adhesives, thermal settings, and thermal plastic adhesives, with quasi-isotropic and cross-ply stacking sequences. Moreover, fasteners included bolts and rivets arranged in various patterns, i.e., one (1*1), three (1*3), (3*1), six (2*3), and nine (3*3). The six bolts configuration possessed the highest strength. The authors said that adding more bolts did not necessarily increase the joint strength, given that more damage area was introduced and that concentrated stress would be induced in the structure. In terms of adhesive selection, it was concluded that choosing adhesives having similar material properties to that of the adherends should be considered in order to obtain a more efficient joint design. Fu and Mallick [36] did a study on the static and fatigue strength of hybrid bolted/bonded joints in a structural reaction injection-molded composite (SRIM). The authors concluded that hybrid joints deliver better static and fatigue performance than adhesive joints in SRIM composites when the clamping force is present. In the year 2005, Kelly [37] numerically investigated the load distortion due to the bolt in hybrid joints. In addition, an instrumented bolt was used to measure the transferred load via the bolt. Finite element results showed that the load transferred by the bolt increased with increasing

adherend thickness and adhesive thickness but decreased when increasing the overlap length, the pitch distance, and the adhesive modulus. His work confirmed what had been stated by Hart-Smith [2] that the "*combination of bonding and bolting can be the most appropriate for thicker structures*". It was concluded that the contribution of bolts would be significant when a joint was flexible either in terms of the joint design or adhesive material. Moreover, by means of an instrumented bolt, a bolt load of about 32% out of 8kN tensile load was measured, which was in good agreement with finite element results.

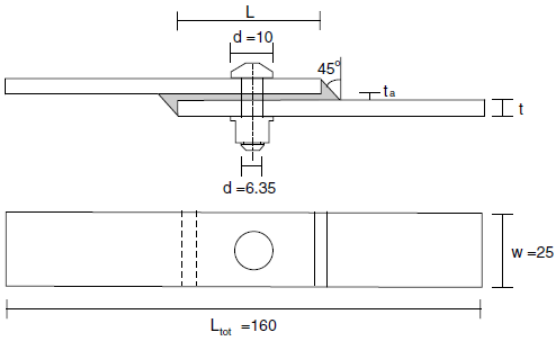

Figure 2.12: Dimension of HBB in Kelly`s work [37].

Kelly continued his work [38] and showed experimentally the differences of load shearing in bonded, bolted, and bonded/bolted hybrid joints. He stated that failure of hybrid joints takes place in two stages; first the adhesive fails, and second, the bolt joint fails. Figure 2.13 shows the failure of hybrid joints with polyurethane and epoxy adhesives and, in both cases, illustrates a crack initiating from the embedded adhesive corner and propagating from the ends of the overlap toward the center.

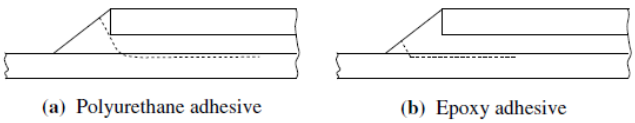

Figure 2.13: Failed mode in the bonded and hybrid joints. Dashed lines show the crack path [38].

Analytical studies are always highly complex and demanding analysis, as they require proper knowledge of material properties, reaction forces, boundary conditions, contact information, and they are governed by equilibrium equations, making it challenging to generate an accurate and realistic model. Analytical solutions of the hybrid joint have attracted the attention of a limited number of authors to conduct parametric studies regarding the behavior of this type of

joint. A semi-analytical solution was developed by Barut and Madenci [39] for the stress analysis of single-lap hybrid (bolted/bonded) composite joints. The authors observed the same simulated results as what takes place in reality via their method, which demonstrated that no load was transferred through the bolt until a certain deboning length was achieved in the adhesive. Once the crack continued propagating and passed this critical length, the bolt contributed to taking a proportional amount of the applied load. When the full unzipping occurred in the adhesive, the bolt took the entire load. Bois et al. [40] proposed an analytical model which was a good replacement for complex FE models. The reliability of their model in predicting the load transfer in the bolt and the adhesive portion of the joint was confirmed when comparing FE with experimental results.

A new geometry for HBB was developed by Vadean and Ouellet [41] by which, the maximum peel stress was successfully decreased within the adhesive layer. Authors were inspired by a special feature in Belleville's spring-type washer (Figure 2.14) through which the clamping force would be brought as close as possible to the edge of the overlap without increasing the washer's thickness and weight (substrate edges also tapered). Consequently, the peel stress at these corresponding spots would be eased. The authors also suggested that the shear stress reduction in the adhesive layer could be achieved by increasing the amount of load transferred through the bolts. Similar to the work done previously [39], Bodjona and Lessard [42] applied the principle of virtual work to develop their proposed method. In contrast to Barut and Madenci's work [39], the nonlinear constitutive behavior of the adhesive was taken into account, and the solution was performed using a mesh-free global Galerkin technique based on Radial Point Interpolating (RPIM) Functions. This method's outcomes are in very good agreement with the results of FEM and experimental data, and they suggest that the hybrid joint strengths would exceed both the bonded joint and bolted joint strengths.

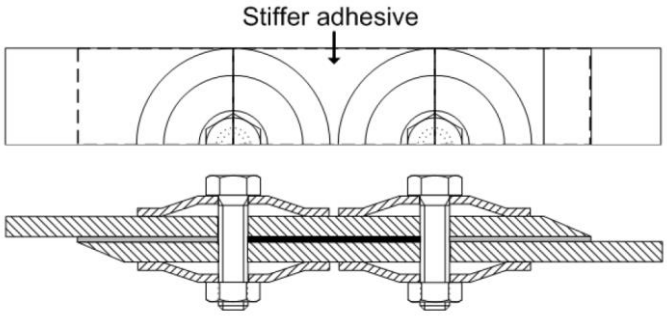

Figure 2.14: New joint geometry of HBB proposed by [41].

Load sharing in hybrid bolted/bonded joints is of significant concern and defined as the proportion of the applied external load, which is transferred by the bolts against that which is carried by the adhesive layer [33]. Bodjona et al. [43] reported a bolt load of 40% (10 kN applied load), which was obtained using an instrumented bolt and validated with numerical 3D FEM and the Global Bolted Joint Method (GBJM [44]) results. It is worth noting that the joint configuration was single lap/single bolt, and used adhesive was elastic-plastic material. The authors` investigation was further completed by studying the effect of materials in blot load sharing [45]. They found out that adhesive's yield strength is singularly the most prominent material parameter affecting the load sharing, and after that, the joint E/D ratio, adhesive thickness, and adhesive hardening slope were figured to be the other influencing factors. In two previous works, authors tried to increase load sharing using a low-modulus adhesive, but again the significant load sharing took place when the adhesives failed. Rather the same authors collaborating with Karthik Prasanna Raju, Gyu-Hyeong Lim [46] used a three dimensional finite element model to study the influence of an interference-fit bolt instead of the conventional neat-fit or clearance fit bolt for improving the load sharing in hybrid joints. An interference-fit HBB joint had roughly 10% higher shared load than a neat-fit HBB joint. Findings showed that the load transferred as soon as the joint underwent loading through a contact between the bolt and edge of the bolt hole.

Statistical methods have been grabbing the attention of researchers, specifically when it comes to taking into account a considerable number of items influencing the outcomes. These techniques may help to reduce the process variation and enhance its effectiveness. Dashore et al. [47] used the Taguchi method to assess the effect of bolt size, clearance bolt, bolt tightening torque, adhesive type, adhesive thickness, overlapping length, and the material used for the joint. The ANOVA method was used to evaluate the contribution of each factor and to find the best combination. They confirmed what had been found [46] that the press-fit fasteners were always the strongest joint given that it does not allow any relative movement between adherends. The following year, 2017, Lopez-Cruz et al. [48] also utilized the ANOVA method to analyze the statistical results obtained from a method called Design of Experiment (DOE). The adherend thickness, adhesive modulus, adhesive thickness, clamping area, and bolt-hole clearance were the factors studied. Outcomes indicated that the hybrid joint was stronger than the underlying bolted or bonded ones, and the ANOVA results showed that the strength of the hybrid joint was mainly influenced by the adhesive mechanical properties, adherend thickness, and bolt-hole clearance.

Italian researchers [49] evaluated the behavior of a single lap bolted/bonded composite joint using a finite element method. The stress distributions in the adhesive layer of the hybrid joint were compared with that of a simple adhesive joint. Moreover, the bolt load was computed and, for some cases, compared with experimental results reported by Kelly [37]. FE results endorsed previous findings from literature stating that the transferred load via the bolts increases when the strength of the structural adhesive is reduced and if the gap between the bolt's shank and the bolt-hole is reduced. Due to the lack of experimental knowledge regarding hybrid multi-bolted/bonded composite joints, Gamdani et al. [50] analyzed the tensile behavior of these types of joints. The fracture of the 3-bolts HBB joints showed that the damage initiation and propagation appeared to be located almost exclusively in the external bolt-holes areas, as displayed in Figure 2.15. results demonstrated that by adding the adhesive, the strength of the three bolts joints increased by 70% for cross-ply laminates and 30% for quasi-isotropic laminates. Moreover, it was suggested that for multi-bolted HBB joints, only external bolts are required.

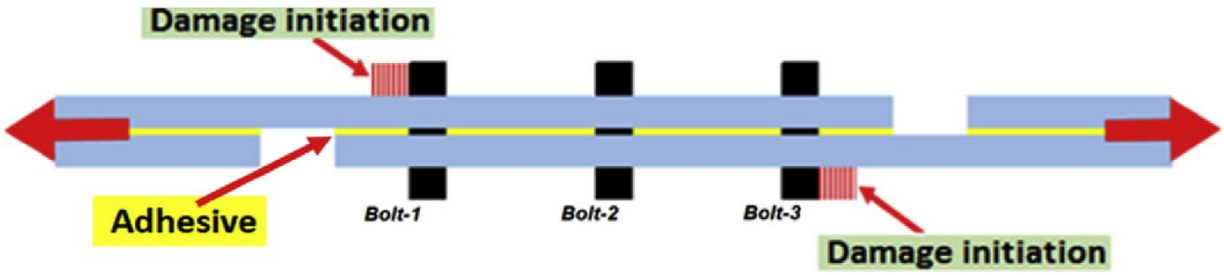

Figure 2.15: Illustration showing the localization of the failure initiation and propagation in a three bolted/bonded composite joint [50].

Xin Li et al. [51] found that the stacking sequence and width to diameter (W/D) ratio are vital factors in designing the hybrid SL composite joints. The results showed that in HBB joints, the bolts could improve the tensile property after the adhesive fails. HBB was found to acquire the highest tensile strength compared with only bolted or only bonded joints, however, the secondary bending phenomenon is a serious concern that may change the fracture mode. The increase of an average of 19.0% in the strength of bonded composite joints after adding a bolt was calculated by Wenhao Li et al. [52], which is partially related to the load transferred via the bolt after adhesive failure initiation and to the improved out-of-plane bending stiffness. Another experimental study

also confirmed that the ultimate strength of the HBB joint is enhanced compared to the underlying joints separately [53]. It was discovered that the addition of a bolt could remarkably increase the adhesive damage initiation strength for the case of a high-compliance adhesive. Romanov et al. [54] claimed that the important factors for strength and stiffness improvement of the two-bolt HBB joint are the load sharing between the bolt and the adhesive, as well as the overlap length. Moreover, the bolt positioning was found to have no effect on the HBB joint stiffness, while it influences the joint strength and load sharing.

2.3 Digital Image Correlation (DIC) Technology

One of the principal methods used to study the structural response of construction or for characterizing the mechanical properties of a material is to measure the strain changes while the concerned item undergoes deformation due to the applied loads. One of the most conventional and highly used devices is resistance strain gauges (SG) which are adhesively installed on the surface of an object (should be completely smooth and clean) and measure the strains. This technique provides accurate data for a specific point where the SG is adhered. However, the data from the SG is restricted to the installation location, which should be easily accessible, clean, and smooth (or can be smoothened). Extensometers are another device that can be used but only provides the changes in the length of an object. Moreover, the aforementioned systems of measuring (SG & extensometer) demand a physical connection with the specimen surfaces, which restricts the freedom of the testing. When a set of strain data points are required for point-wise information, a full-field measurement technique would be highly practical. One of these methods is the digital image correlation (DIC) technique which optically-numerically measures displacement fields and corresponding strains. This method is non-contact and is capable of in-situ testing as well. The background and principal of DIC are concisely explained here; however additional details can be found in [55, 56].

A group of researchers from the University of South Carolina in the 1980s was pioneers in this field [57, 58]. Nowadays, DIC is widely used in a variety of fields of study, including mechanical engineering, biomechanics, metallurgy, civil engineering, and many more, given the enriched results which can be obtained. The implementation of the 2D DIC method consists of three major steps, namely (1) specimen and experimental preparations; (2) recording images of the planar specimen surface before and after loading; (3) processing the acquired images using a

computer program to obtain the desired displacement and strain information [56]. The fundamental concept of digital image correlation underlies the comparison of two digital images of a specimen surface, taken at different times, in order to obtain a quantitative, pointwise track of the test object surface deformation during that time period. Basically, in the 2D DIC method, a calculation area (i.e., region of interest, ROI) is specified in a reference image (undeformed surface) in which the specimen surface is divided into a series of equal size square patterns, as shown in Figure 2.16 (a). The displacements are calculated at each of the points in the virtual grids in order to acquire the full-field deformation (Figure 2.16 (b)) [56].

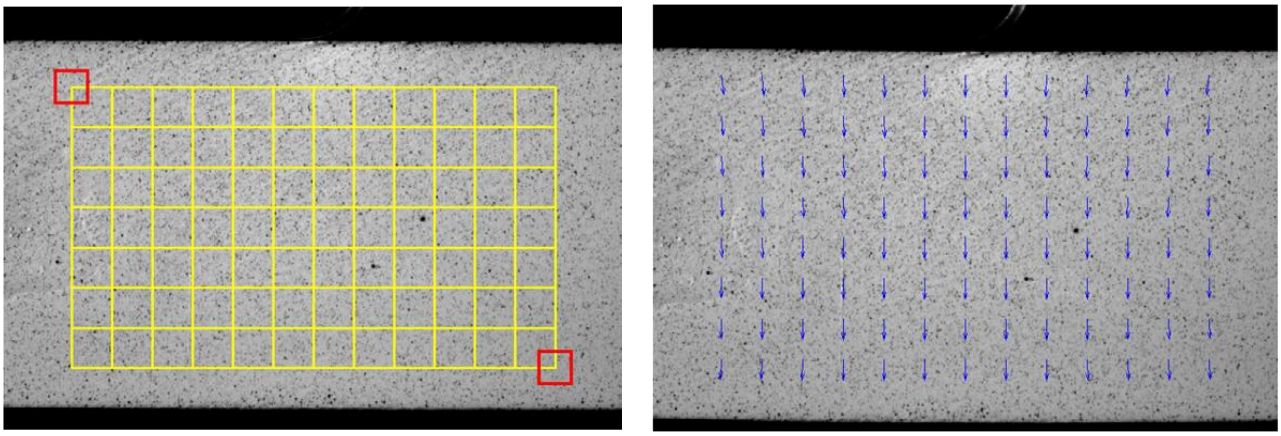

Figure 2.16: Reference image, the imposed red square is the subset used for tracking the motion of its center point, and the intersection points of the yellow grid denote the points to be calculated; (b) the calculated displacement vectors imposed on the deformed image [56].

The basic principle of 2D DIC is tracking (or calculating) the pixel displacement by matching speckles between the un-deformed image and the deformed image (as displayed in Figure 2.17) and then deriving information of strain and strain-rate [59]. In order to calculate the displacements of a point P, a square reference subset of $(2M + 1) \times (2M + 1)$ pixels centered at point $P(x_0, y_0)$ from the reference image are chosen and used to track its corresponding location in the deformed image [56]. The captured images are not compared point-by-point but rather by matching local distributions of pixel intensity (“subsets”) in images of the undeformed and the deformed specimen [60]. The reason behind this is that each subset includes a broader variation in gray levels, which results in better differentiation among subsets and can be identified uniquely in the deformed picture.

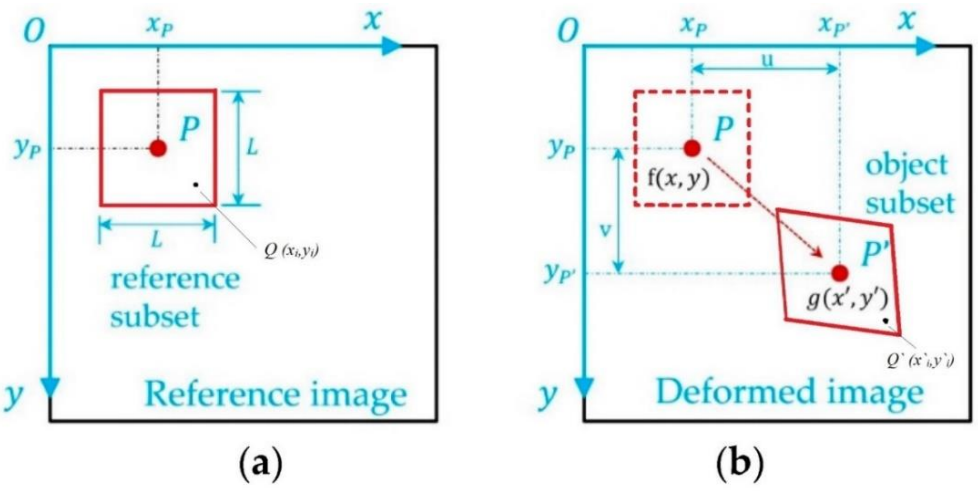

Figure 2.17: Schematic sketch of 2D DIC (a) Un-deformed image, (b) Deformed image. P is a reference point [56].

To evaluate the optimal match (or degree of similarity) between subsets, a cross-correlation (CC) criterion or sum-squared differences (SSD) correlation criterion should be defined in advance before correlation analysis [56]. For the former method, cross-correlation (CC), normalized cross-correlation (NCC), and zero-normalized cross-correlation (ZNCC), and for the latter, sum of the squared differences (SSD), the normalized sum of squared differences (NSS), and the zero-normalized sum of the squared differences (ZNSSD) are the most used algorithms. Based on the literature, it has been concluded that the ZNCC or ZNSSD correlation criterion are the most robust, noise-proof, and reliable ones since they are not sensitive to the offset and linear scale in lighting conditions [56].

Zero-normalized sum of squared differences (ZNSSD)

$$C_{ZNSSD} = \sum_{i=-M}^{M} \sum_{j=-M}^{M} \left[\frac{[f(x_i, y_j) - f_m]}{\Delta f} - \frac{[g(x'_i, y'_i) - g_m]}{\Delta g} \right]^2$$

Zero-normalized cross-correlation (ZNCC)

$$C_{ZNCC} = \sum_{i=-M}^{M} \sum_{j=-M}^{M} \left[\frac{[f(x_i, y_j) - f_m] \times [g(x'_i, y'_i) - g_m]}{\Delta f \Delta g} \right]$$

Once the deformed subset is determined using correlation criterion analysis, the in-plane displacement vector for the center of the subset (point *P* in Figure 2.17) will be yielded. This vector consists of *u* and *v* values in x and y directions. By means of these values and using so-called shape

functions, the displacements of subset pixels (like point Q in Fig 18) can be calculated. The relation between the deformed and the reference coordinates in the subset is defined as:

$$x_i' = x_i + \varepsilon(x_i, y_j)$$
$$y_i' = y_i + \eta(x_i, y_j) \qquad (i, j = -M{:}M) \qquad (2.7)$$

In which the ε and η represent the shape functions and could be defined from the zero-order, in the case where only rigid body translation exists, to higher orders which would allow detecting translation alongside rotation, shear, and normal strains [56].

The sub-pixel interpolation must be used prior to the correlation criteria to have a continuous correlation. The gray level intensity of these points and their derivatives between sample pixels are interpolated to reconstruct image intensity patterns. Researchers have been introduced to a variety of sub-pixel interpolation schemes such as bilinear interpolation, bicubic interpolation, bicubic B-spline interpolation, biquintic B-spline interpolation, and bicubic spline interpolation [56]. As mentioned before, this technique has been widely used in different fields of study. One particular subject is analyzing joints for which DIC is extremely practical and delivers a considerable amount of worthwhile information. In the following sections, the application of DIC in studying bonded, bolted, and hybrid composite joints is surveyed.

2.3.1 DIC with bonded composite joints

As one of the pioneers, who began utilizing DIC to study bonded joints, Colavito et al [61] reported the feasible application of DIC for measuring strains at different regions of adhesively bonded double lap composite joints. The authors demonstrated that DIC technology is capable of recording and observing different behaviors of bonded joints with different adhesive thicknesses. Bonded joint investigations using DIC technology can be classified into two major groups, studies associated with the bondline (BL) region and those related to the surface region of the joints.

2.3.1.1 Bondline studies

The failure of laminated composite bonded single-lap joints often initiates from the overlapped extreme ends where the strain/stress concentrations often occur. However, limited access to the bondline area, specifically overlap ends, brings about difficulties in terms of

experimental investigations. DIC is the best approach to remedy this problem. Wang et al. [62] took advantage of this technology to measure the strain fields near the overlap ends, and good agreement was achieved with FE simulation. Due to having the vivid vision of spew fillet via DIC, experimental outputs confirmed that the spew fillet existence decreased the stress concentrations at overlap ends. Microscope systems can be added to DIC for more in-depth investigations of shear modulus estimation [63] or calculation [64] for different adhesive materials. Using this approach, a microscopically close-view of the adhesive interface area (Figure 2.18) is provided, for which a corresponding strain distribution can be analyzed further. Additionally, the failure mode of the adhesive/adherend interface can be investigated using this system [64].

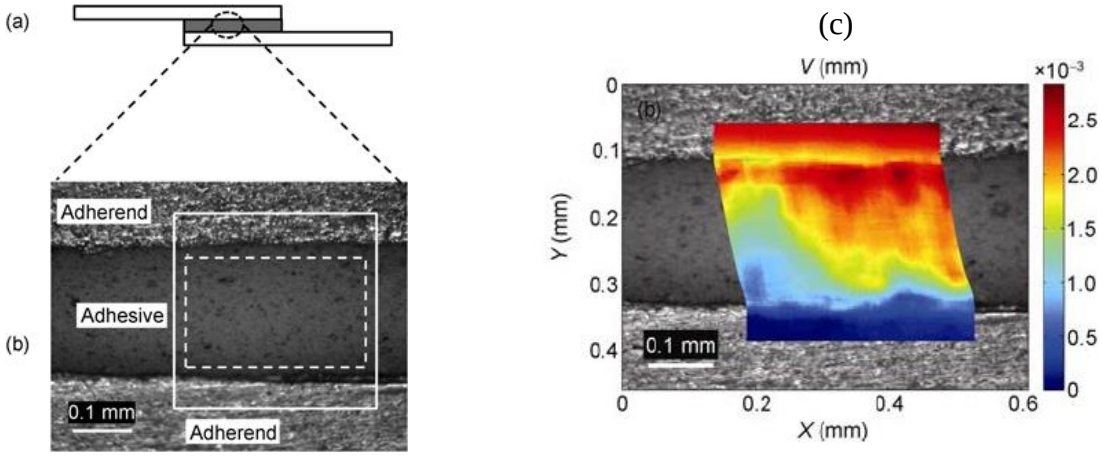

Figure 2.18: Observation on the adhesive interface: (a) the observed area on the adhesive layer; (b) image taken by the microscope system. (c) Displacement fields over the deformed image [64].

3D and 2D DIC were used to observe the evolution of the deformations and strains in composite single-lap bonded joints [65]. DIC results were first compared with that of strain gauges, and good agreement was achieved. 3D DIC successfully provided full-field measurement of in-plane surface strains and out-of-plane surface deformations for composite SL bonded joints. Highly magnified 2D DIC was applied (like the previously mentioned work) to determine the maximum principal strain in the adhesive fillet region. Kumar and his colleagues performed a DIC analysis of bonded joints and compared it with analytical [66] and numerical methods [67]. The peel and shear strain results achieved from DIC were used to calculate the corresponding stresses by assuming a plane strain condition. A comparison between DIC experimental results showed that

corresponding stresses on the BL were considerably higher than those of the theoretical stresses but obtained a better agreement with the results from FEA. Around the same period as Kumar, another team of researchers devoted their efforts to utilizing DIC for studying the stress and strain distributions through-the-thickness, and also for studying damage initiation of a composite within a bonded double butt strap joint [68, 69]. The camera was focused closely on the high peel strain regions identified at the root of the geometric discontinuity between the inner and outer strap to provide meso-scale data. Shear strains were observed to be non-uniform through the thickness of the adhesive, concentrating at the adhesive interface with the outer adherend, where high peel strains were also recorded [69].

Nonetheless, one of the limitations of the adhesive joints is the difficulty in predicting the joint strength owing to the presence of defects in the adhesive due to an improper curing process [70]. Therefore, to understand the joint behavior when these defects are present in a bonded component, an experimental study of CFRP composites SLJ with disbanding defects at the adherend-adhesive interface was conducted by Ping Qiu et al. [70]. DIC results from the BL showed that for the joints with a transverse defect in the BL, much higher strains were found at the edge with the induced defect, leading to the occurrence of serious asymmetry in the strain profiles. While for the joints with an axial defect, the strain profile trend was rather similar to that of the healthy joint. The adhesive strength and its fracture behavior in dissimilar SL joints composing of a composite adherend have been studied benefiting DIC technology [71-74]. DIC results from the joint side view showed that peeling is important in the extremity of the overlap region where failure is initiated [71], and the maximum strain and associated crack appeared first on the overlap end where the lower yield strength adherend is used [72]. Grefe et al. [73] admitted that DIC is a very useful tool to determine the initial crack and its propagation, and they recognized the type of cohesive failure using DIC. Furthermore, the effect of spew fillet was studied through-the-thickness using DIC, and the results demonstrated that the fillet improved the shear and peel strength of the adhesive layer in the overlap region [74]. DIC helped to identify crack initiation forces, stress concentration at the adhesive ends (Figure 2.19), and relative movement between the adhesive and the adherends in SL bonded composite joints [75].

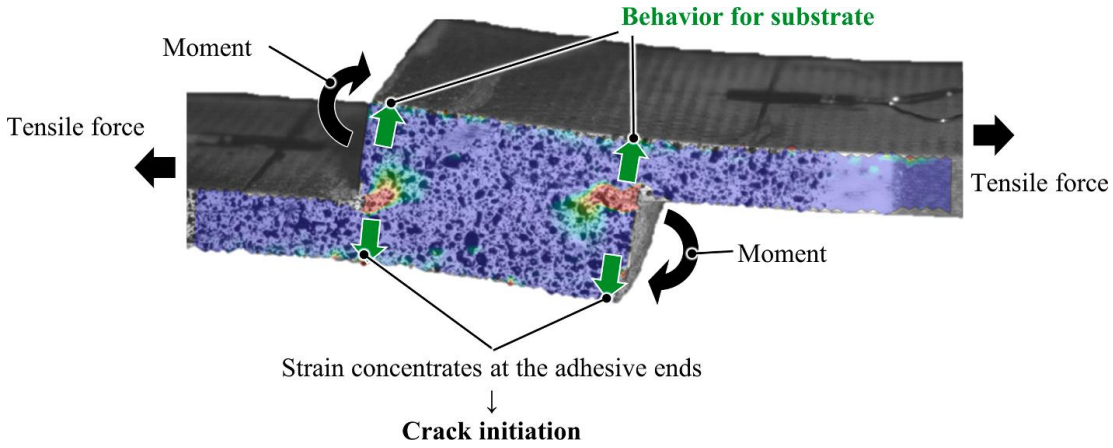

Figure 2.19: Full-field strain image obtained using DIC, and free-body diagram of SLJ specimen subjected to tensile loading [75].

2.3.1.2 Surface studies

Adhesive joints are advantageous when compared to bolted joints, given that they typically possess a lesser amount of stress concentrations and also have a uniform stress distribution in the bonded region. As previously mentioned, however, they sometimes underperform due to the presence of flaws in the BL and at the interface if subjected to an improper curing process. Vijaya et al. [76] managed to use DIC for detecting dry contact kissing bonds in GFRP adhesive joints. DIC results from the surface view confirmed the applicability of this technology for indicating kissing bonds' existence at less than 50% failure load. Bai et al. [77, 78] proposed a hybrid inversion method implemented within both FEM and DIC results to obtain the stress distributions at the adhesive layer of a composite bonded SLJ. Full-field displacement of the outer surface of a composite substrate could be measured by DIC, and then it is converted to that of the inner surface using cubic polynomials. These new values assigned to the adhesive layer, as real boundary conditions, and its stresses could be simulated using a FEM model. 3D DIC can measure the out-of-plane displacement of the joint surface. So, the occurred out-of-plane deformation because of the adhesive debonding in bonded carbon fiber reinforced polymer laminates was found to be the first significant failure, which is responsible for the ultimate failure of the specimen [79]. DIC assisted in monitoring the strain distribution over the surface of the SL composite-titanium bonded joint [80], and it showed a high tensile strain and a high bending and negative strain on the surface of composite and titanium respectively, after starting failure (Figure 2.20).

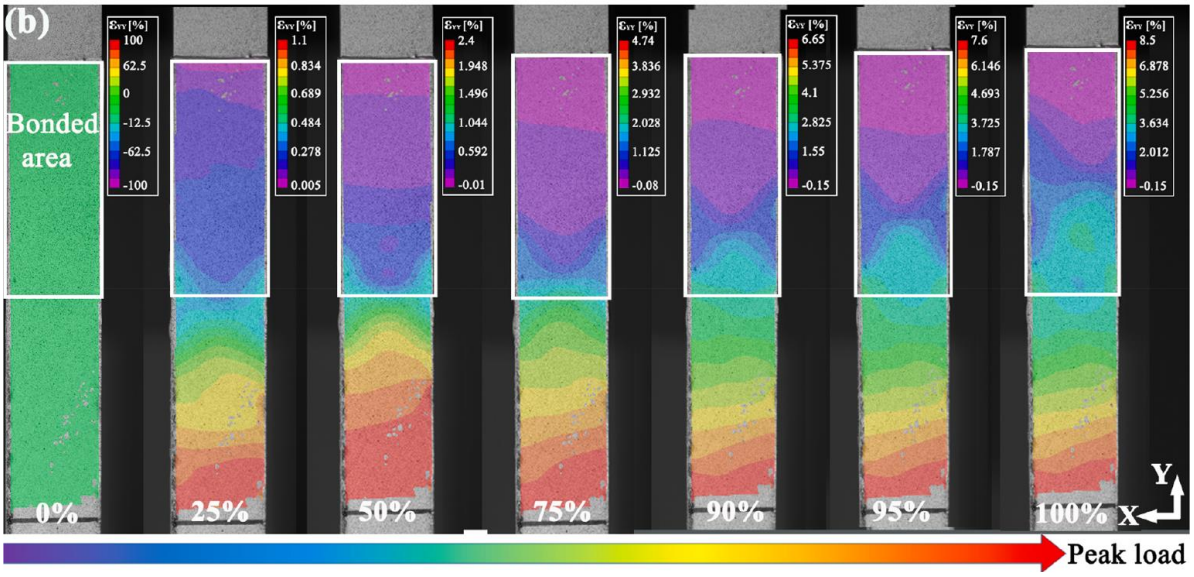

Figure 2.20: Y- direction strain field of dissimilar joints on the surface of composite adherend at different load levels [80].

2.3.2 DIC with bolted composite joints

One of the basic assumptions in DIC is the deformation continuity of a considered surface, which means that any discontinuities, such as cracks or significant relative movement of the structure or components, will disturb the subsets and neighboring points, and subsequently, no results can be provided for that region [56]. Therefore, assessing bolted joints on the BL region does not deliver meaningful outcomes, and researchers have focused mainly on surface investigations. The lateral displacements (or secondary bending, SB) measurements of the surface of a single shear lap joint demand that the strains be measured at certain locations, i.e., the AGARD (Advisory Group for Aerospace Research and Development) points [81]. However, this can be readily accomplished using non-contact optical methods, such as DIC or FEA. The influence of the various parameters on the SB of four fasteners with an aluminum/composite SLJ was performed using FEA alongside DIC [81]. However, digital photos were only taken at zero, 9, and 18 kN. Therefore, the results showed that the overlap reduction caused the SB to increase, whereas reducing the thickness of the aluminum plate caused the SB to decrease. Dupuy et al. [82] increased the photo capturing interval to 5 seconds and compared FEA results with those of DIC, and observed that the curvature of the SB for the metal bolted SLJ.

A liquid-shim is often required to compensate for the assembly tolerances in mechanically-fastened joints. The effect of the introduction of a liquid-shim layer on a thermo-mechanical fatigue response and in-plane strain/out-of-plane deformation of composite-aluminum SLJ were conducted using magnified 2D DIC and 3D DIC by Comer et al. [83, 84]. The presence of liquid shim increased the load eccentricity, and DIC results detected the magnified SB values due to this effect and also identified a likely fatigue crack initiation. 3D DIC outcomes demonstrated that thin composite SL joint experienced higher degrees of out-of-plane displacement, thus increasing the likelihood of fastener pull-through. This was highlighted by Gray et al. [85]. Moreover, SB, which itself appreciably influenced by the taper type, affects the final failure mode. One significant feature of 3D DIC was pointed in which by comparing the out-of-plane deformation of the right-hand-side (RHS) to that of the left-hand-side (LHS) of the joint, the twisting of SLJ can be characterized.

While it is important to assess the stiffness and the ultimate load of the joint, it is proportionally vital to understand the load distribution [86]. Quantifying the load distribution in multi bolted composite joints was restricted to analytical and numerical modeling. The experimental aspect could just be observed while using either instrumented bolts [37, 43] or by installing a row of strain gauges between each bolt-hole [87]. Gray et al. [86] came up with a new method based on DIC results to extract the load distribution in multi-row, multi-column composite SL joints. In order to quantify the load distribution, 3-D DIC was applied to measure the axial strain between each bolt in the joint. This was accomplished by placing a virtual strain gauge halfway between each bolt, which was used to evaluate the average strain across the width of the laminate. Then, the load taken-up by each bolt could be calculated by performing an equilibrium analysis of the joint. Authors spotlighted that 3-D DIC was valid for identifying the point at which the first significant failure event occurred in the joint. Other groups of researchers have continued to use 3D DIC technology to analyze the surface strain distribution and the out-of-plane deformation [88-90]. It has been found that the surface strain is highly concentrated around the holes (Figure 2.21) and that the bolt torque alleviates some of the surface strain concentrations by increasing the friction in the joints [88].

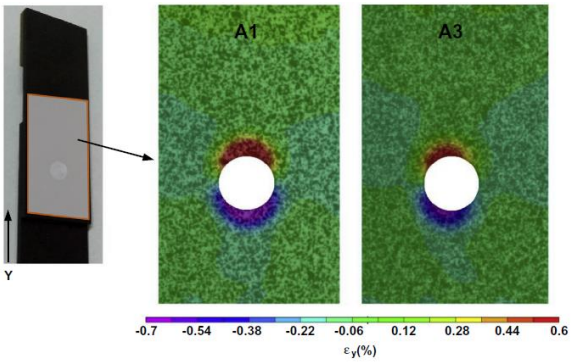

Figure 2.21: Axial strain distribution and concentration around holes [88].

The surface strain concentrations observed (using 3D DIC results) in the specimen can be employed to identify full-field damage onset and to monitor damage progression during loading [89, 91]. The quasi-isotropic laminate experienced the smallest axial compressive and shear strain concentration around the holes resulting in providing the best bearing performance in one bolted single-lap joint. Hu et al. [90, 92] also confirmed that the out-of-plane deformation is substantially influenced by the tightening torque and the laminate stacking sequence (Figure 2.22) [90]. Moreover, DIC results showed that in-plane bearing damages are highly localized in joint with quasi-isotropic lay-up, whereas V-shaped and two paralleled bands along the fiber direction were observed for angel-paly and cross-ply laminate stacking sequences, respectively [92]. In the very recent work [93], the surface results retrieved using DIC demonstrated that owing to increased bolt-hole contact area in interference-fit case, the surface strain concentration is alleviated, while out-of-plane deformation experienced little alteration. Furthermore, a sleeved fastener was found to be more contributive in lessening the surface strain concentration compared with a conventional bolt.

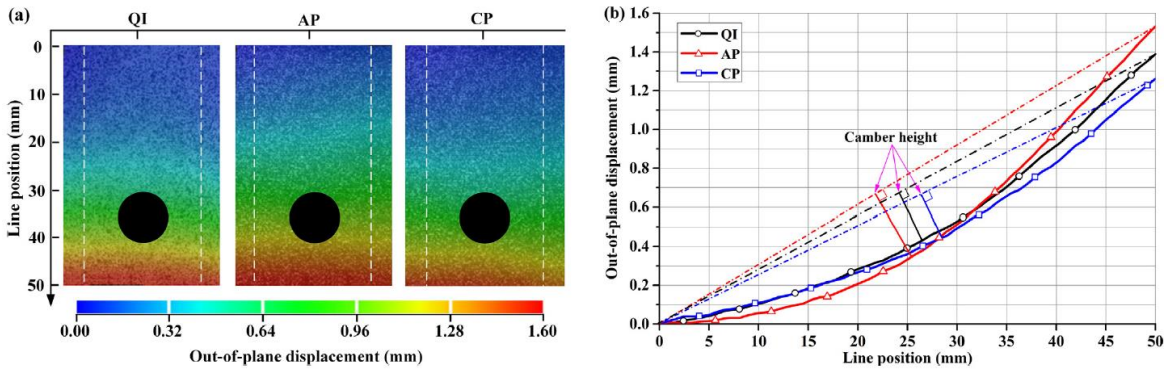

Figure 2.22: Out-of-plane deformation of different lay-ups, quasi-isotropic (QI), angle-ply (AP) and cross-ply (CP). (a) displacement nephogram, (b) average profile of bending laminates [90].

Welding is another technique to connect the composite sub-components, but it is applied just on thermoplastic composite materials due to their inherent properties. DIC was used to study the strain distribution of this sort of joints [94], and shear and peel strain distributions were investigated at the welded joint overlap area. Full field strain measurement provided by DIC contributed to characterize thermoplastic composite joints in order to develop a computational framework [95]. Virtual extensometer provided by DIC was found to be very helpful to ensure accurate extension measurement in woven carbon fiber thermoplastic composite joints [96]. 3D DIC can capture out-of-plane displacement, as mentioned before, and this feature helped Zhao et al. [97] in their study regarding ultrasonic spot welding thermoplastic composite joints. DIC results showed that the overlap rotation and hence secondary bending decreased with increasing number of welded spots. Out-of-plane displacement was recorded using 3D DIC for the case of 3D-printed thermoplastic composite fasteners. The influence of different 3D-printed bolts on secondary bending of composite joint was observed perfectly [98]. The results illustrated that the countersunk head could reduce the joint secondary bending which results in a stiffer joint.

2.3.3 DIC with hybrid bolted/bonded composite joints

The study of the mechanical response and fracture behavior of hybrid bolted/bonded composite joints by means of DIC technology, which is the main concern of the current thesis, are seldom investigated, and there is a very limited numbers of researchers who have put effort into investigating it. However, Canadian institutions and universities have done some work regarding this matter. A group of researchers from Structures and Materials Performance Laboratory of Institute for Aerospace Research National Research Council Canada, Ottawa, started using 2D DIC to determine the strain distribution in bonded and bolted/bonded composite but joints and compared against results from FEM [99]. Strains were measured through thickness and along the bondline in the joint overlap section (Figure 2.23). Overall, a good agreement was achieved between DIC and FEM simulations. Gang Li [100], from the previous group of researchers, individually observed the joint deformation, peak strain, and early damage situation using DIC images in the fatigue behavior of bolted/bonded composite butt joint.

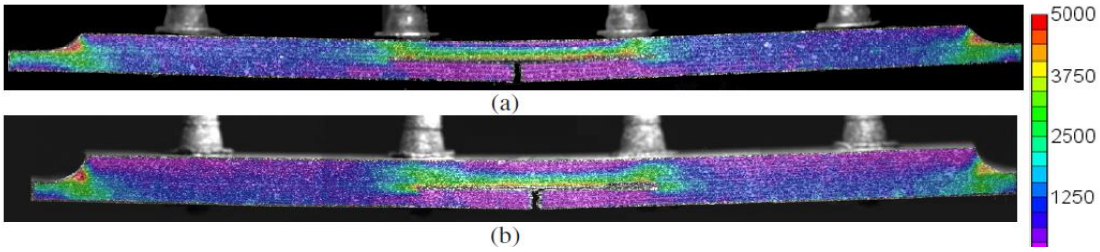

Figure 2.23: Maximum principal strain in bolted/bonded joint measured with DIC [99].

In a collaborative project, for which one of the stakeholders is Carleton University, JiHyun Kim [101] and Pedro Lopes Cruz [102], alongside their FE studies, used 2D DIC in order to experimentally and numerically investigate the response of single-bolted bolted/bonded composite SL joint. The strain on the surface of the joint was studied with 2D [101], but the problem was that 2D DIC could not detect the out-of-plane deformation, which was a key element in the surface characterization. A finer speckle pattern using an airbrush was applied to detect the displacement near the interface between the adhesive and the adherends along the bondline [102]. Authors confirmed that using DIC technology, extensive measurements, and analysis could be obtained and carried out for every single coupon and that for a study on the multi-bolt configurations, it was suggested to take advantage of this 3D DIC bond line approach [102]. In order to design HBB joint with flexible epoxy adhesive, DIC was implemented to perform strain measurement of the specimen surface [103] and the thin bondline of adhesive [104].

Strain distribution and failure characterizations of bolted/bonded dissimilar joints, including composite plate, were investigated using a 3D-DIC system [105-107]. DIC analysis showed that the HBB joint generated more bending, with up to 3.06 mm difference of out-of-plane displacement around the overlap area compared with riveted and bonded joints [105]. Peel strain analysis through-the-thickness of stepped single-side repairs indicated that initial crack mainly appeared on the edge of the adhesive layer between the laminate and substrates (Figure 2.24) [106]. In other work, DIC contributed to fully monitoring the changes in strain contours from progressive failure initiation in the adhesive to reaching the rivet load-bearing stage in HBB joint. It was found that the strain concentration is moved from the edge of the overlap region to the rivet after the adhesive mostly failed [107]. Kim et al. [108] applied 2D-DIC to experimentally study the behavior of bonded and HBB composite joints under tensile loading. It was confirmed that the DIC technology could rapidly and effectively measure the strain field and identify the onset of failure around the bolt during quasi-static loading.

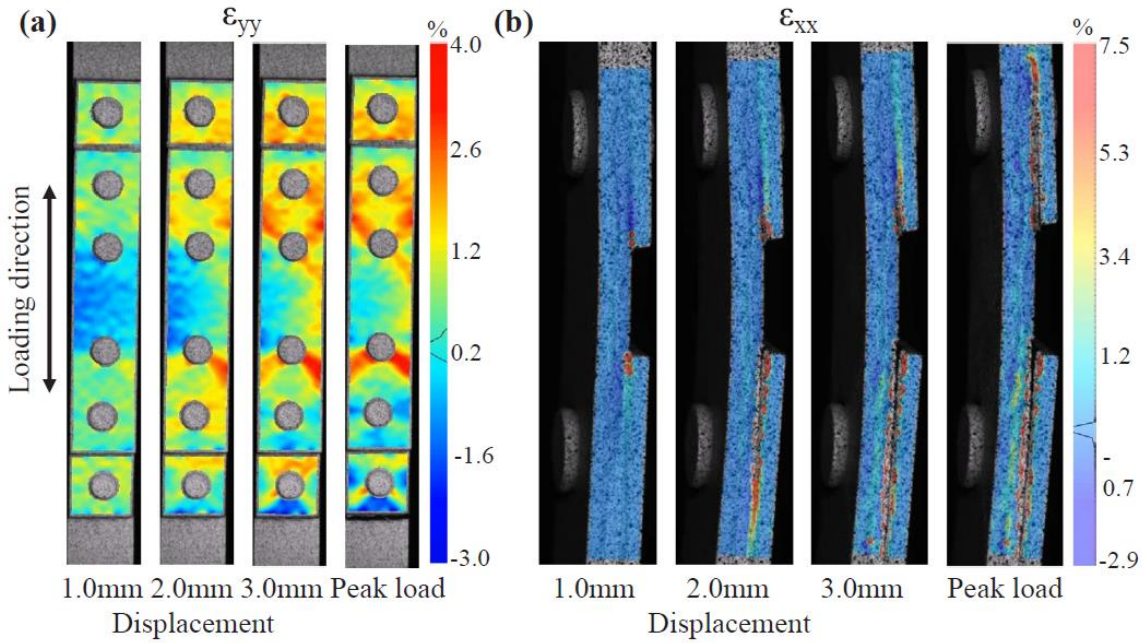

Figure 2.24: Strain distribution at different stages for single-side hybrid repair under (a) front view and (b) side view [106].

2.4 Summary of literature review

The provided literature survey showed that the analysis of SL composite joints is still a serious bone of contention and it requires more in-depth studies. It was tried to review the most relevant work thoroughly to the thesis topic to realize its importance of being more investigated. It was observed that there are a few experimental works have been done about studying the hybrid bolted/bonded single-lap composite joints. Particularly, when it comes to multi-bolted HBB single-lap composite joints, there is a small handful of comprehensive experimental studies, as it is a demanding and challenging task. Consequently, it left a considerable number of issues to be addressed. Theoretical studies to a lesser extent, but the numerical and simulation investigation to a greater extent, dominate a portion of the work in this field. However, what is a real representative of a joint behavior can only be assessed realistically by experiments.

The experimental mechanical characterization of multi-bolted HBB single-lap composite joints is always associated with serious limitations in terms of equipment. Fortunately, Polytechnique Montréal possesses advanced laboratories equipped with proper manufacturing materials and tools alongside modern apparatus, including a DIC system, which overcomes this

obstacle. With the introduction of DIC technology to academia and industry, a good momentum took place among the researchers, yet not enough to make the most of the high potentiality of this robust technique. DIC is an excellent contribution for the purpose of this thesis to effectively observe and analyze various factors, including out-of-plane displacement, strain distribution/concentration on the surface and through-the-thickness, bolt hole elongation, and the like on the strength, behavior, and failure mechanisms of composite joints. To the author's best knowledge, no comprehensive experimental research has been conducted that deals with the analysis of multi-bolted HBB single-lap composite joints, particularly characterized by means of 3D-DIC technology. Thus, it became a primary source of motivation to propose this topic and dig deeper within this field. The outcomes of this research certainly provide worthwhile findings that may eventually yield improved and optimized composite joints.

CHAPTER 3 RESEARCH OBJECTIVES AND COHERENCE OF ARTICLES

3.1 Problem statement and potential solution

Avoiding any redundancies and oversizing and reaching a safe, reliable and optimal composite joint design that possesses more strength and can properly stand against applied load is always a controversial issue amongst the academic and industrial communities. Measuring displacement field and corresponding strain changes during loading delivers crucial insight into the investigation of the mechanical response of a composite structure. Numerical simulations have come into play to compensate for this lack of information. However, they are always prone to accurately define material properties, boundary conditions, loading, geometry specification, contacts, and so on to deliver real outcomes. In terms of experimental approaches, two conventional methods called strain gauges and extensometer are being utilized for displacement and strain measurements. The former is highly restricted to the installation surface (which should be accessible, clean, and smooth) and only provides plane measurement data from one specific point, and the latter delivers the changes in the length of an object.

In order to obtain more realistic and detailed results, the need for practical equipment for the sake of reliable and extensive experimental testing is highly sensed. Here is the place where DIC technology plays a leading role. The superior capability of DIC not only overcomes the drawbacks of the aforementioned approaches, but it also provides a real full-field point-wise measurement of displacements and strains (in-plane or out-of-plane) all along with the test and up to the final failure. Therefore, strain distribution, concentration, load transfer, crack initiation/propagations, failure mechanism, and such related matters can be precisely characterized using this technology. Outcomes of the present study address a worrisome problem regarding the efficient contribution of the bolts, adhesive, adherend lay-up, and geometry on the mechanical behavior of the multi-bolt and hybrid bolted/bonded SL composite joints using experimental DIC results.

3.2 Objectives and related articles articulation

In the light of the literature survey and the stated problem with the proposed solution, the main objective of the present thesis has been formed. It aims to investigate experimentally the

deformation and mechanical behavior as well as the fracture mechanism in the plane and through-the-thickness of multi-bolt and hybrid bolted/bonded single-lap composite joints using 3D Digital Image correlation (3D-DIC) technology. The principal goal of this research work is to carry out an extensive series of experimental studies on the aforementioned composite joints to acquire a better comprehension of their mechanical behavior, which could result in delivering a safe design and optimized structures. In order to accomplish the mentioned main objective, the following four sub-objectives have emerged:

Sub-Objective 1: Quantify and analyze one of the deleterious effects, called secondary bending, in multi-bolt single-lap composite joints.

3D-DIC is capable of measuring the out-of-plane displacement, which in this case represents the secondary bending (SB) effect that occurs because of the geometrical eccentricity of the single-lap joints. The laminate composite materials suffer from brittleness and lack of ductility; hence, they are very susceptible to bending effects like SB, which is the unwanted by-product of the applied tensile load to SL joints. Due to the lack of precise and detailed experimental results characterizing and understanding the SB phenomenon, the first article, presented in Chapter 4, is exclusively dedicated to this matter due to its importance. The paper entitled "*Quantifying of secondary bending effect in multi-bolt single-lap carbon-epoxy composite joints via 3D-DIC*" was published in the journal "*Composite Science and Technology*" on September 5, 2020. In order to revalidate the accuracy and reliability of 3D-DIC results and their trend, the analytical Neutral Line Model (NLM) was adopted, whose outcomes were promising. This chapter focuses only on multi-bolt single-lap composite joints. Two well-known stacking sequences are investigated, namely quasi-isotropic (QI) and cross-ply (CP), for two laminate thicknesses, and their deformation and strength are analyzed considering the SB effect. The obtained results were motivating enough to pursue SB measurement alongside the surface strain distribution in the case of HBB joints as well, which leads to sprouting the idea of Sub-Objective 2:

Sub-Objective 2: Studying the full-field strain distribution and secondary bending/twisting effects in bolted and hybrid bolted-bonded single-lap composite joints.

After measuring and understanding SB in only bolted joints, it is time to extend the work to investigate this phenomenon in the hybrid bolted-bonded case. The work even becomes more broadened to study the full-filed strain distribution of the joint surface and the balance between

bypass and bearing loads as well as exploring/comparing the load transferring mechanism via the bolts in only bolted and hybrid joints. The mentioned fields of study are of great concern in analyzing the tensile behavior and fracture mechanism of multi-bolt fastened joints, and the yielded results are practical leads in proposing a reliable composite joint design. To do so, the second article (presented in Chapter 5) was conducted dealing with the goal of Sub-Objective 2. This work was published in the journal of "*Composite Part B, Engineering*" on the 4th of April 2021, holding the title "*3D-DIC strain field measurements in bolted and hybrid bolted-bonded joints of woven carbon-epoxy composites*". The same laminate lay-up and thicknesses as article one were considered, mentioning the fact that an adhesive was added to have hybrid joints which eventually results in eight different configurations. DIC results clearly illustrated the strain distribution/concentration and bearing effects caused by the bolt in bolted and HBB joints. The mentioned factors, next to some others, make the bolt-holes to deform and elongate, which considerably varies from bolted to hybrid joints. Thus, to be more specific with this matter, the sub-objective 3 is proposed:

Sub-Objective 3: Accurate measurement of hole elongation in woven composite plates and joints, alongside examining the factors affecting it.

The findings of Sub-Objective 2 became a source of inspiration for digging deeper into hole elongation and its development. While fiber-reinforced composite is brittle, the cutout holes in composite plates and joints experience noticeable elongation. This phenomenon is considered as a critical parameter in cyclic loading, but its importance in tensile testing is neglected to some extent, as its experimental measurement is very challenging. DIC is a great asset for accurate measurement of the hole elongation from the surface of a specimen. Therefore, Chapter 6 is presented to trigger this purpose. The related article is named "*Experimental investigation of hole deformation and bolt-hole elongation of woven carbon-epoxy composite plates and joints using DIC technique*", which is submitted to the journal of "*Composite Structures*". In addition to considering the same eight configurations tested in the sub-objective 2, hole deformation of open hole tension (OHT) and bolted filled-hole tension (FHT) specimens are also analyzed to have good basic knowledge regarding this objective (results of this additional section are provided by the master student of Prof. Boukhili, Aouni JR. Lakis, who has finished his studies in the same research group as the thesis author). This chapter presents different interesting results, including the effects of composite lay-up, laminate thickness, hybridization on the hole deformations, and its influence on the

specimens' strength. Through these three sub-objectives, the most that can be benefited from DIC regarding the surface studies are almost carried out. Next, it is time to exploit the potential of DIC regarding the through-the-thickness analysis of HBB joints, which is presented in the final sub-objective:

Sub-Objective 4: Using DIC to study and monitor the strains' development and crack initiation/propagation through-the-thickness of the hybrid single-lap composite joints.

This sub-objective will ultimately use the capability of the optical DIC technology to measure and analyze the strain distribution of limited access areas. The side view of the overlap region is narrow, and only a non-contact approach like DIC can capture this area, specifically from the beginning of the test to the final failure moment. By means of this feature, strain full-field measurements through-the-thickness of the joint overlap section, including both adhesive layer and laminate plates, is doable, which will deliver new experimental findings of this less-investigated region. The related article, which is presented in Chapter 7, is entitled "*Full-field through-the-thickness strain distribution study of hybrid multi-bolted/bonded single-lap composite joints using digital image correlation*", which is under review in the journal of "*Composite Part A: Applied Science and manufacturing*". This work is only dedicated to the hybrid joints with thicker laminates and lay-ups of QI and CP, which results in two configurations. DIC results contributed to detecting the strain components of the mentioned region, which leads to inspecting and following the adhesive failure nucleation and propagation and observing the joints' mechanical responses. This last work is a final study that ends the fulfillment of the stated sub-objectives, which cumulatively bring about complementation to the principal goal of the thesis.

CHAPTER 4 ARTICLE 1: QUANTIFYING OF SECONDARY BENDING EFFECT IN MULTI-BOLT SINGLE-LAP CARBON-EPOXY COMPOSITE JOINTS VIA 3D-DIC

Published in: Journal of Composite Science and Technology, September 2020

Masoud Mehrabian, Rachid Boukhili*

Department of Mechanical Engineering, Polytechnique Montreal, Quebec H3C 3A7, Canada

4.1 Abstract

In this paper, an extensive experimental study was performed to quantify and understand secondary bending (SB) in multi-bolt single-lap joints composed of quasi-isotropic (QI) and cross-ply (CP) carbon/epoxy laminates for two laminate thicknesses. The out-of-plane displacement (OPD), which represents SB, was measured experimentally using a 3D digital image correlation (DIC) system. The SB ratio was quantified as the ratio of out-of-plane displacement (δ_{OPD}) to in-plane displacement (d_t). It is found that δ_{OPD}/d_t ratio measured in CP is approximately 30% higher than in QI. It has also been observed that for a given laminate configuration (CP & QI), the δ_{OPD}/d_t ratio decreases as the tensile load increases. The analytical Neutral Line Model (NLM), which was used in this work, also predicts this trend. Moreover, 3D-DIC measurements show that although δ_{OPD} decreases with increasing modulus of elasticity, it increases with increasing thickness of the laminate.

Keywords

Secondary bending, Three dimensional digital image correlation (3D DIC), Multibolted single-lap composite joints, Neutral line model (NLM)

* Corresponding author.

E-mail address: rachid.boukhili@polymtl.ca (R. Boukhili).

4.2 Introduction

The main concern regarding SL joints is when an applied force generates a bending moment that tends to turn or rotate a subject element. This situation induces secondary bending (SB) and causes out-of-plane displacements (OPDs). SB significantly affects the local strain field and the global response of joints, and OPDs generally diminish the joint stiffness in the longitudinal direction [1], which results in a joint loss of efficiency in aeronautical structures. SB was initially studied by Schijve et al. [2, 3] using an analytical method known as the neutral line model (NLM). The effect of SB in real aircraft structures has been investigated by Schütz and Lowak [4]. SB was primarily measured in terms of either stress or strain [5-9], which is expressed as follows:

$$SB = \frac{\varepsilon_{bot} - \varepsilon_{top}}{\varepsilon_{bot} + \varepsilon_{top}} = \frac{\varepsilon_{bend}}{\varepsilon_{ax}} \approx \frac{\sigma_{bend}}{\sigma_{ax}} \tag{4.1}$$

where the subscripts *top* and *bot* indicate the top and bottom surfaces of the sheets, respectively; *ax* and *bend* refer to the axial and bending strains, respectively. Ireman et al. [7, 9] implemented Eq. (4.1) to determine SB experimentally and compared the results with a developed 3D finite element model [7]. The SB values calculated using Eq. (4.1) illustrated that SB was reduced when significant damage occurred and caused a change in the contact state between the laminate and bolt [9]. Other findings showed that the plate curvature in multibolted joints is equivalent to the SB, which was experimentally measured using strain gauges established around the bolt holes [1, 10].

McCarthy et al. [11] developed an improved 3D FE model that can capture 3D effects in a single-bolt joint, such as SB and twisting. Schijve [2, 3] extended his studies to analyze the effect of SB on the fatigue properties of a structure [12]. NLM method presents a bending factor, which is defined as the ratio of the bending stress to the applied tensile stress. The bending factor was calculated for a three-bolt lap joint with three different row spacing, and it was observed that by increasing the row spacing, the bending factor was reduced. The effect of SB on the triple-row riveted lap aluminum joint fatigue life was investigated experimentally and analytically [13]. The results confirmed that the NLM could be used to evaluate the effects of joint geometry parameters on the magnitude of SB.

A novel FE model, known as the global bolted joint model (GBJM), was developed by Gray and McCarthy [14]. This 3D model discretizes laminates through their thickness, which enables the SB effect to be captured from nodal displacement. The SB of SL single-bolted composite joints was predicted using an enhanced analytical approach by Olmedo et al. [15]. Because the SB effect affects the damage evaluation of multibolted SL composite joints, it was computed via a 3D implicit FE damage model. It was found that the clearance changed the SB of the joints substantially. The progressive damage model (PDM) facilitated the calculation of SB of SL and double-lap composite joints [16]. It was concluded that the decreased contact area and higher stress level arising from SB further accelerated the material damage in single-bolted SL joints. Investigations on the effect of SB on the damage and strength of SL single-bolt interference-fit composite joints showed that this phenomenon and the corresponding delamination could be restrained constructively by bolt preloads [17].

With the advancement in digital image processing, digital image correlation (DIC) technology has emerged, which provides researchers with a noncontact measurement technique, without requiring specific instrumentation, installation, or machinery. Researchers implemented this technique in a variety of composite studies such as investigating strain variations or measuring fibre orientation in short fibre reinforced polymers and so on [18-20]. The OPD of the top surface of a single-bolted countersunk composite joint was measured using 3D DIC and demonstrated good agreement with the numerical results [21]. DIC results demonstrated that tapering SL single-bolted countersunk composite joints significantly affected the degree of SB and consequently the final failure mode [22]. Yunong Zhai et al. [23, 24] experimentally studied the effects of bolt-hole clearance and bolt torque [23] as well as the interface condition [24] on the OPD of SL single-bolt countersunk composite joints. It was found that the bolt torque exerted a slight effect on the out-of-plane deformation, but the OPD was slightly magnified as the clearance increased. The OPD of two groups of single-lap adhesive bonded CFRP laminate was studied using DIC [25]. It was found that the maximum deformation occurred on one side of the specimen but more significantly in the adhesive region.

The present paper aims to quantify experimentally the secondary bending in SLJ via an enhanced analysis of 3D DIC measurements. It is expected that this quantification will clarify the reasons for the low resistance of CP single-lap joints compared to the QI case.

4.3 Methodology

4.3.1 Experimental procedure

4.3.1.1 Material and specimen preparation

Carbon fiber reinforced epoxy (CFRE) laminates were manufactured using the vacuum assisted resin transfer molding (VARTM). The materials specifications of fibre, epoxy resin, bolts and nuts are the same as used in [26, 27]. Two different stacking sequences were designed, namely cross-ply (CP) and quasi-isotropic (QI), whose lay-up and average thickness (after the recommended curing cycle of 24 h) are shown in Table 4.1. A tightening torque of 5 Nm was applied to each of the bolts. Single-Lap (SL) shear bolted joints with three bolts were manufactured according to the ASTM-D5961 standard [28]. The geometrical configuration of the joint is shown in Figure 4.1.

Table 4.1: Stacking sequences and tensile strength of the manufactured laminates.

Code	Lay-up	Plies	Average thickness, *t* (mm)	Tensile strength as per ASTM D3039. (MPa)
CP8	$[(0/90)/(0/90)/(0/90)/(0/90)]_s$	8	1.65	854
QI8	$[(0/90)/(\pm45)/(0/90)/(\pm45)]_s$	8		592
CP12	$[(0/90)/(0/90)/(0/90)/(0/90)/(0/90)/(0/90)]_s$	12	2.63	800
QI12	$[(0/90)/(\pm45)/(0/90)/(\pm45)/(0/90)/(\pm45)]_s$	12		579

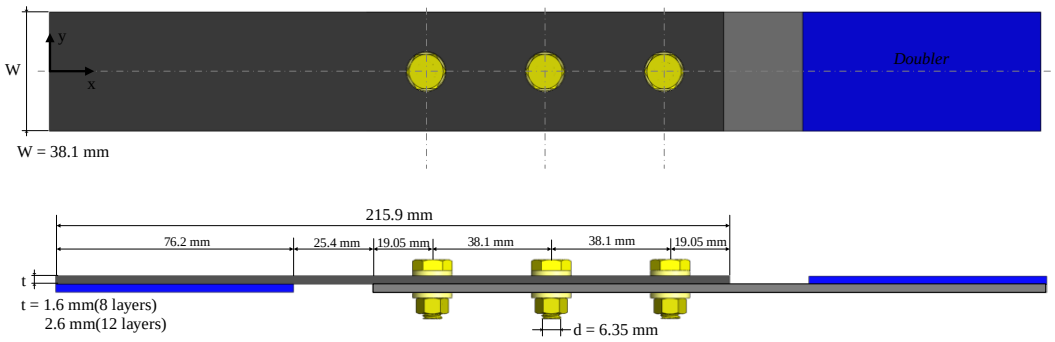

Figure 4.1: Specimen geometry and dimensions, *d* is the hole diameter and *t* is the thickness of the composite panel.

Because DIC method was employed in this study, prior to fastening the bolts, the surface of the specimens was prepared to generate a random gray intensity distribution, that is, a random speckle pattern. First, to remove any dust and debris, the surface was cleaned using isopropyl alcohol; subsequently, a white background was painted with white spray paint. Next, a black speckle pattern was applied onto the white specimens using black archival ink and a roller stamp with dot sizes of 0.026 inches in diameter.

4.3.1.2 Test setup and procedure

For each category of the SL bolted joints investigated, at least four identical specimens were tested under tension loading at a constant standard cross-head displacement rate of 2 mm/min. All mechanical tests were performed on a servo-hydraulic MTS testing machine model 810 with a 100 kN load cell. For all tests, 3D DIC was implemented to measure the OPD of the joint surfaces. The basic principle of DIC is based on tracking the random pattern on the specimen surface, which is performed by matching the local distribution of the pixel concentration, i.e. the subsets, between undeformed and deformed images during a specific time interval. Surface deformation is computationally attained by optimizing a least-squares or cross-correlation function to evaluate the similarity degree between the undeformed specimen and the corresponding deformed specimen in terms of grayscale intensity values [29]. A set of two charge-coupled device (CCD) cameras was mounted vertically on an aluminum extrusion guide bar, and right in front of the specimen such that the specimen surface normal bisected the stereo angle (relative angle between two cameras) [30]. The 3D DIC system and software used is a Vic-3D v 7.2.4 model from Correlated Solutions Inc., USA.

4.3.2 Analytical approach

4.3.2.1 Neutral line model (NLM)

For the analytical investigation of the SB, a one-dimensional NLM was used. Schijve [2, 31] initially proposed this approach for calculating the ratio of bending stress over tensile stress (bending factor, k_b) as well as NLD (neutral line displacement), which means OPD calculated by the NLM. This model was governed by the advanced elastic beam theory, in which the region outside the overlap area and the overlap section (between the extreme bolts) were regarded as a

solid cantilever beam subjected to a tensile load and an internal plane moment owing to the eccentricities. The region outside the overlap area involves a beam with a thickness *t*, whereas the section between the extreme bolts is considered as an integrated beam, which possesses flexural rigidity corresponding to twice the laminate thickness, i.e., *2t* [32]. The severity of SB at the location of the extreme bolt is defined by a calculated coefficient called the bending factor, k_b, which is expressed as follows:

$$k_b = \frac{\sigma_{\text{bending}}}{\sigma_{\text{no min al}}} = \left(\frac{6}{tw}\right)(A_1\, sinh(\alpha_1 l_1) + B_1\, cosh(\alpha_1 l_1)) \tag{4.2}$$

In equation (4.2), *t* is the laminate thickness, *w* is the joint width, $\alpha_1 = \sqrt{P/E^* I_1}$, where P is the applied load; $E^* I$ refers to the bending stiffness of the corresponding section, l_1 is the length of the distance between one extreme bolt and the corresponding end of the joint. A_1 and B_1 are the unknowns which would be determined after solving the equilibrium equations of half of the studied configurations (See Appendix A for details). The coefficient k_b will be obtained afterwards. The NLM is a convenient method for evaluating the SB effect for various joints with different geometries based on determining the NLD and bending stress. Some adopted simplifications, such as bolts are not modeled; the bolt tilting and load transferred by the bolts are neglected; and the presence of middle bolts is ignored in the case of multibolted joints, which may affect the results [13]. Nevertheless, it may be concluded that the NLM can deliver meaningful and comparative information regarding SB in different multibolted joints [12].

4.4 Results and discussion

4.4.1 Effect of the laminate thickness and stacking sequence on the bending factor

Figure 4.2 (a) shows the effect of the stacking sequence and laminate thickness on NLD at the outer bolt as predicted by the NLM. For all the laminates configurations, the NLD increases rapidly as the load increases and then stabilizes as it approaches higher load values. Thinner laminates show smaller NLD and this behavior is well expected because a thinner laminate plate results in a smaller geometrical eccentricity. In addition, Figure 4.2 (a) shows that NLD is lower for CP than

for QI and this can be related to the higher bending stiffness of CP compared to that of QI. A significant contribution of the NLM is displayed in Figure 4.2 (b), which compares the variation of the bending factor k_b for the four lay-ups versus the applied tension load. For the two thicknesses investigated, k_b is found to be higher for CP than for QI. This means that there is relatively more bending in CP than in QI. Considering the inherent higher stiffness of CP, at first sight, this is an unexpected behavior and may denote a limitation of the NLM model. However, as it will be shown in the next sections, this behavior is validated experimentally via appropriate 3D DIC measurements. Actually, according to equation (2), k_b expresses the bending to extension ratio. Although named the «bending factor», mathematically speaking, k_b is not more related to bending than it is related to extension. k_b is a dimensionless ratio expressing the simultaneous occurrence of bending and extension. Bending/extension coupling is a common phenomenon which occurs in non-symmetric structures. Due to the definition of k_b in equation (2), it can be said that a joint with a higher k_b undergoes relatively more bending, which does not necessarily mean more out-of-plane deformation. In this regard, since Figure 4.2 shows that QI has more OPD but lower k_b than CP, this means that there is relatively less bending in the QI joints.

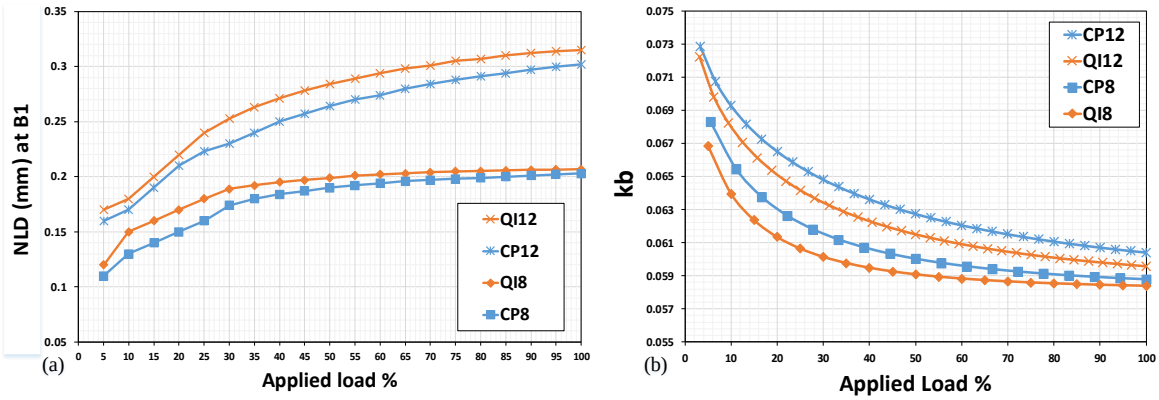

Figure 4.2: Effect of stacking sequence and laminate thickness on (a) NLD and (b) kb.

4.4.2 Effect of the stacking sequence and laminate thickness on the bearing strength

The bearing stress σ^{br} versus bearing strain ε^{br} diagram was used to determine the strength of the three-bolts SL joints in accordance with the ASTM standard D5961 [28] and the methodology outline in [22, 33]. The bearing stress (σ^{br}) is calculated as

$$\sigma^{br} = \frac{P}{k \times D \times h} \tag{4.3}$$

where P is the applied load; D is the hole diameter; h is the thickness of the composite panel; k is the force per hole factor, which is three for the three-fastener tests. The bearing strain (ε^{br}) can be calculated using the following equation:

$$\varepsilon^{br} = \frac{\delta}{K \times D} \tag{4.4}$$

where δ is retrieved from the cross-head displacement, and K is two and one for single-shear and double-shear tests, respectively. Therefore, after acquiring these values, bearing stress/bearing strain curves were plotted for all the performed tests. Figure 4.3 shows representative diagrams for the case QI and CP laminate composite joints from 12 plies thick laminates. For all the joints tests, an initial quasi-linear section can be observed, followed by a visible "knee" point. The knee point corresponds to the transition of the load transfer mechanisms from frictional to load bearing. This trend exhibited good repeatability in all tests performed for identical coupons in each corresponding category. From the original load (P) versus displacement (δ) curves transformed into stress (σ^{br}) – strain (ε^{br}) curves through equations (4.3) & (4.4), as illustrated in Figure 4.4, the derived three important joint properties are the ultimate σ^{br}, the 2%-offset-σ^{br}, and the joint bearing stiffness (E^{br}).

Figure 4.4 summarizes these properties for the four configurations studied (QI-8, QI-12, CP-8 and CP-12). It can be seen that there is no thickness effect on the ultimate σ^{br} and 2%-offset σ^{br}. However, for a given thickness, QI displays a higher strength and lower joint bearing stiffness than CP. The same trend for the bearing strength was reported previously [11, 26, 34]. However, the explanations were mainly hypothetical. For example, [34] concludes that «The joint structure possesses its own response characteristics which are beyond extrapolation», while Gamdani et al [26] notice that based on Open-Hole-Tension tests, the quasi-isotropic configuration is slightly less notch sensitive than the cross-ply configuration. However, in a single lap bolted joint configuration (Figure 4.4), CP is significantly weaker that QI and the justification based on notch sensitivity is not sufficient. The effect of secondary bending (SB) in the loss of resistance observed in CP versus

QI, has not been yet proposed, probably due to a lack of direct evidence. Such direct evidence can be provided by a suitable use of the 3D DIC technique as detailed in the next section.

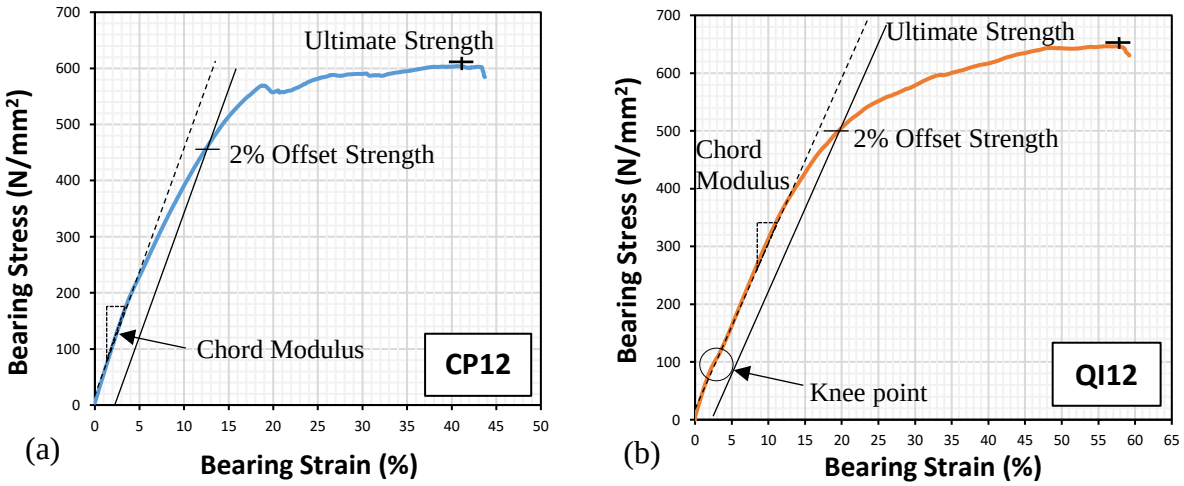

Figure 4.3: Bearing stress/strain curves of three-bolt SL joints: (a) CP12 layers, (b) QI 12 layers.

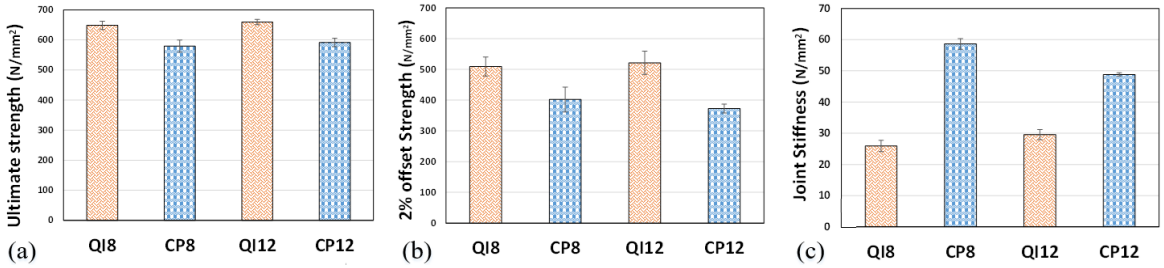

Figure 4.4: Effect of stacking sequence and laminate thickness on (a) ultimate bearing strength (b) 2% offset bearing strength (c) joint bearing stiffness.

4.4.3 Capture of Out of Plane Deformations (OPD) via 3D DIC

Figure 4.5 and 4.6 show the DIC-measured OPDs for each of the four configurations investigated. The dashed red line within the inset pictures in Figure 4.5 and 4.6 shows the path along which the DIC measurements were recorded. The dashed line is located at a distance of 2*d* from the bolt center, where *d* is the bolt-hole diameter. For the face of interest of the joint, the three bolts are labeled as B1, B2, and B3. B1 is the bolt near the free edge, B2 is the central bolt, and B3 is the bolt near the side of the grip. Within this context, it was observed that for all the tests performed, fracture always occurred at B3 via a net tension fracture mode, as reported recently in [27]. To highlight the SB at increasing load levels, the OPD was plotted for 25%, 50%, and 75%

of the failure load (FL). In all the diagrams, the left plot shows the OPD values obtained from the 3D DIC of the dashed red line, and the right plot shows the colorful displacement nephogram. It is noteworthy that the colored bands are not horizontal; this is an indication of the occurrence of a twisting phenomenon (See Appendix A for details).

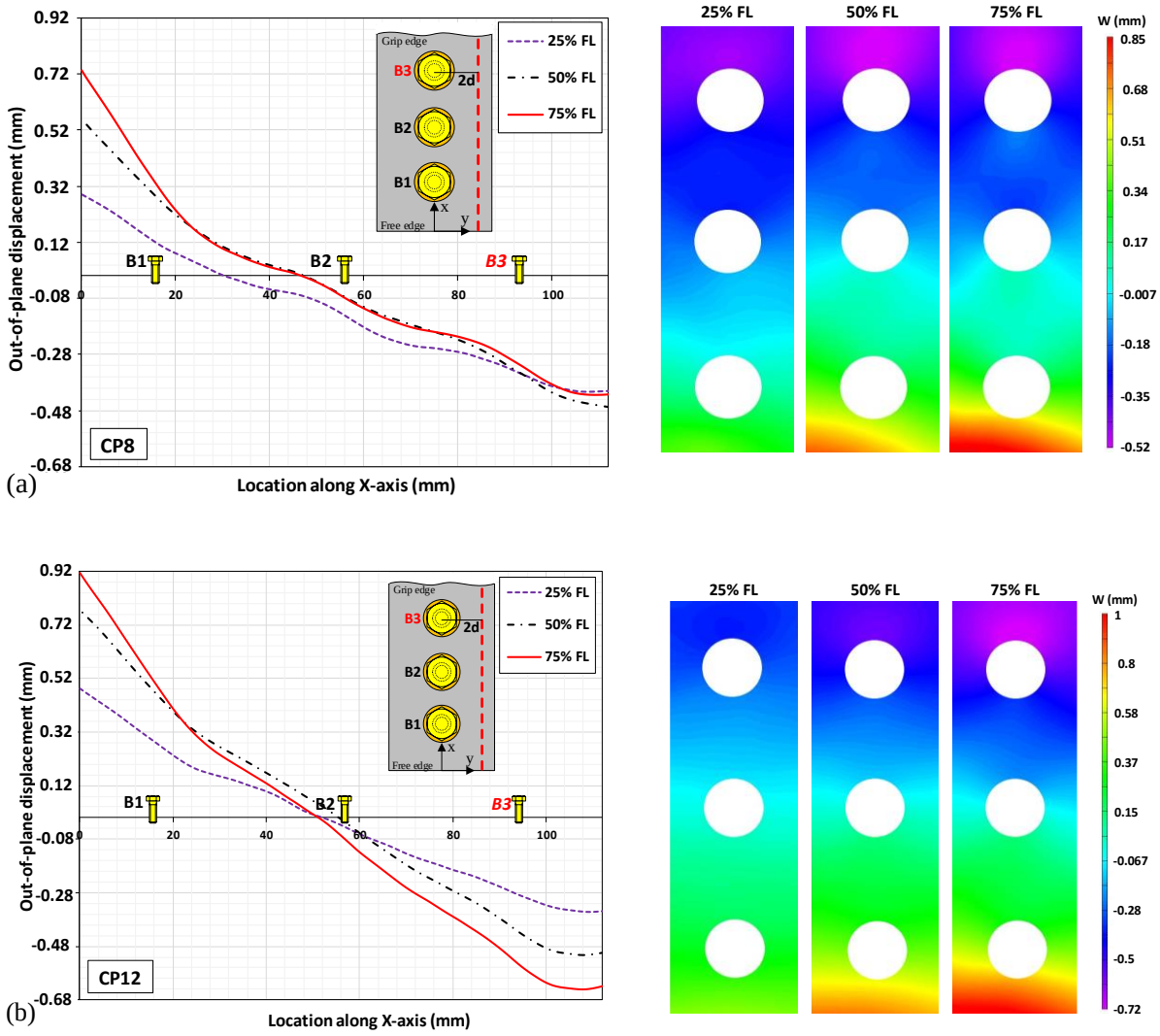

Figure 4.5: Out-of-plane displacements of three-bolt single lap cross-ply (CP) joints at different load levels: (a) 8 layers and (b) 12 layers.

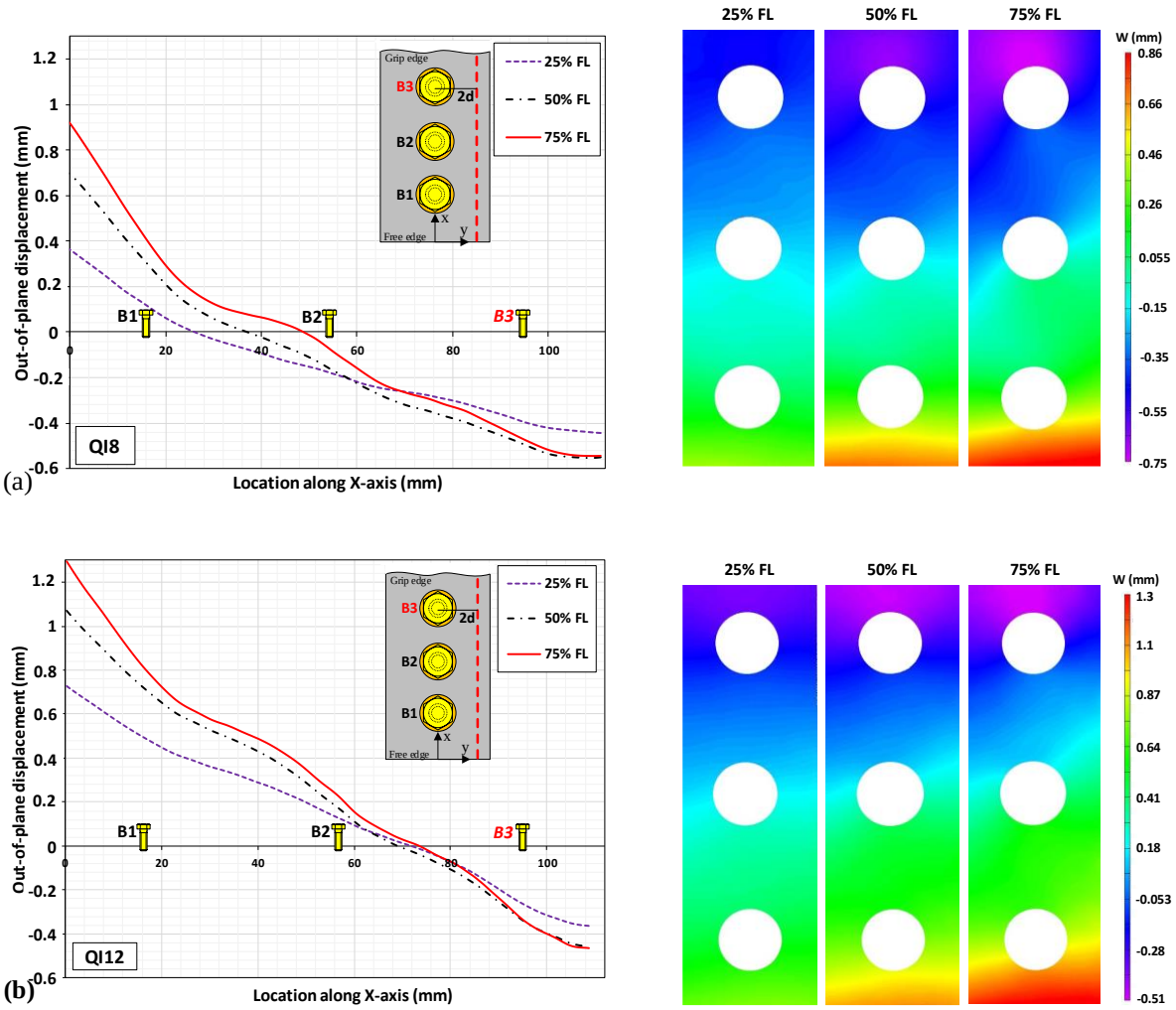

Figure 4.6: Out-of-plane displacements of three-bolt single lap quasi-isotropic (QI) joints at different load levels: (a) 8 layers and (b) 12 layers.

It can be seen for all the curves in Figure 4.5 and 4.6 that the OPD increases with the applied tension load, but the variation is higher in the 25%–50% FL range than in the 50%–75% FL range. This is consistent with the observations regarding Figure 4.2 (a) derived from the NLM, which implies that the eccentricity lessens and the two joint parts become more aligned at the higher level of the applied load. The wavy shape of the OPD curves illustrates the sensitivity of the DIC measurements to local deformations. In fact, numerous bumps are observed in these curves. These bumps show the approximate positions of the bolts. Symmetric bending behavior cannot be expected, with respect to the middle of the joints, specifically in multibolted SL composite joints

with a large overlap length. This asymmetric behavior is likely to be generated owing to (a) twisting in the joints, (b) bolt tilting/slanting, (c) the bolt-hole clearance, (d) defects introduced in the manufacturing process, and (e) the brittle behavior of composite materials. Noteworthy, the thicker joints display more symmetry.

For a given laminate configuration (QI or CP), Figure 4.5 and 4.6 are plotted with the same scale to capture the severity of the OPD in thin and thick plates. The OPDs measured by DIC (Figure 4.5 and 4.6) show that the curve of thick laminates exhibits rather smooth and moderate deflections, whereas that of the thinner laminates experienced more severe local and overall deformations because they were more prone to bolt tilting. This would generate nonlinear deflections on the bolt hole and eventually results in a noticeable induced fluctuation in the SB curves, particularly between the extreme bolts (B1 and B3). With regard to the laminate lay-up, QI underwent noticeable warping primarily around the bolts, as shown in the OPD curves, compared with CP, which can be attributed to the lower bending stiffness of the QI laminates.

Figure 4.7 is another visualization method to illustrate SB in a 3D space. In such an illustration, the bump-like deformation near the B3 bolt is captured accurately. In Figure 4.7, the 3D-view was reconstructed using pixel data values of the surface of interest from the Vic-3D data acquisition. An artificial surface was passed through the point cloud using MATLAB post-processing. The mesh grid of the surface combined with the colorful counter plot distinctly exhibited the induced local/overall deformation and curvature of the joint surface. The effect of bolt rotation on the surface deformation was evident in all three fasteners.

In bolted joints, as the load is increased, the bolt tilts and the bolt head applies pressure on the joint surface through the washer. Consequently, the area below all three fasteners underwent a localized depression and formed a concavity deformation, whereas the area above the bolts bulged out, which can be observed clearly in the 3D and X-Z views as well. The mentioned deformation, which is another demonstration of the bearing stress effect, occurred near all three fasteners and was more appreciable around B3, where the net tensile fracture mode occurred. The induced waviness on the laminate surfaces arising from the depression and lumping, was more noticeable in the thinner plates. This may be attributed to the higher pliability and lower flexural rigidity of the eight-layer laminate.

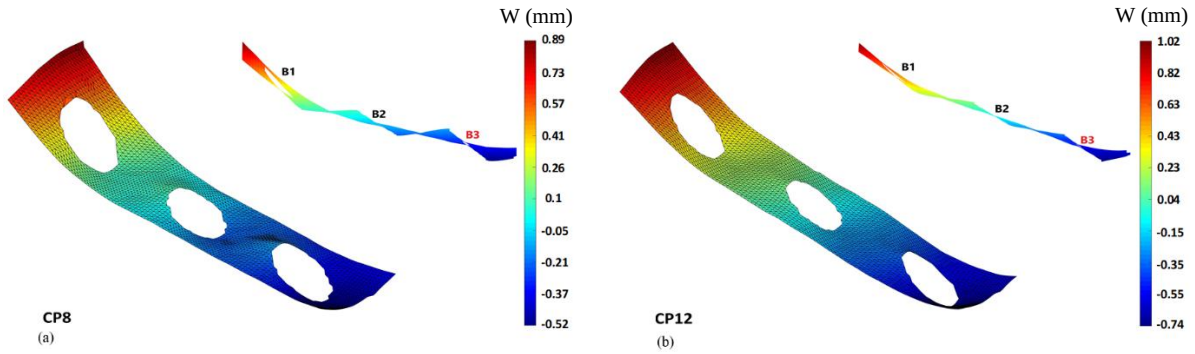

Figure 4.7: 3D nephogram of out-of-plane displacement of (a) cross-ply (CP) 8 and (b) CP 12 configurations.

4.4.4 Quantification of the bending factor

In section 4.4.1, the NLM (Figure 4.2) predicted that QI has more OPD but lower k_b than CP and this means that there is relatively less bending in the QI joints. Concurrently, in section 4.4.2, it was shown that SLJ made of CP laminates displays a surprisingly lower bearing strength σ^{br} than SLJ made from QI laminates. It was proposed that the effect of secondary bending expressed by k_b may be a contributing factor in the pronounced loss of resistance observed in SLJ made of CP. This section intends to provide the experimental equivalent of Figure 4.2 in terms of OPD and k_b (secondary bending). Equation (4.1) defines k_b as the ratio of bending to axial deformations. For the purpose of this investigation and with regard to the available experimental 3D-DIC data, k_b is being defined as:

$$k_b = \delta_{OPD} / d_t \tag{4.5}$$

where δ_{OPD} is the amplitude of out-of-plane displacement provided by the DIC data (Figure 4.5 and Figure 4.6) and d_t is the corresponding axial tensile displacement. The δ_{OPD} and d_t for the four laminate configurations as function of the applied load are presented in Table 4.2. The δ_{OPD} in Table 4.2 are measured between the two extreme bolts and the d_t is also measured between the two extreme bolts. The data from Table 4.2, served to construct Figure 4.8 (a) and (b), which respectively represent the variation of the δ_{OPD} and the bending factor as function of the applied

load. As it can be seen, the general pattern behavior depicted by Figure 4.8 (a) is equivalent to Figure 4.2 (a) and Figure 4.8 (b) is equivalent to Figure 4.2 (b). Figure 4.8 (a) shows that most of the secondary bending materialized by δ_{OPD} occur in the early stages of the loading. The δ_{OPD} almost stabilizes after 50% of the failure load. Also, the fact that bending induces interlaminar shear stresses (ILS) can trigger premature failure should be taken into account. Actually, this behavior is the foundation of the well-known standard short-beam-shear test that measures the ILS strength. Consequently, it can be postulated that because of the induced bending, interlaminar shear cracks develop at the early loading stages and trigger the damage that subsequently weaken the joint strength. It is also remarkable to notice that while according to Figure 4.4 the joint bearing stiffness for CP is almost double that of QI, adversely, in terms of induced secondary bending, Figure 4.8 (a) indicates that the δ_{OPD} in CP is only slightly lower than in QI. Yet, the ratio δ_{OPD} / d_t is significantly higher for CP compared to QI. From a beam theory standpoint [35], acknowledging a relatively high bending displacement combined to a high stiffness indicates that occurrence of high bending stresses. High bending stresses generates high interlaminar shear stresses. All these indications contribute to support the fact that the interlaminar shear stresses are higher in CP than in QI and explains why SLJ made of CP laminates displays a surprisingly lower bearing strength σ^{br} than SLJ made from QI laminates.

The present finding can be used to explain the behavior reported by Skorupa et al [13]. Reporting on the effect of secondary bending for riveted lap joints, Skorupa et al [13] noticed that reducing the thickness of the sheets and increasing the distance between rivet rows lead to considerably longer fatigue lives. The geometry effect described by Skorupa et al [13] can be explained by the well known effect of the length-to-thickness ratio in bending [36] where it is shown that larger length-to-thickness ratio do not favor interlaminar shear stresses. In other words, the increased spacing decreased the SB, which in turn disadvantaged the interlaminar shear stresses, a source of premature failure.

Table 4.2: Effect of the laminate thickness and stacking sequence on the bending factor.

	QI-8	QI-8	QI-8		CP-8	CP-8	CP-8
	25% FL	50% FL	75% FL		25% FL	50% FL	75% FL
δ_{OPD}, mm	0.49	0.76	0.85	δ_{OPD}, mm	0.44	0.61	0.63
d_t, mm	0.47	1.38	2.69	d_t, mm	0.29	0.90	1.56
δ_{OPD} / d_t	1.04	0.55	0.31	δ_{OPD} / d_t	1.51	0.68	0.40
	QI-12	QI-12	QI-12		CP-12	CP-12	CP-12
	25% FL	50% FL	75% FL		25% FL	50% FL	75% FL
δ_{OPD}, mm	0.73	1.02	1.10	δ_{OPD}, mm	0.56	0.87	1.02
d_t, mm	0.56	1.34	2.16	d_t, mm	0.36	0.90	1.56
δ_{OPD} / d_t	1.29	0.76	0.51	δ_{OPD} / d_t	1.55	0.97	0.65

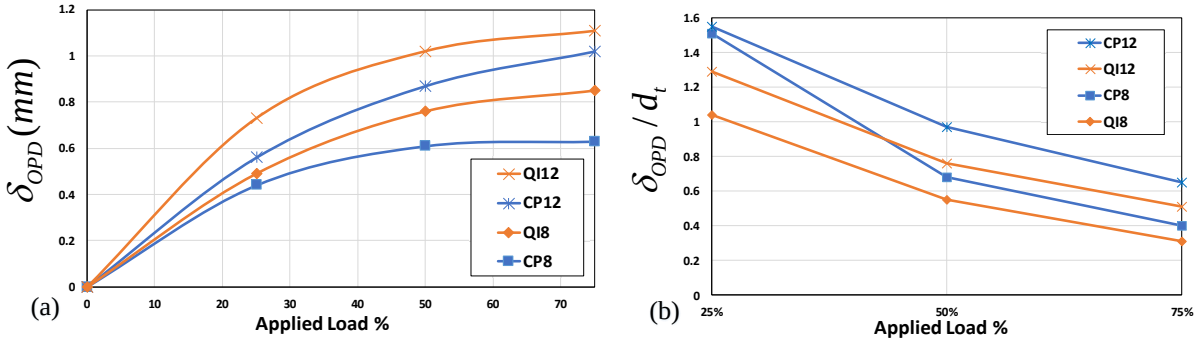

Figure 4.8: Effect of the laminate thickness and stacking sequence on: (a) δ_{OPD} and (b) the bending factor.

4.5 Conclusion

Literature reports several studies on the relative weakness of single-lap bolted joints of laminated composites, however, the existing knowledge is not yet enough to establish a complete understanding of this subject. For example, the tensile strength of composite cross-ply laminates (CP) is higher than that of quasi-isotropic laminates (QI) due to the higher ply content of 0°. From standard Open-Hole-Tension (OHT) and Filled-Hole-Tension (OHT) tests, it is observed that the strength of CP laminates is so affected that it becomes comparable to that of QI laminates. This behavior is explained by the higher notch sensitivity of CP laminates. However, when these laminates are tested for the tensile strength of multi-bolt single-lap joints (SLJ), the strength of joints made from CP laminates is significantly lower than that from QI laminates. Clearly, the higher notch sensitivity of CP laminates does not fully explain the extent of their strength reduction in an SLJ configuration. This investigation is based on the hypothesis that one of the phenomena, which contributes to this inverted behavior, is the induced secondary bending (SB) in the SLJ. This investigation combines analytical and experimental methods to prove this hypothesis. The secondary bending (SB) of single lap (SL) three-bolt carbon/epoxy composite joints was investigated via 3D DIC as a function of stacking sequence and laminate thickness. To characterize this effect analytically, a neutral line model (NLM) was used.

The results obtained show that:

- NLM results demonstrated that thicker joints exhibited larger out-of-plane displacement (OPD) and bending factor (k_b). This behavior was verified by the DIC measurements.
- NLM results demonstrated for the same thickness, quasi-isotropic (QI) exhibited a larger OPD than cross-ply (CP) but lower bending factor (k_b). This behavior was verified by the DIC measurements.
- Although named the «bending factor», mathematically speaking, k_b is not more related to bending than it is related to extension. k_b is a dimensionless ratio expressing the simultaneous occurrence of bending and extension. A joint with a higher k_b undergoes relatively more bending, which does not necessarily mean more out-of-plane deformation.
- The joint bearing stiffness for CP is almost double that of QI. However, induced secondary bending is higher for CP compared to QI. These features indicate that the interlaminar shear

stresses are higher in CP than in QI and explains why SLJ made of CP laminates displays a surprisingly lower bearing strength σ^{br} than SLJ made from QI laminates.

- Both the NLM and the DIC results show that most of the out-of-plane displacement occur in the early stages of the loading. Consequently, it is postulated that because of the induced bending, interlaminar shear cracks develop at the early loading stages and trigger the damage that subsequently weaken the joint strength.

4.6 Acknowledgments

The authors acknowledge the financial support provided by the Natural Sciences and Engineering Research Council of Canada (NSERC) and the Consortium for Research and Innovation in Aerospace in Quebec (CRIAQ). We also thank Bombardier Aerospace, L-3 Communications and Delastek Aeronautique Inc. for their valuable support.

4.7 References

[1] J. Ekh, J. Schön, L.G. Melin, Secondary bending in multi fastener, composite-to-aluminium single shear lap joints, Composites Part B: Engineering 36(3) (2005) 195-208. doi:https://doi.org/10.1016/j.compositesb.2004.09.001.

[2] J. Schijve, Some elementary calculations on secondary bending in simple lap joints, Nationaal Lucht-en Ruimtevaartlaboratorium, 1972.

[3] A. Hartman, J. Schijve, The effect of secondary bending on the fatigue strength of 2014-T3 Alclad riveted joints, Nationaal Lucht-en Ruimtevaartlaboratorium, 1969.

[4] D. Schütz, H. Lowak, The effect of secondary bending on the fatigue strength of joints, Report FB-113, Darmstadt: Laboratorium für Betriebsfestigket (1974).

[5] L. Jarfall, Shear loaded fastener installations, International Journal of Vehicle Design 7(3-4) (1986) 337-380. doi:https://doi.org/10.1504/IJVD.1986.061155.

[6] R.P.G. Muller, An experimental and analytical investigation on the fatigue behaviour of fuselage riveted lap joints: The significance of the rivet squeeze force, and a comparison of 2024-T3 and Glare 3, (1997).

[7] T. Ireman, Three-dimensional stress analysis of bolted single-lap composite joints, Composite structures 43(3) (1998) 195-216. doi:https://doi.org/10.1016/S0263-8223(98)00103-2.

[8] G. Segerfrojd, A. Blom, Fatigue behavior of mechanical joints: a state-of-the-art overview, Higher Education Press, Fatigue'99: Proceedings of the Seventh International Fatigue Congress., 1999, pp. 41-56.

[9] T. Ireman, T. Ranvik, I. Eriksson, On damage development in mechanically fastened composite laminates, Composite Structures 49(2) (2000) 151-171. doi:https://doi.org/10.1016/S0263-8223(99)00130-0.

[10] J. Ekh, J. Schön, Effect of secondary bending on strength prediction of composite, single shear lap joints, Composites Science and Technology 65(6) (2005) 953-965. doi:https://doi.org/10.1016/j.compscitech.2004.10.020.

[11] M.A. McCarthy, C.T. McCarthy, V.P. Lawlor, W.F. Stanley, Three-dimensional finite element analysis of single-bolt, single-lap composite bolted joints: part I—model development and validation, Composite Structures 71(2) (2005) 140-158. doi:https://doi.org/10.1016/j.compstruct.2004.09.024.

[12] J. Schijve, G. Campoli, A. Monaco, Fatigue of structures and secondary bending in structural elements, International Journal of Fatigue 31(7) (2009) 1111-1123. doi:https://doi.org/10.1016/j.ijfatigue.2009.01.009.

[13] M. Skorupa, A. Korbel, A. Skorupa, T. Machniewicz, Observations and analyses of secondary bending for riveted lap joints, International Journal of Fatigue 72 (2015) 1-10. doi:https://doi.org/10.1016/j.ijfatigue.2014.10.008.

[14] P.J. Gray, C.T. McCarthy, A global bolted joint model for finite element analysis of load distributions in multi-bolt composite joints, Composites Part B: Engineering 41(4) (2010) 317-325. doi:https://doi.org/10.1016/j.compositesb.2010.03.001.

[15] A. Olmedo, C. Santiuste, E. Barbero, An analytical model for the secondary bending prediction in single-lap composite bolted-joints, Composite structures 111 (2014) 354-361. doi:https://doi.org/10.1016/j.compstruct.2014.01.015.

[16] L. Zhao, A. Xin, F. Liu, J. Zhang, N. Hu, Secondary bending effects in progressively damaged single-lap, single-bolt composite joints, Results in physics 6 (2016) 704-711. doi:https://doi.org/10.1016/j.rinp.2016.08.021.

[17] K. Zhang, J. Hu, P. Zou, Y. Cheng, B. Luo, H. Cheng, Effect of secondary bending and bolt load on damage and strength of composite single-lap interference-fit bolted structures, Journal of

Composite Materials (2019) 0021998319857463. doi:https://doi.org/10.1177%2F0021998319857463.

[18] A. Bernasconi, M. Carboni, R. Ribani, On the combined use of Digital Image Correlation and Micro Computed Tomography to measure fibre orientation in short fibre reinforced polymers, Composites Science and Technology (2020) 108182. doi:https://doi.org/10.1016/j.compscitech.2020.108182.

[19] A. Djabali, L. Toubal, R. Zitoune, S. Rechak, Fatigue damage evolution in thick composite laminates: Combination of X-ray tomography, acoustic emission and digital image correlation, Composites Science and Technology 183 (2019) 107815. doi:https://doi.org/10.1016/j.compscitech.2019.107815.

[20] G. Seon, A. Makeev, J. Cline, B. Shonkwiler, Assessing 3D shear stress–strain properties of composites using Digital Image Correlation and finite element analysis based optimization, Composites Science and Technology 117 (2015) 371-378. doi:https://doi.org/10.1016/j.compscitech.2015.07.011.

[21] B. Egan, C. McCarthy, M. McCarthy, P. Gray, R. Frizzell, Modelling a single-bolt countersunk composite joint using implicit and explicit finite element analysis, Computational Materials Science 64 (2012) 203-208. doi:https://doi.org/10.1016/j.commatsci.2012.02.008.

[22] P.J. Gray, R.M. O'Higgins, C.T. McCarthy, Effect of thickness and laminate taper on the stiffness, strength and secondary bending of single-lap, single-bolt countersunk composite joints, Composite Structures 107(Supplement C) (2014) 315-324. doi:https://doi.org/10.1016/j.compstruct.2013.07.014.

[23] Y. Zhai, D. Li, X. Li, L. Wang, Y. Yin, An experimental study on the effect of bolt-hole clearance and bolt torque on single-lap, countersunk composite joints, Composite structures 127 (2015) 411-419. doi:https://doi.org/10.1016/j.compstruct.2015.03.028.

[24] Y. Zhai, D. Li, X. Li, L. Wang, An experimental study on the effect of joining interface condition on bearing response of single-lap, countersunk composite-aluminum bolted joints, Composite Structures 134 (2015) 190-198. doi:https://doi.org/10.1016/j.compstruct.2015.08.078.

[25] C. Barile, C. Casavola, G. Pappalettera, P.K. Vimalathithan, Characterization of adhesive bonded CFRP laminates using full-field digital image stereo-correlation and finite element analysis, Composites Science and Technology 169 (2019) 16-25. doi:https://doi.org/10.1016/j.compscitech.2018.10.032.

[26] F. Gamdani, R. Boukhili, A. Vadean, Tensile strength of open-hole, pin-loaded and multi-bolted single-lap joints in woven composite plates, Materials & Design 88 (2015) 702-712. doi:https://doi.org/10.1016/j.matdes.2015.09.008.

[27] F. Gamdani, R. Boukhili, A. Vadean, Tensile behavior of hybrid multi-bolted/bonded joints in composite laminates, International Journal of Adhesion and Adhesives 95 (2019) 102426. doi:https://doi.org/10.1016/j.ijadhadh.2019.102426.

[28] ASTM-D5961/D5961M-13, Standard Test Method for Bearing Response of Polymer Matrix Composite Laminates, ASTM International, 100 Barr Harbor Drive, PO Box C700, West Conshohocken, PA 19428-2959. United States, 2013.

[29] S.H. Daly, Digital image correlation in experimental mechanics for aerospace materials and structures, Encyclopedia of Aerospace Engineering (2010). doi:https://doi.org/10.1002/9780470686652.eae542.

[30] H. Schreier, J.-J. Orteu, M.A. Sutton, Image correlation for shape, motion and deformation measurements, Springer US2009.

[31] J. Schijve, Fatigue of structures and materials, Springer Science & Business Media2001.

[32] A. Skorupa, M. Skorupa, Riveted lap joints in aircraft fuselage: design, analysis and properties, Springer Science & Business Media2012.

[33] M. McCarthy, V. Lawlor, W. Stanley, C. McCarthy, Bolt-hole clearance effects and strength criteria in single-bolt, single-lap, composite bolted joints, Composites science and technology 62(10-11) (2002) 1415-1431. doi:https://doi.org/10.1016/S0266-3538(02)00088-X.

[34] J. Hu, K. Zhang, Q. Yang, H. Cheng, P. Liu, Y. Yang, An experimental study on mechanical response of single-lap bolted CFRP composite interference-fit joints, Composite Structures (2018). doi:https://doi.org/10.1016/j.compstruct.2018.05.016.

[35] P.K. Mallick, Fiber-reinforced composites: materials, manufacturing, and design, CRC press2007.

[36] R. Boukhili, P. Hubert, R. Gauvin, Loading rate effect as a function of the span-to-depth ratio in three-point bend testing of unidirectional pultruded composites, Composites 22(1) (1991) 39-45. doi:https://doi.org/10.1016/0010-4361(91)90101-L.

CHAPTER 5 ARTICLE 2: 3D-DIC STRAIN FIELD MEASUREMENTS IN BOLTED AND HYBRID BOLTED-BONDED JOINTS OF WOVEN CARBON-EPOXY COMPOSITES

Published in: Journal of Composite Part B: Engineering, April 2021

Masoud Mehrabian, Rachid Boukhili*

Department of Mechanical Engineering, Polytechnique Montreal, Quebec H3C 3A7, Canada

5.1 Abstract

In this study, the 3D digital image correlation (3D-DIC) technique is extensively used to explain the tensile behaviors of single-lap only bolted (OB) and hybrid bolted-bonded (HBB) joints via measurement of strain distribution and secondary bending/twisting, as well as balance between bypass and bearing loads. Single-lap multi-bolt joints made of woven carbon-fiber-reinforced epoxy composite laminates were tested using quasi-isotropic and cross-ply configurations for two thicknesses. The 3D-DIC analysis clearly shows that hybridization produces two positive effects: (a) it relieves stress concentration around the bolts and delays damage initiation and thereby the final fracture; (b) it reduces the secondary bending and twisting phenomena and thereby the associated deleterious effects. Moreover, hybridization was found to be more beneficial in thinner multi-bolt single-lap composite joints, where strength retention was doubled. It was also found that the 3D-DIC data depicted the balance between bypass and bearing loads, which is important for the behavioral analysis of multi-bolt fastened joints in general. The competing actions of the bypass and bearing stresses in each joint configuration were measured by tracking the strain evolutions in the regions under the bolts. For increasing applied loads, the bypass action corresponded to increasing strain and bearing action corresponded to decreasing strain.

Keywords

Composites, Bonding, Bolting, Hybrid joints, DIC, Bypass.

---

* Corresponding author.

E-mail address: rachid.boukhili@polymtl.ca (R. Boukhili).

5.2 Introduction

Composite structures have the advantage of maintaining the integrity of a structure by allowing for the production of large and complex components by simple molding, unlike conventional metal structures, which require numerous joints. However, it does not deny the need for joints in composite structures. Reliable applications of composite materials highly depend on using suitable choices for the joining technique as well as laminate lay-up, which are essential for providing safe load-transfer mechanisms and higher mechanical joint efficiencies [1, 2]. There are three main types of joints in composite structures: mechanically fastened, adhesively bonded, and hybrid bolted-bonded (HBB) joints. The former two joining methods have been widely studied for many years, while the latter is still in the early stages of research and development; therefore, it requires extensive research to achieve scientific maturity [3].

Studies concerning bolted-bonded composite joints started in the 1980s, with a series of works by Hart-Smith [4-6]. In 2001, Fu and Mallick [7] studied the fatigue responses of HBB composite joints, and their results showed that hybrid joints have higher static failure loads and longer fatigue lives than adhesive joints. Kelly [8, 9] conducted comprehensive research on single-lap (SL) single-bolted hybrid composite joints, where the load distributions, strengths, and fatigue lives of the hybrid composite joints were analyzed. Analytical models were developed to evaluate the stress [10], predict load transfer in bolts and adhesive joints, and predict the strengths of the bolted-bonded composite joints [11]. Bodjona et al. [12-16] conducted studies on the mechanical behaviors of composite bolted-bonded SL single-bolt joints. A developed computational model showed that significant load sharing occurred in HBB joint, with the bolt carrying up to 40% of the overall applied load [12]. It was found that the adhesive yield strength is the single most important factor in load sharing [13], and such load sharing could be improved using an interference fit [15]. Their recent study showed that for high-compliance adhesives, the addition of fasteners significantly delayed initial failure [16]. Experimental and finite element (FE) studies on multi-bolt thin HBB double lap joints and thick HBB step lap joints were performed by Chowdhury et al. [17-19], who concluded that in HBB step lap joints, placing fasteners closer to the ends of the overlap was vital to suppressing the peak peeling stresses and delaying the effects of early crack initiation [18]. Moreover, the bolts may also act as adhesive bond failsafe mechanisms to prevent sudden catastrophic failures [19]. The design of experiments (DOE) by Lopez-Cruz et al. suggested that in

SL single-bolt HBB composite joints, the strength was mainly governed by adherend thickness, adhesive mechanical properties, and bolt-hole clearance [3].

The number of bolts used in HBB joints is a key parameter for determining the joint load capacity. A semi-analytical model, developed by Paroissien et al. [20], demonstrated that if two bolts are used, the adhesive failure propagates up to the middle of the overlap; thereafter, the fasteners carry the load, similar to a pure bolted joint. Gamdani et al. [21, 22]; their results showed that addition of the adhesive increased the strengths of the three bolt joints by 70% for cross-ply and 30% for quasi-isotropic laminates. It was also found that the outer bolts limited the peel stresses (suggesting that only outer bolts are required in multi-bolt HBB joints), and the adhesive reduced the stress concentration around the bolts. Recent studies on single-bolt hybrid joints have shown that the stacking sequence and *W/D* ratio (*W* is the specimen width and *D* is the hole diameter) are important in the design of hybrid joints [2, 23]. Digital image correlation (DIC) technology provides an easy-to-use non-contact approach to study the behaviors of any type of structure. Researchers have used this technique for composite joints [20, 24-27] yet there remains much to benefit from the maximum potential of the DIC. Recently, the authors used DIC to quantify the secondary bending effects in multi-bolt SL composite joints [28].

According to a previous review on HBB joints [29] and to the best of the authors' knowledge, there is still a substantial lack of knowledge regarding the behaviors of multi-bolt HBB composite joints, and the DIC approach could be of great assistance to explore this topic. The present study aims to analyze the effects of hybridization (adding adhesives between two joint parts) on the strengths, strain distributions, and out-of-plane displacements of multi-bolt single-lap carbon-epoxy composite joints using 3D-DIC technology. In this work, two well-known composite lay-ups, namely the cross-ply (CP) and quasi-isotropic (QI) types, were manufactured using plain weave fabrics. The reason for choosing these configurations is that first, it is recognized that plain weave fabrics (0/90) are commonly used in composites industry because of their ease of manufacturing and advantageous performance/cost ratio. Generally, CP configurations are suitable for most applications, and part fabrications are straightforward, with minimal material wastage. However, if rigidity along the 45° axis is required, or if the structure experiences torsional stress, then the QI configuration yields superior performance, with turning 0/90 woven plies at 45°.

5.3 Experimental procedure

5.3.1 Material and specimen preparations

Carbon-fiber-reinforced epoxy (CFRE) panels were manufactured by the Vacuum Assisted Resin Infusion (VARI) process using the epoxy resin Araldite Renlnfusion 8601/Ren 8602 provided by Huntsman Advanced Materials Americas. In this study, the CFRE composite laminates were composed of either 8 or 12 layers of the 3K plain weave carbon fabric having a surface weight of 193 g/m^2 (5.7 oz/yd^2) [22, 30]. Two different laminate stacking sequences were designed, namely cross-ply (CP) and quasi-isotropic (QI) sequences, whose lay-up and average thickness (after the recommended curing cycle of 24 h) are given in Table 5.1.

Table 5.1: Stacking sequences of the manufactured laminates.

Code	Lay-up	Plies	Average thickness (*t*, mm)
CP8	$[(0/90)/(0/90)/(0/90)/(0/90)]_s$	8	1.65
QI8	$[(0/90)/(\pm45)/(0/90)/(\pm45)]_s$	8	
CP12	$[(0/90)/(0/90)/(0/90)/(0/90)/(0/90)/(0/90)]_s$	12	2.63
QI12	$[(0/90)/(\pm45)/(0/90)/(\pm45)/(0/90)/(\pm45)]_s$	12	

In the lay-up displayed above, (0/90) or (±45) indicates a single layer of each woven ply, which is fabricated from weft yarns woven over and under the warp thread. For all the composite laminates, the warp side was oriented toward the zero direction. The QI lay-up involves 45° fiber placement; thus, a (0/90) cut woven fabric is simply rotated to obtain the (±45) orientation [30].

Single-shear multi-bolted joints were designed and manufactured according to ASTM-D5961 [31]. To fasten the two parts in SL only bolted (OB) joints, steel hex head shear bolts (NAS6204-4) of diameter 6.35 mm as well as nuts (MS21042-4) and cadmium-plated steel washers (NAS1149F0463P) of internal diameter 6.73 mm and external diameter 12.70 mm for both the head and nuts sides were utilized. A tightening torque of 5 Nm was applied to each bolt using the Tohnichi Dial Torque Wrench DB25N-S. A specialized carbide drill of diameter 6.35 mm, obtained

from YG-1 America, Inc., was used to drill the CFRP specimens. Additionally, a wooden sacrificial back-up plate was placed under the specimen to prevent delamination or laminate defects upon push-out of the drill. The only difference between the OB and HBB joints is the application of an adhesive between the faying surfaces. The adhesive used for these joints was the same epoxy resin used to manufacture the composite laminate [22]. For all bonding purposes, a mat surface was used because the application of the peel ply resulted in a sufficiently rough surface texture, which provided the desired bonding characteristics for the faying surfaces.

Obtaining an approved bonding between the joint components requires a controlled system to exert uniform pressures on both surfaces, to allow uniform propagation of the epoxy between the two mat faces. To achieve this, the joint assembly was wrapped in a vacuum bag to provide uniform pressure. Throughout this paper, prefixes OB and HBB are used to indicate the laminate code, e.g., HBB-QI8, to specify the class of configuration as either OB or HBB joint, respectively. The geometrical configurations of the SL OB and HBB composite joints are shown in Figure 5.1. The composite panels were bonded to the specimens as doublers; further, the specimen surface preparation for DIC testing is outlined in [28].

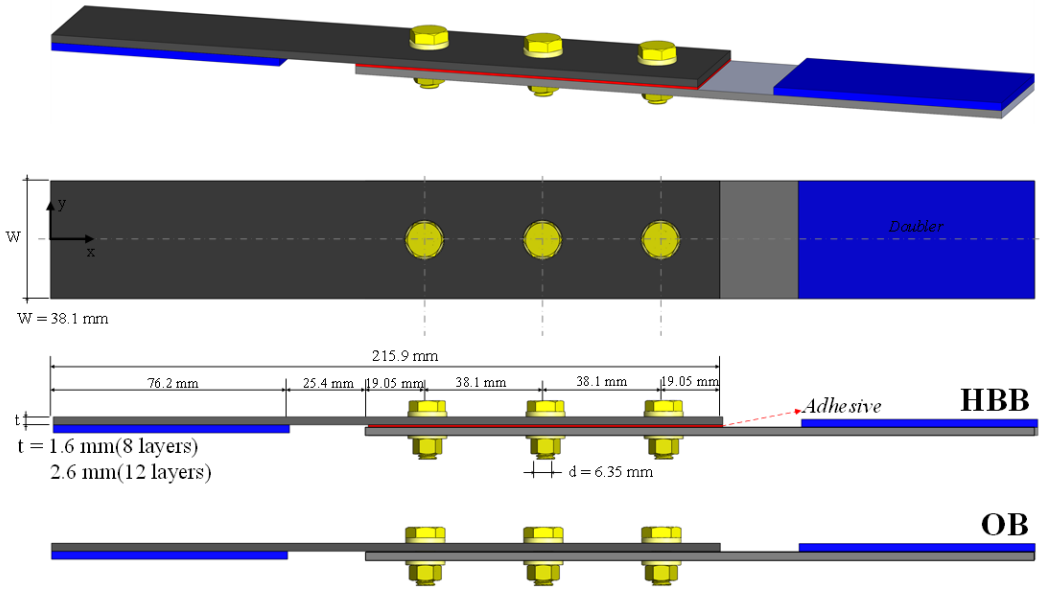

Figure 5.1: Specimen geometry and dimensions used for OB and HBB SL joints.

5.3.2 Test set-up and procedure

For each category of OB and HBB SL joints, at least four identical specimens were tested at a constant standard cross-head displacement rate of 2 mm/min under ambient conditions. All mechanical tests were performed on a servo-hydraulic MTS testing machine (model 810) with a load capacity of 100 kN. In this study, the 3D-DIC method was used extensively to measure the full-field strains and out-of-plane displacements of the surfaces of interest. The principle of this optical non-contact measurement technique is based on tracking (or calculating) random patterns on the specimen surfaces via matching the local distributions of pixel concentrations, i.e., subsets, between the un-deformed and deformed images during specific time intervals. The surface deformation is computationally achieved by optimizing a cross-correlation or least-squares function to evaluate the degree of similarity between the undeformed and deformed specimens in terms of grayscale intensity values [32]. The 3D-DIC system and software used were the Vic-3D v 7.2.4 model from Correlated Solutions Inc. (CSI), USA.

When mounting the DIC setup, once the tripod, cameras, lighting locations are determined and the cameras focus and aperture have been adjusted, calibration should be performed. The 3D calibration procedure calculates variables about the camera imaging and geometry in order to calibrate the intersection of two optical rays formulated in a common coordinate system, known as being a stereo-triangulation process [33]. This requires choosing an appropriate calibration panel (dotted panels supplied by the manufacturer), the size of which should approximately fill the field of view. The selected calibration panel is placed at the location of the specimen (in between the grips), then moved manually in the three axes of translation, and rotated around all the three axes, while an average of six images per axis are captured. Based on the knowledge of the calibration panel geometry, the calibration system has recognition software that identifies the correspondences between target points from the captured images [33]. This also allowed the DIC software to locate each individual target point in 3D space. When the calibration process completed, the software gives the calibration score which is recommended from the company to have a 0.05 score and below. For all the performed tests, an accepted and very low score were achieved which guaranties good quality results.

Furthermore, the two charge-coupled device (CCD) cameras of the 5 megapixel Pointgrey Grasshopper type were used, having pixel sizes of 3.45 **µm** for the camera sensors. However, the

pixel size of the specimen can vary depending on the lens and distance from the specimen, which in this study is approximately 18.5 pixel/mm. With the utilized system and according to the specifications provided by CSI, the in-plane displacement resolution was estimated as FOV/100,000, and the out-of-plane displacement was estimated as FOV/50,000, where FOV is the width of the field of view (FOV of the performed test was approximately 120 mm, so, the in-plane and out-of-plane displacement measurement resolutions are about +/- 1.2 μm and +/- 2.4 μm). The strain resolution estimation was more complex, but was approximately 50 micro-strain locally. In order to have proper focal characteristics, cameras were placed at a distance of approximately 1.5 m from the specimen with a focal length of about 23000 pixels for each camera. A black speckle pattern was applied onto the white specimens using black archival ink and a roller stamp with dot sizes of 0.026 inches in diameter, which was the smallest appropriate speckle size available. The applied speckle pattern allowed a subset size of 29 pixels with the selected step size of 7 pixels. It is noteworthy that there is no particular standard for the accuracy of the entire DIC system because of variability with pattern quality, setup, focus, lighting, etc. However, according to experience and meticulous testing, the accuracy estimates are conservative, and the level of uncertainty quantification in the results is very low, which ensures accuracy of computation.

5.4 Results and discussion

5.4.1 Verification of the 3D-DIC measurements using real strain gauges

In this section, a comparative study is presented to demonstrate the accuracy and reliability of DIC measurements; therefore, the DIC results were compared to those obtained using conventional strain gauges (SGs). A comparative study was performed on the cross-ply material CP12 using standard tensile tests according to ASTM D3039 [34]. It is emphasized that the composite plates manufactured by VARI are characterized by two distinct surfaces, namely a glossy surface that corresponds to the glossy face of the mold and a mat surface that corresponds to removal of the peel-ply layer after molding. In this study, the SG was bonded to the mat surface, while the DIC speckles were painted on the glossy surface. Figure 5.2 (a) shows the SG bonded to the mat surface, and Figure 5.2 (b) shows the DIC speckles on the back side (glossy surface) along with the position of the virtual SG (Vic-3D DIC), whose dimensions correspond to those of the real SG. To ensure that the measurements obtained with the real and Vic-3D DIC SGs correspond

to the same material region, a white paper marked with three parallel lines was lightly attached on the back side, as shown in Figure 5.2 (b).

Figure 5.3 (a) shows the stress–strain curves obtained from the DIC and real longitudinal strain gauge (SG-L). The modulus of elasticity values computed by the DIC and SG-L are 56726 MPa and 55468 MPa, respectively, and the difference between the results of the DIC and real SG were within the range of experimental errors. Moreover, the corresponding strain-time curve is illustrated in Figure 5.3 (b) in which the strain evolution is compared between the DIC and SG-L during the tensile process. The maximum strain recorded by the two methods is all about 0.4%. This comparison confirms the accuracy of the DIC apparatus used in this study.

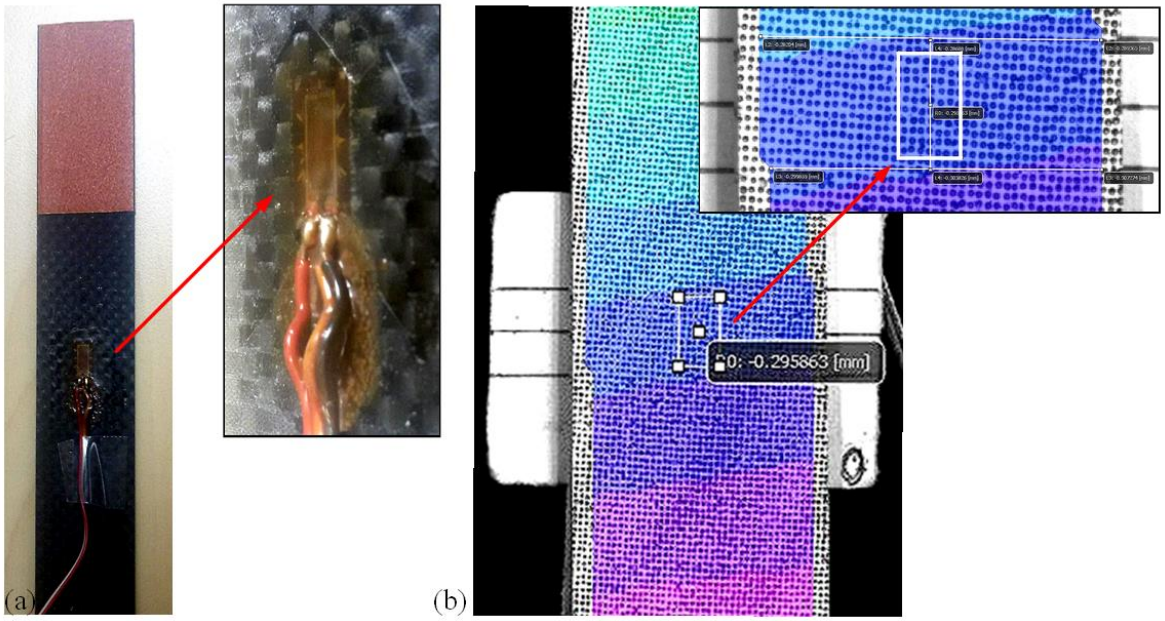

Figure 5.2: (a) Installed SG on the mat surface and (b) locating the virtual strain gauge via Vic-3D.

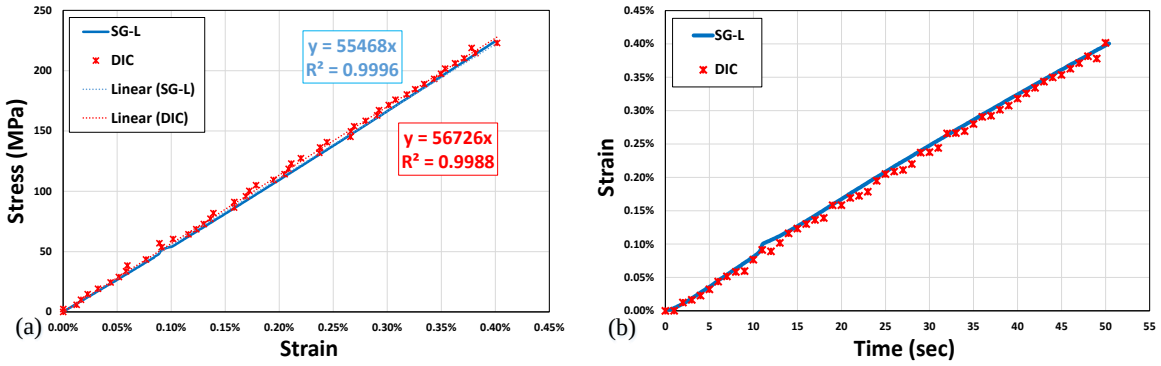

Figure 5.3: Axial strains from the DIC and longitudinal strain gauge (SG-L) versus (a) applied stress, and (b) time.

5.4.2 Strength characteristics of the investigated composite laminates and fastened assemblies

Table 5.2 summarizes all the test results in terms of strength and from three parts. Part-1 includes the unnotched Tensile Strength (TS), the Open-Hole-Tension (OHT), OB, and HBB parts. Part-2 shows the values of the OHT, OB, and HBB normalized by TS. Part-3 reports the OB and HBB values normalized by the OHT strength. All these properties are reported for cross-ply (CP) and quasi-isotropic (QI) configurations and for two laminate thicknesses (8 and 12 plies).

Table 5.2: Strength characteristics of the investigated composite laminates and fastened assemblies.

	Part 1				Part 2			Part 3		
	TS strength in MPa (STD)	OHT strength in MPa (STD)	OB strength in MPa (STD)	HBB strength in MPa (STD)	OHT/TS	OB/TS	HBB/TS	OB/OHT	HBB/OHT	Increase of HBB vs OB
CP8	854 (30)	455 (10)	279 (9)	559 (11)	53%	33%	65%	61%	123%	100%
QI8	592 (9)	384 (7)	326 (11)	494 (16)	65%	55%	83%	85%	129%	52%

CP12	800 (15)	406 (8)	289 (7)	443 (10)	51%	36%	55%		71%	109%	53%
QI12	579 (9)	364 (8)	317 (6)	392 (17)	63%	55%	68%		87%	108%	24%

The most notable feature of Part 1 of Table 5.2 is the fact that with regard to the bolted joints, QI laminates exhibit higher strengths than CP laminates. Therefore, if a woven laminate composite part is intended to be bolted, the QI configuration should be preferred. This also means that the standard OHT resistance is not a reliable indicator of the bolted joint behavior as might sometimes be suggested [35]. In other words, the behavior of the bolted joint is not only controlled by the presence of the hole and its related stress concentration but also controlled by the secondary bending phenomena and associated early delamination, as reported recently [28]. Interestingly, Table 5.2 shows that the addition of the adhesive (HBB) restores the strength rankings of the CP joints over QI (4^{th} column of Part-1). This behavior suggests that hybridization has two positive effects: (a) it relieves the stress concentration around the bolts and delays damage initiation and thereby the final fracture [22]; (b) it diminishes the secondary bending phenomena and hence the associated deleterious effects. Although these may initially seem logical, these explanations are only hypotheses and must be demonstrated experimentally, which is precisely the purpose of using DIC measurements in section 3.4. The purpose of normalization in Part-2, is to determine the stress concentration variation for each situation (OHT, OB, and HBB). Usually, the severity of stress concentration is judged using the OHT/TS ratio; accordingly, it is clear that the CP type is more notch sensitive than the QI type.

The purpose of OB/OHT normalization is to introduce additional mechanisms (other than stress concentration around the hole) that are specifically associated with OB SL joint conjugations. The additional mechanisms are the bearing contact and secondary bending phenomena, and their impacts are equivalent to that of the stress concentration around the hole. The purpose of HBB/OHT normalization is to determine the extent to which the presence of the adhesive helps bypass the deleterious effects of stress concentration around the hole and secondary bending,

thereby improving the joint strength. The multi-bolted joint retains only one-third of the tensile strength of the pristine material, as seen for thin cross-ply plates (CP8). However, if an adhesive is added (HBB), the strength retention is doubled for thin plates. Another proof of the effectiveness of hybridization in thinner joints is shown in Figure 5.4. Observations of the fracture surfaces illustrate that the failure modes in both HBB-CP12 and HBB-QI12 (Figure 5.4 (b) and (d)) are a combination of cohesive and adhesive failures, while that of the 8-layer is a combination of cohesive and light-fiber-tear failure (LFTF) (Figure 5.4 (a) and (c)). The LFTF occurs lightly within the fiber-reinforced plastic (FRP) adherend near the surface, which is characterized by a thin layer of the FRP resin matrix visible on the adhesive and ruptured surfaces [36]. Therefore, the LFTF mode indicates efficient stress transfer between the two joint members.

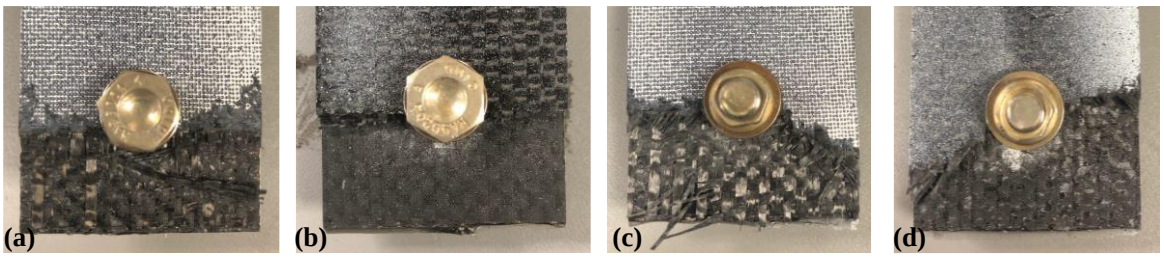

Figure 5.4: Failure modes in (a) HBB-CP8, (b) HBB-CP12, (c) HBB-QI8, and (d) HBB-QI12.

5.4.3 Surface strain distribution in OB and HBB joints

In a previous investigation [22] related to OB and HBB joints with three bolts, it was reported that the final fracture always started on the outer bolt located on the grip side (Figure 5.5), and in the case of the HBB, the central bolt did not seem to bear any load. These behaviors can be analyzed systematically using the 3D-DIC technique, where the two cameras and associated software allow three dimensional measurements of the shapes, displacements, and deformation fields of the test specimens. It is also expected that 3D-DIC analysis will provide a straightforward explanation for the dramatic strength decreases of CP laminates compared to those of QI laminates when used in bolted joints (Table 5.2). These aspects are discussed in detail in the following four subsections. Subsection 5.4.3.1 the evolution of the axial strain in the overlap region; subsection 5.4.3.2 focuses on the strain distribution under the external bolt associated with joint failure; subsection 5.4.3.3 illustrates the balance between the bypass and bearing loads in the OB and HBB

joints; subsection 5.4.3.4 focuses on the region in which the fracture occurs. For the face of interest of the joint, the three examined bolts were labeled as B1, B2, and B3; B1 is the bolt near the free edge, B2 is the central bolt, and B3 is the bolt near the side of the grip. The test results analyzed are based on the 3D-DIC data recorded for eight different single-joint tests, and the corresponding load–displacement responses are shown in Figure 5.6.

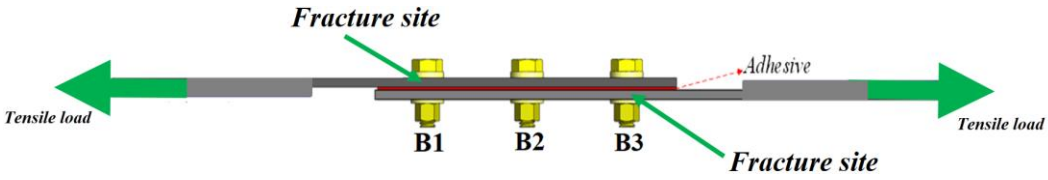

Figure 5.5: Identification of the three bolts and fracture sites of SL joints.

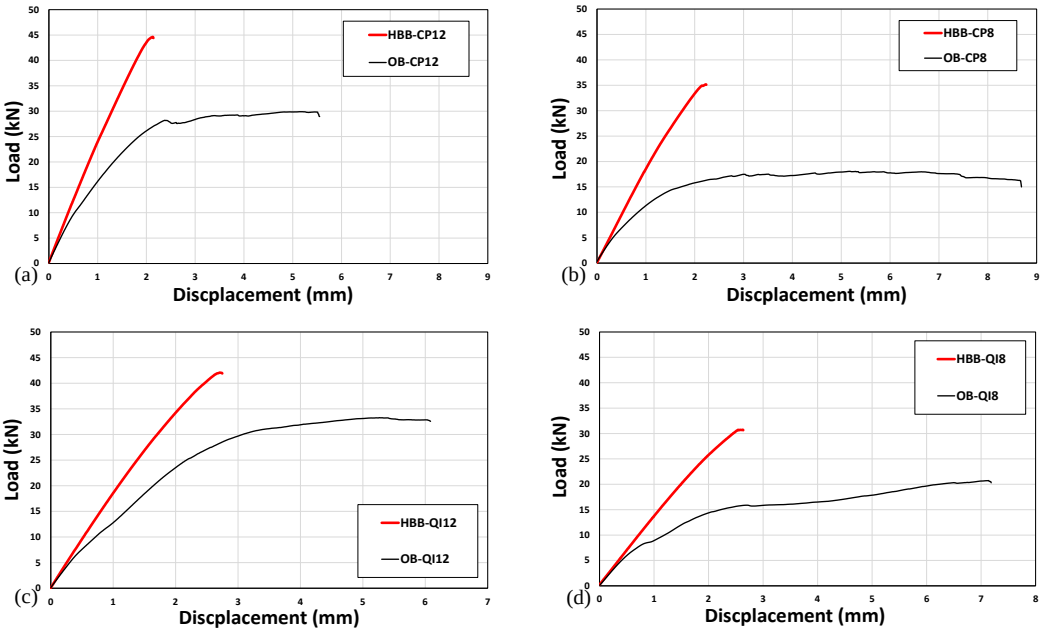

Figure 5.6: Load–displacement behavior of OB vs. HBB joints: (a) CP12, (b) CP8, (c) QI12, and (d) QI8.

5.4.3.1. Interpretation of the observed axial strain field

Figure 5.7 shows the axial surface strain distribution (ε_{xx}) along the loading direction (only the 12-layer configuration is shown here, which also represents that of the 8-layer case) at increasing load levels (25%, 50%, and 75% of the failure load (FL)). The readily apparent characteristics noted in this figure are as follows:

- In OB joints, a vertical line along the load path indicates the compression induced by the bearing action under the bolts. This compression zone is significantly more severe for CP than for QI, although it increases in both cases when moving from the grip side toward the free side. This might be related to the decrease in the ratio of the bypass/bearing load in this direction, which eventually results in the growth of the pressure effect of the bolt shank into the laminate (as detailed in Section 5.4.3.3).
- In the OB joints, two tensile strain concentration zones that are approximately oriented along the ±45° axes are observed and appear more pronounced for QI than for CP. These may be the results of matrix damage and growth of microscopic splitting cracks [26].
- In HBB joints, the vertical compression line disappears, indicating the absence of bearing action. Inversely, the external bolt toward the grip side (B3) is the siege of a high tensile strain concentration for both the CP and QI. The central bolt (B2) appears unstrained, and the bolt toward the free end (B1) is the region where almost no effective load is applied and the adhesive is debonded.

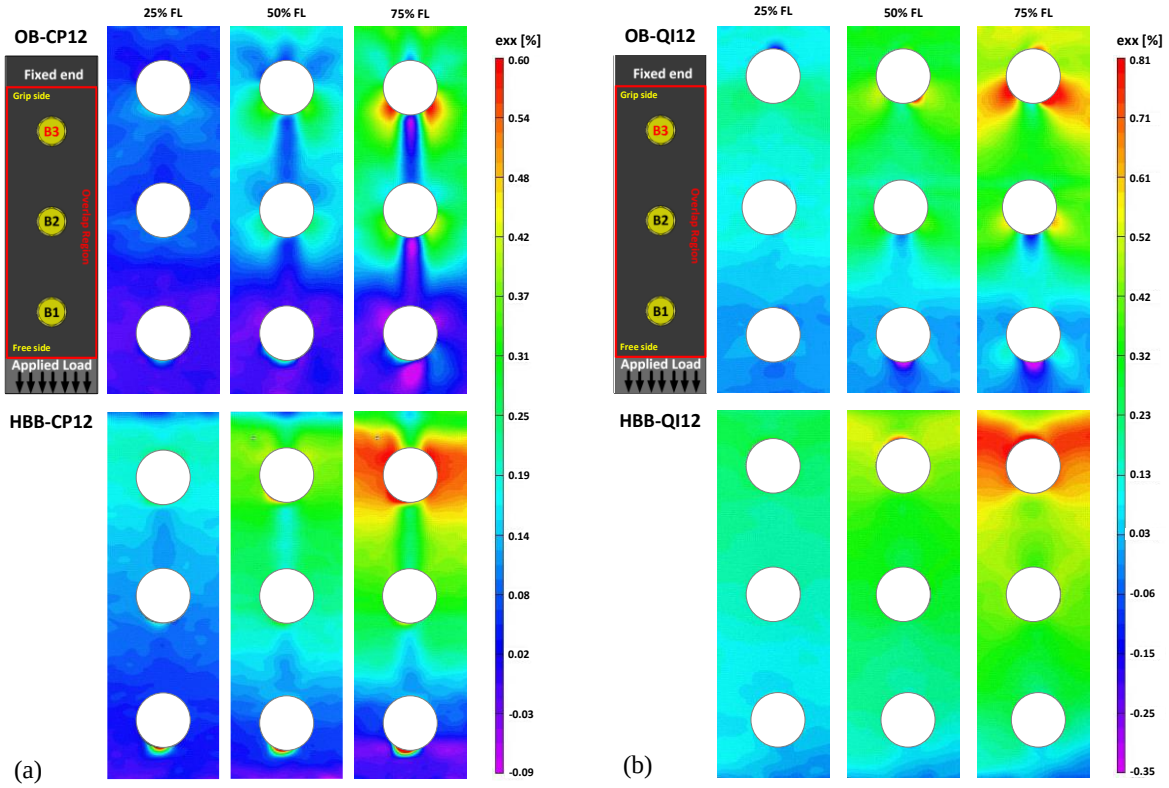

Figure 5.7: Axial surface strain distributions (ε_{xx}) of OB vs. HBB in (a) CP12 and (b) QI12.

The stress on the free end of the overlap is zero, while the facing adherent material is under tension. The resulting shear stress debonds the adhesive, but the extreme bolt prevents debonding from progressing to the middle section. The debonded zone of the free end does not participate in the tensile stress transfer and hence does not display any tensile stress patterns. Accordingly, if the free ends of the CP and QI are compared, it can be concluded that the debonding in CP is more widespread than that in QI.

A 3D plot of the surface strain distribution at 75% FL is shown in Figure 5.8. This figure can assist comparing the surface conditions between OB and HBB. The effect of bearing on e_{xx} distribution is detected clearly in OB, whereas that for HBB is not clearly discerned. Hence, it can be concluded that DIC illustration contributed effectively to see the hybrid joining method impact on bolted joints. Hybridization helps to alleviate the overall strain/stress distribution and noticeably relieves the stress concentration around the middle hole. Moreover, the in-plane bearing damage is reduced to a significant extent, and B2 does not transfer any loads between the two joint members. These contributors truly help CP-bolted joints, which have more stress concentration and notch sensitivity, to sustain more strength than QI joints via addition of adhesive to the shear plane (as also reported in Table 5.2).

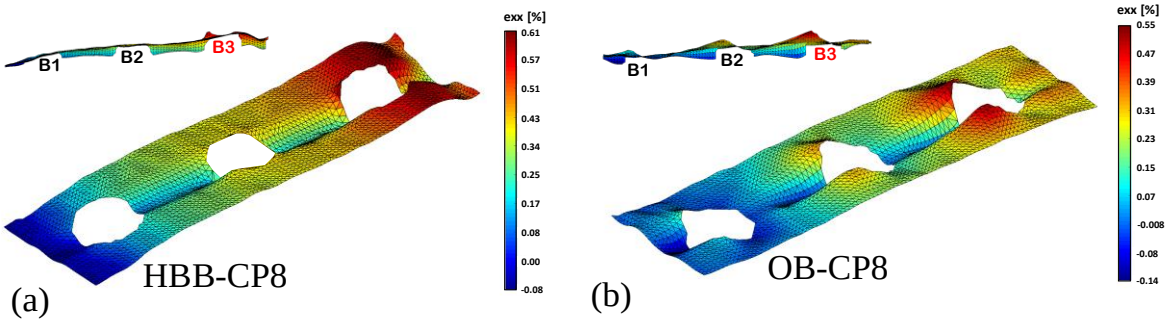

Figure 5.8: 3D nephogram of ε_{xx} distribution: (a) HBB-CP8; (b) OB-CP8.

5.4.3.2. Strain distribution below the leading bolt

To measure the axial strain below B3, where failure occurred, a virtual line perpendicular to the load direction was drawn at a distance of *2d* from the center of the corresponding hole. Figure 5.9 shows the evolution of ε_{xx} between 0% and 90% of the applied load in steps of 10%. In the OB joints and above 90% of the applied load, the measurements are disturbed by extensive bearing damage. The observed edge-to-edge (-20mm to +20mm on Y position) in-plane deformation was caused by both the bearing and bypass loads. A comparison of Figure 5.9 (a) and (c) shows that in CP, the axial strain ε_{xx} of the bearing plane, first increases with increasing load and then decreases until reaching negative values (compression) at 70% of the failure load. However, for QI, the ε_{xx} values remain positive up to 90% of the failure load. The bearing load in CP is associated with fiber compression, shear damage, and matrix compression damage in each layer of the laminate, whereas that in QI causes significant matrix damage only in the 0° plies [37]. Hence, a larger bearing damage area was formed in the CP. It can thus be concluded that QI has better bearing performance than CP, which leads to higher strength retention in QI than CP for bolted joints (Table 5.2).

On the other hand, in HBB joints, the overall edge-to-edge strain values has a growing trend with increasing load. In addition, the ε_{xx} of the bearing plane did not reach negative values, implying that the region below the bolt remained under tension throughout the test. The diagrams in Figure 5.9 show a concavity (depression) that is formed in the deformation curves, around the zero position of the x-axis, where the bolt is located. This depression was formed merely by the bypass load, which flowed around the hole and has its own maximum tensional effect on bilateral sides of the hole. The depression area in HBB-CP was more pronounced than that in HBB-QI.

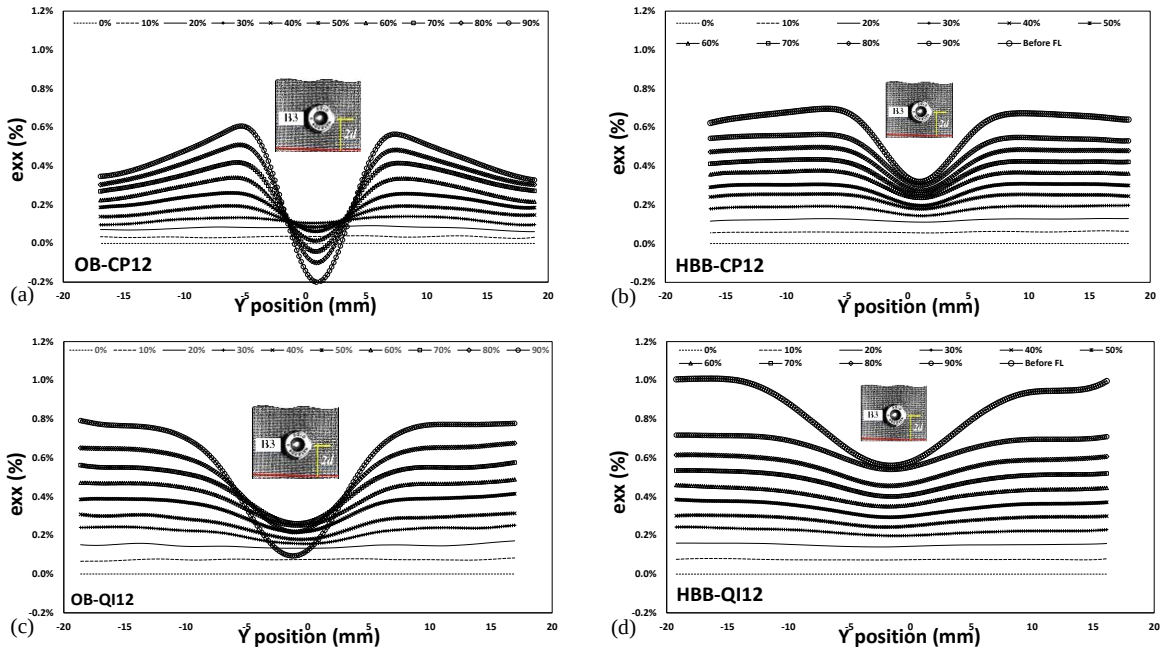

Figure 5.9: Axial surface strain distribution below B3: (a) OB-CP12, (b) HBB-CP12, (c) OB-QI12, and (d) HBB-QI12.

Figure 5.10 shows the variation of the axial (ε_{xx}) and transverse (ε_{yy}) strains below B3 in the OB and HBB joints at a 15 kN tensile load. The first noticeable feature is the increase in ε_{yy} below the bolt of the OB (black lines in Figure 5.10 (a) and (b)), which is an indication of material expansion induced by the bearing action. Meanwhile, for the same position, ε_{xx} decreased significantly (black lines in Figure 5.10 (c) and (d)). For HBB, the variations in ε_{xx} and ε_{yy} were significantly relieved (red lines in Figure 5.10). The second noticeable feature is that for the OB joints, the extent of ε_{xx} variation in the vicinity of the bolt position, which is an indicator of stress concentration, is significantly higher for CP than for QI. A further illustration of the greater benefit of CP from hybridization is highlighted by the gap between the global minima of ε_{xx} curves of the OB versus HBB. This gap is significantly wider for CP than for QI, as seen in Figure 5.10 (c) and (d). The localized results in this section, which focus on B3, demonstrated that the lower bearing performance of OB-CP, compared to OB-QI, resulted in a higher stress concentration in the CP and resulted in associated adverse effects on its performance. However, the addition of adhesive significantly relieved the concentration of the in-plane strain components around B3, which helped preserve the strength of CP provided by their higher 0° plies content, which is more notch sensitive than QI [22, 30]. Overall, the DIC clearly shows the occurrence of the depression zone on the

bearing plane and indicates that its magnitude is highly dependent on the types of joint configuration.

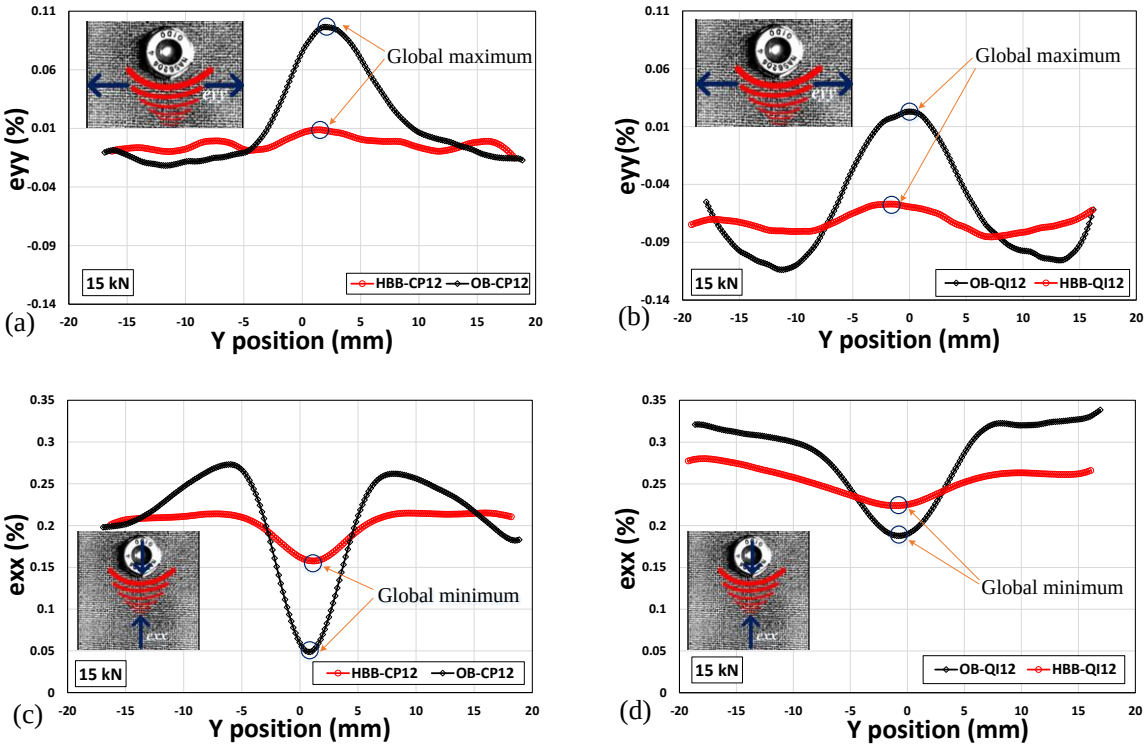

Figure 5.10: Comparison of the surface strain distribution below B3 between OB and HBB at 15 kN: (a) ε_{yy} of CP12, (b) ε_{yy} of QI12, (c) ε_{xx} of CP12, and (d) ε_{xx} of CP12.

5.4.3.3. Axial strain evolutions on the bearing planes of the three bolts

In the preceding sub-section, Figure 5.9 focused on ε_{xx} evolution under B3 along a horizontal line spanning the width, and the notable feature here is the occurrence of a depression whose magnitude depends on the type of joint (CP, QI, OB, or HBB). In this section, the focus is on the extremum depression point (the bearing plane which is located along the longitudinal axis passing through the hole center), and the measurements are extended to the three bolts. The follow-up of the strain shows the tensile strain increase and then decrease to negative values, as is the case for OB.

Figure 5.11 illustrates and compares ε_{xx} evolution on the bearing axis of each bolt of the OB and HBB joints. Thus, three virtual strain gauges (SGs) were placed longitudinally at distances of *2d* from the centers of the bolts (Figure 5.11). The readily apparent feature in Figure 5.11 is that

for the HBB joints, all virtual SGs display steadily increasing positive strain values up to the final failure. However, for the OB joints, the virtual strain gauges display increasing positive strains up to a maximum and then decreasing strains. This behavior is an illustration of the competing actions of the bypass and bearing stresses in each joint configuration. The bypass action corresponds to increasing strain with increase in the applied load, and the bearing action corresponds to decreasing strain with increasing applied load.

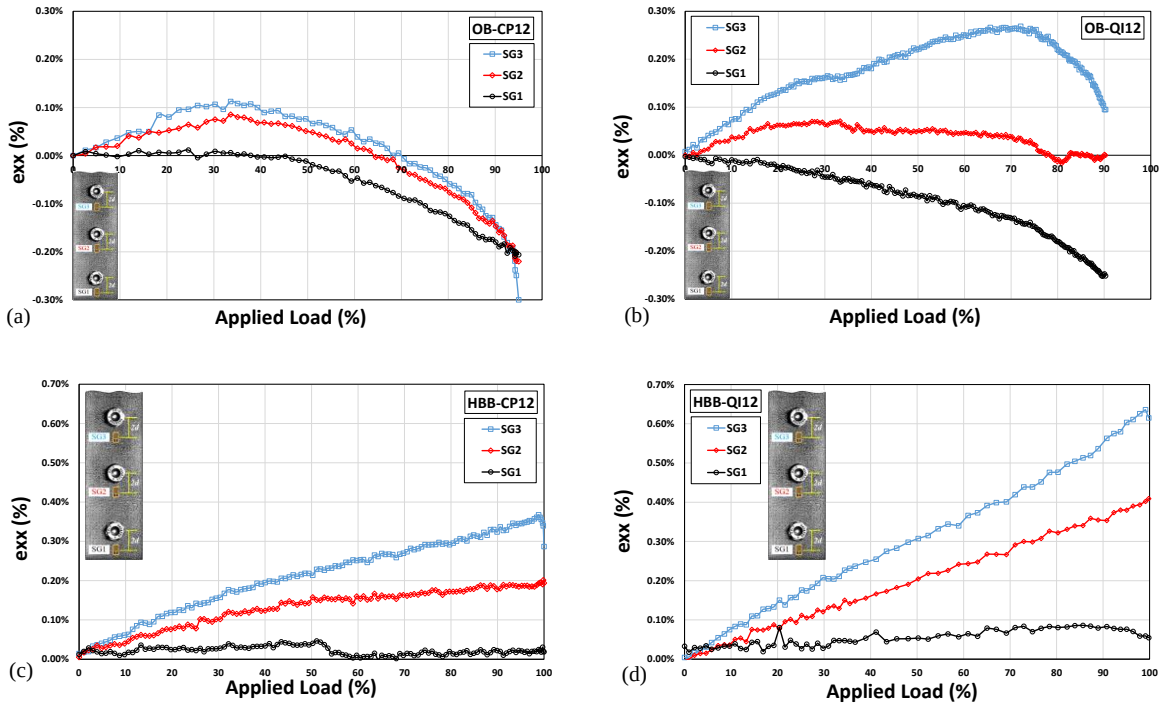

Figure 5.11: Axial strain evolutions on the bearing planes of the three bolts: (a) OB-CP12, (b) OB-QI12, (c) HBB-CP12, and (d) HBB-QI12.

Figure 5.11 (a) shows that in the OB CP, the ε_{xx} of SG3 and SG2 increased gradually up to approximately 35% of the applied load, which corresponds to 10 kN (Figure 5.6), and then all the curves started declining. This might be related to the inception where the bolts start transferring the applied load (knee point [28]). As shown in Figure 5.11 (b), in the OB QI, SG3 continued to increase up to 70% of the applied load and then decreased without reaching a negative strain. Clearly, the bypass action is more active for QI than for CP as far as the external bolts are concerned. It is recalled here that an SL joint under tension is made of two members sliding in

opposite directions. The bolt B3 is similar to bolt B1 when observed from the other member. Consequently, the observed responses of SG3 and SG1 are inverted for the other member. In other words, SG3 and SG1 displayed in Figure 5.11 represent the strains under the external bolts in back-to-back members.

On the other hand, the corresponding curves for the HBB joints displayed completely different behaviors. The retrieved DIC data formed almost a set of linear trend lines, which showed increasing progression. It is interesting to note that, except for SG1, which has an almost zero slope, the slopes of SG2 and SG3 in QI are twice those of CP. The higher ductility behavior of the QI layup than CP might be the reason. As all the HBB curves have upward inclinations, it can be understood implicitly that there is not much bearing action, and the bearing plane experiences longitudinal tensile strain. In all the SG curves of the bolted joints, the upward trends, which are followed by downward trends, denote load transfer to the bolts. However, in HBB joints, all the curves show straight upward trends, which indicate that the adherends are practically under tension upon complete failure. Therefore, it can be concluded that in HBB joints, unlike bolted joints, the load transfer between the adherends is mainly provided by the adhesive, and the bolts do not contribute significantly in this regard. Moreover, the elimination of the bearing effect in HBB joints directly favors joint strength preservation.

5.4.3.4. Initiation spots of the net-tension failures in OB and HBB

Figure 5.12 illustrates the growth of ε_{xx} and initial location of the net-tension failure near B3. The data were retrieved at 25%, 50%, and 75% of the failure load from a series of integrated points placed around B3 (half-circle red line). Contrary to the OHT test in which the high tensile strain region was concentrated at the center-transverse line at the edge of the hole, with the rupture initiating at this point [24, 38-40], the DIC results illustrated that in SL joint experiencing secondary bending (SB), this location changed. Moreover, this spot also varied between OB and HBB joints. Figure 5.12 shows that severe tensile strain concentrations are localized below the bolt for the OB joints and above the bolt for the HBB joints. In OB joints, the load transfer mechanism is provided by the bolts, whereas in HBB, it is provided by the adhesive, and the bolt contact-induced damage is not operative. Consequently, the main operative stress concentration mechanism is on the lateral sides of the hole. Interestingly, ε_{xx} decreased around the center area of the bolt. Owing to SB, a compression bending stress was induced on the outer surface of the laminate, which

was subtracted from the nominal tensile stress, and lowered the values of ε_{xx}. Because the thicker joints have greater SB than the thinner ones [28] (i.e., higher bending stress), a greater reduction in the values of ε_{xx} can be observed in the OB 12-layer configuration. Moreover, the strain/stress concentration was intensified in the OB 12-layer. However, in HBB joints, the thinner configurations showed higher maximum values of ε_{xx} than thicker ones.

Figure 5.13 compares the appearance and changes in the surface cracks and failure patterns in OB-CP/QI 12 and HBB-CP/QI 12 just before failure (BF) and immediately after failure (AF). It can be seen that before failure, the cracks were captured at the bottom side of the hole in the OB, and they commenced at approximately 98% FL. The bearing effect is also pronounced in OB-CP12 and surfaced at approximately 92% FL. However, HBB does not display any visible cracks/bearing manifestations even up to the final failure, which demonstrates the least bolt contribution in load sharing as well as delayed damage initiation as a result of using adhesive. It can thus be concluded that the adhesive contributes effectively to sustaining the laminate strength and decelerating failure, which allows the joint to bear more of the applied load.

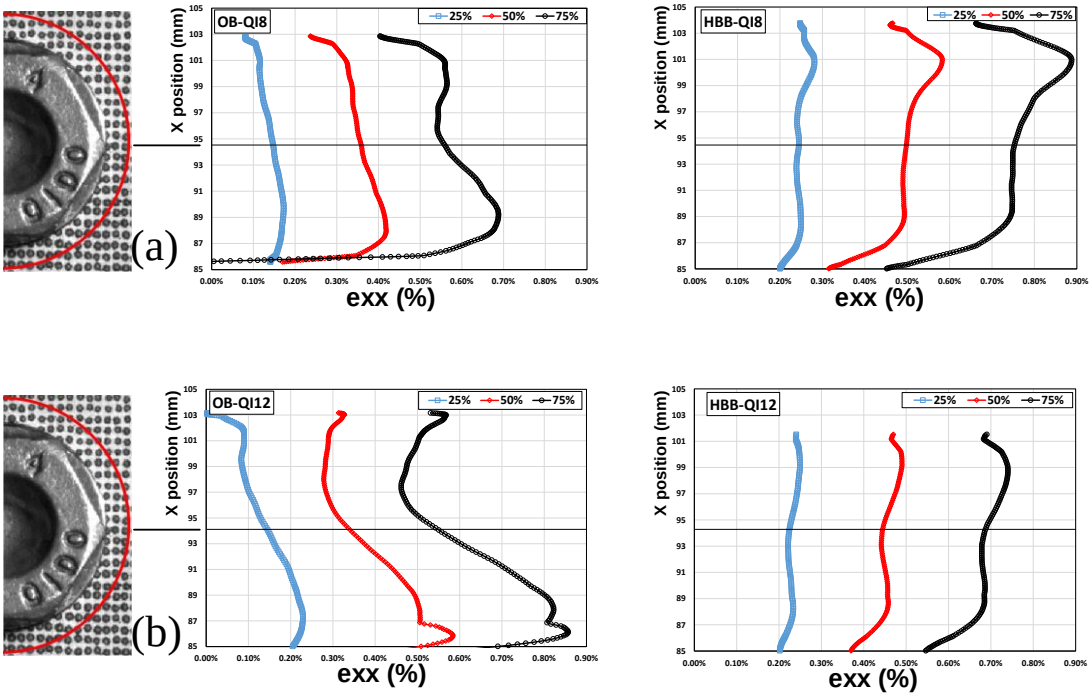

Figure 5.12: Location of the net-tension failure initiation in OB and HBB joints: (a) QI8 and (b) QI12.

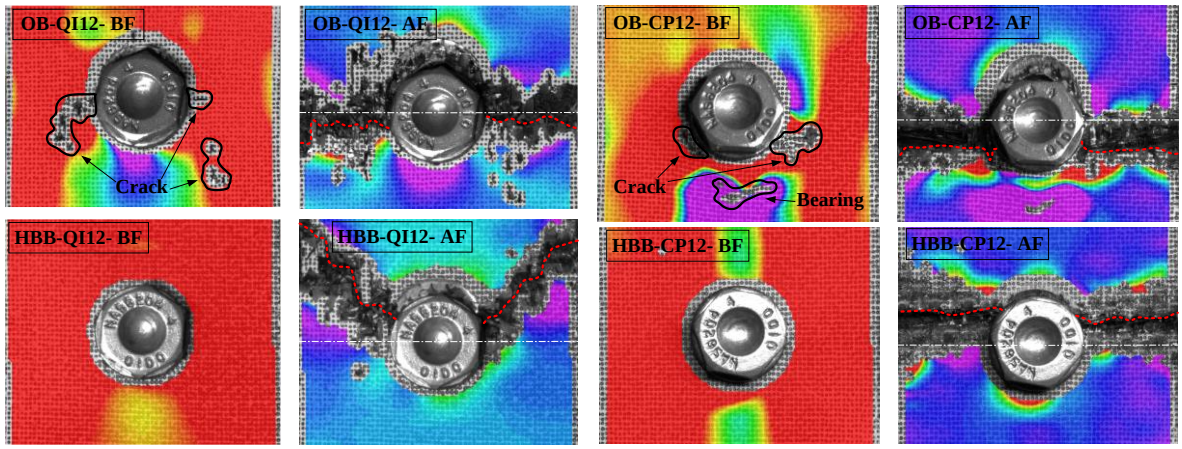

Figure 5.13: Comparison of the surface cracks and failure formations.

5.4.4 Secondary bending and twisting in HBB joints

Consider the multi-bolt single shear lap joint secured by tensile grips, as shown in Figure 5.14 (a), and particularly the overlap region for which the «Grip side » and «Free side» are identified. In a prior investigation [28], it was reported that SB can be measured as the out-of-plane displacement (δ_{OPD}) using a 3D-DIC system. The two dashed parallel lines in Figure 5.14 (b) show the virtual paths along which the DIC measurements are recorded. The virtual dashed lines are located at distances of $2d$ from the bolt center, where d is the bolt-hole diameter. For the face of interest of the joint, the three bolts are labeled as B1, B2, and B3. B1 is the bolt near the free edge, B2 is the central bolt, and B3 is the bolt near the side of the grip.

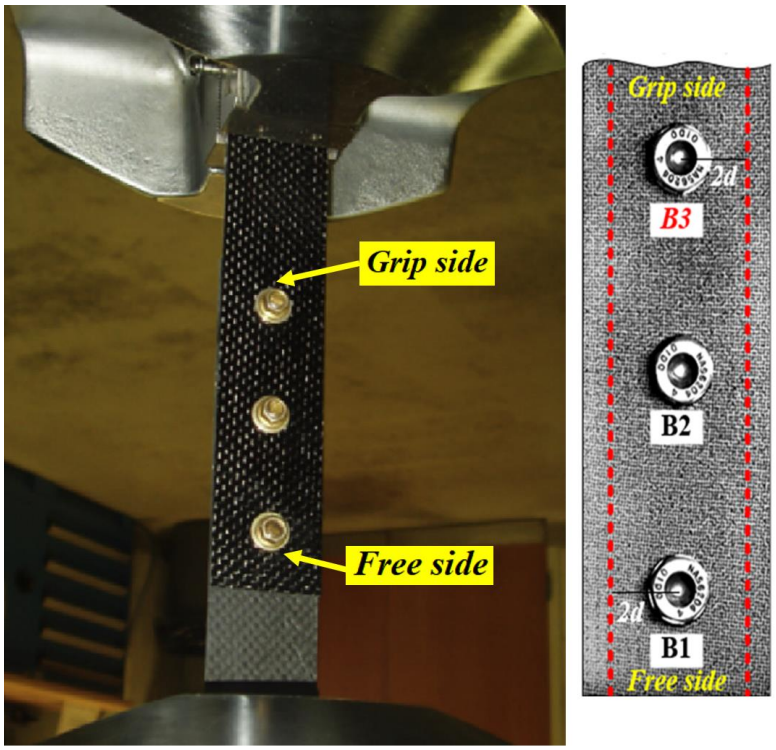

Figure 5.14: (a) Multi-bolt single shear lap joint secured by tensile grips, and the two sides of the overlap region are identified by the «Grip side » and «Free side». (b) Represents the speckled overlap region upon which two virtual parallel lines are identified.

The results of the tracking of δ_{OPD} corresponding to the two parallel virtual lines in Figure 5.14 (b) are plotted for the four laminates investigated (CP8, QI8, CP12, and QI12) for both OB and HBB joints, as shown in Figure 5.15. The inset photo of the joint side view in Figure 5.15 shows the secondary bending direction, and the yellow line represents the surface of interest where the DIC data were retrieved. The following features are observed in Figure 5.15.

- For all the laminate stacking sequences (CP and QI) and thicknesses (8 and 12 plies), δ_{OPD} is always lower for HBB compared to OB. This means that the adhesive restricts secondary bending.
- For a given OB laminate, the δ_{OPD} values of the left and right lines did not superimpose. This meant that the joint was subjected to twisting.

- For a given HBB laminate, the δ_{OPD} values of the left and right lines were almost superimposed. This meant that the adhesive restricted the twisting phenomenon.

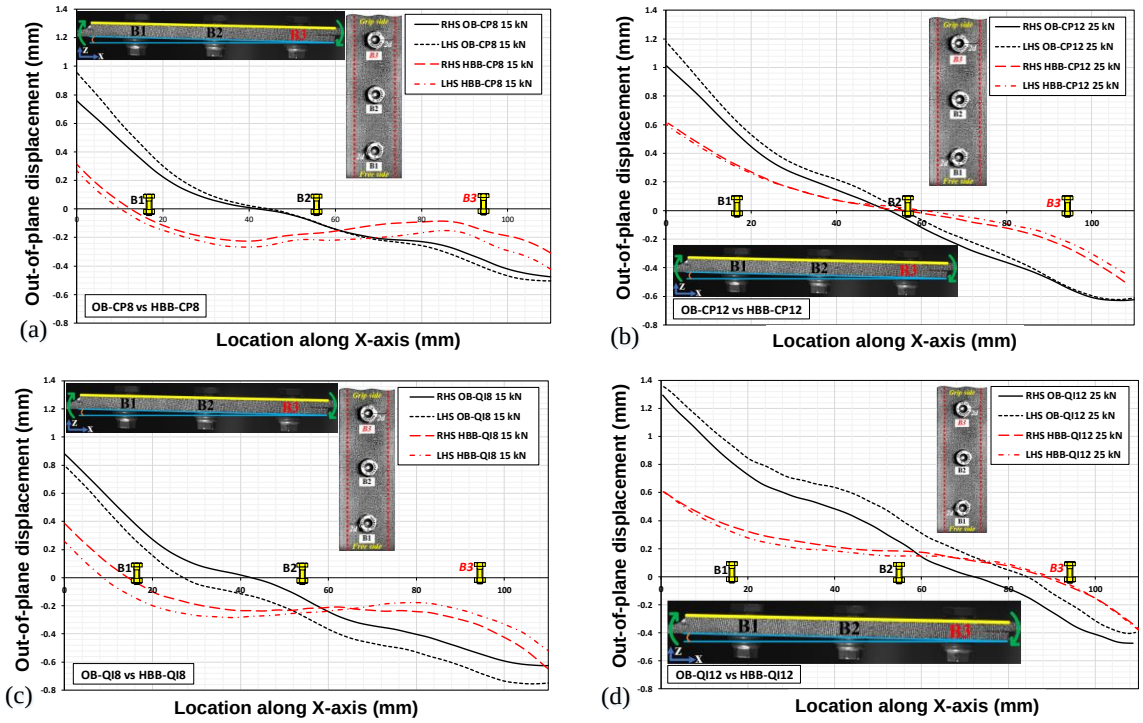

Figure 5.15: Comparison of secondary bending and twisting in OB vs. HBB: (a) CP8, (b) CP12, (c) QI8, and (d) QI12.

Specifically, in the HBB joints, the adhesive decreased δ_{OPD} by approximately 50% and 64% in CP12 and QI12, respectively, and 86% and 70% in CP8 and QI8. This indicates that hybridization is more beneficial for thin laminates. In fact, the δ_{OPD} curves also appear to be more flattened between bolts B1 and B3 in the case of thin laminates. This behavior may be attributed to the smaller geometrical eccentricities of the thinner joints, which lower the induced bending moment. This situation translates to less interlaminar shear stresses, less damage/delamination/deformation around the holes, and less local stress concentrations. These factors collectively contribute to sustaining joint stiffness and strength. Consequently, the reversal of the resistance orders of CP and QI depending on OB or HBB, as shown in Table 5.2, are mainly related to the SB offsets via adhesive bonding.

Figure 5.16 shows a 3D plot of δ_{OPD} from the joint surface to highlight the adhesive effects. First, it is noted that the colored bands are not horizontal for the OB joint compared to the HBB

joint. This feature is a direct indication of twisting. Furthermore, in contrast with OB joints, HBB joints do not display any obvious bearing/deformation effects around the holes. The only notable behavior of the HBB joint in response to the eccentricity of the load is the curvature introduced to the adherent at the overlapping ends. The 3D contour plots of δ_{OPD} show that the middle joint regions of the HBB joints experience significantly less deformations than the external bolt-hole areas, where debonding occurs because of peel stress. In the OB joint, secondary bending prompts the bolt to tilt into the notch, which further increases the bearing damage.

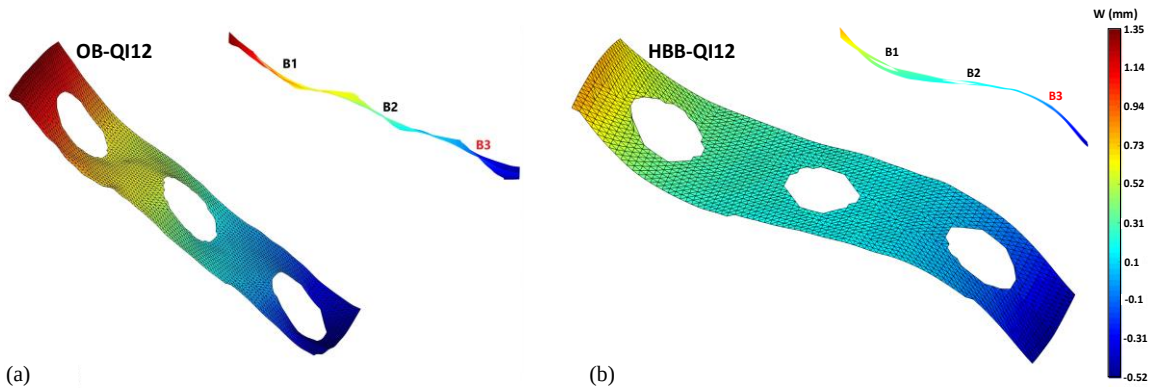

Figure 5.16: Comparison of the 3D nephograms of OPD: (a) OB-QI12 and (b) HBB-QI12.

To obtain a closer view of the deformation around B3, one line parallel to the grip edge was drawn at a distance *d* from the bolt-hole center and above it (Figure 5.17). The OPD profiles along the line are plotted for OB and HBB at equal load levels for comparison. Technically, owing to the load eccentricity, fastener rotation and bolt-head pushing into the surrounding areas cause a local depression, where the line is assigned. The diagrams show that for OB joints, the magnitudes of the depressions increased with increasing load. However, in the HBB joints, no remarkable deformations were observed, as the line was straight and only came downward while the load increased. Therefore, the bolt was not engaged much during load transfer in HBB joins; otherwise, it is assumed that there must be transversal OPD above the bolts (dashed line), similar to those seen in OB joints.

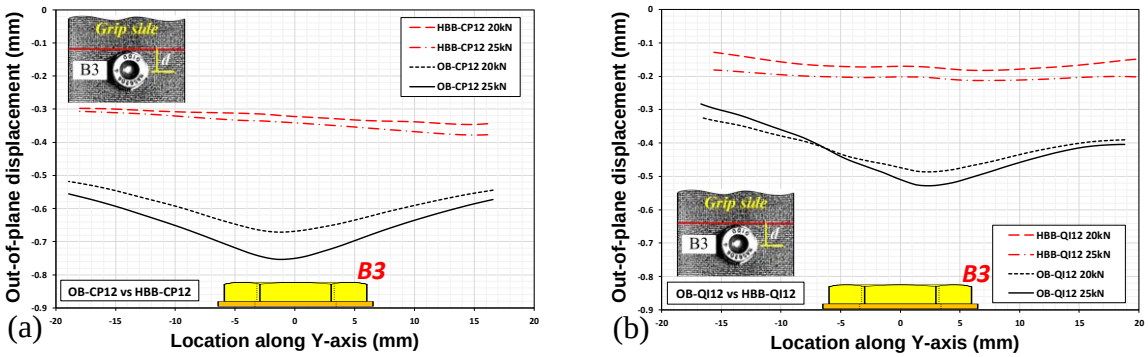

Figure 5.17: Comparison of transversal OPDs in OB and HBB joints at B3: (a) CP12 and (b) QI12.

5.5 Conclusion

In this study, 3D digital image correlation (3D-DIC) was employed to experimentally investigate the influence of hybridization (applying adhesive in bolted joints) on the responses of single-lap three-bolt carbon/epoxy composite joints. The configurations evaluated included two well-known stacking sequences, namely cross-ply (CP) and quasi-isotropic (QI) types, for two thicknesses of 8 and 12 layers. The objective was to investigate the effects of hybridization on the strengths, surface strain distributions, and secondary bending (SB) of the tested configurations. The DIC results contributed to enriching the knowledge in this regard. The following conclusions can be drawn from the experimental results.

- If a structure has to be bolted, it is preferable to choose a QI material unless hybridization, as the HBB/OB strength ratio of CP is almost twice that of QI. Moreover, the results showed that hybridization was better for thin joints than thick joints.

- DIC results showed that hybridization eased the all-round strain/stress distribution as well as the bearing action, while noticeably relieving the stress concentration around the holes, thereby helping CP joints sustain more strength than QI by approximately 13.5%. Nevertheless, QI has better bearing performance than CP, which favors QI for bolted joint applications.

- The axial strain curve of the bearing plane of each bolt showed no advancement in bearing response and indicated almost no load sharing via the bolts in the HBB joints. Furthermore, it was found that hybridization delayed damage initiation, which decelerated the failure process.

- In applications where SB occurrences are more probable, hybridization is highly recommended as the adhesive decreases SB significantly; further, it has better impact on thinner joints. This enables joints to preserve their stiffness and strength by minimizing the interlaminar shear stresses. Moreover, hybridization allowed better performance for thicker joints in terms of twisting reduction.

- The OHT resistance of CP is greater than that of QI but the reverse occurs in the case of OB joints. However, in the case of HBB joints, the superiority of CP is restored.

Finally, it was also noted that 3D-DIC could be a powerful tool to assess the balance between bypass and bearing loads, which is important for the behavioral analyses of fastened joints. Further, 3D-DIC can help better understand the fastening parameters, such as the effects of the bolt-hole fit conditions, clearance, interference, preloads, friction, and lubrication. The suggested topics are the scopes for future work to acquire more knowledge regarding the behaviour of SL multi-bolt composite joints via DIC technology.

5.6 Acknowledgments

The authors acknowledge the financial support provided by the Natural Sciences and Engineering Research Council of Canada (NSERC) and the Consortium for Research and Innovation in Aerospace in Quebec (CRIAQ). We also thank Bombardier Aerospace, L-3 Communications and Delastek Aeronautique Inc. for their valuable support.

5.7 References

[1] Tang H, Liu L. A novel metal-composite joint and its structural performance. Composite Structures. 2018;206:33-41.

[2] Li X, Tan Z, Wang L, Zhang J, Xiao Z, Luo H. Experimental investigations of bolted, adhesively bonded and hybrid bolted/bonded single-lap joints in composite laminates. Materials Today Communications. 2020;24:101244.

[3] Lopez-Cruz P, Laliberté J, Lessard L. Investigation of bolted/bonded composite joint behaviour using design of experiments. Composite Structures. 2017;170:192-201.

[4] Bauer J, Hart-Smith L. Bolted/Bonded Joints in Polymeric Composites. Bolted/Bonded Joints in Polymeric Composites. 1997.

[5] HART-SMITH LJ. Bonded-bolted composite joints. Journal of Aircraft. 1985;22(11):993-1000.

[6] Hart-Smith L. Design Methodology for Bonded-Bolted Composite Joints. Volume I. Analysis Derivations and Illustrative Solutions. MCDONNELL DOUGLAS CORP LONG BEACH CA; 1982.

[7] Fu M, Mallick PK. Fatigue of hybrid (adhesive/bolted) joints in SRIM composites. International Journal of Adhesion and Adhesives. 2001;21(2):145-59.

[8] Kelly G. Load transfer in hybrid (bonded/bolted) composite single-lap joints. Composite structures. 2005;69(1):35-43.

[9] Kelly G. Quasi-static strength and fatigue life of hybrid (bonded/bolted) composite single-lap joints. Composite structures. 2006;72(1):119-29.

[10] Barut A, Madenci E. Analysis of bolted–bonded composite single-lap joints under combined in-plane and transverse loading. Composite Structures. 2009;88(4):579-94.

[11] Bois C, Wargnier H, Wahl J-C, Le Goff E. An analytical model for the strength prediction of hybrid (bolted/bonded) composite joints. Composite Structures. 2013;97:252-60.

[12] Bodjona K, Raju K, Lim G-H, Lessard L. Load sharing in single-lap bonded/bolted composite joints. Part I: Model development and validation. Composite Structures. 2015;129:268-75.

[13] Bodjona K, Lessard L. Load sharing in single-lap bonded/bolted composite joints. Part II: Global sensitivity analysis. Composite Structures. 2015;129:276-83.

[14] Bodjona K, Lessard L. Nonlinear static analysis of a composite bonded/bolted single-lap joint using the meshfree radial point interpolation method. Composite Structures. 2015;134:1024-35.

[15] Raju KP, Bodjona K, Lim G-H, Lessard L. Improving load sharing in hybrid bonded/bolted composite joints using an interference-fit bolt. Composite Structures. 2016;149:329-38.

[16] Bodjona K, Fielding S, Heidari-Rarani M, Lessard L. Effect of adhesive layer compliance on strength of single-lap hybrid bonded-bolted joints. Composite Structures. 2020:113324.

[17] Chowdhury NM, Wang J, Chiu WK, Chang P. Experimental and finite element studies of thin bonded and hybrid carbon fibre double lap joints used in aircraft structures. Composites Part B: Engineering. 2016;85:233-42.

[18] Chowdhury NM, Chiu WK, Wang J, Chang P. Experimental and finite element studies of bolted, bonded and hybrid step lap joints of thick carbon fibre/epoxy panels used in aircraft structures. Composites Part B: Engineering. 2016;100:68-77.

[19] Chowdhury NM, Wang J, Chiu WK, Chang P. Static and fatigue testing bolted, bonded and hybrid step lap joints of thick carbon fibre/epoxy laminates used on aircraft structures. Composite Structures. 2016;142(Supplement C):96-106.

[20] Paroissien E, Lachaud F, Schwartz S, Da Veiga A, Barrière P. Simplified stress analysis of hybrid (bolted/bonded) joints. International Journal of Adhesion and Adhesives. 2017;77:183-97.

[21] Gamdani F, Boukhili R, Vadean A. Tensile behavior of hybrid multi-bolted/bonded joints with carbon/epoxy composites. In: Proceedings of 21st International Conference on Composite Materials (ICCM). Xi'an, 20-25th August 2017.

[22] Gamdani F, Boukhili R, Vadean A. Tensile behavior of hybrid multi-bolted/bonded joints in composite laminates. International Journal of Adhesion and Adhesives. 2019;95:102426.

[23] Li X, Cheng X, Guo X, Liu S, Wang Z. Tensile properties of a hybrid bonded/bolted joint: parameter study. Composite Structures. 2020:112329.

[24] Kashfuddoja M, Ramji M. Whole-field strain analysis and damage assessment of adhesively bonded patch repair of CFRP laminates using 3D-DIC and FEA. Composites Part B: Engineering. 2013;53:46-61.

[25] Hu J, Zhang K, Yang Q, Cheng H, Liu P, Yang Y. An experimental study on mechanical response of single-lap bolted CFRP composite interference-fit joints. Composite Structures. 2018.

[26] Hu J, Zhang K, Xu Y, Cheng H, Xu G, Li H. Modeling on bearing behavior and damage evolution of single-lap bolted composite interference-fit joints. Composite Structures. 2019;212:452-64.

[27] Wang H-T, Wu G, Pang Y-Y, Shi J-W, Zakari HM. Experimental study on the bond behavior between CFRP plates and steel substrates under fatigue loading. Composites Part B: Engineering. 2019;176:107266.

[28] Mehrabian M, Boukhili R. Quantifying of secondary bending effect in multi-bolt single-lap carbon-epoxy composite joints via 3D-DIC. Composites Science and Technology. 2020:108453.

[29] Bodjona K, Lessard L. Hybrid bonded-fastened joints and their application in composite structures: A general review. Journal of reinforced plastics and composites. 2016;35(9):764-81.

[30] Gamdani F, Boukhili R, Vadean A. Tensile strength of open-hole, pin-loaded and multi-bolted single-lap joints in woven composite plates. Materials & Design. 2015;88:702-12.

[31] ASTM-D5961/D5961M-13, Standard Test Method for Bearing Response of Polymer Matrix Composite Laminates. ASTM International, 100 Barr Harbor Drive, PO Box C700, West Conshohocken, PA 19428-2959. United States, 2013.

[32] Daly SH. Digital image correlation in experimental mechanics for aerospace materials and structures. Encyclopedia of Aerospace Engineering. 2010.

[33] Bermudo Gamboa C, Martín-Béjar S, Trujillo Vilches FJ, Castillo López G, Sevilla Hurtado L. 2D–3D Digital Image Correlation Comparative Analysis for Indentation Process. Materials. 2019;12(24):4156.

[34] Materials ACD-oC. Standard test method for tensile properties of polymer matrix composite materials: ASTM International; 2008.

[35] Hallett SR, Green BG, Jiang W-G, Cheung KH, Wisnom MR. The open hole tensile test: a challenge for virtual testing of composites. International Journal of Fracture. 2009;158(2):169-81.

[36] Taib AA, Boukhili R, Achiou S, Gordon S, Boukehili H. Bonded joints with composite adherends. Part I. Effect of specimen configuration, adhesive thickness, spew fillet and adherend stiffness on fracture. International Journal of Adhesion and Adhesives. 2006;26(4):226-36.

[37] Xiao Y, Ishikawa T. Bearing strength and failure behavior of bolted composite joints (part II: modeling and simulation). Composites science and technology. 2005;65(7-8):1032-43.

[38] Pitz EJ, Miron M-C, Major Z. Computational implementation and experimental validation of a micro-mechanics informed progressive damage Strain Invariant Failure Theory. Composites Part B: Engineering. 2018;155:225-36.

[39] Gao X, Yu G, Xue J, Song Y. Failure analysis of C/SiC composites plate with a hole by the PFA and DIC method. Ceramics International. 2017;43(6):5255-66.

[40] Caminero M, Lopez-Pedrosa M, Pinna C, Soutis C. Damage monitoring and analysis of composite laminates with an open hole and adhesively bonded repairs using digital image correlation. Composites Part B: Engineering. 2013;53:76-91.

CHAPTER 6 ARTICLE 3: EXPERIMENTAL INVESTIGATION OF HOLE DEFORMATION AND BOLT-HOLE ELONGATION OF WOVEN CARBON-EPOXY COMPOSITE PLATES AND JOINTS USING DIC TECHNIQUE

Submitted to: Journal of Composite Structures, January 2022

Masoud Mehrabian, Aouni Jr. Lakis, Rachid Boukhili*

Department of Mechanical Engineering, Polytechnique Montreal, Quebec H3C 3A7, Canada

6.1 Abstract

The elongation of the bolt hole is an important parameter for assessing the failure of bolted joints. However, its direct experimental measurement using strain gauges and extensometers is difficult. This article shows that digital image correlation (DIC) can overcome the difficulties and provide important indications of the failure mechanisms of bolted joints. Hole elongation was measured using DIC in the following carbon/epoxy composite configurations: standard open-hole tensile (OHT) and filled-hole tensile (FHT), single-lap shear only-bolted (OB), and single-lap shear hybrid bolted/bonded (HBB) joints. For each configuration, the hole-elongation changes were tracked for cross-ply (CP) and quasi-isotropic (QI) stacking sequences with two thicknesses. In the tensile load direction for OHT and FHT cases, CP showed a greater hole elongation than QI. However, the opposite trend was observed in the transverse direction. In OB joints, bypass loads contributed more to the hole elongation than bearing action. In HBB joints, it has been observed that the adhesive significantly reduced hole elongation, particularly for CP configurations. Moreover, it was found that in HBB joints, hole elongation was independent of laminate lay-up, while it is very determinative in OB joints.

Keywords

Bolt-hole elongation, Hole deformation, Composites, Bolting, Hybrid joints, DIC.

* Corresponding author

E-mail address: rachid.boukhili@polymtl.ca (R. Boukhili)

6.2 Introduction

Carbon-fiber reinforced polymer (CFRP) composites are widely used in primary structures of aircraft, ships, and other applications where high reliability must be maintained during either short-term or long-term operations. This is due to the excellent specific mechanical properties of CFRP materials, such as light weight, high strength, low thermal and electrical conductivity, and high corrosion resistance [1, 2]. Three main classes of joining are used to connect thermoset composite components: mechanical fasteners, adhesive bonding, and hybridization of the two [3]. However, the presence of joints increases the flexibility of the entire structure. The added flexibility leads to not only the elongation of the hole and the associated bearing damage, but also the deformation/rotation of the bolt [4].

Several studies have addressed the hole elongation of open and filled hole specimens. Sawicki and Minguet [5] studied the failure mechanisms of open and filled holes in carbon/epoxy laminates under compressive loads. The addition of a fastener to an open hole specimen creates a load path, called a through-fastener load path, which reduces the deformation around the hole as the bolt takes up the majority of the load. This, in turn, reduces the amount of compressive deformation that the hole exhibits. Sola et al. [6] investigated the damage mechanisms of pin-bearing carbon-fiber composite laminates by considering the displacement of the pin. They found that a large notch elongation may promote the transition from bearing failure to either shear-out or cleavage failure. Saleh et al. [7] studied the effect of a circular hole in open-hole tensile (OHT) carbon-fiber woven composites by incorporating digital image analysis (DIC), which could properly capture the hole elongation of the specimen as it underwent uniaxial tension until failure. Junshan et al. [8] examined the effect of strain on the hole circumference of OHT composite laminates. By utilizing DIC, strain values around the hole were plotted as a function of the angular position with respect to the direction of the applied load. Using these strain values, the elongation of the hole can be calculated.

In the fatigue testing of a joint structure, the hole elongation after N cycles is calculated by subtracting the displacement at the first cycle from that at the Nth cycle [9]. The results obtained previously demonstrated that one of the reasons for bearing failure is the significant elongation of the joint hole, and a high clamp-up torque results in small hole elongations. Strain gauges installed between the blot rows of a multi-bolted joint can be used in quasi-static and fatigue testing to

analyze the strain distribution and load transfer [10, 11]. The measurements could also be considered as a representation of the hole elongation as well. Girard et al. [12] measured hole elongation using an extensometer and showed that the composite lay-up can affect the hole elongation in such a manner that angle-ply and quasi-isotropic (QI) lay-ups present similar hole elongations that are larger than the cross-ply (CP) hole elongation. Hole elongation was considered the ultimate failure mode in the fatigue testing of double-lap, multi-bolt composite joints [13]. It was found that in joints with a loose-fit hole, hole elongation commenced sooner, and clearance had the greatest effect on failure initiation but a lower effect on ultimate failure. Another fatigue testing result showed that long fiber-reinforced leaf spring joints experienced a lower hole elongation than unreinforced or short fiber reinforced for all stress levels tested [14]. Wei et al. [15] considered the bolt-hole elongation (BHE) reaching 4% of the hole diameter as an indication of composite joint failure in fatigue testing. Their results showed that neat fit joints experienced the least BHE compared to other interference fits.

Li et al. [16] experimentally found that the BHE increases as the number of fatigue cycles increases, while it decreases gradually with an increase in interference-fit sizes. X-ray images were used to observe the hole elongation in the single-lap (SL) composite joint. The results showed that the advent of hole elongation is more evident in countersunk fasteners than in non-countersunk fasteners because of the additional compressive deformation induced by the countersunk head of the bolt [17]. The cyclic loading of a composite joint revealed that an abrupt increase in BHE occurred in high-clamp-up torqued configurations, whereas for the low-clamp-up configurations, a gradual BHE increase was observed [18]. An improved finite-element (FE) model for single-bolt SL composite joints was developed by Liu et al. [19]. A good agreement was obtained between the bolt-hole deformation measurement using an extensometer and the FE simulation, which validated the effectiveness of the adjusted 3D FE model.

The combined effects of fatigue loading and seawater ageing on the bearing performance and failure mechanism of SL composite bolted joints were studied by Zhang et al. [20], and they found that the hole elongation, under quasi-static loading, for fatigue-tested specimens was noticeably smaller than that of non-fatigued specimens. Sajid et al. [21] investigated the role of washer size on the BHE of an SL basalt composite joint. A significant hole elongation was observed for larger washer configurations, but no apparent hole elongation was observed for small washer configurations. A computed tomography (CT) scan of an SL riveted woven carbon composite joint

showed that growth in the hole diameter due to hole elongation had its maximum values at the top plies, while it decreased step-wise while moving in the thickness direction to the middle plane and then the bottom plies [22]. CT and scanning electron microscopy (SEM) images also contributed to the observation of fiber kinking and wedge matrix cracking. The interaction of these damage modes leads to the formation of through-thickness shear cracks, the propagation of which causes permanent bolt-hole deformation [23].

While hole elongation is of significant concern in cyclic loading and researchers have focused excessively on it, the hole elongation of fatigue-tested composite joints was observed to be remarkably smaller than that of tensile-tested joints [20]. Therefore, it is important to investigate the hole-elongation phenomenon and its effects on the mechanical behavior of multi-bolted SL composite joints under quasi-static loading. However, in the literature, experimental measurements were primarily performed using displacement records of extensometers mounted on the tested specimen, which are always associated with some errors and inaccuracies due to the movement of the fixture of the tensile test machine. Therefore, the experimental measurement under quasi-static loading is quite challenging.

The present study aimed to use DIC technology to precisely measure the hole-elongation development and its effects for different composite configurations: open-hole tension (OHT) bolted filled-hole tension (FHT), only bolted (OB), and hybrid bolted/bonded (HBB) SL joints. The chosen composite lay-ups are the two well-known types: CP and QI lay-ups, which were manufactured using plain weave fabrics with thicknesses of 8 and 12 layers. The obtained results can assist in gaining a profound understanding of the hole-elongation development and the factors influencing it for the aforementioned configurations. Additionally, the DIC results are expected to provide more details in this regard to contribute to composite joining design for different types of aeronautic structures.

6.3 Experimental procedure

Carbon-fiber epoxy laminates reinforced with epoxy were manufactured using the vacuum-assisted resin infusion (VARI) process. The composite laminates were composed of 3K plain weave carbon fabric with a surface weight of 193 g/m^2 and a commercial Araldite epoxy resin system [24]. The average thicknesses of the panels were approximately 2.6 mm and 1.6 mm for 12 and 8 layers, respectively. The QI and CP laminate configurations were obtained by orienting the

woven plies, the lay-up of which is given in Table 6.1. Moreover, Table 1 lists the average recorded nominal strengths in unnotched tensile standard (TS), OHT, and FHT tests for CP and QI.

Table 6.1: Stacking sequences and tensile strengths of the unnotched (TS), open-hole (OHT), and filled-hole (FHT) configurations of the manufactured laminates.

Code	Lay-up	Plies	Average thickness, *t* (mm), (STD)	Unnotched, TS (MPa), (STD)	Open-hole, OHT (MPa), (STD)	Filled-hole, FHT (MPa), (STD)
CP8	$[(0/90)/(0/90)/(0/90)/(0/90)]_s$	8	1.65 (0.027)	854 (29.8)	455 (9.82)	420 (0.95)
QI8	$[(0/90)/(\pm45)/(0/90)/(\pm45)]_s$	8		592 (9.12)	384 (6.76)	366 (0.3)
CP12	$[(0/90)/(0/90)/(0/90)/(0/90)/(0/90)/(0/90)]_s$	12	2.63 (0)	800 (15.26)	406 (8.4)	442 (1.03)
QI12	$[(0/90)/(\pm45)/(0/90)/(\pm45)/(0/90)/(\pm45)]_s$	12		579 (9)	364 (7.98)	358 (1.18)

The specimens corresponding to TS, OHT, and FHT tests were manufactured according to ASTM-D3039 [25], ASTM-D5766 [26], and ASTM-D6742 [27], respectively. Moreover, SL multi-bolted joints were designed and manufactured according to ASTM-D5961 [28]. The two parts in SL bolted joints were fastened using steel hex-head shear bolts (NAS6204-4) with a diameter of 6.35 mm, nuts (MS21042-4), and cadmium-plated steel washers (NAS1149F0463P) with an internal diameter of 6.73 mm and external diameter of 12.70 mm on both the head and side nuts. A tightening torque of 5 Nm was applied to each bolt using a Tohnichi Dial Torque Wrench DB25N-S. A specialized carbide drill bite with a diameter of 6.35 mm, provided by YG-1 America, Inc., was utilized to drill in the laminate coupons [3]. The HBB joints were manufactured by simply adding an adhesive between the faying surfaces of OB joints. The applied adhesive was the same as the epoxy resin used for manufacturing the composite laminate [29]. Throughout this paper, the prefixes OHT, FHT, OB, and HBB are added to the laminate code, for example, HBB-CP12 and OHT-QI8, to specify the class of configurations. The geometrical configurations of OHT, SL OB,

and HBB composite joints are shown in Figure 6.1. Furthermore, at least four identical coupons were tested for each configuration at a constant standard crosshead displacement rate of 2 mm/min. Uniaxial tests were conducted using a servo-hydraulic MTS machine model 810. The 810 MTS offers extensive testing capabilities and a load capacity of up to 100 kN. It is appropriate for fatigue, fracture, and monotonic tests.

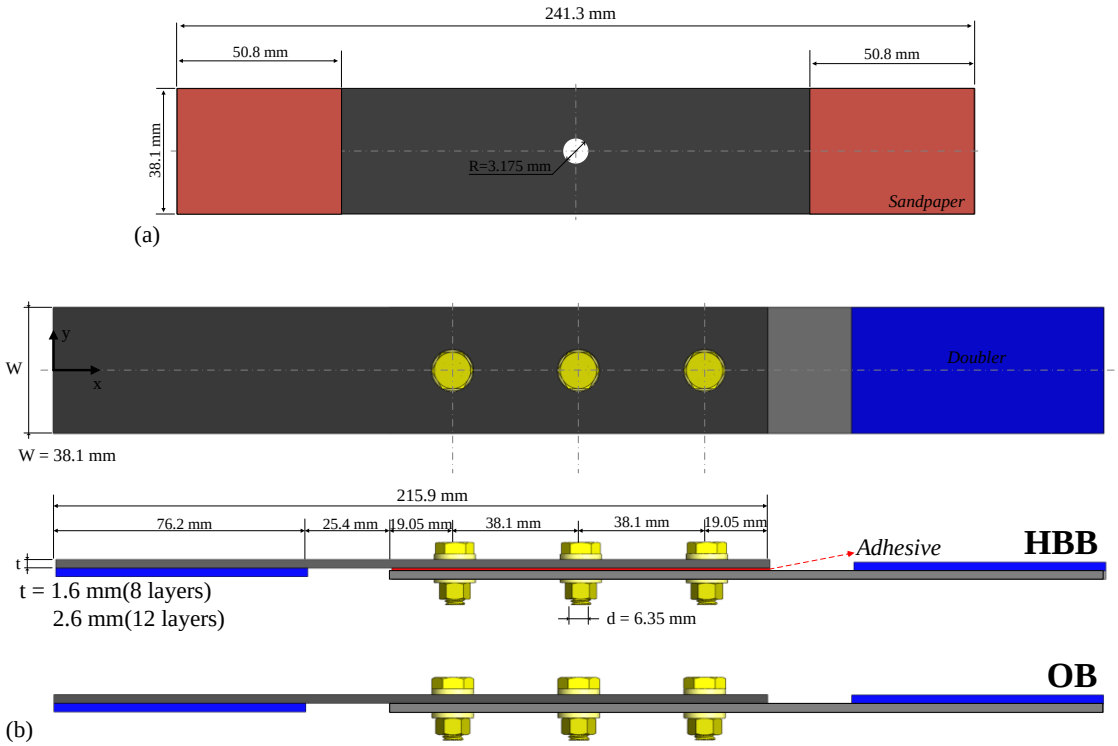

Figure 6.1: Specimen geometry and dimensions for (a) OHT and (b) OB and HBB SL joints.

In this study, DIC technology was used to measure hole deformations. The principle of this optical measurement technique is based on the tracking of a random pattern on the specimen surface by matching the local distribution of pixel concentration, i.e., subsets, between the undeformed and deformed images in a specific time interval. Two 5-megapixel Pointgrey Grasshopper charge-coupled device (CCD) cameras with a pixel size of 3.45 were used for the camera sensor [3]. The setup also included a light source to illuminate the specimens. All specimens were spray-painted with white spray paint, following which a random speckle pattern was applied. The cameras captured photos at a rate of 2 frames per second. The captured images were processed using Vic-3D v7.2.4 (Correlated Solutions Inc., USA). Further details of the DIC system configuration are provided in Ref. [3].

6.4 Results and discussion

6.4.1 Hole deformation

Prior to investigating the hole elongation of OB and HBB joints, this phenomenon was studied for OHT and FHT, which are widely used in the aeronautical industry for material qualification purposes [30, 31]. During tensile testing, the deformation of the hole was measured in the longitudinal and transverse directions. The deformation of the hole along the longitudinal direction (the loading direction) is labeled as LHE, short for longitudinal hole elongation, and that along the transverse direction to the loading is labeled as THC, short for transverse hole compression. As shown in Figure 6.2, the LHE and THC measurements were retrieved by applying two virtual extensometers (VEs) within Vic-3D software: one in the longitudinal direction and the other in the transverse direction.

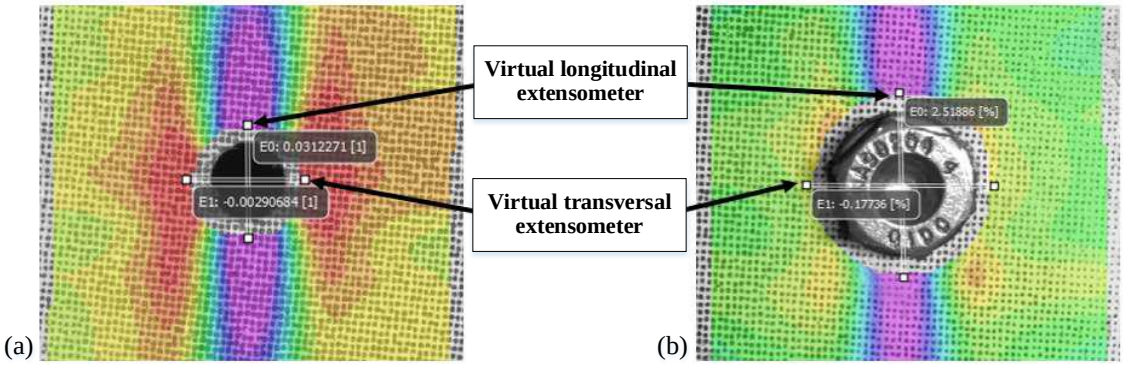

Figure 6.2: Application of virtual extensometers in Vic-3D: (a) OHT and (b) FHT.

Figure 6.3 plots LHE against the applied tensile load of OHT and FHT specimens for each laminate. Because CP laminates have twice as many fibers oriented in the load direction as QI laminates, at first glance, it can be expected that their higher stiffness will result in lower hole elongation. However, for the OHT test, as shown in Figure 6.3 (a), the opposite result is obtained. This result may stem from the fact that the CP configuration has a higher notch sensitivity and stress concentration than the QI configuration [3, 30]; hence, it significantly influences the CP longitudinal hole elongation from the beginning of the test.

It is interesting to observe that for a given thickness in the case of FHT (Figure 6.3 (b)), unlike the OHT case, the hole elongation for the CP configuration is slightly less than that of the

QI configuration up to a certain load. Beyond this load, the CP curves gradually diverge, and a greater hole elongation is observed as compared to the QI configuration. It is suggested that at lower levels of applied load, filling the hole with a clamped bolt greatly reduces the longitudinal and transversal deformation because the bolt upholds the geometric integrity of the hole; consequently, the notch sensitivity does not play a crucial role. However, at higher load levels, the higher stress concentration in the CP configuration results in increased hole elongation. The benefit of the reduction in LHE with a clamped bolt does not seem to contribute to the strength retention of the laminates. Because the holes in the FHT specimens undergo less deformation, the hole boundary exhibits a smaller degree of damage. This, in turn, leads to less energy absorption and, hence, less stress relief, which explains why the FHT specimens in this investigation have a lower tensile strength than the OHT specimens (Table 6.1). Delamination at the edge of the hole during testing leads to a decrease in stress concentration [32]. CP12 is an outlier because its OHT strength is less than its FHT strength. In general, it can be inferred that in a woven carbon-fiber composite plate with a hole, the bolt can provide a good system of control, creating a delaying effect on the stress concentration and notch sensitivity of the corresponding laminate as well as blocking the damage progression to some extent.

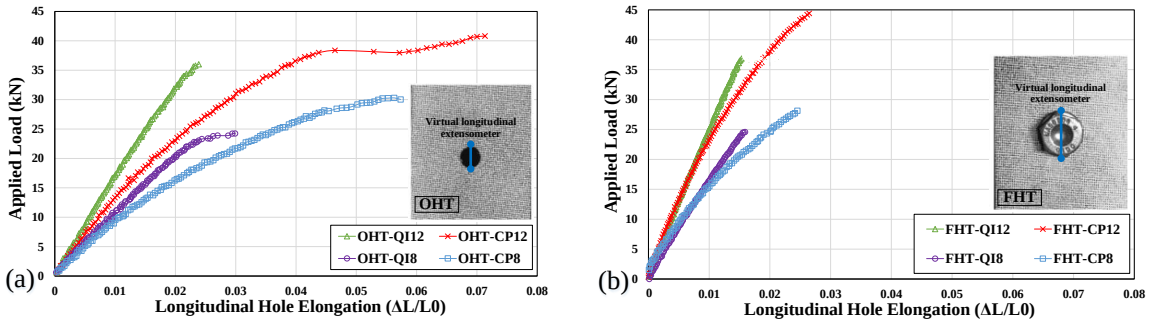

Figure 6.3: Effect of laminate configuration on open- and filled-hole notch deformation: (a) OHT with LHE and (b) FHT with LHE.

Figure 6.4 (a) and (b) show the load–displacement curves of OHT and FHT, respectively. These curves show the macroscopic deformation, which is the total displacement of the specimen between the grips and comprises the LHE. From Figure 6.4 (a) and (b), the laminates in the increasing order of macroscopic elongation are CP12, QI12, CP8, QI8, CP12, CP8, QI12, and QI8. It is interesting to note that this order of elongation is different from that shown in the LHE curves (Figure 6.3 (a) and (b)), in which the values of QI are always greater than those of CP for the given thicknesses. It can be concluded that the load–displacement curves are not reliable in predicting the microscopic elongation of the hole (LHE), and the DIC technique is a necessary tool for extracting such data.

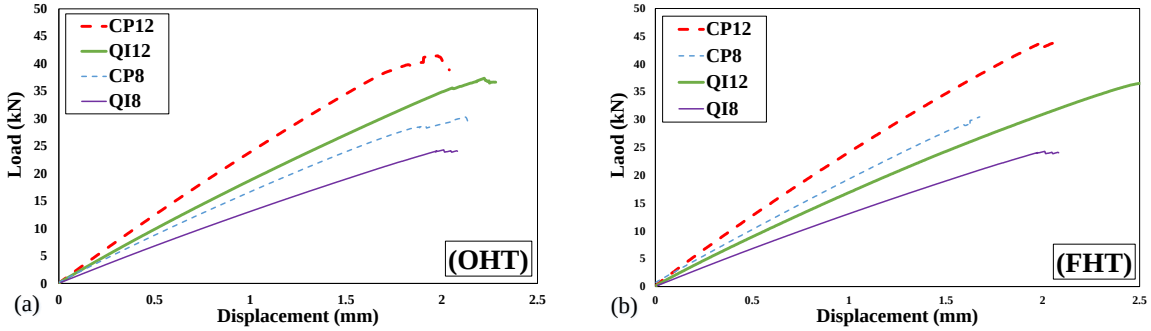

Figure 6.4: Load–displacement curves of CP8, CP12, QI8, and QI12: (a) OHT and (b) FHT.

Figure 6.5 plots THC against the applied tensile load in OHT and FHT specimens for each laminate. The following observations can be made by comparing OHT with FHT:

- The clamped bolt upholds the geometric integrity of the hole because FHT laminates have a lower THC than OHT laminates.
- CP laminates, which have a large LHE, possess a lower THC than QI laminates. This implies that the hole elongates more in CP than in QI, while the CP hole exhibits less THC than the QI hole. This trend was observed for both OHT and FHT specimens (Fig. 5 (a) and (b), respectively).

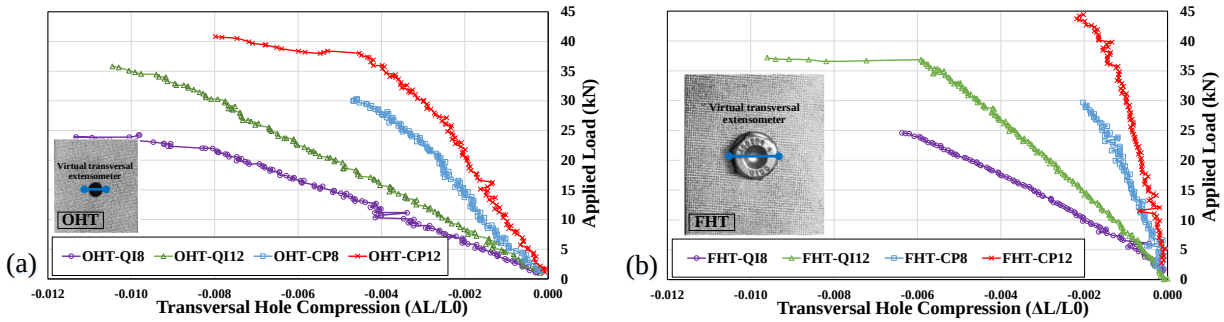

Figure 6.5: The effect of laminate configuration on open- and filled-hole notch deformation: (a) OHT with THC and (b) FHT with THC.

The difference in LHE and THC between CP and QI may occur because of the 45° plies in the QI laminate. Figure 6.6 illustrates the strain contour plots (longitudinal and transverse) at 40% of the failure load for CP12 and QI12. The arrows depict the direction and magnitude of the strains with respect to the axis of the peak strains for each strain plot. As shown in Figure 6.5 (a), the axis of the peak strains is the transversal axis from the hole edge to the free edge of the specimen. The axis of the peak strains is dependent on the laminate configuration and whether the strain is longitudinal or transversal. As shown in Figure 6.6 (a), the peak longitudinal strains (ε_{xx}) for CP12 are concentrated at the hole boundary and stay elevated along the longitudinal direction owing to the 0° plies. The axis of symmetry for the strains coincides with the y-axis. However, the axis of the peak strains for QI12 (Figure 6.6 (b)) is at an angle of approximately 45° to the y-axis (butterfly pattern). The fact that the CP peak strains pull perpendicularly to the hole boundary and those of QI pull at an angle from the hole boundary might explain why the LHE of the CP configuration is higher than that of the QI configuration (Figure 6.3).

The perpendicular deformation of the hole has increased leverage over the longitudinal deformation as compared to deformation at an angle. The peak transversal strains (ε_{yy}) for CP12 (Figure 6.6 (c)) are concentrated at the hole boundary and stay somewhat elevated along the longitudinal direction. This trend is similar to that exhibited in the longitudinal strain plots; however, there is a clear difference. The compressive transversal strains occur in half of the specimen (upper-right and lower-left sides of the notch) with no clear axis of symmetry. The QI lay-up exhibits (Figure 6.6 (d)) the same 45° axis, along which the peak compressive strains are

distributed. This favors an increase in THC values for QI compared to CP lay-ups. Although CP12 and QI12 were used here as examples, CP8 and QI8 exhibited the same phenomenon. This result indicates that the laminate lay-up has a significant influence on the overall hole deformation of the composite plate.

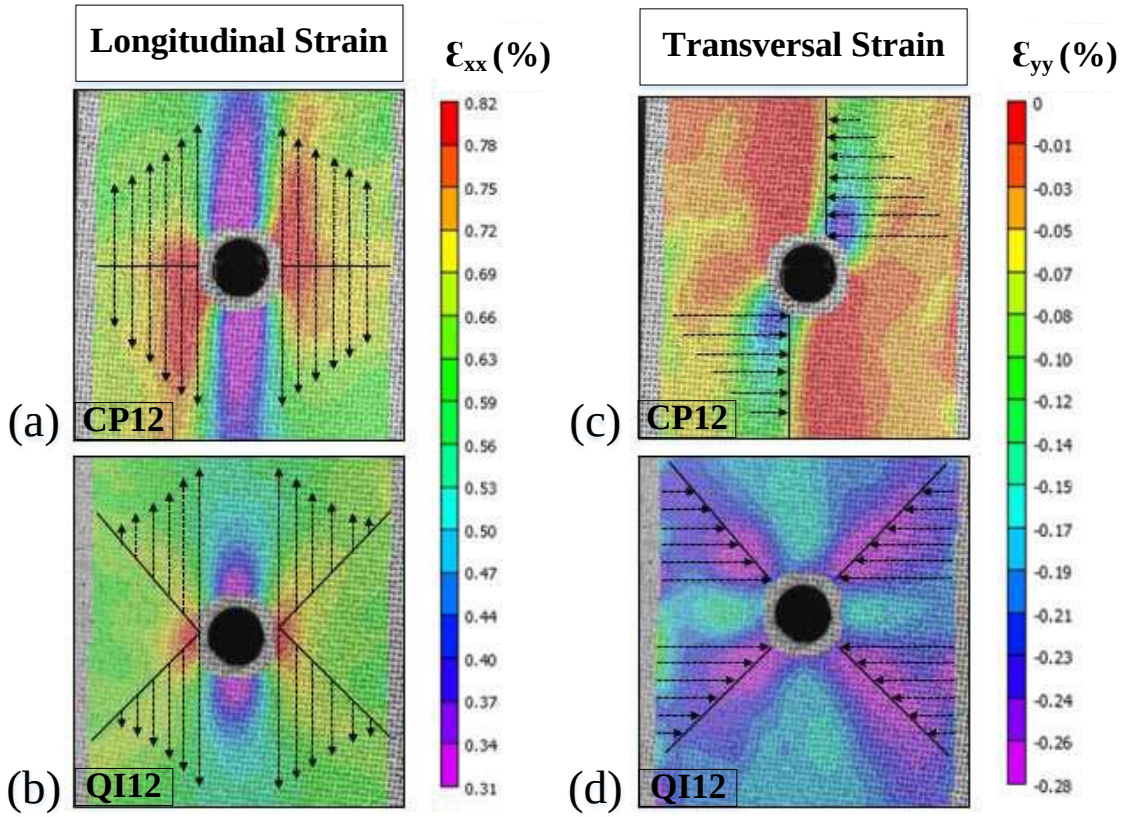

Figure 6.6: Strain contours at 40% of the failure load for longitudinal strains of (a) CP12 and (b) QI12, as well as transversal strains of (c) CP12 and (d) QI12.

6.4.2 Bolt hole elongation (BHE) in joints

Following the investigation of hole deformation in OHT and FHT, this section investigates the same phenomenon for SL joints with significantly different geometrical configurations and behaviors. The test results were analyzed based on the DIC data recorded for eight different SL joint configurations (see Table 6.1), the corresponding failure loads and load–displacement curves of which are shown in Figures 6.7 and 6.8, respectively. As previously mentioned, the BHE (also

called hole wear in fatigue testing) is of significant concern in the cyclic and quasi-static loading of a joint. Similar to the previous section, three VEs were placed diametrically in the axial direction at the bolt positions (Figure 6.9 (b)) and labeled as VE3, VE2, and VE1. This section comprises the following three subsections: Section 6.4.2.1 studies the case of OB joints (Figures 6.10-6.11), Section 6.4.2.2 investigates HBB joints (Figures 6.12-6.13), and finally, Section 6.4.2.3 compares the two configurations, i.e., OB vs HBB, in a bar chart (Figure 6.14) to determine the effect of hybridization on hole elongation development.

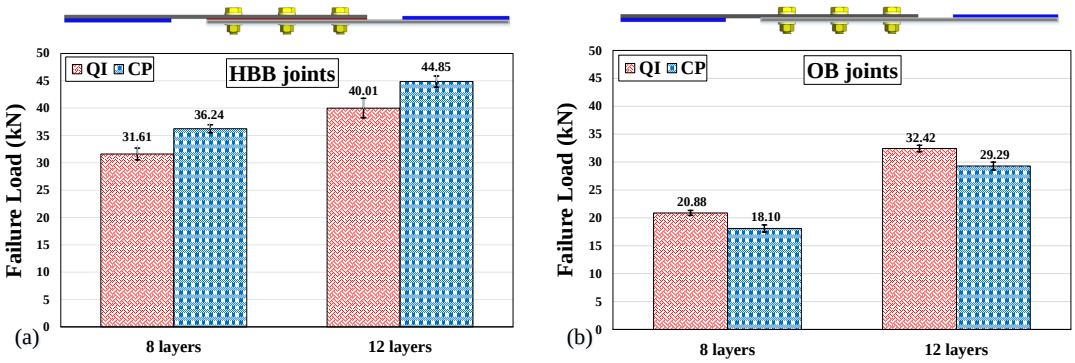

Figure 6.7: Failure loads of CP and QI with 8 and 12 layers: (a) HBB and (b) OB.

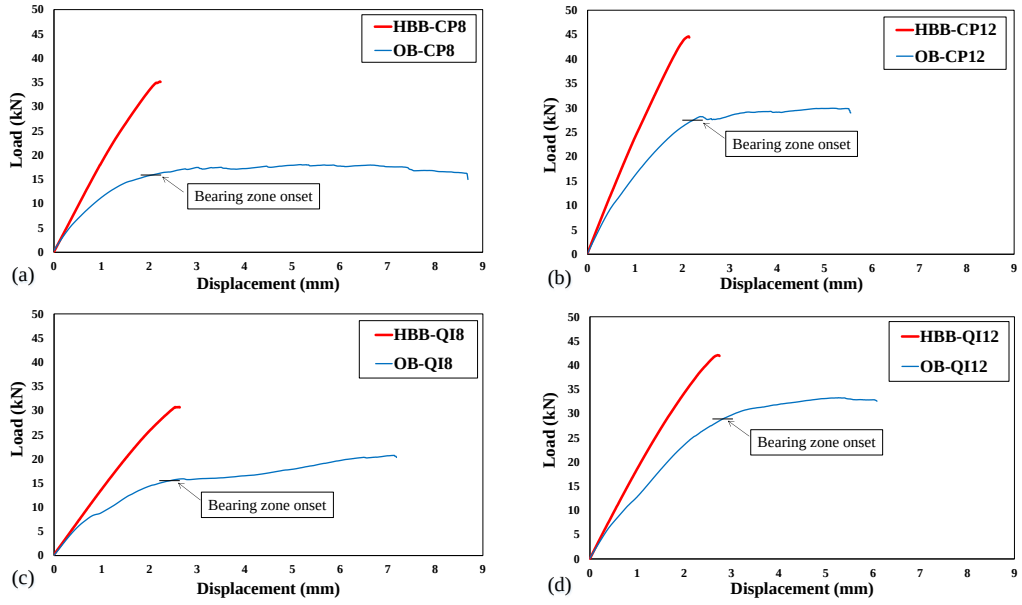

Figure 6.8: Load–displacement curves with the indication of bearing zone onset of OB vs HBB joints, (a) CP8, (b) CP12, (c) QI8 and (d) QI12.

6.4.2.1 BHE of only-bolted (OB) joints

In general, BHE describes the deformation of the hole caused by both the bearing load through the bolt shank pressure [33] and the bypass load around the hole. Figure 6.9 (a) shows a schematic of the contribution of the bearing and bypass loads around the critical bolt, i.e., B3, where net-tension failure occurs owing to the highest value of bypass/bearing load ratio. Moreover, Figure 6.9 (b) illustrates the position of the previously mentioned VEs.

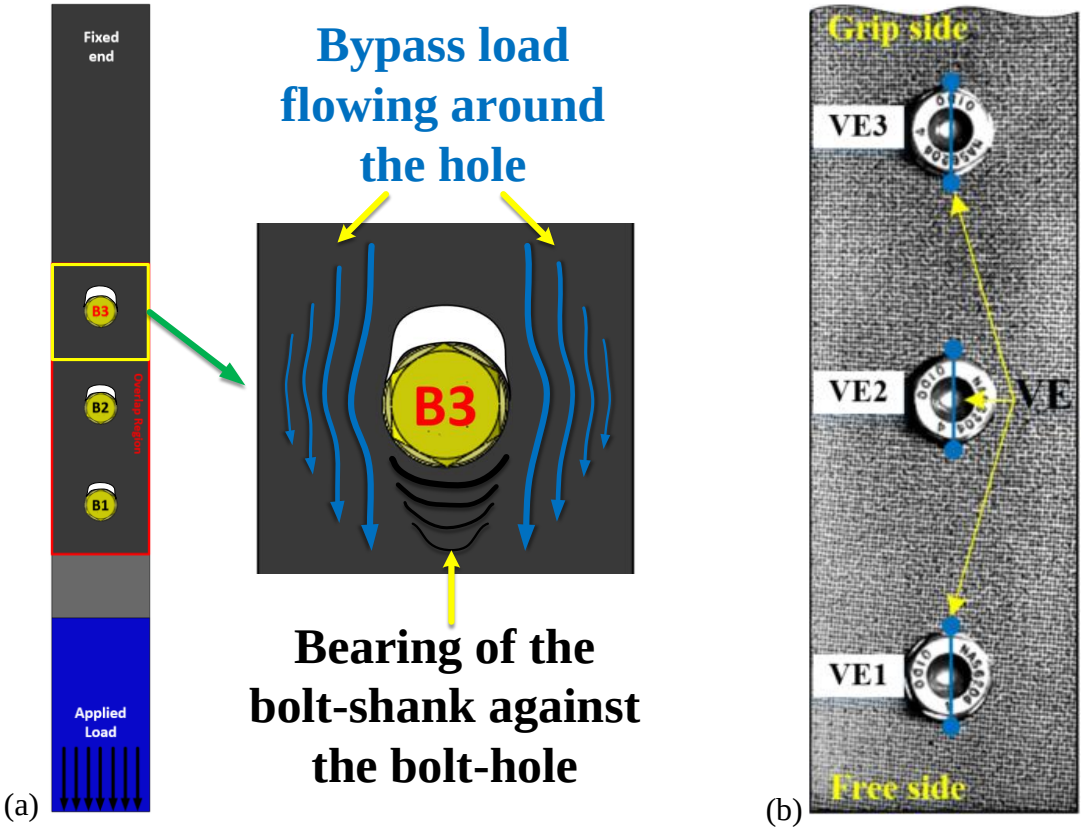

Figure 6.9: (a) Exaggerated schematic of the BHE in an SL joint and (b) the placement of three VEs at the hole position in DIC software.

Figure 6.10 shows the BHE of the OB joints up to the load level corresponding to the onset of bearing damage identified in Figure 6.8. A curve fit of the DIC data was used to improve visualization. For all the laminate lay-ups (CP and QI) tested, BHE gradually decreased when proceeding from hole 3 (grip side) towards hole 1 (free side). This is due to the stepwise reduction in the bypass/bearing load ratio in the mentioned direction [3]. Therefore, it could be suggested that the influence of the bypass load is greater than that of the bearing action in forming the hole

elongation for a given laminate lay-up of the multi-bolted SL composite joint. The results for the thinner joints (see Appendix B) illustrate that at equal load levels, thinner configurations experienced more longitudinal hole elongation than the thicker ones, which seemed to be more pronounced at B3. In SL joints, this phenomenon may be attributed to the higher induced bending stress in thicker joints due to the greater geometrical eccentricity [34]. Consequently, at the fastener location, the outer surface of thicker laminates may experience more compression than thinner ones, which can lead to an overall reduction in BHE.

The relationship between BHE and tensile loading can represent the BHE stiffness. The curves of CP exhibited two distinguishable segments of BHE stiffness. The first segment of the curves is predominantly linear and has a high slope. In the second segment, the slope of the curves abruptly starts to decrease, crossing the QI whose curves are rather single-slope and indicating minor changes in BHE stiffness. It is interesting to note that the same behavior is also observed in the FHT case (Figure 6.3(b)), in which CP experienced a lower BHE than QI for both thin and thick configurations at lower load levels. However, as the load increased, the BHE curves of CP surpassed those of QI, resulting in greater elongation in CP. It is worth noting that with an acceptable estimation, the CP curves of VE3, VE2, and VE1 surpassed those of QI at approximately 40%, 55%, and 60% of the failure load, respectively. Therefore, it can be observed that for B3, the crossing of the curves occurred much sooner and approximately at the moment of transition where the load transfer mechanism changed from friction between faying surfaces to bolt load bearing [34]. According to the previously mentioned percentages, the bolt shanks of B2 and B1 are considered to have come into contact with the bolt hole with a noticeable delay compared to that of B3. Figure 6.11 shows another representation of the transition of the load transfer mechanism occurring at the B3 location. To do so, a virtual yellow line (inset in Figure 6.11) perpendicular to the load direction was drawn from edge to edge (Y position ranging from -20 mm to +20 mm) and at a distance of *2d* (*d* is the hole diameter) from the center of the corresponding hole. The results show the evolution of longitudinal deformation from 10% to 90% of the failure load in steps of 20%. It can be seen that at lower load levels (10% and 30%), the distribution of longitudinal deformation, i.e., axial strain, below the bolt is more level than that of the higher ones. This could be attributed to the friction forces engaged between the faying surfaces of the plates, which subsequently prevented the bolts from load transferring at lower load levels. Moreover, Figure 6.11 illustrates the consequence of the greater BHE of CP compared to QI in terms of bearing formation

under B3. The higher strength of the OB joint made of QI compared to that made of CP shown in Figure 6.7 may be explained by the fact that QI experiences less hole elongation than CP. Indeed, hole elongation in bolted joints is associated with local bearing damage around the bolt holes [3].

As stated previously, BHE is associated with the combination of the bearing action and the bypass load, where the stress concentration of the former is more severe than that of the latter [35] and may alter the magnitude of BHE for a given laminate thickness. Thus, the observation of CP curves surpassing those of QI could be explained by the fact that the stress concentration is intensified when the number of 0° plies increases and lessened when the portion of ±45° plies increases. As the applied load increases, the stress concentration becomes a dominant factor in generating delamination and macrocracking within the laminate, specifically around the holes. Therefore, as the load increases, the CP lay-up, which has greater bearing deformation, experiences a greater stress concentration than QI, which eventually leads to the higher BHE. Overall, it can be concluded that in SL multi-bolted composite joints, the rate of increase of BHE is highly dependent on the laminate lay-up, and a laminate with a lower content of 0° plies undergoes less hole wear, resulting in a higher restored strength.

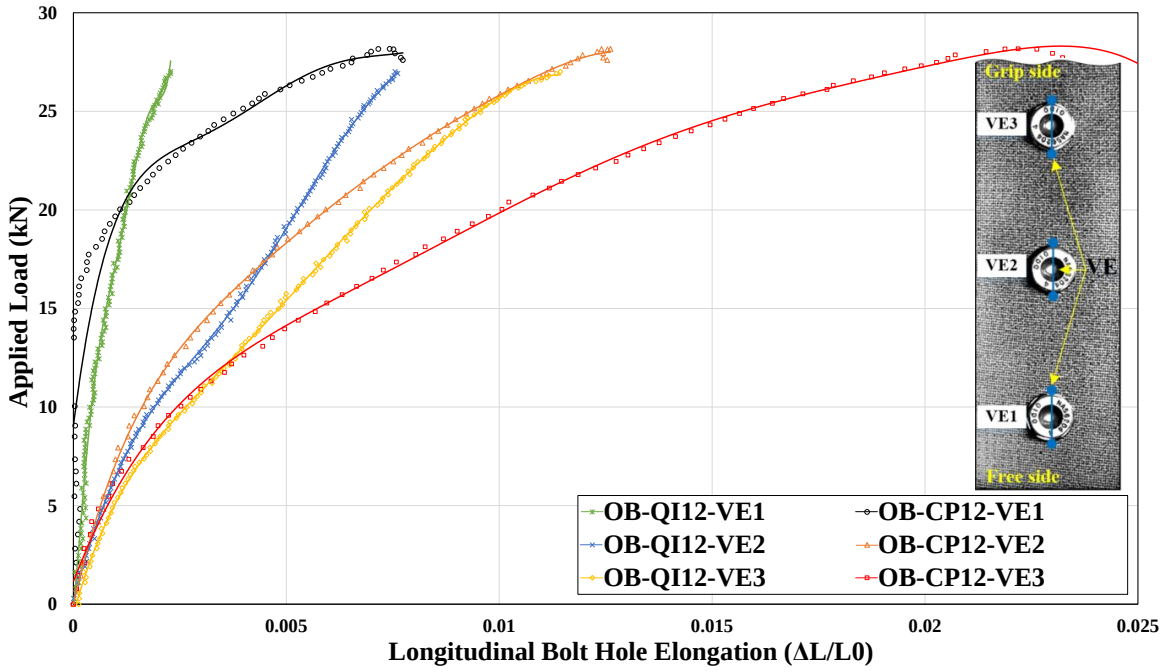

Figure 6.10: Bolt-hole elongation of OB-CP12 and OB-QI12 (the same pattern occurs for 8 layers; see Appendix B).

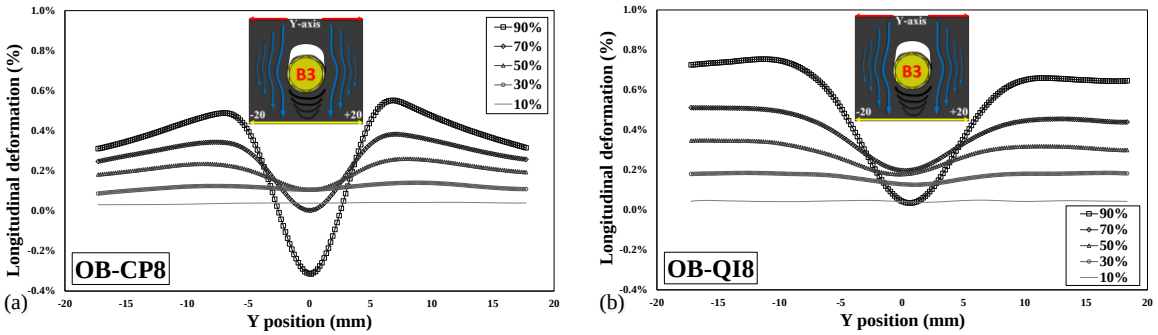

Figure 6.11: Longitudinal deformation below B3 at 10%, 30%, 50%, 70%, and 90% of the failure load: (a) OB-CP8 and (b) OB-QI8 (the same pattern occurs for 12 layers; see Appendix B).

6.4.2.2 BHE of hybrid bolted-bonded (HBB) joints

Figure 6.12 shows that for HBB joints, similarly to OB joints, BHE decreases when moving from B3 to B1. It is important to highlight that among the two main factors that contribute to hole elongation in SL bolted joints, the bypass load plays the predominant role in the HBB joints as the added adhesive cancels out the bearing effect to a substantial extent [3]. Unlike the OB joints in which bearing action is actively operative and alters the BHE (Figure 6.10), the curves of HBB remained mostly straight, which indicates minor changes in BHE stiffness throughout the test (Figure 6.12). This suggests that hybridization effectively eliminates the effects of stress concentration and notch sensitivity, which are noticeably influenced by the bearing act, in OB composite joints. It should be noted that since 12-layer laminate is stiffer than 8-layer laminate, the BHE stiffness (curve slope) of each hole of the former is greater than that of the latter (see Appendix B for the corresponding figure of 12-layer joints).

It is striking to underline that the BHE values of each peer-to-peer hole of CP and QI are almost equal for both 8 and 12 layers, which clearly indicates the independence of BHE from the laminate stacking sequence and bolt movement in the HBB SL composite joints studied herein. Furthermore, as there is no presence of fair share of bearing act in forming the hole elongation; therefore, it can be inferred that in multi-bolted hybrid composite joints, the dominant mechanism of load transmission between the two joint members is driven by the adhesive itself to a significant

extent. Similar to Figure 6.11, the surface deformations under B3 for CP and QI are shown in Figure 6.13. It can be observed that the curves do not cross each other, and the concavity shape (depression) is formed merely by the bypass load [3], which flows around the hole and is the main contributor to the hole elongation development of HBB joints.

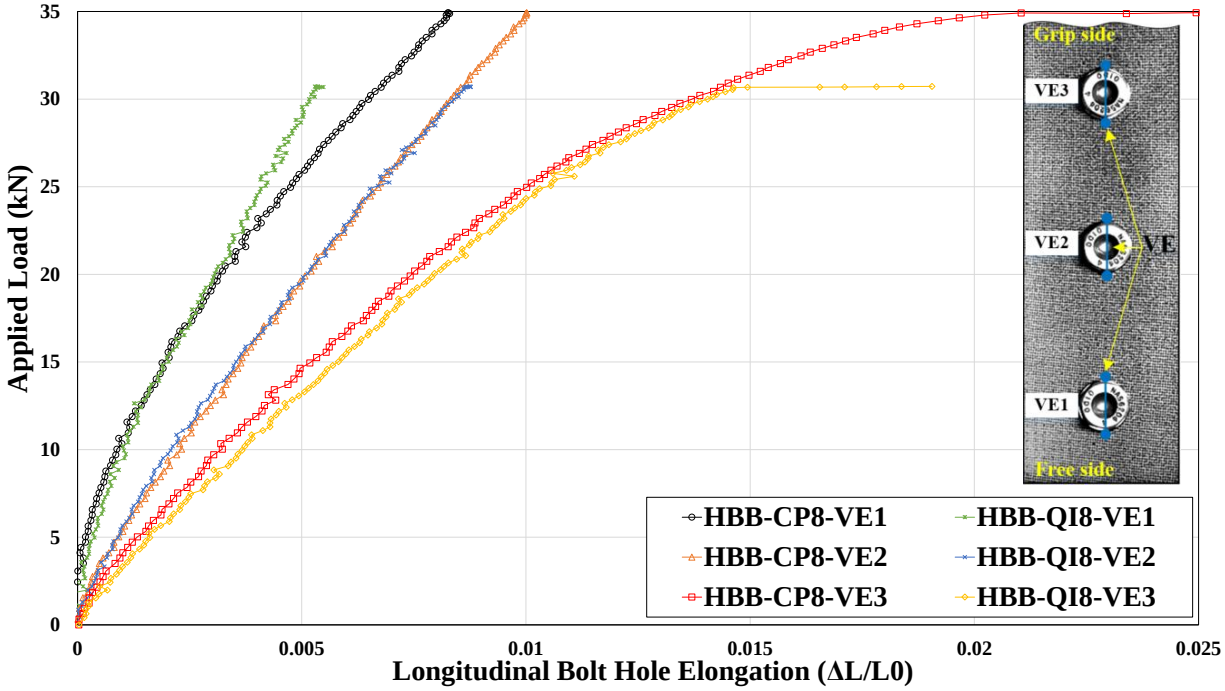

Figure 6.12: BHE of HBB-CP8 and HBB-QI8 (the same pattern occurs for 12 layers; see Appendix B).

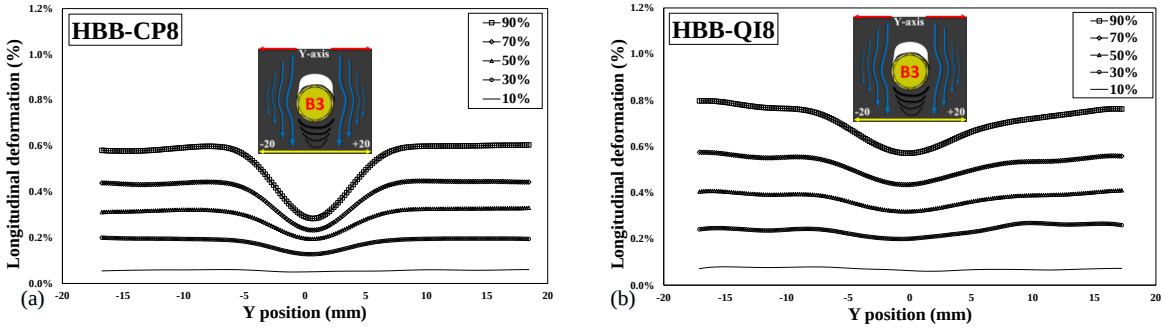

Figure 6.13: Longitudinal deformation below B3 at 10%, 30%, 50%, 70%, and 90% of the failure load: (a) HBB-CP8 and (b) HBB-QI8 (the same pattern occurs for 12 layers; see Appendix B).

6.4.2.3 BHE in OB versus HBB: CP and QI

Figure 6.14 compares the BHE for OB and HBB joints with investigated laminates of 8 layers. The load level (15 kN) corresponds to the onset of bearing damage in the OB joints, as shown in Figure 6.8. Therefore, the hole elongation values of CP are greater than those of QI, as was observed previously at higher load stages. Moreover, for a given thickness, the elongations of each hole of CP and QI, for example, bolt-hole 2 (BH2), are approximately identical in the HBB joint, whereas they markedly differ in the OB joint. This may suggest that hybridization significantly eliminates the hole elongation caused by the bearing effect, which is due to the bolt movement/tilting in OB configurations. According to Figure 6.14, hybridization decreases hole elongation, especially in the critical bolt (B3), and this decrease is more pronounced for CP than for QI. This occurred because, in comparison with QI, CP experiences a more severe stress concentration and notch sensitivity around the holes, and the added adhesive relieves it significantly. Better performance of the adhesive in creating a dramatic reduction in the BHE of CP, the adhesive assists this configuration to substantially sustain its strength, as shown in Figure 6.7.

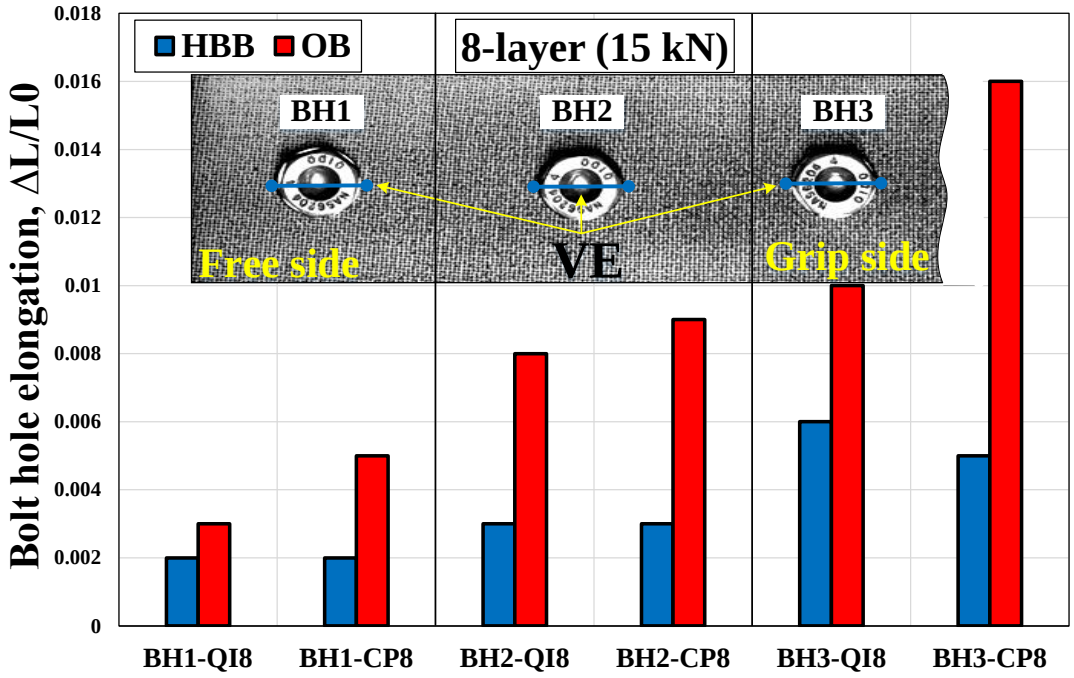

Figure 6.14: Comparison of BHE in OB8 versus HBB8 of CP and QI joints at a load level of 15 kN (the same pattern occurs for 12 layers; see Appendix B).

6.5 Conclusion

This study focused on highlighting the use of DIC to properly monitor hole elongation in woven laminated composites. DIC hole elongation was measured in the following carbon/epoxy composite sample configurations: standard open-hole tensile (OHT) and filled hole tensile (FHT) specimens, single-lap shear only bolted joint (OB) and single-lap shear hybrid-bolted-bonded joint (HBB).

In the case of OHT, for a given stress level, the total displacement of the specimen between grips was lower for CP than for QI laminates, and this behavior appears logical because CP is stiffer than QI. However, during the same tests, the longitudinal hole elongation (LHE) was higher for CP than for QI laminates, implying that the total displacement cannot indicate the state of deformation of the hole. During the same tests, the transverse hole compression (contraction) was measured, and against expectations, QI retracted more than CP. In other words, for CP, the hole elongated more than for QI but retracted less. The fact that the retraction was less for CP can be explained by the inherently lower Poisson's ratio (ν_{xy}) of CP compared to QI. However, the mechanism underlying the higher LHE in CP is unclear. It must be noted that the aforementioned behavior was verified for two different laminate thicknesses. Asserting that the hole elongates more but retracts less for CP as compared to QI amounts to stating that the effective diameter of the hole increases in the case of CP, which explains the greater sensitivity to the notch of CP reported in the literature. The same behavior was observed for the case of FHT, except that the difference in LHE between CP and QI was observed only at high stress levels.

The same pattern behavior of FHT was replicated with multi-bolt OB joints, although some specific features emerged due to the fact that in multi-bolt OB, the load sharing between the three bolts increases when moving from the free end to the grip end. Bolt B3 at the grip end, which experienced the highest load, initially behaved similarly in CP and QI, but at approximately 40% of the ultimate load, the elongation of the bolt hole in CP increased at a greater rate than for QI. Moreover, it was found that in multi-bolted SL composite joints, the influence of the bypass load was greater than the bearing action in forming the hole elongation.

BHE was considerably reduced in HBB than in OB. In fact, the results showed that the studied CP and QI laminates behave similarly until the onset of failure. The BHE of bolt B3 in CP surpassed that in QI, and the same was observed for bolt B2. Furthermore, hybridization

significantly reduced BHE, which was more pronounced in CP than in QI. This is due to the effective stress concentration relief that occurred around the CP bolt hole because of the adhesive. Hybridization also aids in sustaining the strength of the HBB-CP joints.

6.6 Acknowledgments

The authors gratefully acknowledge the financial support provided by the Natural Sciences and Engineering Research Council of Canada (NSERC).

6.7 References

[1] Mehrabian M, Golmakani M. Nonlinear bending analysis of radial-stiffened annular laminated sector plates with dynamic relaxation method. Computers & Mathematics with Applications. 2015;69:1272-302.

[2] Davies P, Rajapakse YD. Durability of composites in a marine environment: Springer, 2014.

[3] Mehrabian M, Boukhili R. 3D-DIC strain field measurements in bolted and hybrid bolted-bonded joints of woven carbon-epoxy composites. Composites Part B: Engineering. 2021:108875.

[4] Vangrimde B, Boukhili R. Analysis of the bearing response test for polymer matrix composite laminates: bearing stiffness measurement and simulation. Composite structures. 2002;56:359-74.

[5] Sawicki AJ, Minguet PJ. Failure mechanisms in compression-loaded composite laminates containing open and filled holes. Journal of Reinforced Plastics and Composites. 1999;18:1708-28.

[6] Sola C, Castanié B, Michel L, Lachaud F, Delabie A, Mermoz E. Bearing fatigue of composite laminates: Damage monitoring and fatigue life prediction. Composites Part B: Engineering. 2017;110:487-96.

[7] Saleh MN, Wang Y, Yudhanto A, Joesbury A, Potluri P, Lubineau G, et al. Investigating the potential of using off-Axis 3D woven composites in composite joints' applications. Applied Composite Materials. 2017;24:377-96.

[8] Hu J, Zhang K, Cheng H, Liu P, Zou P, Song D. Stress analysis and damage evolution in individual plies of notched composite laminates subjected to in-plane loads. Chinese Journal of Aeronautics. 2017;30:447-60.

[9] Chen H-S. The static and fatigue strength of bolted joints in composites with hygrothermal cycling. Composite structures. 2001;52:295-306.

[10] Starikov R, Schön J. Fatigue resistance of composite joints with countersunk composite and metal fasteners. International journal of fatigue. 2002;24:39-47.

[11] Starikov R, Schön J. Quasi-static behaviour of composite joints with protruding-head bolts. Composite structures. 2001;51:411-25.

[12] Girard C, Dano M-L, Picard A, Gendron G. Bearing behavior of mechanically fastened joints in composite laminates--Part I: strength and local strains. Mechanics of Advanced Materials and Structures. 2003;10:1-21.

[13] Lawlor VP, Mccarthy MA, Stanley W. An experimental study of bolt–hole clearance effects in double-lap, multi-bolt composite joints. Composite structures. 2005;71:176-90.

[14] Subramanian C, Senthilvelan S. Effect of reinforced fiber length on the joint performance of thermoplastic leaf spring. Materials & Design. 2010;31:3733-41.

[15] Wei J, Jiao G, Jia P, Huang T. The effect of interference fit size on the fatigue life of bolted joints in composite laminates. Composites Part B: Engineering. 2013;53:62-8.

[16] Li J, Zhang K, Li Y, Liu P, Xia J. Influence of interference-fit size on bearing fatigue response of single-lap carbon fiber reinforced polymer/Ti alloy bolted joints. Tribology International. 2016;93:151-62.

[17] Nezhad HY, Egan B, Merwick F, McCarthy CT. Bearing damage characteristics of fibre-reinforced countersunk composite bolted joints subjected to quasi-static shear loading. Composite structures. 2017;166:184-92.

[18] Giannopoulos IK, Doroni-Dawes D, Kourousis KI, Yasaee M. Effects of bolt torque tightening on the strength and fatigue life of airframe FRP laminate bolted joints. Composites Part B: Engineering. 2017;125:19-26.

[19] Liu F, Lu X, Zhao L, Zhang J, Hu N, Xu J. An interpretation of the load distributions in highly torqued single-lap composite bolted joints with bolt-hole clearances. Composites Part B: Engineering. 2018;138:194-205.

[20] Zhang K, Li H, Cheng H, Luo B, Liu P. Combined effects of seawater ageing and fatigue loading on the bearing performance and failure mechanism of CFRP/CFRP single-lap bolted joints. Composite structures. 2020;234:111677.

[21] Sajid Z, Karuppanan S, Sallih N, Kee K, Shah S. Role of washer size in mitigating adverse effects of bolt-hole clearance in a single-lap, single-bolt basalt composite joint. Composite structures. 2021;266:113802.

[22] Torres-Arellano M, Bolom-Martínez MdJ, Franco-Urquiza EA, Pérez-Mora R, Jiménez-Arévalo OA, Olivier P. Bearing Strength and Failure Mechanisms of Riveted Woven Carbon Composite Joints. Aerospace. 2021;8:105.

[23] Cao Y, Zuo D, Zhao Y, Cao Z, Zhi J, Zheng G, et al. Experimental investigation on bearing behavior and failure mechanism of double-lap thin-ply composite bolted joints. Composite structures. 2021;261:113565.

[24] Gamdani F, Boukhili R, Vadean A. Tensile behavior of hybrid multi-bolted/bonded joints in composite laminates. International Journal of Adhesion and Adhesives. 2019;95:102426.

[25] ASTM D3039/D3039M-14, Standard Test Method for Tensile Properties of Polymer Matrix Composite Materials, ASTM International, 100 Barr Harbor Drive, PO Box C700, West Conshohocken, PA 19428-2959. United States (2014). ASTM International West Conshohocken, PA; 2014.

[26] ASTM D5766-D5766M-11: Standard Test Method for Open-hole Tensile Strength of Polymer Matrix Composite Laminates, ASTM International, 100 Barr Harbor Drive, PO Box C700, West Conshohocken, PA 19428-2959. United States (2011). ASTM; 2011.

[27] ASTM-D6742/D6742M-12, Standard Practice for Filled-Hole Tension and Compression Testing of Polymer Matrix Composite Laminates, ASTM International, 100 Barr Harbor Drive, PO Box C700, West Conshohocken, PA 19428-2959. United States (2012). ASTM; 2012.

[28] ASTM-D5961/D5961M-13, Standard Test Method for Bearing Response of Polymer Matrix Composite Laminates. ASTM International, 100 Barr Harbor Drive, PO Box C700, West Conshohocken, PA 19428-2959. United States, 2013.

[29] Gamdani F, Boukhili R, Vadean A. Fatigue behavior of hybrid multi-bolted-bonded single-lap joints in woven composite plates. International journal of fatigue. 2022:106738.

[30] Gamdani F, Boukhili R, Vadean A. Tensile strength of open-hole, pin-loaded and multi-bolted single-lap joints in woven composite plates. Materials & Design. 2015;88:702-12.

[31] Tomblin J, Seneviratne W. Laminate statistical allowable generation for fiber-reinforced composite materials: lamina variability method: Office of Aviation Research and Development, Federal Aviation Administration, 2009.

[32] Portanova MA, Masters J. Standard methods for filled hole tension testing of textile composites. NASA Contractor Report. 1995;198263.

[33] Lim JB, Nethercot D. Stiffness prediction for bolted moment-connections between cold-formed steel members. Journal of constructional steel research. 2004;60:85-107.

[34] Mehrabian M, Boukhili R. Quantifying of secondary bending effect in multi-bolt single-lap carbon-epoxy composite joints via 3D-DIC. Composites Science and Technology. 2020:108453.

[35] Skorupa A, Skorupa M. Differences between the fatigue behaviour of longitudinal lap joints in a pressurized fuselage and laboratory lap joint specimens. Riveted Lap Joints in Aircraft Fuselage: Springer; 2012. p. 11-26.

CHAPTER 7 ARTICLE 4: FULL-FIELD THROUGH-THE-THICKNESS STRAIN DISTRIBUTION STUDY OF HYBRID MULTI-BOLTED/BONDED SINGLE-LAP COMPOSITE JOINTS USING DIGITAL IMAGE CORRELATION

Under review: Journal of Composite Part A: Applied Science and Manufacturing, Sep. 2021

Masoud Mehrabian[a], Rachid Boukhili[b]*

[a b] Department of Mechanical Engineering, Polytechnique Montreal, Quebec H3C 3A7, Canada

7.1 Abstract

This study proposes a digital image correlation (DIC) technique for through-the-thickness deformations (x-z plane) of multi-bolted single-lap (SL) shear hybrid bolted/bonded joints (HBB) made of carbon/epoxy composite laminates. Through-the-thickness peel strain (ε_{zz}), shear strain (ε_{xz}), and longitudinal strain (ε_{xx}) are obtained throughout the overlap region during the entire tensile test. It is observed that real-time monitoring of the strain in the overlap region informs the location of the failure before the load reaches 50% of its ultimate value. ε_{zz}-load curves for both the overlap ends superimpose perfectly up to approximately 40 - 50% of the applied tensile load. ε_{zz} curves of the two ends diverge considerably beyond that level. Similar behavior occurs for ε_{xz} and confirmed for the two laminate stacking sequences; quasi-isotropic (QI) and cross-ply (CP) laminate stacking sequences. It is also found that peel and shear strains, as well as joint rotation in CP, are higher than those of QI. These results can be useful in designing this type of joint.

Keywords

Polymer-matrix composites, Hybrid joints, Through-the-thickness, Digital Image Correlation (DIC), Peel/Shear strains

* Corresponding author.

E-mail address: rachid.boukhili@polymtl.ca (R. Boukhili).

7.2 Introduction

A composite material structure has the advantage of being manufactured with the minimum number of joints possible due to the integration of several components into one piece. Next to the other well-known benefits of composite materials include light weight, high strength/stiffness, and corrosion resistance [1], the abovementioned feature provides less discontinuity to the entire structure, which in turn results in better structural efficiency performance. However, it is still necessary to join composite components, and the two main traditional techniques to accomplish this are mechanical fastening and adhesive bonding [2]. Both strategies have pros and cons, which creates challenges in choosing an appropriate option that corresponds to a specific application. For example, adhesive bonding offers uniform stress distribution and less stress concentration, but a promising surface treatment is required to achieve good adhesive bonding strength [3, 4] and avoid bondline defects such as voids, cracks, and kissing bonds [5, 6]. Conversely, mechanical fasteners do not suffer from such issues, but they introduce stress concentrations and increase the overall weight [7].

An alternative method combining both techniques was first proposed and studied by Hart-Smith in 1982, which has since attracted significant interest among researchers in academia and industry [8]. This combination is hereafter referred to as hybrid bolted/bonded (HBB) joins. The interesting features of HBB joints create an opportunity for a vast domain of new research to investigate the behavior of this type of joint. Consequently, a significant number of questions need to be addressed. A great deal of experimental and numerical work has been conducted on different aspects of HBB joints, including strength, fatigue life, load distributions/sharing, adhesive layer properties, and joint geometry [7, 9-17]. Experimental analysis of single-lap (SL) HBB composite joints is more complicated compared to the separate constituents as it simultaneously deals with the structural mechanism of bonded and bolted joints. A new technology called digital image correlation (DIC) has recently been used, which efficiently eliminates some experimental testing and analysis obstacles. This non-contact image processing-based approach is very useful in terms of strain/stress analysis as it provides full-field strain distribution from all surfaces around the desired object. Therefore, DIC turns out to be very practical for a through-the-thickness analysis of SL composite joints.

A significant amount of work has been carried out regarding the through-the-thickness of the adhesively bonded joints because the strain concentration and crack initiation/propagation can be properly captured from the SL joint side view using DIC [18-25]. For instance, Kumar et al. investigated the strain and stress distribution in the bondline region of a composite SL joint and found that the peel strain increased quickly after the crack began to spread [18, 19]. DIC contributed to the analysis and quantification of the incidence of deformation on the adherends and adhesive during the tensile tests. Additionally, valuable information was supplied, such as the bending moment, load distribution, and stress state of the joint [22]. Sun et al. managed to characterize the bondline fracture process using DIC, observing that this process was symmetric for joints with similar adherends [23]. Moreover, it was found that the DIC system could monitor the adhesive strain to predict the strength of the bonded joints. Recently, Zheng et al. implemented DIC to determine the strain distribution at the side interface of aged water-immersed adhesive joints [25]. They observed that the influence of the filet on the SL joints improved the peel and shear strengths of the adhesive layer in the overlap area.

DIC technology is widely available and has been used in the research community. However, only a small number of studies have focused on experimentally investigating the through-the-thickness for HBB joints, that is, from the joint side view [26-29]. Past research has confirmed the DIC robustness in strain distribution analysis, monitored the crack development from initiation to propagation, and analyzed the failure process from the beginning to the end of the test. Therefore, DIC was utilized extensively in the present experimental study to comprehensively analyze the full-field strain distribution through-the-thickness of multi-bolt HBB SL composite joints. The choice of multi-bolt joints originates from parent papers dealing with multi-bolt joints [12, 30]. At least three bolts are required in real applications to achieve maximum load transfer and proper joint stiffness [30]. Two well-known laminate lay-ups, namely quasi-isotropic (QI) and cross-ply (CP), were manufactured using carbon fabrics. It is recognized that plane weave [0/90] fabrics are frequently used in the composite industry due to their ease of manufacture and advantageous performance/cost ratio. However, a quasi-isotropic configuration provides superior performance if rigidity along the 45-degree axis is required for structural design purposes to reduce torsional stress. This requires adequate [0/90] turning of the woven plies at 45° [2]. The focus of this study was on the influence of the joint configurations on the strain distribution, fracture process, and joint rotation.

7.3 Experimental details

7.3.1 Material and specimen fabrication

Carbon-fiber-reinforced epoxy laminate panels were fabricated utilizing the vacuum assisted resin transfer molding (VARTM) process. A 3 K plain weave carbon fabric with a surface weight of 193 g/m^2 (5.7 oz/yd^2) was used as the reinforcement mechanism, and the epoxy resin Araldite Renlnfusion 8601/Ren 8602 (provided by Huntsman Advanced Materials Americas) was used as the matrix system. CP and QI stacking sequences (composed of 12 layers) were manufactured and the lay-up and average thickness (after the recommended curing cycle of 24 h) are provided in Table 7.1. In the lay-up presented in Table 7.1, (0/90) or (±45) specifies a single layer of each woven ply, which is fabricated from weft yarns woven over and under the warp thread [12, 30].

Table 7.1: Stacking sequences of the laminated composite panels.

Code	Lay-up	Plies	Average thickness (t, mm)
CP	$[(0/90)/(0/90)/(0/90)/(0/90)/(0/90)/(0/90)]_s$	12	2.63
QI	$[(0/90)/(\pm45)/(0/90)/(\pm45)/(0/90)/(\pm45)]_s$	12	

Hybrid multi-bolted/bonded (HBB) single-lap (SL) composite joints were designed and manufactured according to ASTM-D5961 [31]. The plates were attached using bolts and adhesives. Mechanical fasteners were composed of steel hex head shear bolts (NAS6204-4) with a diameter of 6.35 mm, nuts (MS21042-4), and cadmium-plated steel washers (NAS1149F0463P) with internal and external diameters of 6.73 and 12.70 mm, respectively, for the head and nut sides. A tightening torque of 5 Nm was applied to each bolt using a Tohnichi Dial Torque Wrench DB25N-S. More details are available in Refs. [2, 30, 32]. The adhesive applied to these joints was the same epoxy resin used to manufacture the composite laminate [12]. A mat surface was used for all bonding purposes because of its adequate rough surface texture for the application of the peel ply, which results in the desired bonding characteristics for the faying surfaces [2]. The joint assembly

was wrapped in a vacuum bag to provide uniform pressure and create an approved bonding between the joint components. The geometrical configuration of the SL HBB composite joint is shown in Fig. 1. The specimen surface preparation for DIC testing is explained in Ref. [32]. As this study analyzes the through-the-thickness of the joint, the main X-Z coordinate system is assigned to the joint side surface, X-Y is the plane of the laminate, and the strain components are named accordingly. The X-axis is aligned with the applied load direction, and the positive side of the Z-axis is towards the bolt head. The fracture ends, i.e. overlap ends, and fracture sites, where the final net-tension failure always begins, are shown in Figure 7.1.

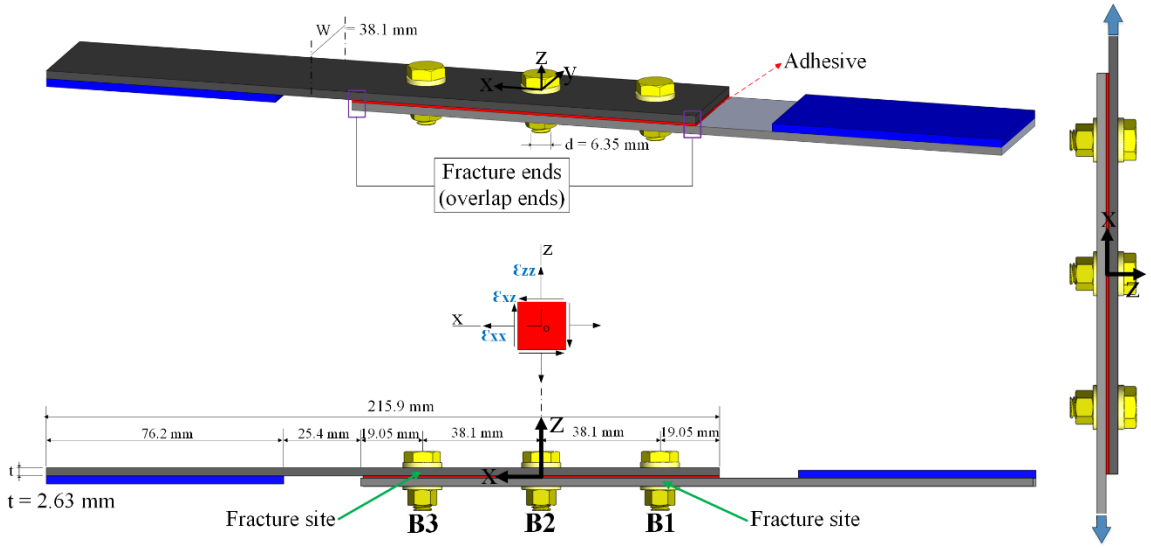

Figure 7.1: Specimen geometry/dimensions, identification of the three bolts, fracture ends (overlap ends) and fracture sites in the joint as well as strain components within the adhesive layer.

7.3.2 Test set-up and procedure

Three identical specimens were tested for CP and QI joint configurations at a constant standard cross-head displacement rate of 2 mm/min. A servo-hydraulic MTS testing machine (Model 810) equipped with a load cell capacity of 100 kN was utilized to perform the mechanical tests. DIC technology was employed to measure the full-field strain components of the joint side surfaces, that is, the through-the-thickness. The principle of the DIC technique is based on tracking random patterns on the surfaces of interest by matching the local distributions of pixel concentrations, i.e., subsets, between the deformed and undeformed digital images during

particular time intervals. The displacement field is computationally achieved by optimizing a cross-correlation or least-squares function to evaluate the degree of similarity between the undeformed and deformed specimens in terms of grayscale intensity values [33]. The DIC system software used was the Vic-3D v 7.2.4 model (Correlated Solutions Inc. (CSI), USA). Comprehensive details regarding the utilized DIC system, including setup mounting, calibration, specifications, resolution, and accuracy are outlined in Refs. [2, 32]. According to previously reported results and comparisons, the level of uncertainty in the results is very low, which ensures the accuracy of computation and delivers good quality outcomes [2, 32].

7.4 Results and discussion

7.4.1 Load-displacement curves

The continuous recording of the deformation of the sample in the thickness plane during the tensile test associates the images acquired at different load levels, as illustrated in Figure 7.2. The load-displacement curves of the two HBB configurations (CP and QI) were tested with load levels A, B, C, D, and E, which correspond to 0%, 25%, 50%, 75%, and the final failure load (FL) of the applied load, respectively, as shown in Figure 7.2 (a). The transverse plane containing the bondline at the marked load levels is displayed in Figure 7.2 (b). According to the load-displacement curves, the CP joint possessed a higher stiffness and breaking load than the QI joint. Two small observable bumps, which negligibly changed the stiffness, could be observed between points D and E. These bumps are attributed to sudden adhesive debonding, as illustrated in the insets of Figure 7.2 (a).

The identification of the rotation of the joint, caused by the characteristic eccentricity of the SL joint, was made possible by careful analysis of the image during loading. For this purpose, image A was taken as a reference, and two yellow lines were placed on the longitudinal edges of the joint. Subsequently, the angle of rotation (θ) progression could be identified in images B to E, as illustrated in Figure 7.2 (b). The rotation created out-of-plane displacements, also known as secondary bending (SB), which increased the stress concentration at the overlap ends and led to crack initiation and propagation along the bondline. Details using DIC results will be further discussed in the following sections. The incidence of the crack is identified by red dashed circles

on the curves, and are outlined in solid red line at the end of the overlaps, i.e. the fracture end, as shown in Figure 7.2 (b).

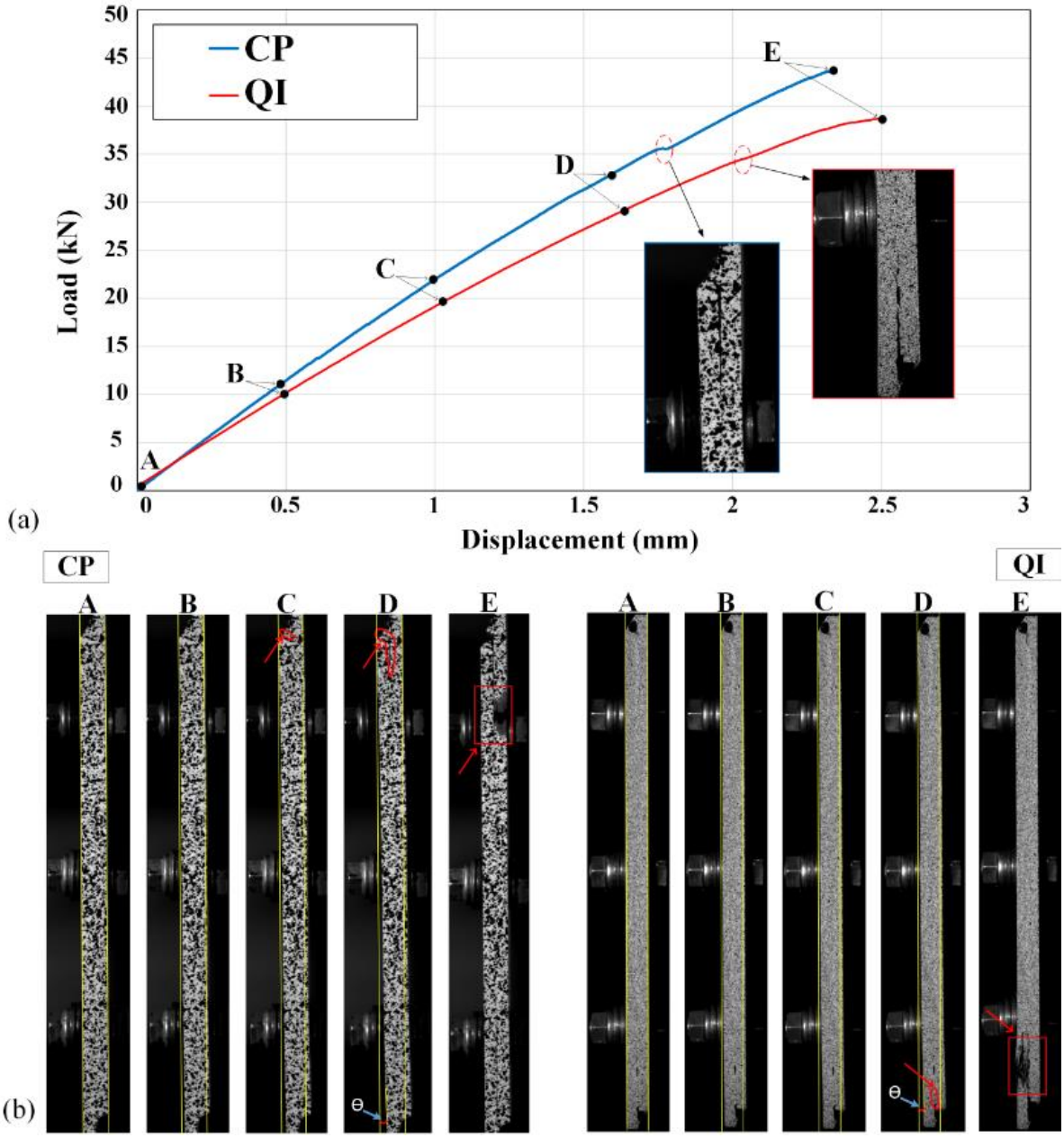

Figure 7.2: (a) Load–displacement curves and (b) corresponding images of the progressive failure process for CP and QI. Yellow lines indicate the longitudinal edges of the joint, and red dashed circles and solid shapes indicate the incidence of cracks.

7.4.2 Digital image correlation analysis

7.4.2.1 Strain field analysis of adhesive bondline

The load value in the SL joint can be divided into the bending moment, peel force, and shear force [26], which creates the through-the-thickness strain components such as peel strain (ε_{zz}), shear strain (ε_{xz}), and longitudinal strain (ε_{xx}). The full-field peel strain (ε_{zz}) and shear strain (ε_{xz}) distributions on the side surfaces of the two configurations at increasing load levels are illustrated in Figure 7.3 and 7.4, respectively. The peel and shear strains are highly concentrated at the overlap ends (compared to the joint center), which indicates that the peel and shear forces predominantly occur in these regions. The eccentric load path induced a bending moment whose maximum value was reached close to the overlap ends [32]. This phenomenon resulted in higher peel stress in the bondline and generating premature failure (cracks) of the adhesive layer at the extreme ends of the overlap (also spew filet) [18, 19]. Overall, the results demonstrate that the values of the peel and shear strains in CP were remarkably higher than those of QI.

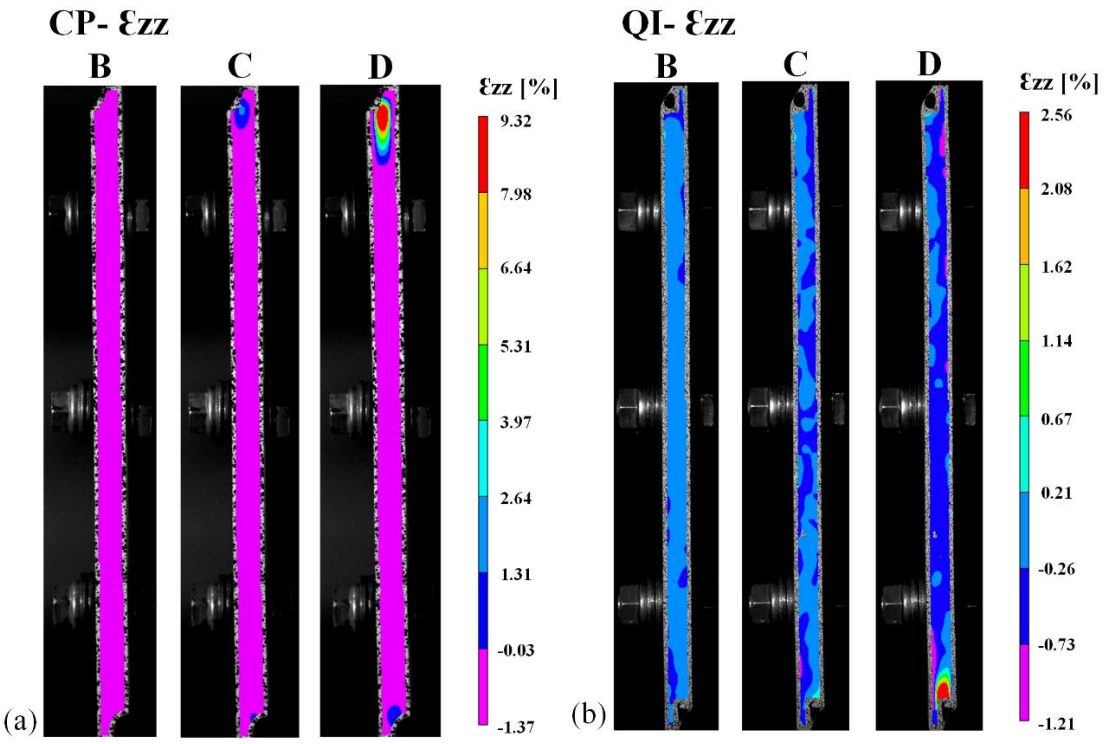

Figure 7.3: Side view of the distribution of the peel strain (Ɛzz) contour of: (a) CP and (b) QI at different applied load levels of 25% (B), 50% (C), and 75% (D).

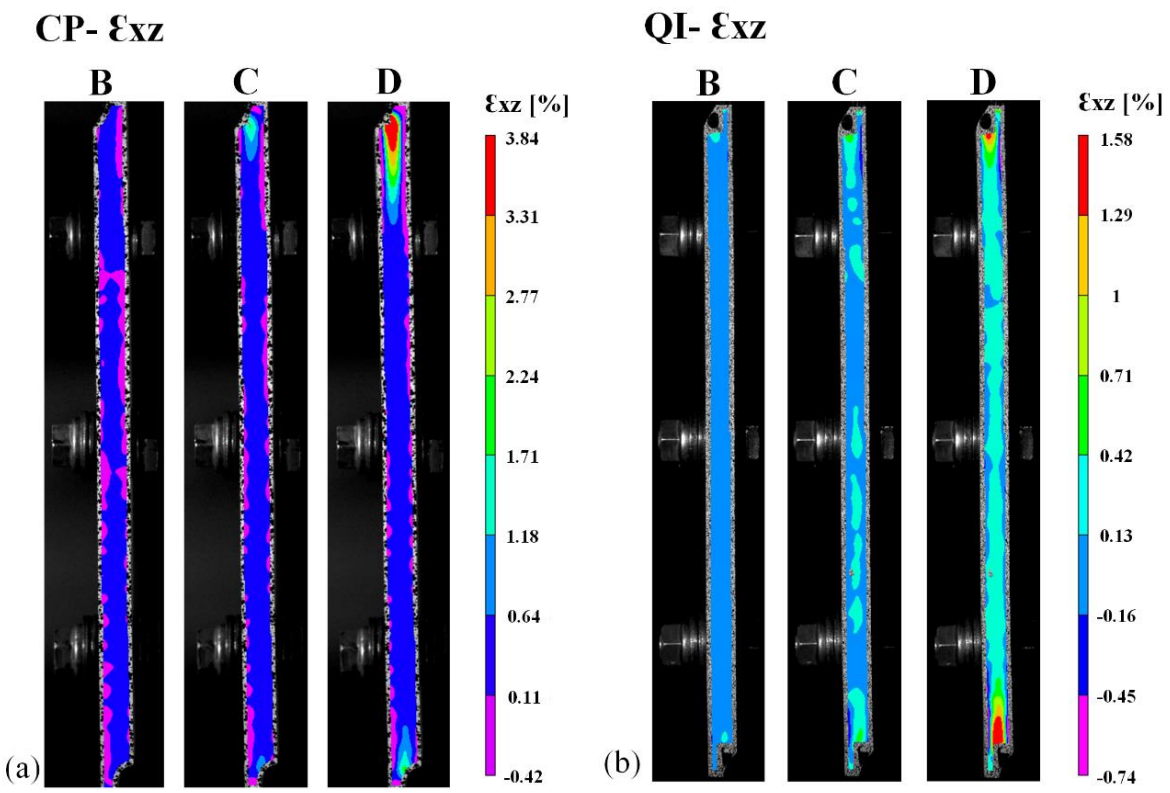

Figure 7.4: Side view of the distribution of the shear strain (Ɛxz) contour of: (a) CP and (b) QI at different applied load levels of 25% (B), 50% (C), and 75% (D).

The evolution of the peel ($Ɛ_{zz}$) and shear ($Ɛ_{xz}$) strains along the adhesive layer are shown in Figure 7.5. One path was defined along the adhesive bondline to retrieve the corresponding strain profiles from the DIC software, represented by the red line in Figure 7.5 (e). The -60 and +60 values are the distances (mm) in the X direction from the joint center, where the origin of the coordinate system (X-Z) is positioned. It is worth noting that the movement and rotation of this red line corresponded to any movement and rotation of the joint itself. The three fastened bolts were labeled as B1, B2, and B3. B1 and B3 are the extreme bolts, located on the potential fracture sites and labeled in red in Figure 7.5. B2 is the central bolt, as shown in Figure 7.1. The strain components in the region of the bondline were analyzed considering the range of 30% to 50% of the failure load as crack formations became more prevalent beyond this range, which can lead to correlation errors.

The results illustrate that the peel and shear strains peaked at the overlap ends (outside of B1 and B3, towards the grip side), while they reached a minimum in the inner section of the overlap region (between B1 and B3). The shear strain (ε_{xz}) of the adhesive layer was formed by the contributions of normal (Z direction) and longitudinal (X direction) deformations of the bondline. The adhesive deformation in CP was greater than that in QI in the normal direction, that is, the peel strain, as shown in Figure 7.3 and 7.5. Additionally, the DIC results demonstrate that the longitudinal deformation of the edges of the CP plate was greater than that of QI in the overlap region (as it will be further discussed in Section 7.4.2.3 Joint rotation). Thus, this may result in a higher deformation of the CP adhesive layer in the longitudinal direction. These factors may collectively cause CP to attain greater shear strain distribution (ε_{xz}) in the bondline compared to QI.

The analytical and simulation models presume to have a symmetrical adhesive displacement/strain profile with respect to the SL joint center. However, this does not occur in practice, particularly with long overlap length of the present investigated joints, which are also exposed to secondary bending and twisting effects [2, 32]. Another reason for asymmetrical strain distribution (or crack growth) might be due to the unbalanced displacement in the entire joint structure, where more displacement takes place in the moving grip than in the stationary grip [19]. Therefore, this asymmetrical behavior causes the total deformation of the adhesive in the outer region of the external bolts, i.e. B3 in CP and B1 in QI, became greater than that of the opposite side. Consequently, this clarifies why the crack nucleated earlier on the mentioned sides of both configurations. Nevertheless, the strain profiles show that the extreme bolts effectively controlled the strain growth over the overlap inner region (between B1 and B3), which further delayed the crack propagation/spread toward the joint central side. Moreover, the curves demonstrate the importance of the peel and shear strain components in crack initiation at the overlap ends of the SL hybrid multi-bolted composite joints.

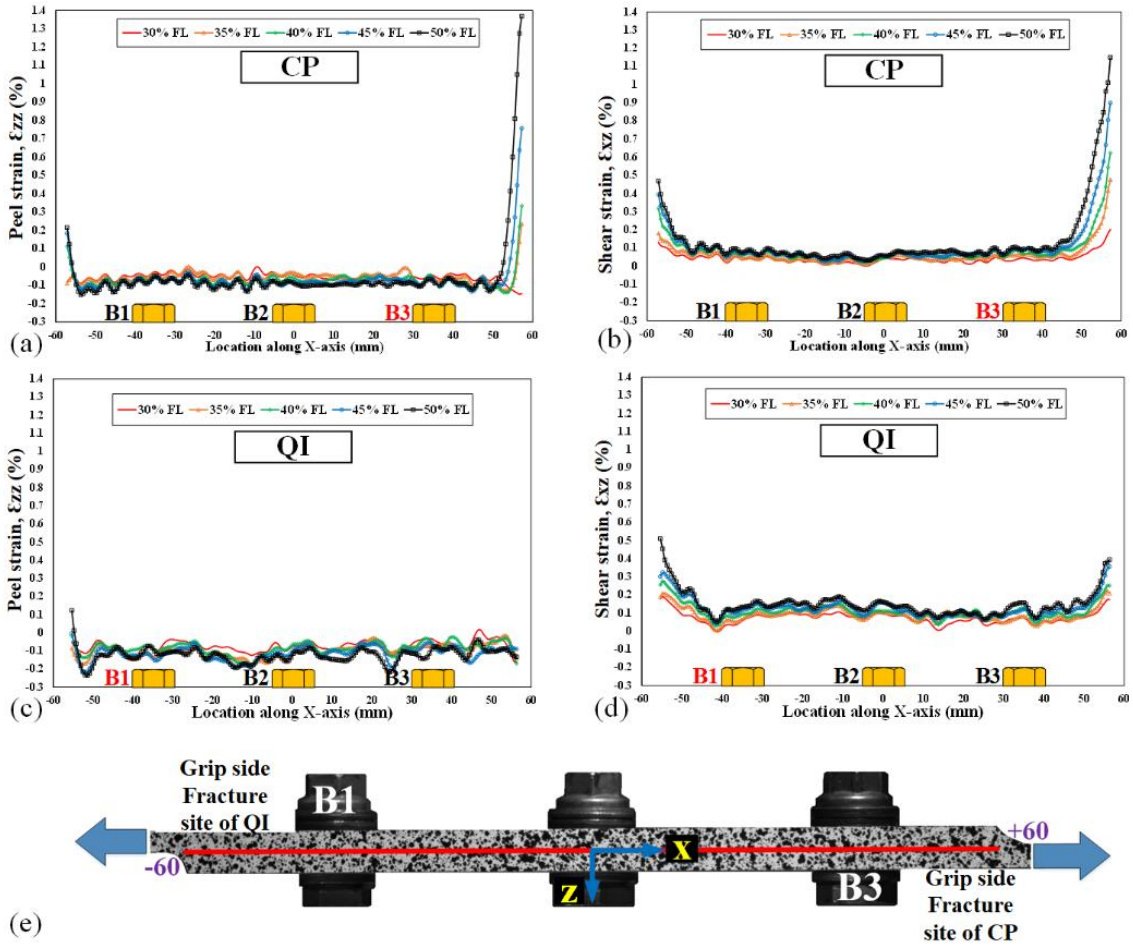

Figure 7.5: (a) and (b) Peel and shear strain changes profile along the bondline of CP, respectively. (c) and (d) Peel and shear strain changes profile along the bondline of QI, respectively. (e) Three bolted hybrid joints under tensile loading. The red line represents one path along the adhesive bondline.

The principal strain represents the maximum (or minimum) possible normal strain at a particular point of a structural element, where the shear strain is theoretically zero at that principal plane. The maximum normal strain is calculated with the shear, peel, and longitudinal strains, expressed as:

$$\varepsilon_1 = \frac{\varepsilon_{xx} + \varepsilon_{zz}}{2} + \sqrt{\left(\frac{\varepsilon_{xx} - \varepsilon_{zz}}{2}\right)^2 + \left(\frac{\varepsilon_{xz}}{2}\right)^2} \tag{7.1}$$

According to equation 7.1, and as it can be seen, it includes the contribution of all three main strain components. Hence, it is a good and critical strain value to perform a proper comparison between the CP and QI adhesive bondline states. The distribution of the principal strain (ε_1) is plotted at a load level of 20 kN to compare the strain values and distribution between the two joint configurations, as shown in Figure 7.6. The peak strain values in CP were significantly greater than that of QI (fracture sites should be compared with each other), similar to the observations from Figure 7.5. The values of the average calculated principal strains between B1 and B3 for CP and QI were very close (a difference of approximately 1%). This negligible difference implies that the mounting bolts could properly control the strain evolution in the adhesive layer and make it laminate lay-up independent in that zone. Furthermore, it is noted that the distribution of the principal strain was similar to that of the shear strain [23, 34]. Therefore, it can be concluded that the shear strain is of great importance in the failure of the adhesive layer of SL hybrid multi-bolted/bonded composite joints.

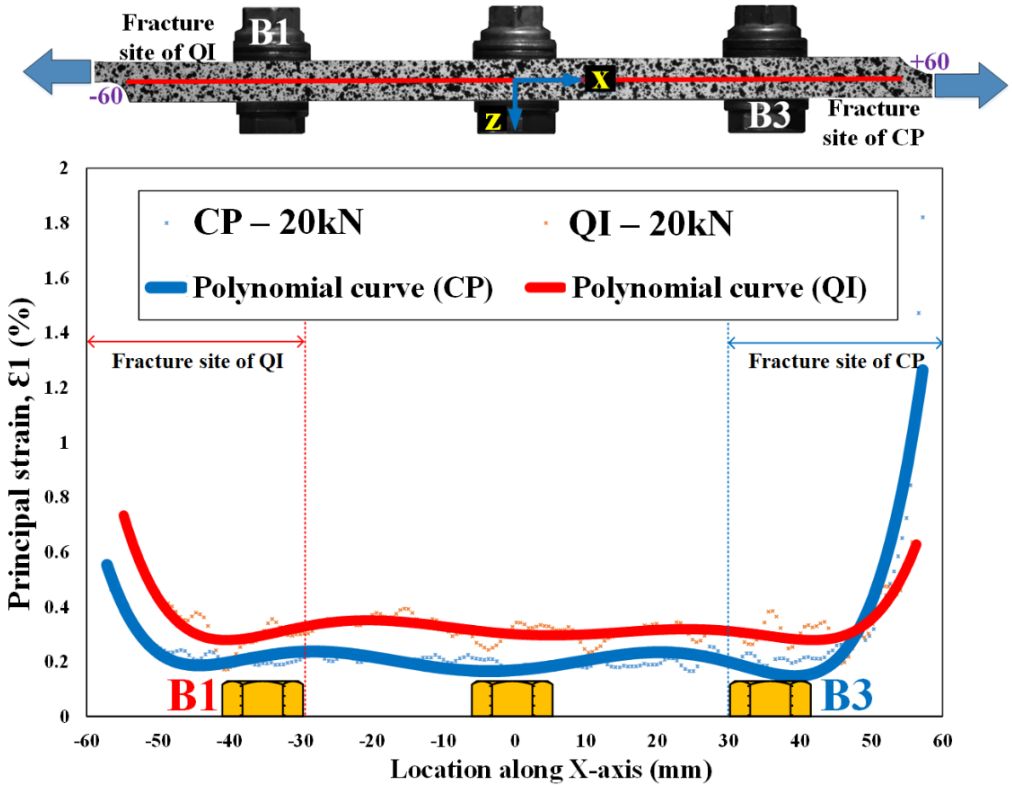

Figure 7.6: Principal strain distribution along the bondline of CP and QI at 20 kN. (A polynomial curve is fitted to the scattered data).

7.4.2.2 Strain analysis at the overlap ends

A close-up view of what occurred to the peel and shear strains at the extreme overlap ends of the two configurations during the tensile process up to 75% FL is shown in Figure 7.7. To do so, two virtual strain gauges (SG1 and SG2) were placed at the overlap ends to record the strain changes, as shown in Figure 7.7 (e). The results show that the strain components at these locations progressed as the load increased. The curves for both configurations can be divided into two different stages. In stage one, the peel and shear strain of the ends (SG1 and SG2) developed rather slowly and coincidently with limited difference up to the onset of stage two. During stage one, the adhesive layer was slightly deformed due to the small induced bending moment to the bondline [25].

In stage two, the strain curves of the fracture end, i.e. SG1 for CP and SG2 for QI, suddenly deviated which was followed by a dramatic growth and surpassed that of the opposite end, whose progression remained almost unchanged. This behavior resulted from the crack nucleation on the corresponding end and its propagation towards the joint center. The induced bending moment in stage two increased and the end of the adhesive bondline deformed significantly. Therefore, the strain development and the difference between the strains at both ends increased rapidly [25]. Moreover, it can be noticed that the rate and intensity of the strain growth of the fracture end were greater in CP than QI in stage two. It can be concluded from the observed results that the development rate of peel and shear strains of the overlap ends played a key role in determining the failure location (fracture site) in SL hybrid multi-bolted/bonded composite joints.

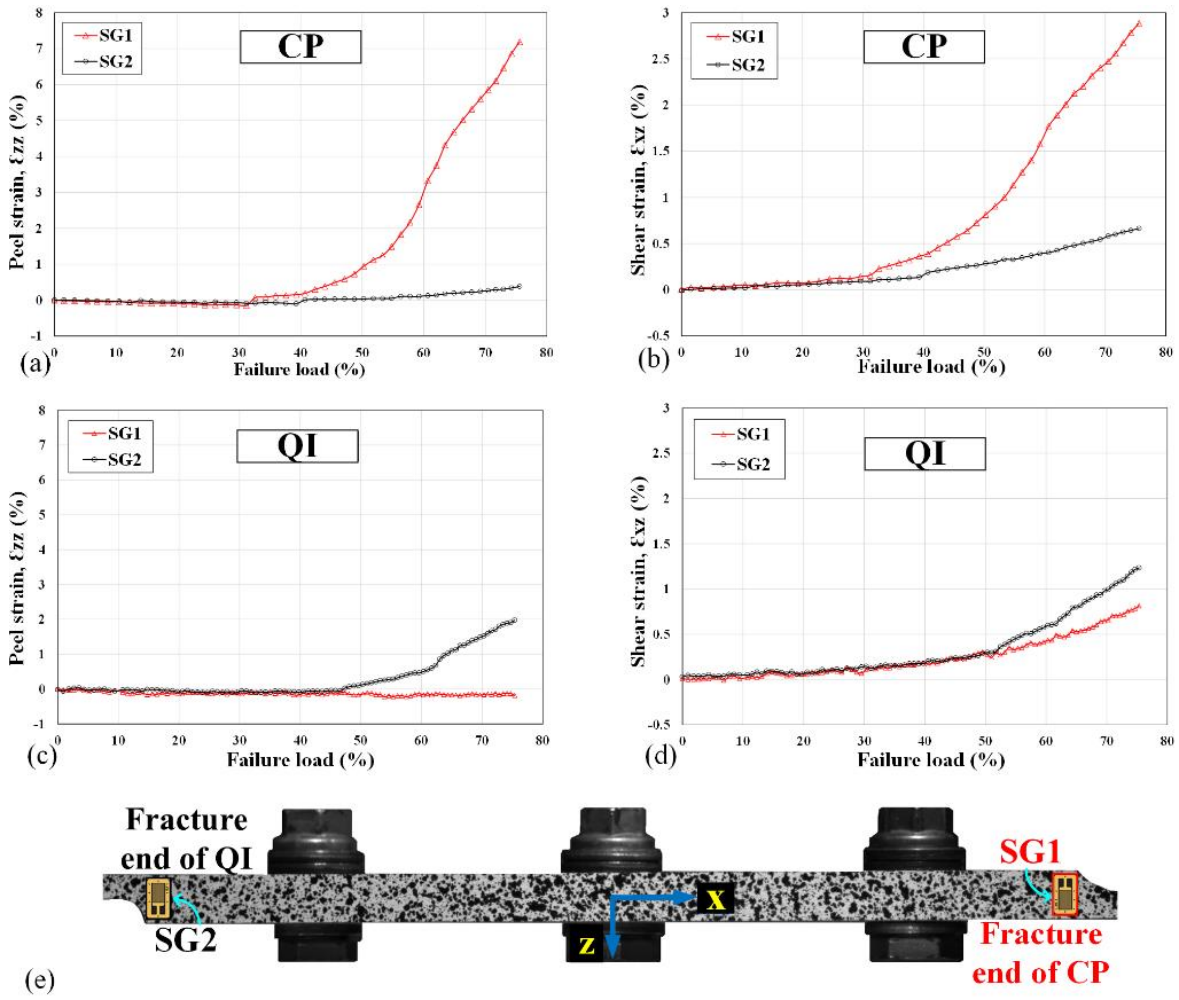

Figure 7.7: Peel and shear strain development at the ends of the adhesive bondline for: (a) and (b) CP, and (c) and (d) QI, respectively. (e) Strain gauges location.

The two strain components between CP and QI were compared due to the importance of the peel and shear strain advancement of the fracture end, as shown in Figure 7.8. As previously mentioned, the induced bending moment had a maximum value at the overlap ends and increased with load. However, after a certain amount of applied load, this increase significantly influenced the fracture end. The peel strain development at the fracture ends of the two configurations is shown in Figure 7.8 (a). Up to a certain load level, the entire HBB joint structure behaved like an integrated bulk material rather than an adherend/adhesive system. In other words, the entire system, which underwent traction in the X direction, experienced compression in the Z direction, and acquired negative peel strain values. This mechanical response fairly represents the Poisson's ratio effect,

in which a bulk material tends to contract in a direction that is perpendicular to the traction load direction, stretching the material.

Afterward, the Poisson's ratio effect was disturbed by changing the sign of the peel strain from negative to positive. This transition process introduced failure initiation or crack nucleation, which occurred sooner in CP than QI, as shown in the encircled areas in Figure 7.8 (a). The corresponding critical load percentages for the failure initiation of the three tested specimens in each configuration for HBB joints were approximately 30% - 40% and 40% - 50% FL for CP and QI, respectively. However, the crack nucleation occurred much later in only-bonded joints, measuring at over 80% FL [23, 35]. Furthermore, the trend of the peel strain curves first diminished with an increase in the applied load, but dramatically increased immediately after the failure initiation, as shown in Figure 7.8 (a). This suggests that the tightening pressure provided by the bolts helped preserve the entire joint as an integrated structure at the start of the tensile test. Changes in the trend of the shear strain curves at the failure initiation moment were not very noticeable, while increasing the slope of the curves at higher load levels was obviously detectable, as shown in Figure 7.8 (b). Furthermore, the rate of slope increase in the shear strain was less than that of the peel strain. Thus, it can be deduced that the peel strain is the leading strain component, which initiates the crack, in SL HBB composite joints.

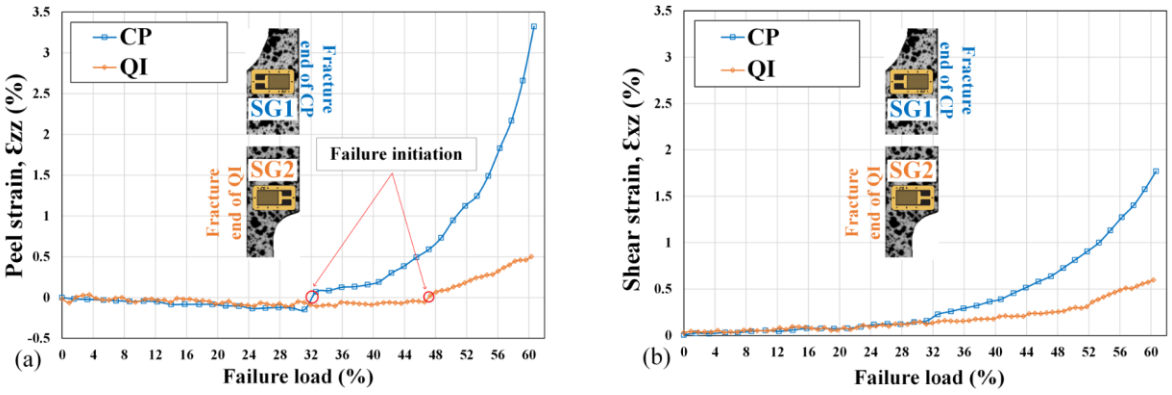

Figure 7.8: Comparing the: (a) peel and (b) shear strains at the fracture ends of CP and QI, and the detection of the failure initiation moment.

The curves of peel (ε_{zz}), shear (ε_{xz}), and longitudinal (ε_{xx}) strain evaluations across the thickness of the fracture end of the CP and QI configurations at 25 kN are shown in Figure 7.9 (a)

and (b), respectively. DIC results were retrieved from section A-A, as shown in Figure 7.9 (d). The approximate location of the adhesive bondline is indicated by the gray vertical lines in Figure 7.9 (a) and (b). The overall magnitude of the peel and shear strain curves of CP was superior to that of QI. However, the same changes/trends in the longitudinal strain curves could be observed. As concluded in the previous sections, this reconfirmed the dominance of the peel strain in comparison with the other strain components at the adhesive layer on the fracture end location in the SL hybrid composite joints. This is contrary to what was reported by Ref. [20] which stated that shear strain had the highest value and greatest influence at the ends of the bondline of the double-butt strap composite joint, which did not experience the secondary bending effect.

The applied tensile load was later accompanied by a by-product bending moment, which created all three stress components in the adhesive layer, namely, the peel stress (σ_{zz}), longitudinal stress (σ_{xx}), and shear stress (σ_{xz}). The DIC strain results helped to calculate these stress components, assuming a plane strain condition and neglecting the material nonlinearity of the adhesive. The following equation was used:

$$\begin{Bmatrix} \sigma_{xx} \\ \sigma_{zz} \\ \sigma_{xz} \end{Bmatrix} = \frac{E_a}{(1+\upsilon_a)(1-2\upsilon_a)} \times \begin{bmatrix} (1-\upsilon_a) & \upsilon_a & 0 \\ \upsilon_a & (1-\upsilon_a) & 0 \\ 0 & 0 & \left(\frac{1-2\upsilon_a}{2}\right) \end{bmatrix} \begin{Bmatrix} \varepsilon_{xx} \\ \varepsilon_{zz} \\ 2\varepsilon_{xz} \end{Bmatrix} \tag{4.2}$$

where E_a (2.1 GPa) and υ_a (0.35) are the elastic modulus and Poisson ratio of the adhesive, respectively. The calculated values of the CP and QI experimental stresses were compared to perform a quantitative analysis, as shown in Figure 7.9 (c). In terms of all the stress components, the superiority of CP over QI still remained. In addition, peel stress remained the most significant among the stress components, while shear stress was the least important. In CP, the composite layer adjacent to the adhesive was 0/90, which allowed the load to be transferred efficiently in the load-bearing fibers of the two substrates [24]. Conversely, the layer adjacent to the adhesive for QI was (±45). This affected the in-plane stress distribution and led to higher shear and longitudinal stresses as a result of better load carrying via the adhesive layer in CP compared to QI. It is known that the peeling effect occurs in the out-of-plane stress class. According to Ref. [32], the CP configuration undergoes relatively more bending, which could be responsible for the higher peel stress value of

the adhesive layer in CP compared to QI. Therefore, it could be inferred that one of the reasons for the higher load-carrying capacity of CP could be related to the greater load carried via the adhesive layer in the former configuration, regardless of the higher peel stress.

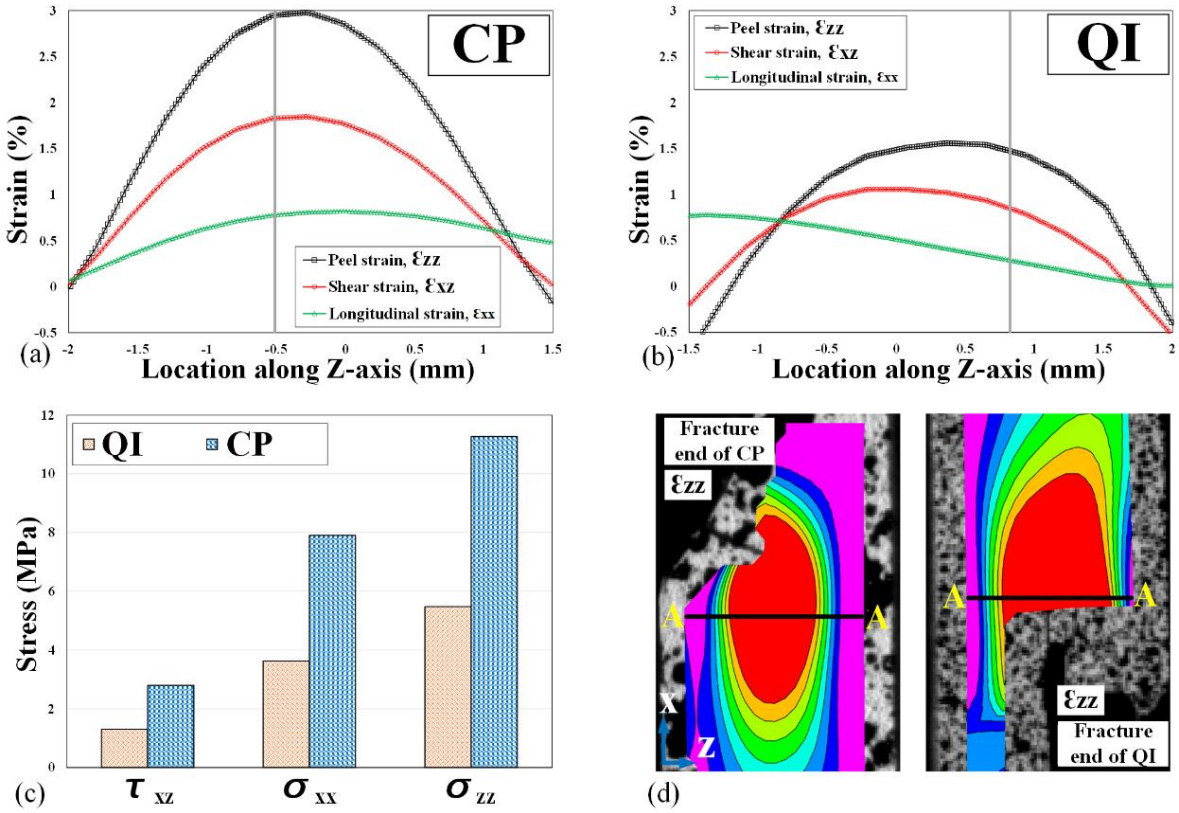

Figure 7.9: Strain component distribution curves of the fracture end at 25 kN for: (a) CP and (b) QI. The approximate location of the adhesive bondline is indicated by the gray vertical lines. (c) Stress components of the adhesive layer. (d) Position of section A-A and contour plot of peel strain (Ɛzz) distribution at the fracture end.

7.4.2.3 Joint rotation

The applied tensile load created a so-called by-product secondary bending (SB) because of the inherent geometrical eccentricity in the structure of an SL joint, which tended to rotate the joint [32]. The out-of-plane displacement (caused by SB) from the surface view was analyzed by the authors [2, 32]. Considering the side view, the out-of-plane displacement can be characterized by moving in the Z direction, which further created an angle θ, as shown in Figure 7.10 (b). This angle was measured by quantifying the divergence of the joint section between the extreme bolts (green

line) with respect to the vertical axis (dashed blue line). This path, that is, the green line, was chosen because of the negligible amount of laminate non-linear deformation in the Z direction of that area. Moreover, these areas experienced significant curvature because of the extensive debonding that occurred in the overlap region outside of the extreme bolts, which did not provide meaningful data for joint rotation measurement.

The joint rotation, i.e. angle θ, throughout the tensile process and prior to 'before failure' (BF) shows that the angle increased with load, as shown in Figure 7.10. It is interesting to see that CP experienced more rotation than QI in the HBB type, unlike only-bolted joints in which QI has a higher SB (greater angle) than CP [32]. The higher rotation of CP may in turn intensify the peel stress at the end of the adhesive layer compared to QI, as shown in Figure 7.9 (c). Consequently, the stress condition at the overlap ends deteriorated, which led to premature cracking in CP sooner than QI, as shown in Figure 7.8. Moreover, the difference between the θ of the two configurations is clearly rather small until the halfway point of the applied load, where the θ for CP was approximately 20% higher than that of QI. Subsequently, the difference increased significantly until BF, almost doubling. This can be attributed to the onset of crack nucleation/propagation, which occurred in the range of 30% - 50% FL in both configurations, as shown in Figure 7.8(a).

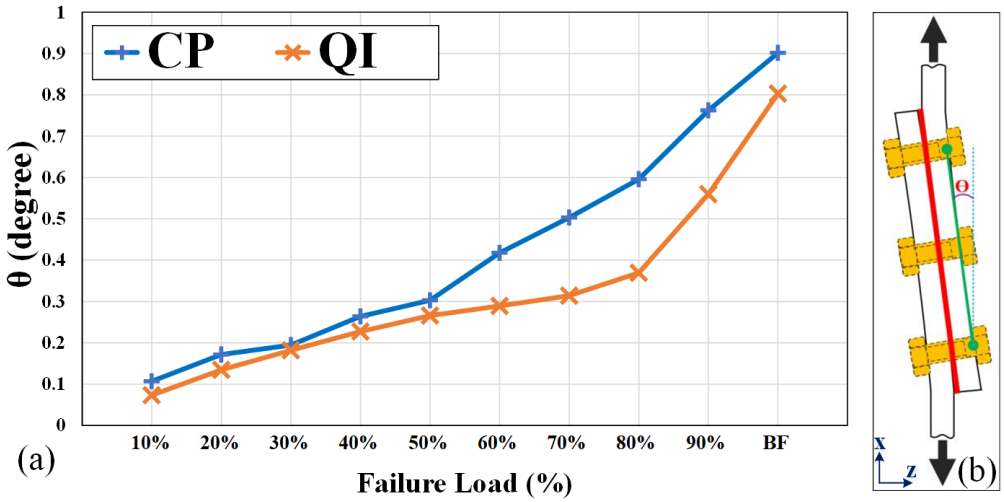

Figure 7.10: (a) Comparison of the joint rotation between CP and QI during the tensile process. (b) Schematic photo of a rotated joint. The green line represents the divergence of the joint section between the extreme bolts. The dashed blue line represents the vertical axis.

The distribution of the longitudinal strain (ε_{xx}) of the composite substrate (plates) edges at 30 kN are shown in Figure 7.11. This strain was measured within the overlap region and through the longitudinal edges of the two substrates of the joints. The data of these edges were retrieved and are represented by the two red lines located on top and bottom of the overlap region in Figure 7.11. A polynomial curve of order two was fitted to obtain a better observation of the strain distribution trend because the data were scattered. Results showed that strain values started from almost zero on the free side (indicated in the figure) and reached the maximum on the grip side at the opposite end. It appears that there is a contradiction between the results shown in Figure 7.2 and 7.11, where QI experienced more displacement than CP and there was greater ε_{xx} distribution of CP than QI in the overlap region, respectively. It should be noted that the reported displacements in Figure 7.2 are the result of grip-to-grip measurements, which include deformation of the joint sections outside of the overlap area, where CP showed a higher modulus of elasticity than QI. This suggests that the geometrical eccentricity with the associated SB may yield different results in terms of the longitudinal deformation of the overlap region in HBB joints.

Furthermore, it is witnessed that the trend of ε_{xx} distribution in CP is remarkably greater than that of QI. This may lead to two interesting effects; first, a higher longitudinal stress in the adhesive layer of CP, as shown in Figure 7.9, and second, a greater shear strain distribution in the CP bondline, as discussed in Section 7.4.2.1. The other purpose of using this figure is to investigate another contributor in the joint rotation. The unbalanced ε_{xx} distribution could be a factor to rotate the joint. Thus, the higher magnitude and distribution of the longitudinal strain (ε_{xx}) in the CP plate compared to QI could be another reason for increased rotation in the former configuration. Considering the outcomes of this section, it can be concluded that CP rotated more than QI as a result of adding an adhesive to the bolted joints, which is in contrast to the only-bolted counterparts [32]. Therefore, the higher rotation of the CP aggravated the stress condition at the fracture end, which resulted in early crack initiation, as shown in Figure 7.8 (a).

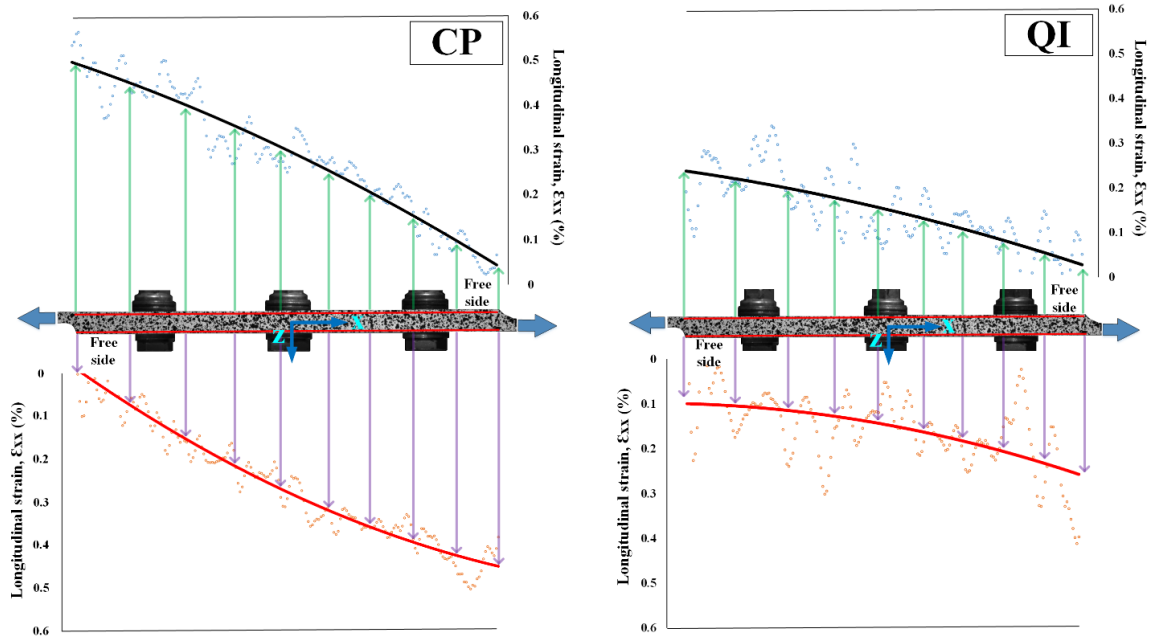

Figure 7.11: Comparing the longitudinal strain (Ɛxx) distribution of the longitudinal side edges of CP and QI at 30 kN. The red lines represent the data of the longitudinal edges.

7.5 Conclusion

In this study, digital image correlation (DIC) technique was chosen to provide a better understanding of the strain distribution through-the-thickness of hybrid multi-bolted/bonded (HBB) composite joints. The investigated lay-ups are the well-known cross-ply (CP) and quasi-isotropic (QI) which were composed of 12 layers. The DIC analysis was very beneficial in acquiring the full-field strain distribution and stress quantification of the adhesive bondline, as well as the joint rotation during the tensile testing process. The following conclusions can be drawn from this experimental study.

- The DIC results showed that the extreme bolts effectively controlled the strain growth of the adhesive layer in the overlap inner region, which consequently arrested the crack propagation/spread toward the joint center. Moreover, this controlling system enabled the strain evolution rather being independent from the laminate lay-up in the mentioned region.
- The growth rate of the peel and shear strains of the overlap ends played a predominant role in determining the fracture end for SL HBB composite joints.

- The peel stress/strain was the most influential at the fracture end, triggering crack nucleation. Unlike the composite bonded joints, in which the crack initiates when the load is over 80%, cracks occurred in hybrid multi-bolted/bonded SL composite joints much sooner, in the range of 30% - 50% of the applied load.
- The stress values and strain increase rate of the adhesive bondline at the overlap end were noticeably higher in CP than QI. This can be related to the greater bending and load transfer that occurred in the adhesive layer of CP compared to QI.
- Despite the fact that CP experienced premature cracking sooner than QI at the overlap end, the higher strength of the former configuration may stem from better load-carrying capacity via its adhesive layer.
- Unlike the only-bolted joints, CP rotated more than QI in HBB, which led to early crack nucleation at the fracture end of the CP. Moreover, the magnitude of the difference between the rotation angles of the two configurations after crack nucleation almost doubled compared to before cracking.

Finally, it was proven that DIC is a very powerful tool for analyzing the strain distribution of the adhesive bondline, crack initiation, and fracture behavior of hybrid bolted/bonded single-lap composite joints. These results can be useful in designing this type of joint.

7.6 Acknowledgments

The authors gratefully acknowledge the financial support provided by the Natural Sciences and Engineering Research Council of Canada (NSERC) and the Consortium for Research and Innovation in Aerospace in Quebec (CRIAQ). We also thank Bombardier Aerospace, L-3 Communications, and Delastek Aeronautique Inc. for their valuable support.

7.7 References

[1] Mehrabian M, Golmakani M. Nonlinear bending analysis of radial-stiffened annular laminated sector plates with dynamic relaxation method. Computers & Mathematics with Applications. 2015;69(10):1272-302.

[2] Mehrabian M, Boukhili R. 3D-DIC strain field measurements in bolted and hybrid bolted-bonded joints of woven carbon-epoxy composites. Composites Part B: Engineering. 2021:108875.

[3] Takeda T, Yasuoka T, Hoshi H, Sugimoto S, Iwahori Y. Effectiveness of flame-based surface treatment for adhesive bonding of carbon fiber reinforced epoxy matrix composites. Composites Part A: Applied Science and Manufacturing. 2019;119:30-7.

[4] Lim SJ, Cheon J, Kim M. Effect of laser surface treatments on a thermoplastic PA 6/carbon composite to enhance the bonding strength. Composites Part A: Applied Science and Manufacturing. 2020;137:105989.

[5] Vijaya Kumar RL, Bhat MR, Murthy CRL. Evaluation of kissing bond in composite adhesive lap joints using digital image correlation: Preliminary studies. International Journal of Adhesion and Adhesives. 2013;42(Supplement C):60-8.

[6] Tao R, Alfano M, Lubineau G. In situ analysis of interfacial damage in adhesively bonded composite joints subjected to various surface pretreatments. Composites Part A: Applied Science and Manufacturing. 2019;116:216-23.

[7] Romanov VS, Heidari-Rarani M, Lessard L. A parametric study on static behavior and load sharing of multi-bolt hybrid bonded/bolted composite joints. Composites Part B: Engineering. 2021;217:108897.

[8] Hart-Smith L. Design Methodology for Bonded-Bolted Composite Joints. Volume I. Analysis Derivations and Illustrative Solutions. MCDONNELL DOUGLAS CORP LONG BEACH CA; 1982.

[9] Bodjona K, Fielding S, Heidari-Rarani M, Lessard L. Effect of adhesive layer compliance on strength of single-lap hybrid bonded-bolted joints. Composite Structures. 2021;261:113324.

[10] Zhang H, Li C, Xu M, Liu Z, Jia D, Zhang Y. A novel method for damage analysis of CFRP single-lap bolted, bonded and hybrid joints under compression. Composite Structures. 2020;251:112636.

[11] Li X, Cheng X, Guo X, Liu S, Wang Z. Tensile properties of a hybrid bonded/bolted joint: parameter study. Composite Structures. 2020:112329.

[12] Gamdani F, Boukhili R, Vadean A. Tensile behavior of hybrid multi-bolted/bonded joints in composite laminates. International Journal of Adhesion and Adhesives. 2019;95:102426.

[13] Lopez-Cruz P, Laliberté J, Lessard L. Investigation of bolted/bonded composite joint behaviour using design of experiments. Composite Structures. 2017;170:192-201.

[14] Bodjona K, Raju K, Lim G-H, Lessard L. Load sharing in single-lap bonded/bolted composite joints. Part I: Model development and validation. Composite Structures. 2015;129:268-75.

[15] Graham D, Rezai A, Baker D, Smith P, Watts J. The development and scalability of a high strength, damage tolerant, hybrid joining scheme for composite–metal structures. Composites Part A: Applied Science and Manufacturing. 2014;64:11-24.

[16] Kelly G. Quasi-static strength and fatigue life of hybrid (bonded/bolted) composite single-lap joints. Composite structures. 2006;72(1):119-29.

[17] Kelly G. Load transfer in hybrid (bonded/bolted) composite single-lap joints. Composite structures. 2005;69(1):35-43.

[18] Kumar RV, Bhat M, Murthy C. Experimental analysis of composite single-lap joints using digital image correlation and comparison with theoretical models. Journal of Reinforced Plastics and Composites. 2013;32(23):1858-76.

[19] Vijaya kumar R, Bhat M, Murthy C. Analysis of composite single lap joints using numerical and experimental approach. Journal of Adhesion Science and Technology. 2014;28(10):893-914.

[20] Crammond G, Boyd SW, Dulieu-Barton JM. Evaluating the localised through-thickness load transfer and damage initiation in a composite joint using digital image correlation. Composites Part A: Applied Science and Manufacturing. 2014;61(Supplement C):224-34.

[21] Qiu P, Shi J, Zheng J. Experimental Investigation on Adhesive Bonded Joints of Carbon Fiber Composite Laminates Containing Disbond Defect. ASME 2017 Pressure Vessels and Piping Conference: American Society of Mechanical Engineers; 2017. p. V005T11A13-VT11A13.

[22] Bamberg P, Reisgen U, Schiebahn A, Barbosa J, Marx B, Coelho R. Digital Image Correlation Analysis Of The Effects Of The Overlap Length, Adhesive Thickness And Adherends Yield Strength Over Similar And Dissimilar Joints Of High Strength Steel And Aluminum Alloys. International Journal of Adhesion and Adhesives. 2018.

[23] Sun G, Liu X, Zheng G, Gong Z, Li Q. On fracture characteristics of adhesive joints with dissimilar materials–An experimental study using digital image correlation (DIC) technique. Composite Structures. 2018;201:1056-75.

[24] Grefe H, Kandula M, Dilger K. Influence of the fibre orientation on the lap shear strength and fracture behaviour of adhesively bonded composite metal joints at high strain rates. International Journal of Adhesion and Adhesives. 2020;97:102486.

[25] Zheng G, Liu C, Han X, Li W. Effect of spew fillet on adhesively bonded single lap joints with CFRP and aluminum-alloy immersed in distilled water. International Journal of Adhesion and Adhesives. 2020:102590.

[26] Li M, Luo W, Chen Y, Yang X. Full-field strain distribution and failure characteristics of CFRP-repaired steel structures. Engineering Failure Analysis. 2020;115:104664.

[27] Cruz PL. Experimental and Numerical Study on Bolted/Bonded Composite Joints for Aircraft: Carleton University Ottawa; 2016.

[28] Li G. Fatigue performance characterization of a composite butt joint configuration. Composites Part A: Applied Science and Manufacturing. 2013;51(Supplement C):43-55.

[29] Backman D, Li G, Sears T. Determining the strain distribution in bonded and bolted/bonded composite butt joints using the digital image correlation technique and finite element methods. Optical Measurements, Modeling, and Metrology, Volume 5. 2011:401-6.

[30] Gamdani F, Boukhili R, Vadean A. Tensile strength of open-hole, pin-loaded and multi-bolted single-lap joints in woven composite plates. Materials & Design. 2015;88:702-12.

[31] ASTM-D5961/D5961M-13, Standard Test Method for Bearing Response of Polymer Matrix Composite Laminates. ASTM International, 100 Barr Harbor Drive, PO Box C700, West Conshohocken, PA 19428-2959. United States, 2013.

[32] Mehrabian M, Boukhili R. Quantifying of secondary bending effect in multi-bolt single-lap carbon-epoxy composite joints via 3D-DIC. Composites Science and Technology. 2020:108453.

[33] Daly SH. Digital image correlation in experimental mechanics for aerospace materials and structures. Encyclopedia of Aerospace Engineering. 2010.

[34] Ruiz P, Jumbo F, Huntley J, Ashcroft IA, Swallowe G. Experimental and numerical investigation of strain distributions within the adhesive layer in bonded joints. Strain. 2011;47(1):88-104.

[35] Sawada T, Kawamori T, Matsunaga M, Fujiyasu Y, Ueki Y. An experimental study for identifying crack initiation forces in single-lap bonded joints. Engineering Fracture Mechanics. 2021;241:107372.

CHAPTER 8 GENERAL DISCUSSION

During the course of the present thesis, we mainly focused on investigating the mechanical behavior and fracture mechanism of two types of multi-bolt single-lap composite joints, namely only-bolted and hybrid bolted/bonded, using the non-contact image processing-based technology called Digital Image Correlation (DIC). The results of this research are presented in four articles, composing the core of this thesis, through which the four sub-objectives were fulfilled. Worth mentioning that two conference papers have also been orally presented within these years of research. This chapter provides a brief review of the work and a general discussion of some major outcomes of the thesis, which are presented through the sequential order of the conducted articles.

The very first step of reaching the main objective of the thesis was initiated by performing a study about one simple but the deleterious and unavoidable effect in the structure of single-lap joints called secondary bending (SB). Precise experimental characterization of this item through conventional testing equipment is almost impossible, but DIC ignited this idea to turn it into a possible task. The two well-known and industrial-used laminate lay-ups were selected, namely cross-ply (CP) and quasi-isotropic (QI). The composite panels, composed of woven carbon fiber embedded in the epoxy resin matrix, were manufactured by the vacuum assisted resin infusion (VARI) process and with two thicknesses, 8 and 12 layers. In order to have a hybrid joint, an adhesive, which is the same epoxy resin used to manufacture the composite panels, was added between the two joint member parts. Totally, the number of all configurations investigated in this thesis is eight. However, and as a start, the first objective was exclusively devoted to the only-bolted joints, i.e., four configurations. DIC Results showed that thicker joints have larger out-of-plane displacement due to higher geometrical eccentricity. Based on the calculation, CP was found to be stiffer than QI (both 8 and 12 layers), while the opposite was observed in terms of ultimate strength. This is counter intuitive as the former lay-up has more 0^o ply content than the latter, but the higher notch sensitivity of CP laminate takes a portion of the responsibility for this response. DIC measurement of out-of-plane displacements (OPD) alongside Neutral Line Model (NLM) calculations assisted here to demonstrate that another responsible for this inverted behavior is the induced secondary bending. While QI exhibited larger OPD than CP, the latter lay-up experienced greater bending than the former, which consequently affected the ultimate strength.

The second part of this work was inspired by the results of the first objective to see and analyze the SB and some other items in the case of hybrid joints. The entire eight configurations were examined in this part. The main goal of this work (covering sub-objective 2) was to observe and analyze the effect of hybridization, and it started with the measurement of surface strain distribution which is followed by assessing secondary bending and twisting effects. In the first work, DIC results were verified with the NLM method, and here in the second study, they were compared against real strain gauges measurements, which showed very good agreement and confirmed the accuracy of the DIC apparatus and the performed tests. DIC illustration clearly showed and compared the strain distribution pattern (in 2D and 3D vision) among CP and QI lay-up and, more importantly, between only-bolted and hybrid joints. Strain concentration and bearing action were distinguishable in only-bolted cases, while they seemed to disappear in hybrid joints. It justified why CP configurations possessed higher strength than QI in HBB joints, contrary to what happened in only-bolted joints of the first objective, as the added adhesive alleviated the overall strain distribution and remarkably relieved the stress concentration around the middle hole. Moreover, tracking the strain development below each bolt proved the fact that the adhesive governs the main load transferring mechanism in HBB joints since no tangible bearing action occurred in the vicinity of the corresponding bolts. Furthermore, OPD measurements illustrated that the applied adhesive restricted the secondary bending and twisting effects to a decent extent.

In the previous investigation, the occurred bearing action alongside the by-pass load caused some deformation in the shape of bolt-holes. Therefore, it was highly sensed to deal with this phenomenon, which was called bolt-hole elongation (BHE), in a separate study. The embedded software in the DIC system, named Vic-3D, provides an inspection tool that works like an extensometer, but virtually. It enabled us to measure the hole elongation accurately from the first to the last moment of testing. This measurement with the real extensometer is always associated with major errors and cannot deliver a proper result. It was observed that in the case of only-bolted joints, there is a non-linear relationship between BHE and tensile loading. At the lower levels of the applied load, CP and QI behaved similarly, but further in the test, the BHE of CP gradually acquired more values than that of QI. The higher notch sensitivity of CP laminate was responsible for this behavior. The mentioned non-linear relationship completely disappeared in the case of HBB joints, showing the fact that hybridization can significantly alter BHE response due to relieving the strain concentration in the vicinity of the bolt-holes. Moreover, results showed that

for an equal amount of the applied load, thinner joints experienced more BHE than the thicker ones for both only-bolted and hybrid cases.

Finally, the major experimental challenge in terms of through-the-thickness analysis of the overlap region of hybrid joints was overcome using the DIC system. While researchers have very considered this area, its geometrical dimensions and difficult-to-access characterization caused many disturbances for experimental investigation. Specimen surface preparation for DIC testing, which includes cleaning the surface of interest, painting it in white, and applying a black speckle pattern meticulously to generate an approved random gray intensity distribution, was difficult for this area, but it was managed to accomplish properly. Figure 8.1 shows the testing setup and the prepared mounted specimen. DIC contributed effectively to detecting and monitoring the evolution of the strain components of this region during the entire tensile test. The major strains are peel and shear, which played a critical role in the initiation and propagation of the crack within the adhesive layer. DIC results helped detect the load corresponding to the adhesive failure initiation. It was found that the crack nucleated much sooner in the HBB joint compared with the only-bonded cases. The effectiveness of DIC technology was reconfirmed.

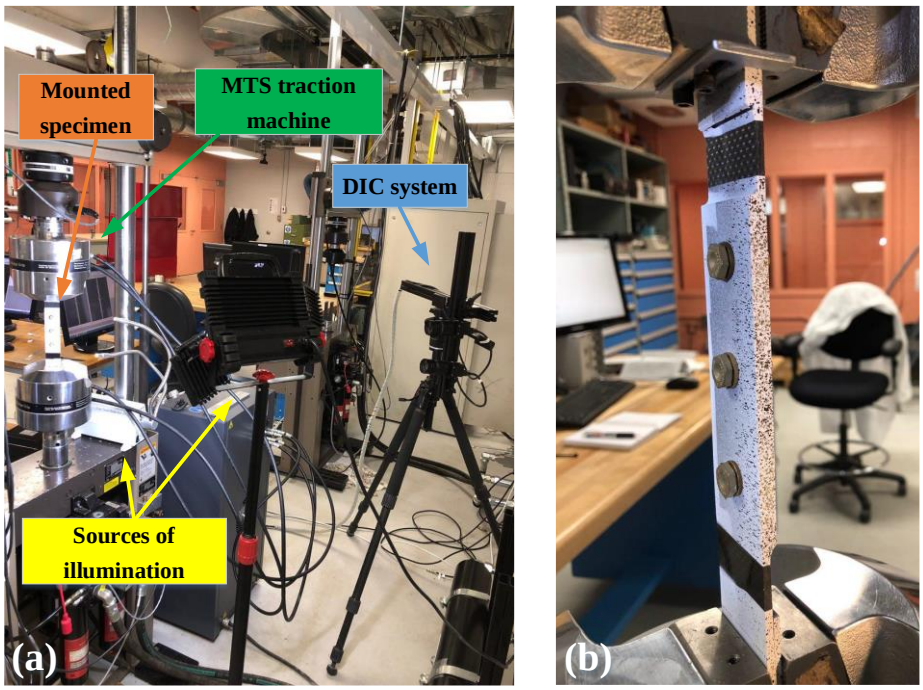

Figure 8.1: (a) The entire DIC setup, (b) prepared surface of the specimen.

To facilitate following the procedural steps from the beginning to the end and obtaining the results in this research work, the following flowchart is provided in Figure 8.2.

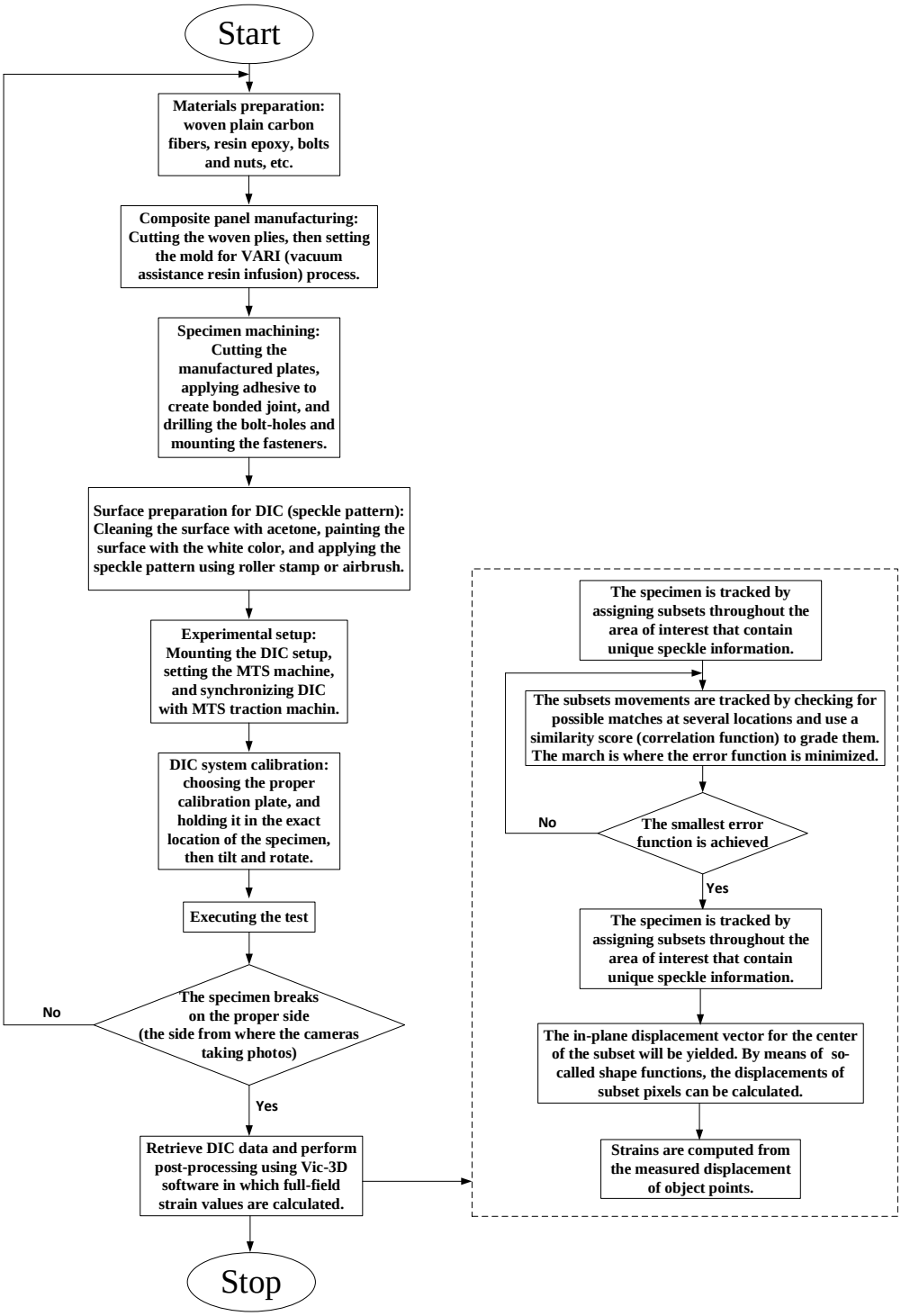

Figure 8.2: Procedural steps of the work.

CHAPTER 9 CONCLUSION AND FUTURE WORK

Mechanical joints are the weakest link of composite structures. In practice, the two main reasons for the success of composites are their proven fatigue performance, and secondly, their suitability in reducing the number of mounted parts, which reduces the number of joints and the final cost. However, as discussed before, the need for fastening techniques remains inevitable and thus a source of problems [109]. Therefore, there is a need to characterize the mechanical behavior of composite joints with a hands-on approach. The main objective of this research work is to perform a series of experimental studies using 3D-DIC technology to investigate the mechanical behavior of multi-bolt and hybrid bolted/bonded single-lap composite joints. It contributes to enriching knowledge and comprehension in this regard, which could be eventually helpful for designing optimized and safe structures.

9.1 Summary of the concluding remarks

The following concluding remarks can summarize the major take-outs of the work carried out in this thesis:

- An applied tensile force to a single-lap (SL) joint makes it rotate due to the geometrical eccentricity, which consequently generates a bending moment. This condition induces secondary bending (SB) which forms out-of-plane displacement (OPD). DIC and NLM results showed that thicker bolted joints experienced larger OPD and bending factor (k_b). Moreover, quasi-isotropic (QI) bolted joint illustrated a larger OPD than cross-ply (CP) one, but lower k_b. This coefficient, k_b, is the ratio of bending stress over tensile stress, which can express the severity of SB at the desired location of an SJ joint. Therefore, only-bolted CP joints undergo relatively more bending, resulting in higher interlaminar shear stresses in the laminate and lessens bearing strength, while CP's bearing stiffness is almost double that of QI.

- The only-bolted SL composite joints experience the most OPD in the early stages of the loading, which was proved by the obtained results of both DIC and NLM. This results in developing interlaminar shear cracks and associated damages at these stages.

- The DIC results showed that hybridization is suggested for SL bolted composite joints as the adhesive decreases SB significantly. This minimizes the interlaminar shear stresses,

which ultimately yields in preserving bolted joints' stiffness and strength. Moreover, the applied adhesive eases the surface strain distribution and noticeably relieves the stress concentration around the holes. In addition, hybridization reduces bolt-hole elongation (BHE) remarkably, which is more pronounced in CP than QI due to the effective stress concentration relief that happens in CP. The mentioned factors help CP joints to sustain their strength. On the other hand, QI bolted joints demonstrated better bearing performance resulting in higher strength than CP bolted ones. Therefore, it could be suggested that for the bolted joint applications, QI is preferable, while CP should be chosen for where the hybridization is applicable.

- It was found by DIC measurements that there is no tangible load sharing through the bolts in multi-bolted hybrid joints. Moreover, the added adhesive delays damage initiation of the laminate plates, which finally results in failure process deceleration.
- The BHE is formed by two factors, namely bearing action and by-pass load, in which the influence of the latter was found to be more than the former in hole elongation of multi-bolted joints. DIC results showed the holes in CP elongate more than that of QI in only bolted joints, while the holes of the studied configurations elongate similarly until the onset of failure in HBB case. It is worth mentioning again that hybridization significantly reduced BHE, which was more pronounced in CP than in QI. Moreover, the fastened bolts in only-bolted joints can control and reduce stress concentration (which is an influential factor in hole elongation formation) at the early stages of the loading, when most OPD occurs.
- The DIC results from the overlap side view, i.e., through-the-thickness, demonstrated the controlling role of the extreme bolts in the strain growth of the adhesive layer, which consequently arrests the crack propagation towards the overlap center. It should be noted that the crack initiation is mostly formed owing to the peel strain at the overlap end. Tracking the peel strain development helped to determine the moment of crack initiation and the corresponding load. It was found that it occurs in the range of 30%-50% of the applied load, contrary to the composite bonded joints in which the crack nucleates when the load reaches over 80%.

- Observing the rotation of the hybrid joint from the side view revealed that CP rotates more than QI, unlike the only-bolted case. It might be the reason for earlier crack initiation at the fracture end of the CP compared to QI.

9.2 Contributions and Impacts

The main contribution and originality of this work are in terms of employing DIC and using the obtained results to assess the strain distribution/ concentration, measuring the out-of-plane displacements, spotting and tracing the fracture initiation/propagation, observing the load transferring mechanism, and studying the effect of hybridization on the behavior of multi-bolted composite joints. All these features will contribute to characterizing and predicting the joint mechanical responses and eventually assisting in designing a reliable, durable, and safe joint. The outcomes of this research are advantageous to the academic studies to compare their work and having different insight in this field to develop their ideas. It is expected that the results not only provide a specific contribution to aerospace applications but also will be directly applicable to a range of other structures in the transportation, automotive, nautical, naval, and wind energy structures. The purposeful use of DIC has resulted successfully in the following contributions:

Title	Current status
Quantifying of secondary bending effect in multi-bolt single-lap carbon-epoxy composite joints via 3D-DIC Masoud Mehrabian, Rachid Boukhili ***Journal of Composites Science and Technology, p. 108453, 2020.***	Published
3D-DIC strain field measurements in bolted and hybrid bolted-bonded joints of woven carbon-epoxy composites Masoud Mehrabian, Rachid Boukhili ***Journal of Composites Part B: Engineering, p. 108875, 2021.***	Published
Experimental study of the hybridization effect on bolt-hole elongation of multi-bolted single-lap composite joints using DIC Masoud Mehrabian, Rachid Boukhili ***65th Aeronautics Conference, A CASI Virtual Series, June 14-18 (2021).***	Presented orally

Surface and through-the-thickness strain distribution study of multi-bolted and hybrid multi-bolted-bonded single-lap composites joints using DIC Masoud Mehrabian, Rachid Boukhili ***36TH INTERNATIONAL CONFERENCE OF THE POLYMER PROCESSING SOCIETY (26-29 September 2021)***	Presented orally
Full-field through-the-thickness strain distribution study of hybrid multi-bolted/bonded single-lap composite joints using digital image correlation Masoud Mehrabian, Rachid Boukhili ***Submitted in Journal of Composites Part A: Applied Science and Manufacturing.***	Under review
Experimental investigation of hole deformation and bolt-hole elongation of woven carbon-epoxy composite plates and joints using DIC technique Masoud Mehrabian, Aouni Jr. Lakis, Rachid Boukhili ***Submitted in Journal of Composite Structures.***	Under review

9.3 Future work

Following the work carried out during this thesis, the potentials and limitations were recognized. Therefore, several recommendations can be considered for future work as follows:

- Implementing numerical simulation using finite element (FE) packages, like Abaqus, can open up a door to have significant insight deeply into the behavior of the composite joints. A complementary study comparing the results retrieved from DIC with that of FE simulation could be a practical project. For example, DIC outcomes could be used as an input to FE simulation to have a more realistic model. This hybrid method can contribute to investigating different aspects like measuring bypass and bearing loads within the joints or calculating the portion of the load transferred via bolts and adhesive.
- It would be interesting to characterize and evaluate the failure mechanism of SL composite joints with hybridized laminate material (i.e., Carbon & Glass reinforcements) and different stacking sequences (cross-ply and quasi-isotropic) under static loading. Carbon fibers have a high tensile strength-to-weight ratio, while they are very expensive. On the other hand, Glass fibers are cheaper and slightly more flexible. Thus, their combination may help adding more flexibility to the joints, resulting in reducing secondary bending and its associated destructive effects.

- The upgraded version of DIC software can show the results at the further free edges and boundaries. In addition, increasing the frequency of photo capturing could assist in the detection of damage initiation/propagation. These features can be implemented simultaneously to monitor the failure mechanism under static or cyclic loading.
- 3D-DIC is a powerful tool to analyze the behavior of composite fastened joints. Therefore, it is recommended to use it to broaden the knowledge about the effects of influential parameters like clearance, bolt-hole fit conditions, preloads, interference, adhesive properties/thickness, friction, and the like.

REFERENCES

[1] R. W. Messler, *Joining of materials and structures: from pragmatic process to enabling technology*: Butterworth-Heinemann, 2004.

[2] L. Hart-Smith, "Design Methodology for Bonded-Bolted Composite Joints. Volume I. Analysis Derivations and Illustrative Solutions," MCDONNELL DOUGLAS CORP LONG BEACH CA1982.

[3] W. Broughton, L. Crocker, and M. Gower, *Design requirements for bonded and bolted composite structures*: National Physical Laboratory, 2002.

[4] D. o. D. Handbook, "Composite materials handbook, volume 3: polymer matrix composites—materials usage, design and analysis," ed: Department of Defense Handbook Horsham, PA, 2002.

[5] P. E. Irving and C. Soutis, *Polymer composites in the aerospace industry*: Woodhead Publishing, 2019.

[6] L. J. Hart-Smith, "Bolted joint analyses for composite structures—current empirical methods and future scientific prospects," in *Joining and Repair of Composite Structures*, ed: ASTM International, 2004.

[7] A. a. Ataş and C. Soutis, "Subcritical damage mechanisms of bolted joints in CFRP composite laminates," *Composites Part B: Engineering*, vol. 54, pp. 20-27, 2013.

[8] A. M. G. Coelho and J. T. Mottram, "A review of the behaviour and analysis of bolted connections and joints in pultruded fibre reinforced polymers," *Materials & Design*, vol. 74, pp. 86-107, 2015.

[9] S. D. Thoppul, J. Finegan, and R. F. Gibson, "Mechanics of mechanically fastened joints in polymer–matrix composite structures – A review," *Composites Science and Technology*, vol. 69, pp. 301-329, 2009/03/01/ 2009.

[10] P. Camanho, S. Bowron, and F. Matthews, "Failure mechanisms in bolted CFRP," *Journal of reinforced plastics and composites*, vol. 17, pp. 205-233, 1998.

[11] F. Liu, J. Zhang, L. Zhao, A. Xin, and L. Zhou, "An analytical joint stiffness model for load transfer analysis in highly torqued multi-bolt composite joints with clearances," *Composite Structures*, vol. 131, pp. 625-636, 2015.

[12] H. Huth, "Influence of fastener flexibility on the prediction of load transfer and fatigue life for multiple-row joints," in *Fatigue in mechanically fastened composite and metallic joints*, ed: ASTM International, 1986.

[13] F. Liu, X. Lu, L. Zhao, J. Zhang, N. Hu, and J. Xu, "An interpretation of the load distributions in highly torqued single-lap composite bolted joints with bolt-hole clearances," *Composites Part B: Engineering*, vol. 138, pp. 194-205, 2018/04/01/ 2018.

[14] G. Kelly, "Joining of carbon fibre reinforced plastics for automotive applications," Farkost och flyg, 2004.

[15] S. Ebnesajjad, *Handbook of adhesives and surface preparation: technology, applications and manufacturing*: William Andrew, 2010.

[16] M. Banea and L. F. da Silva, "Adhesively bonded joints in composite materials: an overview," *Proceedings of the Institution of Mechanical Engineers, Part L: Journal of Materials: Design and Applications*, vol. 223, pp. 1-18, 2009.

[17] F. Campbell, "Secondary adhesive bonding of polymer-matrix composites," *Materials Park, OH: ASM International, 2001.*, pp. 620-632, 2001.

[18] F. C. Campbell Jr, *Manufacturing technology for aerospace structural materials*: Elsevier, 2011.

[19] L. Hart-Smith, "Advances in the analysis and design of adhesive-bonded joints in composite aerospace structures," 1974.
[20] O. Volkersen, "Nietkraftverteiligung in zugbeanspruchten nietverbindungen mit konstanten laschenquerschnitten," *Luftfahrtforschung,* vol. 1, pp. 15–41, 1938.
[21] M. a. R. Goland, E., "The stresses in cemented joints," *Journal of Applied Mechanics,* vol. 11, pp. A17-A27, 1944.
[22] L. Hart-Smith, "Adhesive-bonded single-lap joints," *NASA CR-112236,* vol. 114, 1973.
[23] L. Hart-Smith, "Adhesive Bonded Double Lap Joints," *NASA CR-112235,* 1973.
[24] L. F. da Silva, P. J. das Neves, R. Adams, and J. Spelt, "Analytical models of adhesively bonded joints—Part I: Literature survey," *International Journal of Adhesion and Adhesives,* vol. 29, pp. 319-330, 2009.
[25] L. F. M. da Silva, P. J. C. das Neves, R. D. Adams, A. Wang, and J. K. Spelt, "Analytical models of adhesively bonded joints—Part II: Comparative study," *International Journal of Adhesion and Adhesives,* vol. 29, pp. 331-341, 2009/04/01/ 2009.
[26] S. Budhe, M. Banea, S. de Barros, and L. da Silva, "An updated review of adhesively bonded joints in composite materials," *International Journal of Adhesion and Adhesives,* vol. 72, pp. 30-42, 2017.
[27] R. B. Heslehurst, *Design and analysis of structural joints with composite materials*: DEStech Publications, Inc, 2013.
[28] S. Panigrahi, "Damage analyses of adhesively bonded single lap joints due to delaminated FRP composite adherends," *Applied Composite Materials,* vol. 16, pp. 211-223, 2009.
[29] D. ASTM, "5573-99. Standard practice for classifying failure modes in fiber-reinforced-plastic (FRP) joints," *Annual book of ASTM standards,* vol. 15, 2002.
[30] A. A. Taib, R. Boukhili, S. Achiou, S. Gordon, and H. Boukehili, "Bonded joints with composite adherends. Part I. Effect of specimen configuration, adhesive thickness, spew fillet and adherend stiffness on fracture," *International Journal of Adhesion and Adhesives,* vol. 26, pp. 226-236, 2006.
[31] L. Hart-Smith, "Analysis and design of advanced composite bounded joints," 1974.
[32] J. R. Weitzenböck and D. McGeorge, "Science and technology of bolt-adhesive joints," in *Hybrid adhesive joints*, ed: Springer, 2011, pp. 177-199.
[33] K. Bodjona and L. Lessard, "Hybrid bonded-fastened joints and their application in composite structures: A general review," *Journal of Reinforced Plastics and Composites,* vol. 35, pp. 764-781, 2016.
[34] M. L. Stewart, "An experimental investigation of composite bonded and/or bolted repairs using single lap joint designs," in *Proceedings of the 1997, Structural Dynamics, and Materials Conference. Part*, 1997.
[35] W.-H. Lin and M.-H. R. Jen, "The strength of bolted and bonded single-lapped composite joints in tension," *Journal of Composite Materials,* vol. 33, pp. 640-666, 1999.
[36] M. Fu and P. K. Mallick, "Fatigue of hybrid (adhesive/bolted) joints in SRIM composites," *International Journal of Adhesion and Adhesives,* vol. 21, pp. 145-159, 2001/01/01/ 2001.
[37] G. Kelly, "Load transfer in hybrid (bonded/bolted) composite single-lap joints," *Composite structures,* vol. 69, pp. 35-43, 2005.
[38] G. Kelly, "Quasi-static strength and fatigue life of hybrid (bonded/bolted) composite single-lap joints," *Composite structures,* vol. 72, pp. 119-129, 2006.
[39] A. Barut and E. Madenci, "Analysis of bolted–bonded composite single-lap joints under combined in-plane and transverse loading," *Composite Structures,* vol. 88, pp. 579-594, 2009.

[40] C. Bois, H. Wargnier, J.-C. Wahl, and E. Le Goff, "An analytical model for the strength prediction of hybrid (bolted/bonded) composite joints," *Composite Structures,* vol. 97, pp. 252-260, 2013.
[41] A. Vadean, "DESIGN IMPROVEMENT OF HYBRID COMPOSITE JOINTS BY AXIOMATIC DESIGN," in *Proceedings of the 7th International Conference on Axiomatic Design*, 2013.
[42] K. Bodjona and L. Lessard, "Nonlinear static analysis of a composite bonded/bolted single-lap joint using the meshfree radial point interpolation method," *Composite Structures,* vol. 134, pp. 1024-1035, 2015.
[43] K. Bodjona, K. Raju, G.-H. Lim, and L. Lessard, "Load sharing in single-lap bonded/bolted composite joints. Part I: Model development and validation," *Composite Structures,* vol. 129, pp. 268-275, 2015.
[44] P. Gray and C. McCarthy, "A global bolted joint model for finite element analysis of load distributions in multi-bolt composite joints," *Composites Part B: Engineering,* vol. 41, pp. 317-325, 2010.
[45] K. Bodjona and L. Lessard, "Load sharing in single-lap bonded/bolted composite joints. Part II: Global sensitivity analysis," *Composite Structures,* vol. 129, pp. 276-283, 2015.
[46] K. P. Raju, K. Bodjona, G.-H. Lim, and L. Lessard, "Improving load sharing in hybrid bonded/bolted composite joints using an interference-fit bolt," *Composite Structures,* vol. 149, pp. 329-338, 2016.
[47] S. Dashore, M. M. Patil, and B. Ahuja, "Load Distribution in Hybrid (Adhesive & Bolted) Joint," 2016.
[48] P. Lopez-Cruz, J. Laliberté, and L. Lessard, "Investigation of bolted/bonded composite joint behaviour using design of experiments," *Composite Structures,* vol. 170, pp. 192-201, 2017.
[49] E. Armentani, M. Laiso, F. Caputo, and R. Sepe, "Numerical FEM Evaluation for the Structural Behaviour of a Hybrid (bonded/bolted) Single-lap Composite Joint," *Procedia Structural Integrity,* vol. 8, pp. 137-153, 2018.
[50] F. Gamdani, R. Boukhili, and A. Vadean, "Tensile behavior of hybrid multi-bolted/bonded joints in composite laminates," *International Journal of Adhesion and Adhesives,* vol. 95, p. 102426, 2019.
[51] X. Li, Z. Tan, L. Wang, J. Zhang, Z. Xiao, and H. Luo, "Experimental investigations of bolted, adhesively bonded and hybrid bolted/bonded single-lap joints in composite laminates," *Materials Today Communications,* vol. 24, p. 101244, 2020.
[52] W. Li, S. Guo, I. K. Giannopoulos, S. He, and Y. Liu, "Strength enhancement of bonded composite laminate joints reinforced by composite Pins," *Composite Structures,* vol. 236, p. 111916, 2020.
[53] K. Bodjona, S. Fielding, M. Heidari-Rarani, and L. Lessard, "Effect of adhesive layer compliance on strength of single-lap hybrid bonded-bolted joints," *Composite Structures,* vol. 261, p. 113324, 2021.
[54] V. S. Romanov, M. Heidari-Rarani, and L. Lessard, "A parametric study on static behavior and load sharing of multi-bolt hybrid bonded/bolted composite joints," *Composites Part B: Engineering,* vol. 217, p. 108897, 2021.
[55] H. Schreier, J.-J. Orteu, and M. A. Sutton, *Image correlation for shape, motion and deformation measurements*: Springer US, 2009.

[56] B. Pan, K. Qian, H. Xie, and A. Asundi, "Two-dimensional digital image correlation for in-plane displacement and strain measurement: a review," *Measurement science and technology*, vol. 20, p. 062001, 2009.

[57] T. Chu, W. Ranson, and M. A. Sutton, "Applications of digital-image-correlation techniques to experimental mechanics," *Experimental mechanics*, vol. 25, pp. 232-244, 1985.

[58] M. Sutton, C. Mingqi, W. Peters, Y. Chao, and S. McNeill, "Application of an optimized digital correlation method to planar deformation analysis," *Image and Vision Computing*, vol. 4, pp. 143-150, 1986.

[59] J. Lian, Q. Ouyang, X. Zhao, F. Liu, and C. Qi, "Uniaxial Compressive Strength and Fracture Mode of Lake Ice at Moderate Strain Rates Based on a Digital Speckle Correlation Method for Deformation Measurement," *Applied Sciences*, vol. 7, p. 495, 2017.

[60] S. H. Daly, "Digital image correlation in experimental mechanics for aerospace materials and structures," *Encyclopedia of Aerospace Engineering*, 2010.

[61] K. Colavito, J. Gorman, E. Madenci, and S. Smeltzer, "Refinements in digital image correlation technique to extract adhesive strains in lap joints," in *50th AIAA/ASME/ASCE/AHS/ASC Structures, Structural Dynamics, and Materials Conference 17th AIAA/ASME/AHS Adaptive Structures Conference 11th AIAA No*, 2009, p. 2504.

[62] Z. Wang, L. Wang, W. Guo, H. Deng, J. Tong, and F. Aymerich, "An investigation on strain/stress distribution around the overlap end of laminated composite single-lap joints," *Composite structures*, vol. 89, pp. 589-595, 2009.

[63] L. C. S. Nunes, "Shear modulus estimation of the polymer polydimethylsiloxane (PDMS) using digital image correlation," *Materials & Design*, vol. 31, pp. 583-588, 2010/01/01/ 2010.

[64] B. Guo, H. Xie, J. Zhu, H. Wang, P. Chen, and Q. Zhang, "Study on the mechanical behavior of adhesive interface by digital image correlation," *Science China Physics, Mechanics and Astronomy*, vol. 54, pp. 574-580, April 01 2011.

[65] A. Comer, K. Katnam, W. Stanley, and T. Young, "Characterising the behaviour of composite single lap bonded joints using digital image correlation," *International Journal of Adhesion and Adhesives*, vol. 40, pp. 215-223, 2013.

[66] R. V. Kumar, M. Bhat, and C. Murthy, "Experimental analysis of composite single-lap joints using digital image correlation and comparison with theoretical models," *Journal of Reinforced Plastics and Composites*, vol. 32, pp. 1858-1876, 2013.

[67] R. Vijaya kumar, M. Bhat, and C. Murthy, "Analysis of composite single lap joints using numerical and experimental approach," *Journal of Adhesion Science and Technology*, vol. 28, pp. 893-914, 2014.

[68] G. Crammond, S. Boyd, and J. Dulieu-Barton, "Through-thickness load transfer in adhesively bonded composite joints," in *Imaging Methods for Novel Materials and Challenging Applications, Volume 3*, ed: Springer, 2013, pp. 111-114.

[69] G. Crammond, S. Boyd, and J. Dulieu-Barton, "Evaluating the localised through-thickness load transfer and damage initiation in a composite joint using digital image correlation," *Composites Part A: Applied Science and Manufacturing*, vol. 61, pp. 224-234, 2014.

[70] P. Qiu, J. Shi, and J. Zheng, "Experimental Investigation on Adhesive Bonded Joints of Carbon Fiber Composite Laminates Containing Disbond Defect," in *ASME 2017 Pressure Vessels and Piping Conference*, 2017, pp. V005T11A013-V005T11A013.

[71] F. A. Stuparu, D. A. Apostol, D. M. Constantinescu, C. R. Picu, M. Sandu, and S. Sorohan, "Local evaluation of adhesive failure in similar and dissimilar single-lap joints," *Engineering Fracture Mechanics*, vol. 183, pp. 39-52, 2017/10/01/ 2017.

[72] G. Sun, X. Liu, G. Zheng, Z. Gong, and Q. Li, "On fracture characteristics of adhesive joints with dissimilar materials–An experimental study using digital image correlation (DIC) technique," *Composite Structures*, vol. 201, pp. 1056-1075, 2018.

[73] H. Grefe, M. Kandula, and K. Dilger, "Influence of the fibre orientation on the lap shear strength and fracture behaviour of adhesively bonded composite metal joints at high strain rates," *International Journal of Adhesion and Adhesives*, vol. 97, p. 102486, 2020.

[74] G. Zheng, C. Liu, X. Han, and W. Li, "Effect of spew fillet on adhesively bonded single lap joints with CFRP and aluminum-alloy immersed in distilled water," *International Journal of Adhesion and Adhesives*, p. 102590, 2020.

[75] T. Sawada, T. Kawamori, M. Matsunaga, Y. Fujiyasu, and Y. Ueki, "An experimental study for identifying crack initiation forces in single-lap bonded joints," *Engineering Fracture Mechanics*, vol. 241, p. 107372, 2021.

[76] R. L. Vijaya Kumar, M. R. Bhat, and C. R. L. Murthy, "Evaluation of kissing bond in composite adhesive lap joints using digital image correlation: Preliminary studies," *International Journal of Adhesion and Adhesives*, vol. 42, pp. 60-68, 2013/04/01/ 2013.

[77] R. Bai, S. Bao, Z. Lei, and C. Yan, "INVERSION ANALYSIS FOR INTERFACIAL STRESS OF COMPOSITE SINGLE-LAP JOINT BASED ON FULL-FIELD DEFORMATION AND FEM," 2017.

[78] R. Bai, S. Bao, Z. Lei, C. Yan, and X. Han, "Finite element inversion method for interfacial stress analysis of composite single-lap adhesively bonded joint based on full-field deformation," *International Journal of Adhesion and Adhesives*, vol. 81, pp. 48-55, 2018.

[79] C. Barile, C. Casavola, G. Pappalettera, and P. K. Vimalathithan, "Characterization of adhesive bonded CFRP laminates using full-field digital image stereo-correlation and finite element analysis," *Composites Science and Technology*, vol. 169, pp. 16-25, 2019.

[80] T. Zou, J. Fu, J. Qin, L. Li, and Z. Liu, "Failure analysis of composite-to-titanium single lap adhesive joints subjected to tensile loading," *Engineering Failure Analysis*, vol. 129, p. 105734, 2021.

[81] J. Ekh, J. Schön, and L. G. Melin, "Secondary bending in multi fastener, composite-to-aluminium single shear lap joints," *Composites Part B: Engineering*, vol. 36, pp. 195-208, 2005.

[82] J. Dupuy, F. Lachaud, R. Piquet, and J. Huet, "Finite element model matching based on optical measurement fields on single shear lap joint," in *Application of Imaging Techniques to Mechanics of Materials and Structures, Volume 4*, ed: Springer, 2010, pp. 53-62.

[83] A. Comer, J. Dhôte, W. Stanley, and T. Young, "Thermo-mechanical fatigue analysis of liquid shim in mechanically fastened hybrid joints for aerospace applications," *Composite Structures*, vol. 94, pp. 2181-2187, 2012.

[84] J. Dhôte, A. Comer, W. Stanley, and T. Young, "Study of the effect of liquid shim on single-lap joint using 3D Digital Image Correlation," *Composite Structures*, vol. 96, pp. 216-225, 2013.

[85] P. J. Gray, R. M. O'Higgins, and C. T. McCarthy, "Effect of thickness and laminate taper on the stiffness, strength and secondary bending of single-lap, single-bolt countersunk composite joints," *Composite Structures*, vol. 107, pp. 315-324, 2014/01/01/ 2014.

[86] P. J. Gray, R. M. O'Higgins, and C. T. McCarthy, "Effects of laminate thickness, tapering and missing fasteners on the mechanical behaviour of single-lap, multi-bolt, countersunk composite joints," *Composite Structures,* vol. 107, pp. 219-230, 2014/01/01/ 2014.

[87] V. P. Lawlor, M. A. Mccarthy, and W. Stanley, "An experimental study of bolt–hole clearance effects in double-lap, multi-bolt composite joints," *Composite structures,* vol. 71, pp. 176-190, 2005.

[88] Y. Zhai, D. Li, X. Li, L. Wang, and Y. Yin, "An experimental study on the effect of bolt-hole clearance and bolt torque on single-lap, countersunk composite joints," *Composite structures,* vol. 127, pp. 411-419, 2015.

[89] A. Haris, T. Tay, and V. Tan, "Experimental analysis of composite bolted joints using digital image correlation," 2017.

[90] J. Hu, K. Zhang, Q. Yang, H. Cheng, P. Liu, and Y. Yang, "An experimental study on mechanical response of single-lap bolted CFRP composite interference-fit joints," *Composite Structures,* 2018.

[91] X. Hu, A. Haris, M. Ridha, V. Tan, and T. Tay, "Progressive failure of bolted single-lap joints of woven fibre-reinforced composites," *Composite Structures,* vol. 189, pp. 443-454, 2018.

[92] J. Hu, K. Zhang, Y. Xu, H. Cheng, G. Xu, and H. Li, "Modeling on bearing behavior and damage evolution of single-lap bolted composite interference-fit joints," *Composite Structures,* vol. 212, pp. 452-464, 2019.

[93] G. Xu, K. Zhang, H. Cheng, B. Luo, B. Liang, Y. Cheng, *et al.*, "An experimental study on mechanical behavior and failure mechanism of sleeved fasteners and conventional bolt for composite interference-fit joints," *Thin-Walled Structures,* vol. 170, p. 108537, 2022.

[94] H. Shi, I. Fernandez Villegas, and H. Bersee, "An investigation on the strain distribution of resistance welded thermoplastic composite joints," in *53rd AIAA/ASME/ASCE/AHS/ASC Structures, Structural Dynamics and Materials Conference 20th AIAA/ASME/AHS Adaptive Structures Conference 14th AIAA*, 2012, p. 1448.

[95] J. R. Newkirk, C. M. Degen, and A. Romkes, "Characterization of Thermoplastic Matrix Composite Joints for the Development of a Computational Framework," in *Mechanics of Composite and Multi-functional Materials, Volume 6*, ed: Springer, 2018, pp. 11-19.

[96] A. N. Dickson and D. P. Dowling, "Enhancing the bearing strength of woven carbon fibre thermoplastic composites through additive manufacturing," *Composite Structures,* vol. 212, pp. 381-388, 2019.

[97] T. Zhao, C. Rans, I. F. Villegas, and R. Benedictus, "On sequential ultrasonic spot welding as an alternative to mechanical fastening in thermoplastic composite assemblies: A study on single-column multi-row single-lap shear joints," *Composites Part A: Applied Science and Manufacturing,* vol. 120, pp. 1-11, 2019.

[98] W. Li, S. Guo, I. K. Giannopoulos, M. Lin, Y. Xiong, Y. Liu, *et al.*, "3D-printed thermoplastic composite fasteners for single lap joint reinforcement," *Composite Structures,* vol. 282, p. 115085, 2022.

[99] D. Backman, G. Li, and T. Sears, "Determining the strain distribution in bonded and bolted/bonded composite butt joints using the digital image correlation technique and finite element methods," in *Optical Measurements, Modeling, and Metrology, Volume 5*, ed: Springer, 2011, pp. 401-406.

[100] G. Li, "Fatigue performance characterization of a composite butt joint configuration," *Composites Part A: Applied Science and Manufacturing,* vol. 51, pp. 43-55, 2013/08/01/ 2013.

[101] J. Kim, "Experimental Investigation of Mechanical Behaviour of Hybrid Bolted/Bonded Joints for Aircraft," Carleton University Ottawa, 2016.
[102] P. L. Cruz, "Experimental and Numerical Study on Bolted/Bonded Composite Joints for Aircraft," Carleton University Ottawa, 2016.
[103] G.-H. Lim, K. Bodjona, K. P. Raju, S. Fielding, V. Romanov, and L. Lessard, "Evolution of mechanical properties of flexible epoxy adhesives under cyclic loading and its effects on composite hybrid bolted/bonded joint design," *Composite Structures*, vol. 189, pp. 54-60, 2018.
[104] G.-H. Lim, M. Heidari-Rarani, K. Bodjona, K. P. Raju, V. Romanov, and L. Lessard, "Mechanical characterization of a flexible epoxy adhesive for the design of hybrid bonded-bolted joints," *Polymer Testing*, vol. 79, p. 106048, 2019.
[105] Y. Chen, M. Li, X. Yang, and W. Luo, "Damage and failure characteristics of CFRP/aluminum single lap joints designed for lightweight applications," *Thin-Walled Structures*, vol. 153, p. 106802, 2020.
[106] M. Li, W. Luo, Y. Chen, and X. Yang, "Full-field strain distribution and failure characteristics of CFRP-repaired steel structures," *Engineering Failure Analysis*, vol. 115, p. 104664, 2020.
[107] G. Sun, X. Xia, X. Liu, Q. Luo, and Q. Li, "On quasi-static behaviors of different joint methods for connecting carbon fiber reinforce plastic (CFRP) laminate and aluminum alloy," *Thin-Walled Structures*, vol. 164, p. 107657, 2021.
[108] J. Kim, P. Lopez-Cruz, M. Heidari-Rarani, L. Lessard, and J. Laliberté, "An experimental study on the mechanical behaviour of bonded and hybrid bonded-bolted composite joints using digital image correlation (DIC) technique," *Composite Structures*, vol. 276, p. 114544, 2021.
[109] F. Gamdani, R. Boukhili, and A. Vadean, "Tensile strength of open-hole, pin-loaded and multi-bolted single-lap joints in woven composite plates," *Materials & Design*, vol. 88, pp. 702-712, 2015.

APPENDICES

APPENDIX A: SUPPORTING INFORMATION

Neutral line model (NLM)

For the analytical investigation of the SB, a one-dimensional NLM was used. Schijve [1, 2] initially proposed this approach for calculating the ratio of bending stress over tensile stress (bending factor) as well as OPD (w), which occur in SL/strap butt joints owing to the geometrical eccentricity of their structure. Figure A-1 shows the schematics of the out-of-plane deformation of a three-bolt single-lap joint associated with SB, and the eccentricity of half the splice thickness ($e = t/2$).

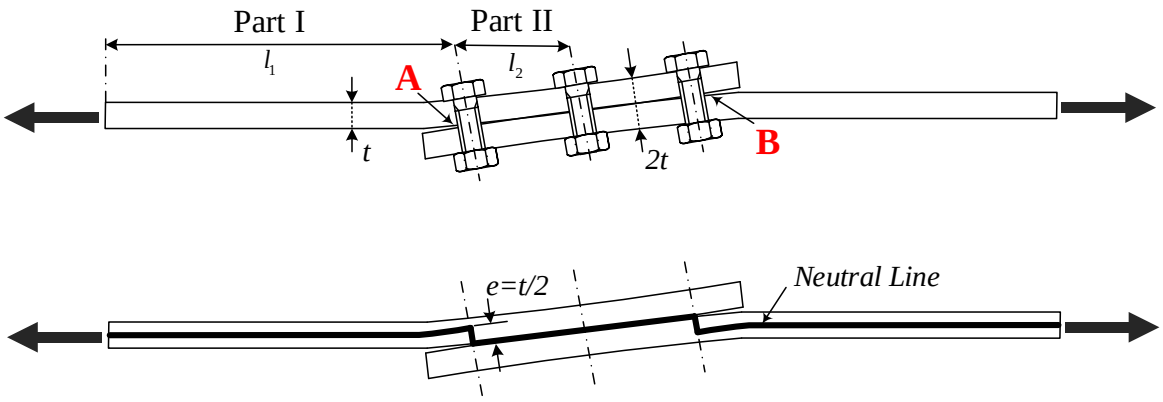

Figure A-1: Secondary bending in three-bolt single-lap joint subjected to tensile loading.

This model was governed by the advanced elastic beam theory, in which the region outside the overlap area (Part I in Figure A-2(b)) and the overlap section (Part II in Figure A-2(b)) were regarded as a solid cantilever beam subjected to a tensile load and an internal plane moment owing to the eccentricities. The former case involves a beam with a thickness t, whereas the latter is considered as an integrated beam, which possesses flexural rigidity corresponding to twice the laminate thickness, i.e., $2t$ [3].

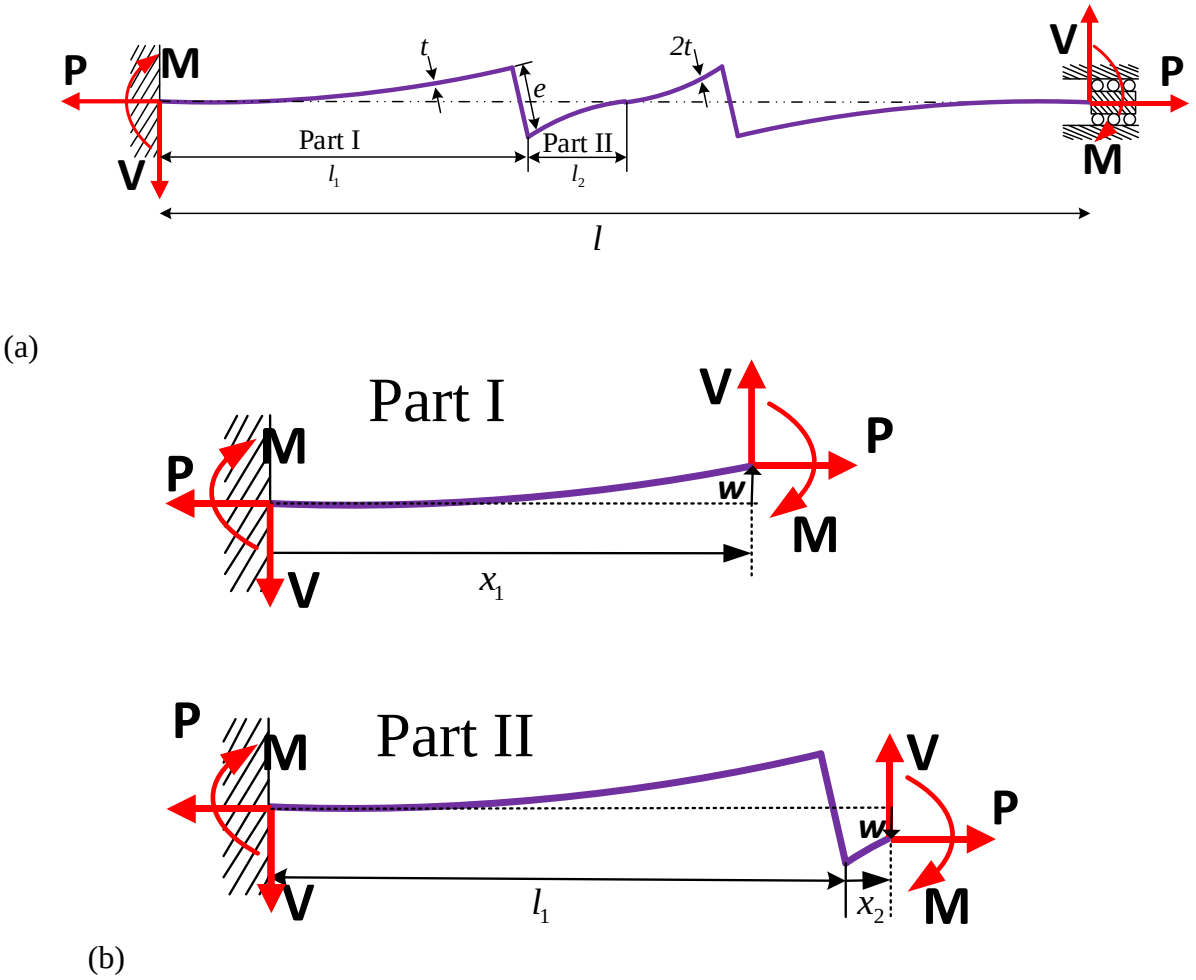

Figure A-2: (a) NLM of bolted joint with fixed clamp conditions; (b) Free diagram and boundary conditions of two main parts of NLM.

In this method, the displacement of the neutral line indicates that the SL joint response corresponds to the applied load. It is assumed that the joint behavior is symmetric with respect to the middle bolt; hence, half of the joint is decomposed into two parts, namely Parts I and II, after which by driving the equilibrium equations and solving them, SB can be analyzed [4]. The static equilibrium equation for the entire joint, which is shown in Figure A-2(a) in the form of the neutral line of the beam, is written as follows:

$$2M - Vl = 0 \tag{1}$$

By applying a sectional cut for Part 1 (Figure A-2(b)), the bending moment of this section (M_x) can be calculated from the differential equation for the vertical displacement *w* of the neutral line, as follows:

$$M_x = M + Pw_1 - Vx_1 = E^* I_1 \left(\frac{d^2 w}{dx^2} \right)_1 \tag{2}$$

where V and M are the internal reaction force and moment, respectively; P is the applied load; $E^* I$ refers to the bending stiffness of the corresponding section. It is noteworthy that the symbol E^* is used for correcting the Young's modulus ($E^* = E/(1-\upsilon^2)$) to prevent anticlastic bending in thin panels, which may result in a small increase in the bending stiffness [2]. I is the inertia moment of the joint cross-section ($I = wt^3/12$, w is the width of the specimen). For brevity, the following relations were utilized: $\alpha_1^2 = P/E^* I_1$ and $q = V/P$. By substituting Eq. (1) into Eq. (2), a second-order linear nonhomogeneous differential equation can be expressed as follows:

$$\left(\frac{d^2 w}{dx^2} \right)_1 - \alpha_1^2 w_1 = \alpha_1^2 \left(\frac{ql}{2} - qx_1 \right) \tag{3}$$

The solution for this equation can be obtained using hyperbolic functions as follows:

$$w_1 = A_1 \sinh(\alpha_1 x_1) + B_1 \cosh(\alpha_1 x_1) + \left(qx_1 - \frac{ql}{2} \right) \tag{4}$$

The boundary conditions for Part 1 at $x_1 = 0$ are

$$\begin{gathered} w_1 = 0 \\ \left(dw/dx_1 \right) = 0 \end{gathered} \tag{5}$$

By applying the boundary condition, the following equations are obtained:

$$B_1 - \frac{ql}{2} = 0 \tag{6}$$

$$A_1\alpha_1 + q = 0 \tag{7}$$

The same procedure should be performed for Part II, whose differential equation is

$$M_x = M + Pw_2 - V(l_1 + x_2) = E^* I_2 \left(\frac{d^2 w}{dx^2}\right)_2 \tag{8}$$

Considering $\alpha_2^2 = P/E^* I_2$ and by substituting Eqs. (1) into Eq. (8), Eq. (8) becomes

$$\left(\frac{d^2 w}{dx^2}\right)_1 - \alpha_2^2 w_2 = \alpha_2^2 \left(\frac{ql}{2} - q(x_2 + l_1)\right) \tag{9}$$

The following hyperbolic function delivers the solution for Eq. (9):

$$w_2 = A_2 \sinh(\alpha_2 x_2) + B_2 \cosh(\alpha_2 x_2) + \left(q(x_2 + l_1) - \frac{ql}{2}\right) \tag{10}$$

The governing boundary conditions for Part II at $x_2 = 0$ are as follows:

$$\begin{aligned} w_{2,x_2=2} &= w_{1,x_1=l_1} - e \\ \left(\frac{dw}{dx}\right)_{2,x_2=0} &= \left(\frac{dw}{dx}\right)_{1,x_1=l_1} \end{aligned} \tag{11}$$

The results are as follows:

$$A_1 \sinh(\alpha_1 l_1) + B_1 \cosh(\alpha_1 l_1) = B_2 + e \tag{12}$$

$$A_1\alpha_1 \cosh(\alpha_1 l_1) + B_1\alpha_1 \sinh(\alpha_1 l_1) = A_2\alpha_2 \tag{13}$$

The last boundary condition is associated with the middle of the joint, i.e., $x_2 = l_2$; and the second half is assumed to yield an analogous response:

$$w = 0 \tag{14}$$

Considering that $l/2 = l_1 + l_2$, the following equation can be derived:

$$A_2 \sinh(\alpha_2 l_2) + B_2 \cosh(\alpha_2 l_2) = 0 \tag{15}$$

Therefore, by summarizing Eqs. (6), (7), (12), (13), and (15), a system of five equations and five unknowns is obtained as follows:

$$B_1 - \frac{l}{2} q = 0$$

$$A_1 + \frac{1}{\alpha_1} q = 0$$

$$A_1 \sinh(\alpha_1 l_1) + B_1 \cosh(\alpha_1 l_1) - B_2 = e \tag{16}$$

$$A_1 \cosh(\alpha_1 l_1) + B_1 \sinh(\alpha_1 l_1) - \frac{\alpha_2}{\alpha_1} A_2 = 0$$

$$A_2 \sinh(\alpha_2 l_2) + B_2 \cosh(\alpha_2 l_2) = 0$$

After solving the equation system, the unknowns A_1, B_1, A_2, B_2, and q can be determined. In a multibolted SL joint, the maximum bending moment always occurs at the extreme bolt (in this case, $x_1 = l_1$) where failure occurs. Using Eqs. (1), (2), and (4), the bending moment at the mentioned location can be expressed as

$$M(x_1 = l_1) = P\left(A_1 \sinh(\alpha_1 l_1) + B_1 \cosh(\alpha_1 l_1)\right) \tag{17}$$

The bending stress and nominal stress at $x_1 = l_1$ are defined as follows:

$$\sigma_{nominal} = \frac{P}{t} \tag{18}$$

$$\sigma_{bending} = \frac{M(x_1 = l_1) y}{I} \tag{19}$$

The severity of SB at a certain location is often defined by a coefficient called the bending factor, k_b, which is expressed as follows:

$$k_b = \frac{\sigma_{bending}}{\sigma_{nominal}} = \left(\frac{6}{tw}\right)\left(A_1 \sinh(\alpha_1 l_1) + B_1 \cosh(\alpha_1 l_1)\right) \tag{20}$$

Supporting results

Comparison of DIC measurements and NLM predictions

OPDs measured by DIC and predicted using the NLM are compared in Figure A-3. The comparison was performed for the case of the three-bolt CP 12-layer configuration, at 25% of the failure load (FL) and in the region between the extreme bolts. The corresponding values of the OPD were calculated using Eq. (10). As shown in Figure A-3, a satisfactory approximation is obtained between the experimental and analytical approaches. The observed deviation between the NLM and the measured data may be due to the fact that the NLM models the region as an integrated beam with a thickness of $2t$. In fact, the supposed integrated beam comprises two parts that slide against each other.

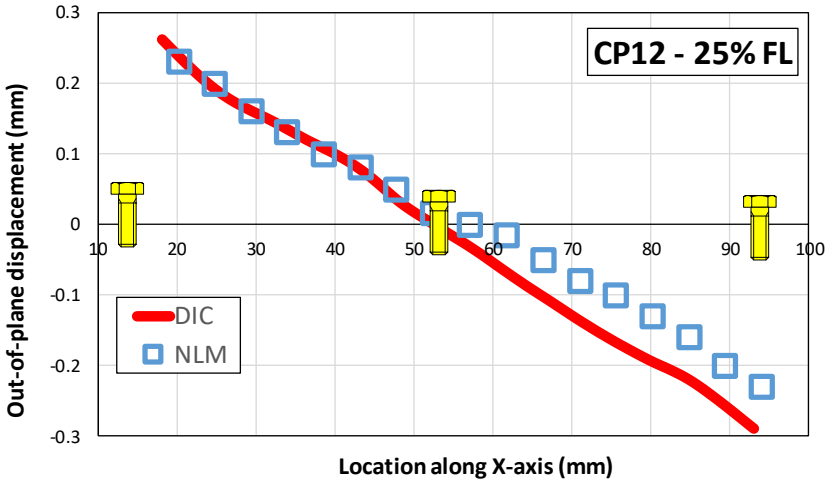

Figure A-3: Comparison of out-of-plane displacement computed by 3D DIC and calculated by NLM for three-bolt CP12 joint.

Joint twisting

It was mentioned in the paper that one of the reasons causing the non-horizontal colored bands of Figure 4.5 and 4.6 is the twisting effect. This phenomenon was captured by comparing the differences between the OPD on the right- and left-hand sides of the joint surface. The inset images in Figure A-4 shows two dashed red lines constructed at a distance of *2d* from the centerline of the holes on the left and right sides of the joint surface. The out-of-plane deformations along these two lines were recorded for the entire test. However, in Figure A-4, the deformation states at 75% of the FL is shown for illustration. It is noteworthy that the specimens were placed meticulously in the testing machine grips to avoid any pre-established twisting, which might be introduced to the joint coupon. While this effect occurs in real structural applications, it cannot be quantified easily using experimental point measurement techniques or numerical simulations. The results show that 3D DIC is a concrete tool to well capture this byproduct of SB (also known as tertiary bending).

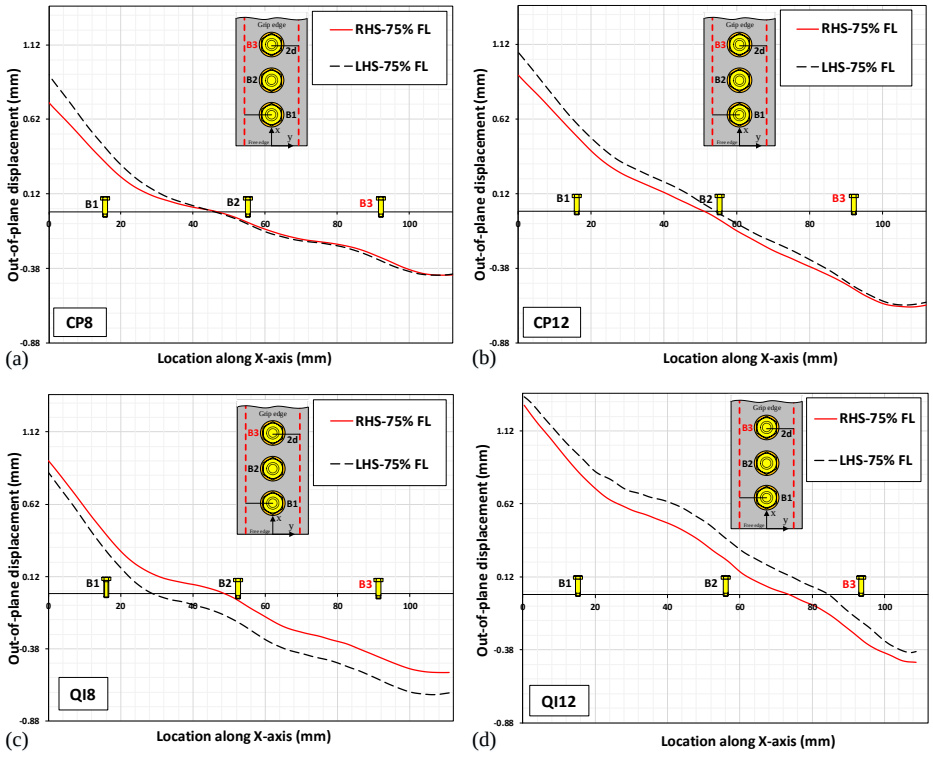

Figure A-4: Twisting of the cross-ply (CP) and quasi-isotropic (QI) joints as a result of secondary bending: (a) CP8, (b) CP12, (c) QI8 and (d) QI12.

Generally, twisting in SL composite joints emanates as a results of a combination of several factors, including (a) extension-shear and bending-twisting coupling, which occur only in anisotropic plates such as laminated structures [5], (b) rotation or slanting of mechanical fasteners owing to geometrical eccentricity, and (c) the existence of $\pm 45^0$ plies on the structure of the laminates. As the bolts are inclined because of case (b), a nonuniform contact area through the laminate thickness is established between the bolt shank and bolt hole, yielding different contact pressures exerted on the -45^0 plies than the $+45^0$ ones [6]. Therefore, the QI lay-up, which is composed of $\pm 45^0$ plies at different positions from the top to bottom of the laminate, i.e., different contact pressures on the corresponding plies, should experience a greater degree of twisting compared with the CP that has a constant fiber arrangement through the thickness.

A comparison of Figure A-4 shows that QI laminates show a more pronounced twisting than CP laminates. This complies with plate laminate theory (PLT) predictions [5]. In fact, according to plate laminate theory [5], the relation between the bending moments (M_{xx}, M_{yy}, and M_{xy}) and curvatures (k_{xx}, k_{yy}, and k_{xy}) for a balanced symmetric laminate can be expressed as shown in Eqs. 21–23.

$$[M] = [D][k] \tag{21}$$

$$\begin{bmatrix} k_{xx} \\ k_{yy} \\ k_{xy} \end{bmatrix} = \frac{1}{D_0} \begin{bmatrix} D_{11}^0 & D_{12}^0 & D_{16}^0 \\ D_{12}^0 & D_{22}^0 & D_{26}^0 \\ D_{16}^0 & D_{26}^0 & D_{66}^0 \end{bmatrix} \begin{bmatrix} M_{xx} \\ M_{yy} \\ M_{xy} \end{bmatrix} \tag{22}$$

$$\begin{aligned} k_{xx} &= \frac{D_{11}^0}{D_0} M_{xx} \\ k_{yy} &= \frac{D_{12}^0}{D_0} M_{xx} \\ k_{xy} &= \frac{D_{16}^0}{D_0} M_{xx} \end{aligned} \tag{23}$$

The elements of the D_{ij}^0 matrix are functions of the laminate elastic properties (i.e., stiffness matrices A, B, and D as defined in PLT). This equation shows that element D16 couples the bending moment M_{xx} with twisting (torsional) deformation k_{xy}. In other words, even though no

twisting moment is applied, the specimen tends to twist [5]. However, in CP laminates, $D_{16} = 0$ and consequently no twisting will be induced by the bending moment. As mentioned above, many factors are contribute to the induced twisting; hence, even when $D_{16} = 0$ for CP, a certain amount of twisting still occurred.

It can be inferred that a multibolted SL composite joint with a more homogenized lay-up arrangement through the thickness can preferably restrain a joint from the twisting effect, whereas it is affected by the induced SB. Twisting disturbs the overall and local surface deflection as well as the symmetry in the strain/stress distribution, which is detrimental to the composite joints and may alter the failure mode. This second byproduct of the tension load is an important issue for bonded and hybrid bonded/bolted SL composite joints; however, it is discovered in this study that for the only bolted case also plays a predominant role, which has rarely been addressed hitherto.

References

[1] J. Schijve, Some elementary calculations on secondary bending in simple lap joints, Nationaal Lucht-en Ruimtevaartlaboratorium, 1972.

[2] J. Schijve, Fatigue of structures and materials, Springer Science & Business Media2001.

[3] A. Skorupa, M. Skorupa, Riveted lap joints in aircraft fuselage: design, analysis and properties, Springer Science & Business Media2012.

[4] J. Schijve, G. Campoli, A. Monaco, Fatigue of structures and secondary bending in structural elements, International Journal of Fatigue 31(7) (2009) 1111-1123. doi:https://doi.org/10.1016/j.ijfatigue.2009.01.009.

[5] P.K. Mallick, Fiber-reinforced composites: materials, manufacturing, and design, CRC press2007.

[6] M.A. McCarthy, C.T. McCarthy, V.P. Lawlor, W.F. Stanley, Three-dimensional finite element analysis of single-bolt, single-lap composite bolted joints: part I—model development and validation, Composite Structures 71(2) (2005) 140-158. doi:https://doi.org/10.1016/j.compstruct.2004.09.024.

APPENDIX B: SUPPORTING RESULTS

For the sake of brevity in the manuscript, in case of observing the same trend between the two different thicknesses, just one is reported and readers are asked to refer to the Appendix A. In this section, all those missing figures are brought to help readers study them and do comparisons wherever is required.

Figure B-1 shows the bolt hole elongation of only-bolted (OB) joints of cross-ply (CP) and quasi-isotropic (QI) lay-up with 8 layers. The corresponding Figure for 12-layer is illustrated in Figure 6.10 of the manuscript.

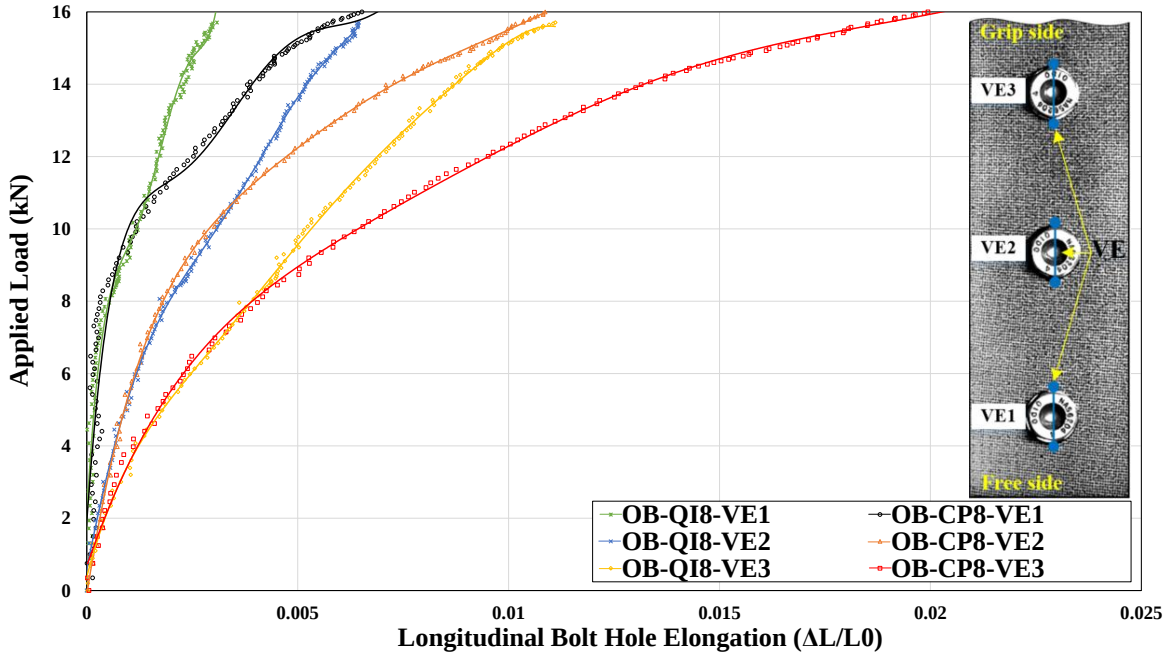

Figure B-1: Bolt hole elongation of OB-CP8 and OB-QI8.

Figure B-2 shows longitudinal deformation below B3 at 10%, 30%, 50%, 70% and 90% of the applied load for only-bolted cross-ply (CP) and quasi-isotropic (QI) lay-up with 12 layers. The corresponding Figure for 8-layer is illustrated in Figure 6.11 of the manuscript.

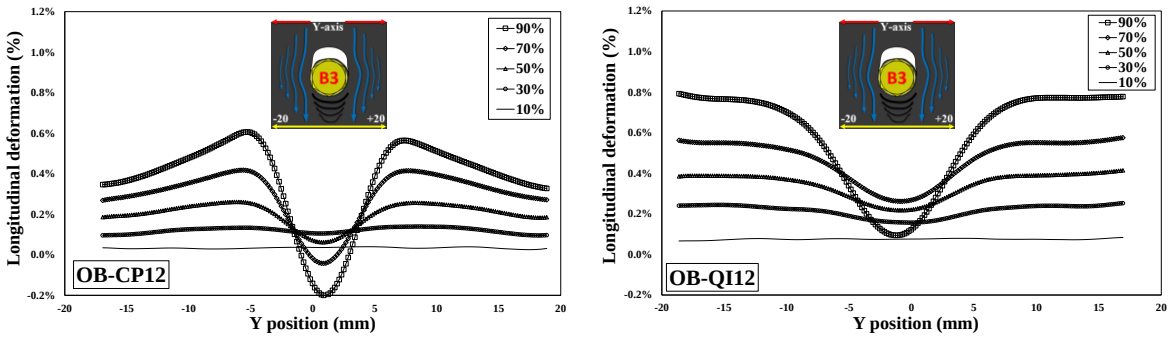

Figure B-2: Longitudinal deformation below B3 at 10%, 30%, 50%, 70% and 90% of the applied load: (a) OB-CP12 and (b) OB-QI12.

Figure B-3 shows the bolt hole elongation of hybrid-bolted-bonded (HBB) joints of cross-ply (CP) and quasi-isotropic (QI) lay-up with 12 layers. The corresponding Figure for 8-layer is illustrated in Figure 6.12 of the manuscript.

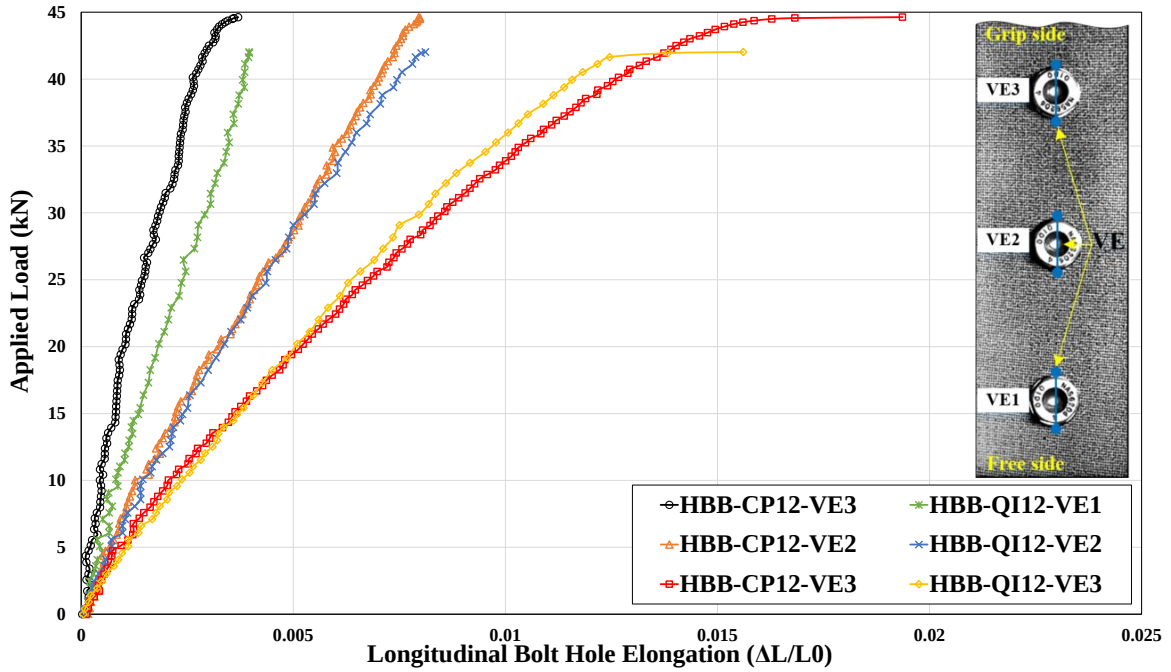

Figure B-3: Bolt hole elongation of HBB-CP12 and HBB-QI12.

Figure B-4 shows longitudinal deformation below B3 at 10%, 30%, 50%, 70% and 90% of the applied load for hybrid-bolted-bonded cross-ply (CP) and quasi-isotropic (QI) lay-up with 12 layers. The corresponding Figure for 8-layer is illustrated in Figure 6.13 of the manuscript.

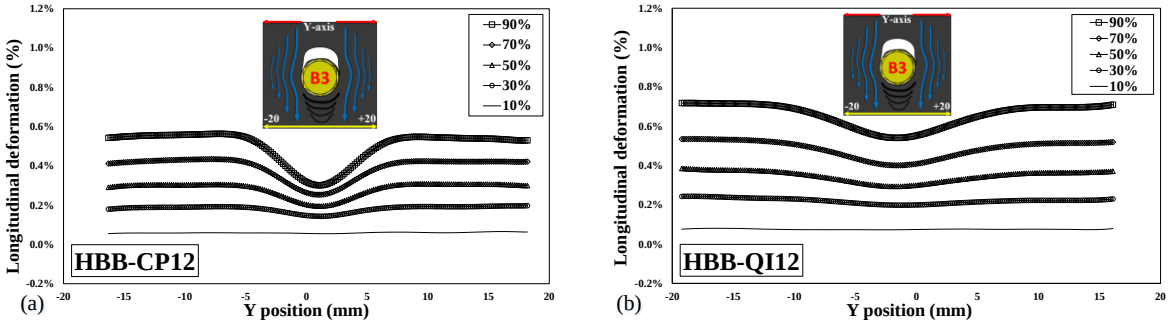

Figure B-4: Longitudinal deformation below B3 at 10%, 30%, 50%, 70% and 90% of the applied load: (a) HBB-CP12 and (b) HBB-QI12.

Figure B-5 compares BHE for only-bolted and hybrid-bolted-bonded for the investigated laminates of 12 layers. The load level (25 kN) corresponds to the onset of the bearing damage in only-bolted joints. The corresponding Figure for 8-layer is illustrated in Figure 6.14 of the manuscript.

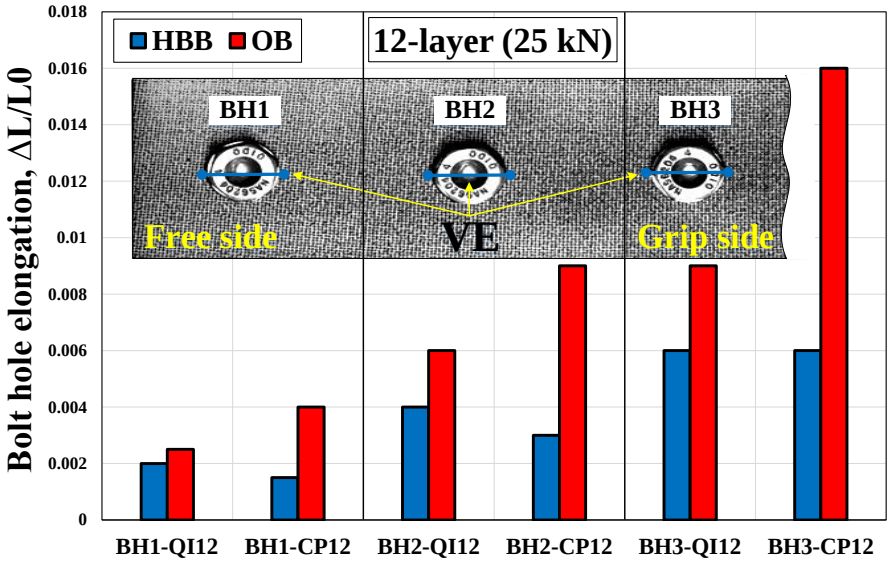

Figure B-5: Comparison of BHE in OB12 versus HBB12 of CP and QI joints at a certain load level of 25kN.